Ministry of Science and Higher Education of the Russian Federation
Russian National Committee on Theoretical and Applied Mechanics
Russian National Committee for IFToMM
(International Federation for the
Promotion of Mechanism and Machine Science)
Siberian Branch of the Russian Academy of Sciences
Khristianovich Institute of Theoretical and Applied Mechanics
of the Russian Academy of Sciences
Central Aerohydrodynamic Institute
Novosibirsk State University

International Conference on the Methods of Aerophysical Research

August 8 – 14, 2022
Novosibirsk, Russia

Abstracts
Part I

Edited by A.N. Shiplyuk

Novosibirsk
Siberian Branch of the Russian Academy of Sciences
2022

UDK 533.6+532.5.013.4+551.5:371.3
ВВК В253.33я431(0)

ICMAR'2022 is sponsored with:
Fund "Science and culture support centre"

International Conference on the Methods of Aerophysical Research (Novosibirsk, Russia, August 8 – 14, 2022): Abstracts. Pt. I / Ed. A.N. Shiplyuk; Ministry of Science and Higher Education of the Russian Federation [et al.]. – Novosibirsk: SB RAS, 2022. – 235 p.

The 21st International Conference on the Methods of Aerophysical Research (ICMAR 2022) is to be held on August 8–14, 2022. ICMAR 2022 conference is dedicated to the 65th anniversary of ITAM SB RAS.
Abstracts of the conference are published in this collection. It includes the main topics ICMAR 2022 which there are:

- Methods of flow diagnostics;
- CFD methods and codes: problems of modeling and verification.

They are distributed through four sections:

- Wind Tunnels and Gas-Dynamic Facilities, Methods of Flow Diagnostics;
- Stability, Turbulence and Separation;
- Gas Dynamics of Internal and External Flows;
- Methods of Aerophysical Research in Interdisciplinary Problems;

The last section of ICMAR deals with the use of Aerophysical Research Methods in medicine, biology, chemistry, ecology, and another fields.

Some ICMAR 2022 papers could be published at the Russian Journals only.

ISBN 978-5-6047889-6-7 (ч. 1)
ISBN 978-5-6047889-5-0

DOI: 10.53954/9785604788967_3

INVESTIGATION OF THE DEVELOPMENT OF THE FREQUENCY SPECTRUM OF AN ACOUSTIC SIGNAL WITH A SMOOTH INCREASE IN THE SPEED OF A FREE ISOTHERMAL JET IN A RESONATING CHAMBER USING A ROBOTRON MEASURING MICROPHONE

A.A. Abdrashitov[1], E.A. Marfin[1], E.A. Plakhova[2]

[1]Institute of Power Engineering and Advanced Technologies
FRC Kazan Scientific Center, Russian Academy of Sciences

[2]Kazan (Volga Region) Federal University
420111, Kazan, Russia

The results of an experimental study of the generation of periodic pressure oscillations in a cylindrical chamber with two side covers when a round air jet flows onto a sharp edge of the outlet are presented. The evolution of the frequency response of the jet-tone of the hole from its appearance at a jet velocity of about 2 m/s to the excitation of the first acoustic resonance mode at the Helmholtz frequency was studied. The jet-tone was a family of harmonics that progressively became more complex as the Reynolds number increased. Amplitude jumps between harmonics were noted with a smooth increase in the jet velocity until the first mode appeared. The sequential appearance of a family of acoustic modes on jet-tone harmonics with a further increase in the jet velocity is studied. Modes at the Helmholtz frequency arose alternately on the jet-tone harmonics, starting from the highest harmonic. The first mode arose at the highest harmonic; the second mode arose at the previous harmonic, and so on. The final mode arose on the fundamental harmonic of the jet-tone and had the maximum amplitude. With a further increase in the Reynolds number, periodic pressure oscillations turned into disordered turbulent pulsations. With a sufficient chamber size and jet velocity, azimuthally and half-wave resonance appeared at the highest harmonic of the jet-tone. The largest Reynolds number at which a resonance at the Helmholtz frequency was observed was 10^5.

The jet velocity at the nozzle outlet was measured indirectly, by an Oven pressure transducer, using the static pressure drop (slowly varying pressure component) across the nozzle. Measurement of the amplitude of pressure fluctuations in the chamber (rapidly changing pressure component) was carried out in a direct way, using an RFT MV 201 Robotron microphone (MK 221 capsule with a sensitivity of 54 mV/Pa) with an error of ±1 dB, in the range of 2…20 kHz.

The recorded signals were digitized by a 14-bit analog-to-digital converter (ADC) E14-440 with a sampling frequency S = 10 kHz and transferred to a personal computer. The program Power Graph 3.3.8. was used to register and process signals [1, 2].

The experimental model was made from a piece of plastic pipe *1* (Fig. 1) with plexiglass covers *2* and *4*. Holes *3* and *5* were made in the covers for pumping air through the chamber [3]. A measuring microphone *6* and a fitting *7* were mounted in the front cover to measure the static pressure inside the chamber. The model was mounted in the cover of an evacuated cylinder (balloon).

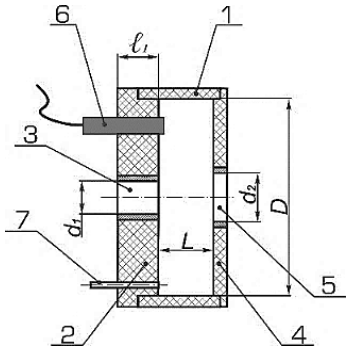

Fig. 1. Scheme of assembly of the experimental model.

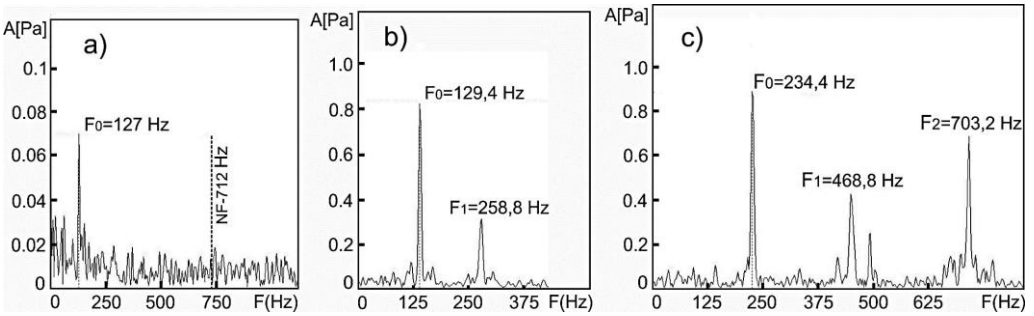

Fig. 2. The emergence and development of jet-tone harmonics.
W = 1.8 (*a*), 3.4 (*b*), 5.2 (*c*) m/s.

In each experiment, a smooth increase in the jet velocity from zero was performed. The values of pressure drop across the nozzle and pressure fluctuations in the chamber were recorded in the time domain as an oscillogram. A windowed Fourier-transform of the microphone signal corresponding to pressure fluctuations in the chamber was performed, and the parameters were converted from the time domain to the frequency one. Then the frequency spectra were analyzed. A technique for identifying and numbering elements of the frequency spectrum (harmonics) was developed.

With a smooth increase in the jet velocity to a value of $W \sim 1.8$ m/s, periodic pressure fluctuations occurred in the chamber at a frequency F_0 of several tens of hertz – a jet-tone of the hole appeared (Fig. 2,*a*). Its frequency was much lower than the natural frequency f_N of the chamber, and resonance did not occur. The tone amplitude at the first moment slightly exceeded the least significant bit (LSB).

As the jet velocity increased to 3.4 m/s, the amplitude of the first peak – the fundamental harmonic - rapidly increased along the ordinate axis (see the ordinate scale), and the peak shifted in frequency on the abscissa axis to the right, towards increasing frequency. Another peak appeared – the first harmonic F_1 – at the double frequency of the fundamental harmonic F_0 (Fig. 2,*b*). With a further increase in speed to 5.2 m/s, the second harmonic F_2 appeared at a frequency multiple of the frequency of the fundamental harmonic (Fig. 3,*c*). With a smooth increase in speed jet, the entire family of harmonics shifted in the direction of increasing frequency along the abscissa axis, and the predominant amplitude could jump from one to another. When the harmonic F_2 reached the lower edge of the gain band of the resonator, resonance began.

REFERENCES

1. **Abdrashitov A.A., Marfin E.A., Chachkov D.V.** Experimental study of a borehole acoustic radiator with a ring in a long cylindrical chamber // Acoustical Physics. 2018. Vol. 64, No. 2. P. 237–244. doi.org/10.1134/S106377101802001X.
2. **Abdrashitov A.A., Marfin E.A., Chachkov D.V., Chefanov V.M.** Effect of nozzle shape on amplitude of well acoustic emitter generation // Acoustical Physics. 2018. Vol. 64, No. 4. P. 492–502. doi.org/10.1134/S1063771018030016.
3. **Morel Th.** Experimental study of a jet-driven Helmholtz oscillator // J. Fluid Engineering. 1979. Vol. 101, Iss. 3. P. 383–390. doi.org/10.1115/1.3448983.

DOI: 10.53954/9785604788967_5

EFFECT OF THE MOMENT OF INERTIA AND THE INITIAL ANGLE OF ATTACK ON THE ASPECTS OF SELF-OSCILLATIONS OF SEGMENTAL-CONICAL BODY AT MACH NUMBER M = 1.75

N.P. Adamov, E.A. Chasovnikov, N.A. Mishchenko

Khristianovich Institute of Theoretical and Applied Mechanics SB RAS
630090, Novosibirsk, Russia

The subject of the study is a segmental-conical body. The forebody has a segmental form with a large radius and the rear part has a form of tapering conoid. The goal of the current study is to investigate the stability of the body having free angle of attack oscillation and to study the effect of the moment of inertia. Tests were conducted at T-313 supersonic blowdown wind tunnel based at ITAM SB RAS using a transversive rod setup [1] at Mach number M = 1.75. Model is presented in two variants with identical geometry but different moments of inertia $I_1 = 1.2\ 10^{-3}$ kg·m^2 and $I_2 = 5.6\ 10^{-4}$ kg·m^2. Axis of rotation is located at the symmetry axis of the model. For the angle of attack measurement the angular position digital sensor with discretization frequency of 1 kHz was used.

Studies have shown that for given flow parameters, self-oscillations of the model occur. Depending on the initial perturbation, scenarios of a decrease or increase in the amplitude manifest reaching the limiting oscillation amplitude of about 40°. At initial angle deviation close to 0° amplitude has no significant increase. Self-induced oscillations with hard excitation are observed.

Study shows that both models have dynamic behavior Fig. 1 and Fig. 2. The limit amplitude of self-oscillation does not significantly depend on the moment of inertia of the model. Moreover, for the first time a special instability of the amplitude of oscillation was recorded at

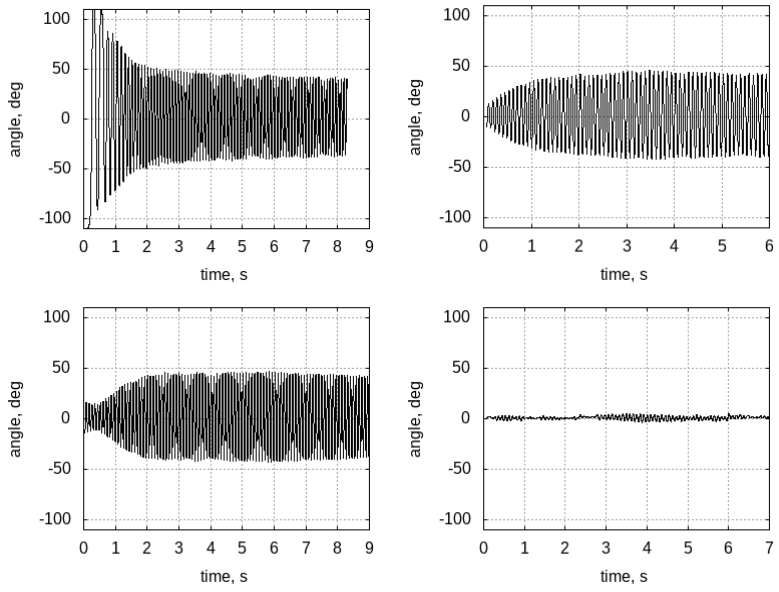

Fig. 1. Angle of attack history with moment of inertia $I_1 = 1.2\ 10^{-3}$ kg·m^2 at M = 1.75, Re = $2.1 \cdot 10^6$ at different initial angles.

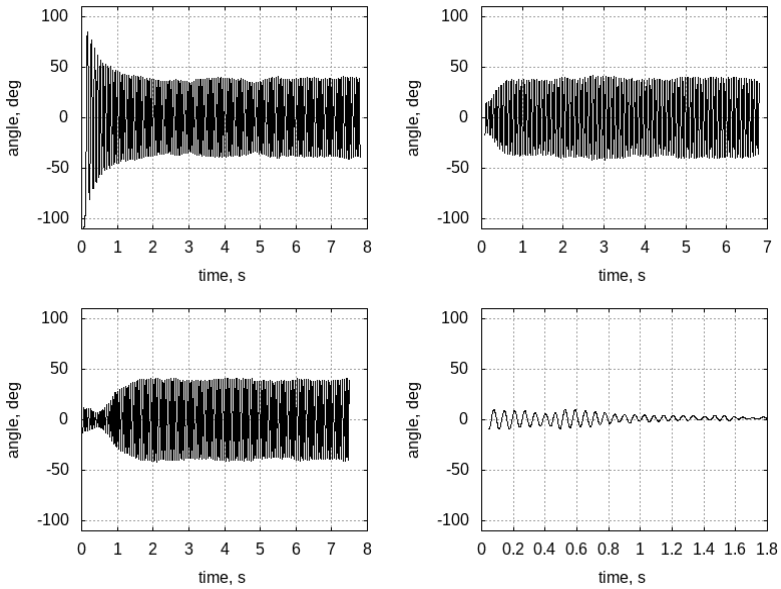

Fig. 2. Angle of attack history with moment of inertia $I_2 = 5.6\ 10^{-4}$ kg·m^2 at M = 1.75, Re = $2.1 \cdot 10^6$ at different initial angles.

initial angle of about 10°. That instability evolution accompanied by amplitude decrease followed by its increase up to the limit amplitude.

The research was carried out within the state assignment of Ministry of Science and Higher Education of the Russian Federation (project No. 121030500161-0). The study was conducted at the Equipment Sharing Center “Mechanics” of ITAM SB RAS.

REFERENCE

1. Adamov N.P., Kharitonov A.M., Chasovnikov E.A., Dyad’kin A.A., Krylov A.N., Aleksandrov E.N. Experimental study of aerodynamic characteristics of a reentry vehicle on a setup with free oscillations at supersonic velocities // Thermophys. Aeromech. 2016. Vol. 23, No. 6. P. 791–800.

DOI: 10.53954/9785604788967_7

EXPERIMENTAL STUDY OF THE RELATIONSHIP OF PULSATIONS OF THE FREE FLOW AND THE DISTURBANCES OF THE BOUNDARY LAYER OF A SHARP PLATE AT MACH NUMBER M = 2.5

L.V. Afanasev, A.D. Kosinov,
A.A. Yatskikh, N.V. Semionov, V.L. Kocharin

Khristianovich Institute of Theoretical and Applied Mechanics SB RAS
630090, Novosibirsk, Russia

The laminar-turbulence transit in supersonic boundary layers is a one of the most important problems in modern aerodynamics. Despite the fact that this problem investigation more than half of century, the modern methods cannot predict the location of laminar-turbulent transition with necessary accuracy. A comparison of the results of direct numerical modeling and experimental studies in wind tunnels clearly shows the imperfection of computational models that do not take into account the noise of aerodynamic installations.

At the moment, there are a number of works devoted to the study of the relationship between the pulsations of the incoming flow and the boundary layer of flat plates [1–3], but these works are limited by the Mach number M = 2. This work is devoted to the consideration of the relationship between free flow pulsations and the boundary layer at Mach number M = 2.5 and the Reynolds unit numbers $11 \cdot 10^6$ m^{-1} and $6 \cdot 10^6$ m^{-1}.

The experiment was conducted in wind tunnel T-325 ITAM SB RAS, at Mach number M = 2.5, and the Reynolds unit numbers $11 \cdot 10^6$ m^{-1} and $6 \cdot 10^6$ m^{-1}. The pulsations of incoming flow and boundary layer were registered by constant temperature hot-wire probes. Hot-wire of the CTA-2017 series were used. Measurements were performed at an overheat equal to 0.8. The signals of CTA were recording by ADC L-Card E10-20, digitization frequency equal 750 kHz, the implementation length was 2^{20} points. The scheme of the experiment is present in Fig. 1 and Fig. 2.

Details about the technique of using weak shock waves to introduce perturbations are described in other works [4–6].

The results obtained show that at Reynolds unit number $\mathrm{Re}_1 = 11 \cdot 10^6$ m^{-1} coefficient of correlation negligible small, but at $\mathrm{Re}_1 = 11 \cdot 10^6$ m^{-1} coefficient of correlation takes values about 0.25–0.3. This fact is interesting, because in the work [7] it was noted that the correlation coefficient increases monotonically with the Mach number. Direct comparison with paper [1] shows the deviation from these

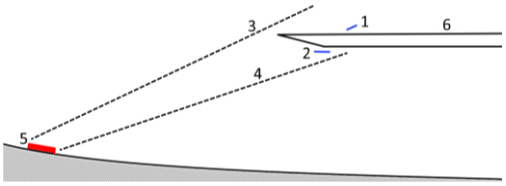

The scheme of the experiment.
1 and *2* are a location of a hot-wire probes, 3 and 4 are the location of shock waves, 5 is a 2D roughness, 6 is model of flat plate with blade leading edge.

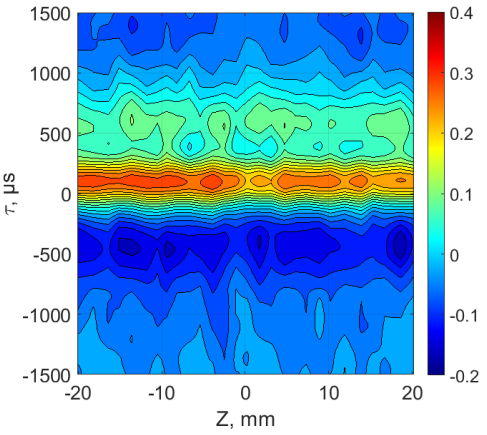

The space-time distribution of the cross-correlation coefficient in section parallel to the leading edge.
The distance from the leading edge is 60 mm.
$\mathrm{Re}_1 = 6 \cdot 10^6$ m^{-1}, M = 2.5.

remarks at the Reynolds unit number $Re_1 = 11 \cdot 10^6$ m^{-1}. This circumstance pushes us to the need to study the dependence of the correlation coefficient of the perturbations of the incoming flow and the perturbations of the boundary layer on the number of Reynolds units.

The research was carried out within the framework of the Program of Fundamental Scientific Research of the state academies of sciences in 2013–2020 (project No. AAAA-A17-117030610125-7). Experiments were carried out using the equipment of the Joint Access Center "Mechanics".

REFERENCES

1. **Afanasev L.V., Kosinov A.D., Yermolaev Yu.G., Semionov N.V.** About the relationship between disturbances in a free supersonic flow and disturbances in a boundary layer at Mach number 2 // Siberian Journal of Physics. 2020. Vol. 15, No. 2. P. 50–60. (in Russ.).
2. **Afanasev L.V., Kosinov A.D., Yatskikh A.A., Kocharin V.L., Semionov N.V., Yermolaev Y.G.** Cross-correlation measurement of disturbance initiated by weak shock wave in the flat plate boundary layer with blunt leading edge at Mach 2 // Proc. Int. Conf. on the Methods of Aerophys. Research **(**ICMAR 2020**) (**Novosibirsk, Russia, 1–7 November 2020): AIP Conference Proceedings. 2021. Vol. 2351, No. 1. Art. 040035. 5 p. DOI: 10.1063/5.0051980
3. **Afanasev L.V., Kosinov A.D., Yatskikh A.A., Kocharin V.L., Semionov N.V., Yermolaev Y.G.** Measurement of the correlation of disturbances from a weak shock wave and pulsations of the boundary layer of a flat plate with a blunted leading edge at Mach 2 // Int. Conf. on the Methods of Aerophys. Research (Novosibirsk, Russia, November 1 –7, 2020): Abstr. Pt. II. Novosibirsk: Parallel, 2020. P. 3–4.
4. **Kocharin V.L., Kosinov A.D., Yatskikh A.A., Afanasev L.V., Ermolaev Yu.G., Semionov N.V.** The experimental study of the weak shock wave action on the boundary layer of the sweep flat plate // J. Phys.: Conf. Ser. 2019. Vol. 1404. Art. 012083. 4 p.
5. **Kocharin V. L., Afanasev L. V., Kosinov A. D., Yatskikh A. A., Semionov N. V., Yermolaev Y. G.** Experimental investigation of effect of an external wave on supersonic boundary layer of the blunt flat plate // High-Energy Processes in Condensed Matter (HEPCM 2019): Proc.of the XXVI Conf. on High-Energy Processes in Condensed Matter (Novosibirsk, Russia 3–5 April 2019): AIP Conference Proceedings. 2019. Vol. 2125, No. 1, Art. 030104. 6 p. DOI:10.1063/1.5117486.
6. **Kocharin V.L., Yatskikh A.A., Prishchepova D.S., Panina A.V., Yermolaev Y.G., Kosinov A.D., Semionov, Afanasev L.V.** Experimental study of the impact of N-wave on heat transfer in a boundary layer of a flat plate at the Mach number 2 // Proc. Int. Conf. on the Methods of Aerophys. Research **(**ICMAR 2020**) (**Novosibirsk, Russia, 1–7 November 2020): AIP Conference Proceedings. 2021. Vol. 2351, No. 1. Art. 040036. 4 p. DOI:10.1063/5.0051930
7. **Kendall J.M.** Wind tunnel experiments relating to supersonic and hypersonic boundary layer transition // AIAA Journal. 1975. Vol. 13. P. 290–299.

DOI: 10.53954/9785604788967_9

SIMULATION OF DETONATION OF INHOMOGENEOUS MIXTURES OF ALUMINUM PARTICLES INTERACTION WITH CLOUDS OF INERT PARTICLES BASED ON PARALLEL TECHNOLOGIES

A.A. Afanasenkov, S.A. Lavruk, T.A. Khmel

Khristianovich Institute of Theoretical and Applied Mechanics SB RAS
630090, Novosibirsk, Russia

The problems of explosion and fire safety in industry attract increased attention, which is associated with possible large destruction during explosions and detonation. The aim of this work is to develop a physical-mathematical model that makes it possible to analyze the conditions for detonation attenuation and quenching in inhomogeneous concentrations of aluminum particles by clouds of inert particles, taking into account their phase transformations. The numerical technology of calculations was also improved using program code parallelization based on the OpenMP library.

The physical-mathematical model [1] was adopted as a basis. Accounting for the processes of melting of inert particles upon reaching the melting temperature was carried out as follows. The total energy of inert particles was written as:

$$E_3 = c_{v3}T_3 + \frac{u_3^2}{2} + kQ_l\,, \tag{1}$$

where

$$k = \begin{cases} 0, T_3 < T_l = 2327K, \\ \dfrac{E_3 - \dfrac{u_3^2}{2} - c_{v3}T_l}{Q_l}, \; T_3 = T_l, \; 0 < k < 1, \\ 1, T_3 > T_l \end{cases}$$

is the proportion of melted alumina, Q_l is specific heat of fusion of the inert phase.

Calculations have shown that taking into account melting (1) has a significant effect on the result when the size of inert particles is less than 5 μm. For larger particles, the influence is less, since the time of heating of particles to the melting temperature is much longer than the characteristic times of detonation flows [2].

The parallelization technology proceeded as follows, the OpenMP library was connected and memory was allocated for each of the arrays used. During the tests, it was found that the same calculation option using parallel programming on eight threads is 2.85 times faster than on one thread, and the average time for the period differs by 3.37 times. It should be noted that when grinding the mesh, the reduction in time will be more significant. The figure shows a comparison of the obtained values of the gas temperature in the one-dimensional problem of the interaction of a detonation wave with a cloud of particles using parallelization based on the OpenMP library and on a single processor. It can be seen that the results are in complete agreement with each other.

A series of parametric calculations was carried out with varying initial concentrations of both combustible and inert particles. Mixtures with a non-uniform distribution of combustible particles in space, in particular, with a transverse concentration gradient in the channel, were also considered. As a result, dependences of the deficit of the mean detonation wave velocity in

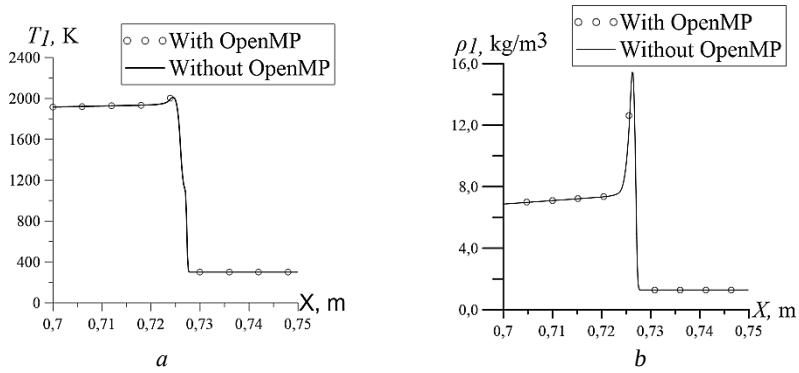

Comparison of results using the OpenMP library and on the same processor.

Parameter profiles at t =0 .5 ms in problem of interaction of detonation in aluminum-oxygen mixture with inert alumina cloud: gas temperature (*a*); gas density (*b*).

a cloud of inert particles on their volume concentration for inhomogeneous mixtures were obtained.

The reported study was funded by RFBR, project number 20-08-00295.

REFERENCES

1. **Fedorov A. V., Kratova Y. V.** Calculation of detonation wave propagation in a gas suspension of aluminum and inert particles // Combust. Explos. Shock Waves. 2013. Vol. 49, № 3. P. 335–347.
2. **Bedarev I.** Micro-level modeling of the detonation wave attenuation by inert particles // Therm. Sci. 2019. Vol. 23. P. 439–445.

DOI: 10.53954/9785604788967_11

CONTROLLED SYNTHESIS OF COMPOSITE CORE – SHELL NANOPARTICLES IN PLASMACHEMICAL REACTOR

S.M. Aulchenko[1,2], E.V. Kartaev[1]

[1]Khristianovich Institute of Theoretical and Applied Mechanics
630090, Novosibirsk, Russia

[2]Novosibirsk State Architectural-Building University
630090, Novosibirsk, Russia

The numerical study of an effect of the different techniques of injecting the precursors on the characteristics of composite nanoparticles has been carried out for two variants of the model of the synthesis of 'titania core – silica shell' particles in the flow-type plasmachemical reactor based on the chloride method. The data regarding the core size of the composite particles, the thickness of their shell as well as the fractions of titania particles with and without silica shell have been obtained for the aforementioned techniques of interest. One of the techniques to control the parameters of the composite particles is the variation of the character of flow motion by means of injection of side jets. The control variables are the position of injection of the side jets, their mass flow rate as well as the composition of gaseous components of the jets. The cases of presence or the absence of silicon tetrachloride vapors in the side jets correspond to either separate or joint oxidation of the precursors.

For computations the two variants of the model of the synthesis of the composite powder have been invoked. For the first variant with full coverage of the core, the total area of titania particles that might be covered with silica shell with minimal thickness equal to the diameter of silica monomer is evaluated. Correspondingly, the fraction of titania particles completely covered by silica shell is calculated [1]. In the second variant of the synthesis a fraction of surface area of each titania particle in the computational volume covered by silica layer is derived [2]. It is implied that there is no coagulation of titania particles completely covered with silica. Whilst in the model there is a possibility of coagulation of titania particles that incompletely covered with silica layer. Both variants of the model of the synthesis of 'titania core – silica shell' particles are grounded on the experimentally confirmed information that the characteristic time of agglomeration of titania nanoparticles is of two order less than that of silica nanoparticles.

The distribution of mean-weghted size of particles and that of logarithm of particle number concentrations along the reactor for the second variant of the model are presented in Fig. 1. It is seen from the figure that at the reactor outlet pure titania nanoparticles are absent. This is a result of the process of coagulation of titania nanoparticles and fur-ther formation of silica layer upon all of them, it may be witnessed by view of curve *1* in the figure. Specifically, for the scheme 3 in the second variant of the model with partial silica coverage of titania particles in the region of deceleration of the mainflow in front of second side jet the process of transformation of titania particles to composite ones prevails over their coagulation (even though a fraction of surface of titania particles covered with silica is small). Thus, the particle core for scheme 3 is less than that for scheme 1 and vice versa shell thickness for scheme 3 is larger compared with that for scheme 1. This scenario is quite opposite to that occurred the case of implementing the variant of the model with full silica coverage of titania particles. The features of curve *5* describing a behaviour of mass average fraction of the surface covered with silica shell (stepped regions, non-monotonous character) might be explained by the limitation imposed on minimal silica shell thickness equal to the diameter of silica monomer. In addition, this behaviour seems to be condi-

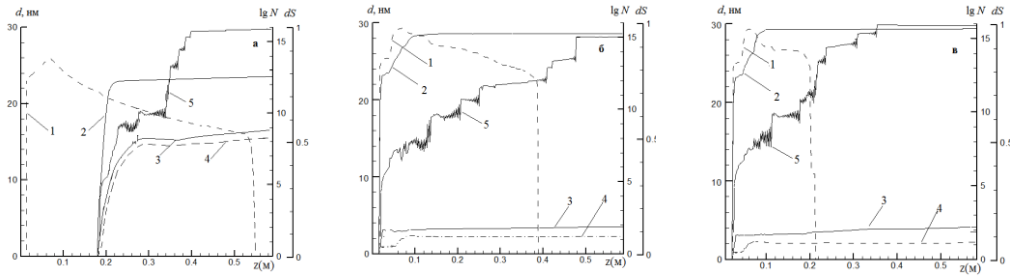

a *b* *c*

Distributions of mean-weighted particle diameter (nm) and the logarithm of the number density of particles (the second variant of the model with incomplete silica coverage of titania particles).

a – separate injection of the precursors (scheme 1), *b* – joint injection of the precursors (scheme 2), *c* – joint injection of the precursors with the injection of the side jet (scheme 3);

1 – logarithm of the number density of titania particles, *2* – logarithm of the number density of composite particles, *3* – the diameter of the composite particles, *4* – the core diameter of composite particles, *5* – the fraction of surface of titania particles covered with silica.

tioned by a decrease of the fraction of covered surface of particles as result of the transformation of pure titania particles into composite ones which have a small fraction of covered surface.

The research was partly carried out within the state assignment of Ministry of Science and Higher Education of the Russian Federation (project No. 121030500145-0). This work was also carried out with partial financial support from the Russian Foundation for Basic Research (Grant No. 18-08-00219 a).

REFERENCES

1. **Aulchenko S.M., Kartaev E.V.** Modeling the one-stage synthesis of composite particles of the nucleus-shell type in separate oxidation of titanium and silicon tetrachlorides in a plasmachemical reactor // Journal of Engineering Physics and Thermophysics. 2020. Vol. 93, No. 1. P.108–113.
2. **Aulchenko S.M., Kartaev E.V.** Modeling of synthesis of composite “core-shell” particles on the basis of joint oxidation of titanium and silicon tetrachlorides in a plasma-chemical reactor // Journal of Applied Mechanics and Technical Physics. 2020. Vol. 61, No. 4. P. 566–572.

DOI: 10.53954/9785604788967_13

RESEARCH OF CONJUGATE HEAT TRANSFER IN A COLLECTOR OF A COMPLEX SHAPE OF AN EXTERNAL FINS

E.S. Baimetova[1], M.R. Koroleva[2]

[1]Kalashnikov Izhevsk State Technical University
426069, Izhevsk, Russia

[2]Udmurt Federal Research Center of the Ural Brunch RAS
426067, Izhevsk, Russia

High demand and a wide range of applications of oil coolers in industry, determines the interest of researchers in this type of energy installations. Currently, oil coolers of various geometries are used for continuous operation of a wide class of technological equipment in various fields. In view of this, studies of methods for intensifying heat exchange processes in channels of various configurations remain relevant and in demand.

The work is devoted to numerical modeling of conjugate heat exchange of the internal channels of the oil cooler with a developed ex ternal surface, taking into account the thermal conductivity of the housing material. The cooling section is made in the form of a flat pipe with longitudinal internal channels of rectangular cross section and a developed external surface with multiple fins [1].

The process of cooling the internal flow of the working fluid – hydraulic oil Lukoil Geyser ST-32 by forced blowing of the oil cooler with a directed air flow is investigated within the framework of the problem of conjugate heat exchange of the internal element of a single cooling section when setting the symmetry conditions on the side faces of the design area. The cooling section [2] housing is made of aluminum. When constructing a mathematical model of the oil cooler refrigerating process, the following assumptions were used: the material of the rectangular channel is isotropic, the roughness of the material is not taken into account. The simulation is carried out on the basis of solving the fluid conservation equations for the domains of air (air) and hydraulic fluid (oil) together with the equation of thermal conductivity in a solid for the oil cooler body (alum). To simulate the motion of gaseous compressible media, the system of equations was supplemented by the equation of state of an ideal gas. The system of partial derivatives constructed in this way on the basis of conservation equations is solved approximately by the finite volume method in a stationary staging based on the opensource toolkit of the OpenFOAM platform. Basic boundary conditions: conditions of 4 genera at the boundaries of alum/oil and air / alum, for the air domain the inlet velocity is 5 m s, the inlet temperature is 293 K, the outlet pressure is zero gradient, for the oil domain the inlet pressure is $(4–10)\cdot10^5$ Pa, the inlet temperature 333K, at the outlet of the oil domain, the pressure is $(1–5)\cdot10^5$ Pa. In addition, the condition of sticking and the condition of symmetry on the lateral borders were used on the impermeable walls.

As a result of the calculations, the distributions of the velocity, pressure, temperature and heat flow fields near the impermeable surfaces of the considered fragment of the outer fins of the oil cooler were obtained, integral thermophysical characteristics of the air flow before and after the passage of the fins elements were obtained. Figure 1 shows the structure of the air flow when flowing around a single cooling element.

From Fig. 1, it can be seen that the structure of the air flow is characterized by the formation of a return zone behind a single element of the cooling section, which is due to the geometry of the section – the presence of a ledge, behind which the formation of a vortex structure is observed. At the same time, in the zone of narrow slit gaps (Fig.1, *b*), when the injected air interacts with the external fins of the element, a layered homogeneous vortex-free flow is observed.

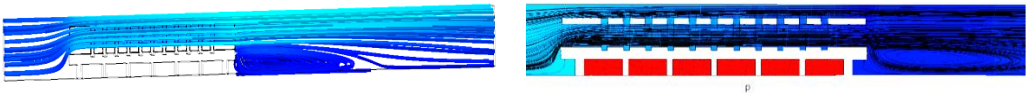

a *b*

Fig. 1. The structure of the air flow in the form of spatial current tubes (*a*) and current lines in the middle section (*b*).

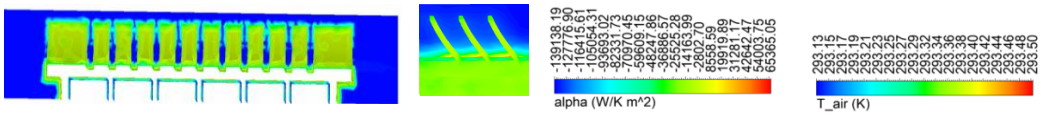

Fig. 2. Distribution of heat transfer coefficient from liquid to housing, from housing to air and discharge air temperature field.

The temperature distribution over the volume of the structure of a single element of the cooling section and the heat transfer coefficient over the oil/alum contact surface of the internal channels of a single element of the cooling section were also investigated. During the calculations, uneven heating of the cooling section housing was observed with the localization of the temperature maximum in the area of the internal central channels, along the length of the channel, the heat transfer from the oil to the housing material decreases, and also, due to the small distance between the channels, the minimum heat transfer coefficient at maximum temperatures of the liquid and the housing is observed in the interchannel region. In the same place, in the central channels, it is fixed of heat flows caused by the mutual influence of internal channels is fixed, leading to the provision of additional heat supply to the hydraulic fluid flowing in the central channels. From the distribution of heat transfer fields from oil to aluminum and from structure to air (Fig. 2), it is clear that the external profiling of the housing allows increasing the efficiency of convective heat exchange – the maximum heat transfer coefficients correspond to the intercostal grooves, however, the dimensions of the external fins require optimization to increase the efficiency of the oil cooler.

In the work was carried numerical modeling of aerohydrogas dynamics and conjugate heat transfer in the hydraulic oil cooling device, the effectiveness of additional fins and profiling of the external developed surface of the oil cooler is shown, as well as the need for constructive optimization of the external fins.

REFERENCES

1. **Baimetova E.S, Koroleva M.R., Chernova A.A.** Application of mathematical modeling methods to solve the problem of optimizing the geometry of the developed outer surface of an industrial oil cooler // International Scientific Conference on the Application of Virtual Reality Technologies and Related Information Systems in Interdisciplinary Tasks FIT-M 2020 (Russia, Moscow, Desember 17–19, 2020): Coll. of conf. abstracts. Moscow, 2020. P. 117–123. DOI:10.38006/907345-75-1.2020.117.123.
2. **Koroleva M.R., Terent'ev A.N., Chernova A.A.** Hydrodynamics of a collector of complex shape // Bulletin of the Rybinsk State Aviation Technological Academy n. a. P.A. Solovyov. 2021. № 3 (58). P. 50–55.

DOI: 10.53954/9785604788967_15

INFLUENCE OF WENO CLASS NUMERICAL SCHEMES ON LARGE EDDY SIMULATIONS OF BASIC TURBULENT FLOWS

S.V. Bakhne, A.I. Troshin

Central Aerohydrodynamic Institute
140180, Zhukovsky, Moscow region, Russia

Nowadays, large eddy simulation (LES) and hybrid RANS/LES methods are considered as promising approaches for solving practical and academic CFD problems. These methods involve the use of low-dissipative numerical schemes which is due to the need for accurately resolving the scales of motion near the grid cut-off. Symmetrical schemes which fit this requirement may become unstable or at least unacceptably oscillating near steep gradients of a solution. Upwind schemes are generally too dissipative. There is a popular approach of adopting a hybrid method which combines these two types of schemes, forming a weighted average from them. Typically, the blending function is rather complex and includes several constants, including flow-dependent ones. An example is the scheme developed by the M.Kh. Strelets group [1].

The main goal of the current work is to assess modern WENO class numerical schemes which can compete with [1] in the framework of LES without introducing flow-dependent constants. According to [2], the most promising schemes of this class are WENO-ZM [3] and WENO-SYMBOO [4]. In the paper, a comparison of these schemes with baseline WENO5, CD6 and hybrid schemes is presented.

First of all, 1D tests were performed. Analysis of linear advection equation showed that all considered WENO class schemes achieve 5th order of accuracy on smooth solutions (left figure) and produce sharp non-oscillatory solutions near discontinuities (right figure), in contrast to CD6 scheme. Similar results were obtained with Burgers' equation. In all these computations, 7th order explicit Runge – Kutta time integration scheme was adopted to minimize the temporal discretization errors.

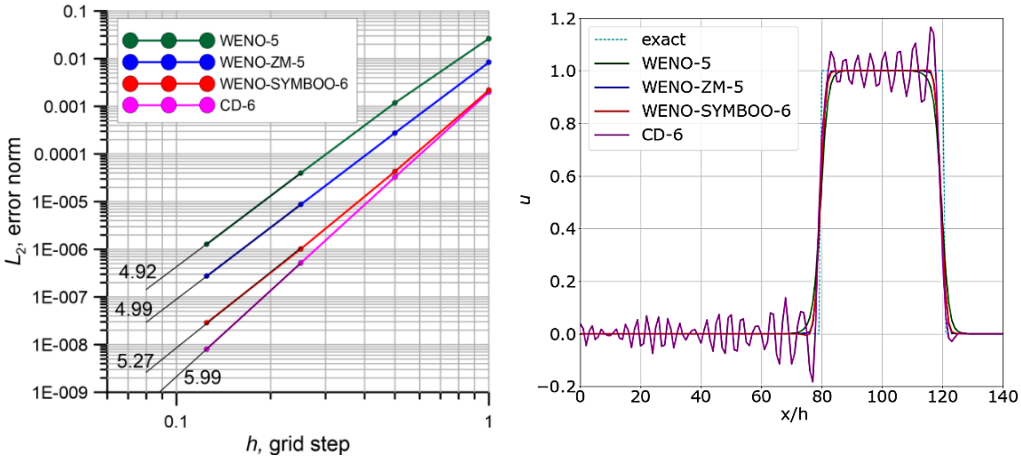

Grid convergence on smooth solution (left) and solution behavior near the discontinuities (right) obtained with linear advection equation.

After that, LES of homogeneous isotropic turbulence decay and of a temporally evolving turbulent shear layer have been performed with the same set of numerical schemes. Computational code *zFlare* (TsAGI) was adopted on multiblock structured grids. Full compressible LES equation system was solved with SST-based DDES closure. 3rd order Heun's RK time integration method was adopted. All simulations were performed in a cubic domain with periodic boundary conditions and grids up to 256^3 cells. Interestingly, in these tests both classical and new WENO class schemes performed worse than hybrid WENO5/CD6 scheme [1], demonstrating higher level of dissipation in high-wavenumber region. Possible reasons for such behavior of the schemes are discussed.

The research was supported by a grant from the Russian Science Foundation No. 21-71-10105, https://rscf.ru/en/project/21-71-10105/

REFERENCES

1. **Guseva E.K., Garbaruk A.V., Strelets M.K.** An automatic hybrid numerical scheme for global RANS-LES approaches // International Conference PhysicA.SPb/2016 (1–3 November 2016, Saint Petersburg, Russian Federation): Proc. IOP Conference Series: Journal of Physics. 2017. Vol. 929. Art. 012099. 6 p URL: https://iopscience.iop.org/article/10.1088/1742-6596/929/1/012099/pdf.
2. **Li H., Luo Y., Zhang S.** Assessment of upwind/symmetric WENO schemes for direct numerical simulation of screech tone in supersonic jet // Journal of Scientific Computing. 2021. Vol. 87, No. 1. P. 1–39.
3. **Zhao S., Lardjane N., Fedioun I.** Comparison of improved finite-difference WENO schemes for the implicit large eddy simulation of turbulent non-reacting and reacting high-speed shear flows // Computers & Fluids. 2014. Vol. 95. P. 74–87.
4. **Nathan J., Datta V.** A bandwidth and order optimized WENO interpolation scheme for compressible turbulent flows: AIAA paper 2011-366, 2011

DOI: 10.53954/9785604788967_17

CALIBRATION OF DIFFERENTIAL SUBGRID STRESS MODEL BASED ON THE RESULTS OF DIRECT NUMERICAL SIMULATION

R.A. Balabanov, A.I. Troshin

Central Aerohydrodynamic Institute
140180, Zhukovsky, Moscow region, Russia

Nowadays most of large eddy simulations (LES) are conducted with algebraic or differential subgrid viscosity models. However, the geometrical configuration complexity of resolved velocity gradients observed in each point allows to suggest that adoption of more advanced differential subgrid stress models (LES-DRSM) could improve the results of LES. General structure of such models is as follows [1]:

$$\frac{\partial\left(\overline{u_i'u_j'}\right)}{\partial t}+\frac{\partial}{\partial x_k}\left[\underbrace{\overline{u_k}\cdot\overline{u_i'u_j'}}_{convection}+\underbrace{\overline{u_i'u_j'u_k'}}_{turbulent\ transport,\ C_{ijk}}-\underbrace{\nu\frac{\partial\overline{u_i'u_j'}}{\partial x_k}}_{diffusion}+\underbrace{\frac{1}{\rho}\left(\overline{p'u_i'}\delta_{jk}+\overline{p'u_j'}\delta_{ik}\right)}_{pressure\ transport}\right]=$$

$$=\underbrace{-\overline{u_i'u_k'}\frac{\partial\overline{u_j}}{\partial x_k}-\overline{u_j'u_k'}\frac{\partial\overline{u_i}}{\partial x_k}}_{production}-\underbrace{\frac{1}{\rho}\left(\frac{\partial}{\partial x_j}\overline{u_i'p'}+\frac{\partial}{\partial x_i}\overline{u_j'p'}\right)}_{pressure-strain\ term,\ \Phi_{ij}}-\underbrace{2\nu\left(\overline{\frac{\partial u_i'}{\partial x_k}\frac{\partial u_j'}{\partial x_k}}\right)}_{dissipation,\ \varepsilon_{ij}}.$$

Here the correlations are written in the Germano decomposition form [2].

In this study, the models for unclosed terms in this equation were chosen and a priori calibration of their coefficients was conducted. For this purpose, statistical analysis of direct numerical simulation database [3] for isotropic turbulence was employed.

For the dissipation rate tensor, the following locally isotropic model was taken:

$$\varepsilon_{ij}=\frac{2}{3}\varepsilon\delta_{ij},\quad\text{where}\quad\varepsilon=\nu\left(\overline{\frac{\partial u_i'}{\partial x_k}\frac{\partial u_i'}{\partial x_k}}\right)=\frac{\tilde{k}}{k}\frac{k^{3/2}}{\Delta}\left(\frac{C_E}{1+C_{E1}II+C_{E2}II^2}\right),\quad II=a_{ij}a_{ij},\quad\tilde{k}=\frac{1}{7}\sum_{i=1}^{7}k_i.$$

It includes dependency on the second anisotropy tensor invariant of and on the local distribution of resolved subgrid energy. When the filter size Δ falls within the inertial range, the coefficients take the following values: $C_E=0.7$, $C_{E1}=C_{E2}=1.0$.

Two models were considered for the pressure-strain term. The first one (linear) was based on Rotta formula and written in terms of subgrid variables:

$$\Phi_{ij}=\frac{1}{\rho}\overline{p'\left(\frac{\partial u_i'}{\partial x_j}+\frac{\partial u_j'}{\partial x_i}\right)}=-C_m\frac{k^{1/2}}{\Delta}\left(\overline{u_i'u_j'}-\frac{2}{3}\delta_{ij}k\right)+\frac{2}{5}k\left(\frac{\partial\overline{u}_i}{\partial x_j}+\frac{\partial\overline{u}_j}{\partial x_i}\right).$$

The calibration of its single coefficient C_m yielded a value of 1.0. This model turned out to have flaws associated with unphysical behavior of the PDF of this coefficient. Due to this fact, a second, quadratic in “slow” part model of the pressure-strain term was considered which has the following form:

$$\Phi_{ij} = \frac{k^{3/2}}{\Delta}\left(-C_1 a_{ij} - C_2\left(a_{ik}a_{kj} - \frac{a_{kl}a_{kl}\delta_{ij}}{3}\right)\right) + C_3 k S_{ij} + C_4 k\left(a_{ik}S_{kj} + a_{jk}S_{ki} - \frac{2}{3}a_{kl}S_{kl}\delta_{ij}\right) + C_5 k\left(\Omega_{ik}a_{kj} + \Omega_{jk}a_{ki}\right).$$

Five coefficients of this model were calibrated by solving an overdetermined linear algebraic equation system with least squares method which resulted in the values $C_1 = 0.8$, $C_2 = -1.0$, $C_3 = 0.8$, $C_4 = 0.3$, $C_5 = 0.3$. The calibration was carried out using twenty different snapshots in a cubic 256^3 point domain, five snapshots in 512^3 point domain, and three snapshots in 1024^3 point domain. Statistical convergence was shown as well as the filter width independency if the filter width falls within the inertial range. Comparison of the pressure-strain models showed that the second model has a correlation coefficient 20-50% higher than the first one depending on the region size. This result is illustrated in the figure.

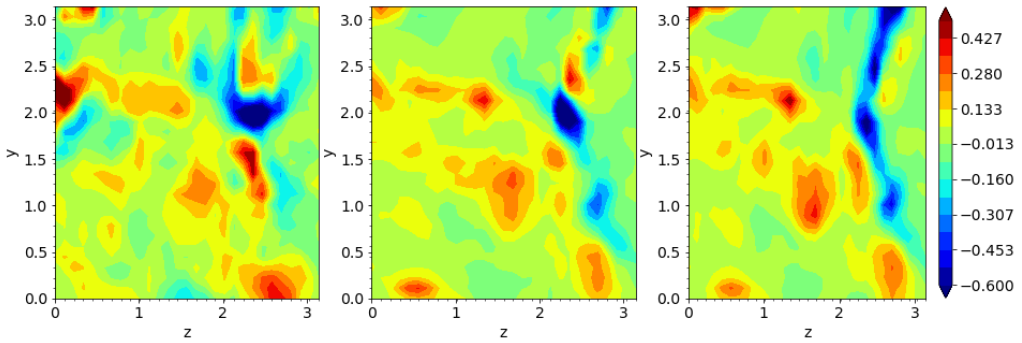

Instantaneous contours of pressure-strain component Φ_{23}: filtered direct numerical simulation data [3] (left), second model (middle), first model (right).

Moreover, the calibration of triple correlation model was carried out which had a form originally proposed by Mellor and Herring within the framework of RANS [4]:

$$C_{ijk} = -C_{3m}\Delta k^{1/2}\left(\frac{\partial}{\partial x_i}\overline{u_j' u_k'} + \frac{\partial}{\partial x_j}\overline{u_i' u_k'} + \frac{\partial}{\partial x_k}\overline{u_i' u_j'}\right).$$

It was shown that PDFs of C_{3m} coefficient calculated for ten independent components of C_{ijk} tensor had positive maxima close to each other with mean value $\langle C_{3m} \rangle = 0.08$.

Based on the results obtained, a subgrid scale model of LES-DRSM class was formulated. The first results of isotropic turbulence decay simulations are presented conducted using *zFlare* code (TsAGI).

The research was supported by a grant from the Russian Science Foundation No. 21-71-10105, https://rscf.ru/en/project/21-71-10105/.

REFERENCES

1. **Deardorff J.W.** The use of subgrid transport equations in a three-dimensional model of atmospheric turbulence // ASME Journal of Fluids Engineering. 1973. Vol. 95, No. 3, P. 429–438.
2. **Germano M.** Turbulence: The filtering approach // Journal of Fluid Mechanics. 1992. Vol. 238, P. 325–336.
3. **Perlman E., Burns R., Li Y., Meneveau C.** Data exploration of turbulence simulations using a database cluster // Proc. of the ACM/IEEE Conference on High Performance Networking and Computing, SC 2007 (USA, Reno, Nevada, November 10–16, 2007). ACM Press, 2007. Art. 23. 11 p. DOI:10.1145/1362622.1362654
4. **Mellor G.L., Herring H.J.** A survey of mean turbulent field closure models // AIAA Journal. 1973. Vol. 11. P. 590–599.

DOI: 10.53954/9785604788967_19

TEMPERATURE MEASUREMENTS OF THE CONDENSING NANOPARTICLES IN A GAS VAPOR TORCH BY OPTICAL METHODS

M.G. Baronskiy[1], G.A. Pozdnyakov[2], Vl.N. Snytnikov[1], V.N. Snytnikov[1]

[1]Boreskov Institute of Catalysis SB RAS
630090, Novosibirsk, Russia

[2]Khristianovich Institute of Theoretical and Applied Mechanics SB RAS
630090, Novosibirsk, Russia

The laser methods for the synthesis of nanoparticles, in particular, with the use of a cw CO_2 laser for the vaporization of a substance, makes it possible to obtain ultrafine powders. During the laser vaporization, a radiating vapor torch is produced. When the molecular vapor of the evaporated substance condenses in a vapor torch, clusters and nanoparticles themselves are formed, which are characterized by a narrow size distribution of particles [1]. The temperature of nanoparticles in a vapor torch varies from the target vaporization temperature to the ambient gas temperature. Thus, formed nanoparticles have temperatures at which various catalytic reactions can be initiated on their surface. The present work is devoted to the study of the laser vaporization process of an Al_2O_3 powder by focused radiation from a cw CO_2 laser followed by condensation of nanoparticles in a cocurrent inert gas flow. The aim of the work was to obtain data for constructing a computational model for changing the temperature of the resulting vapor torch with nanoparticles in the laser radiation field.

Two methods of temperature measurement were used: spectral and color pyrometry [2, 3] in the near infrared region. The first method was implemented according to the scheme shown in Fig. 1; the scheme of the color pyrometry method is shown in Fig. 2.

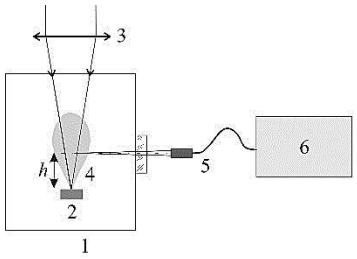

Fig. 1. Scheme of the spectral method.

1 – vaporization chamber, *2* – vaporized Al_2O_3 sample, *3* – laser irradiation, *4* – condensing vapor torch, *5* – light guide, *6* – spectrophotometer S-100.

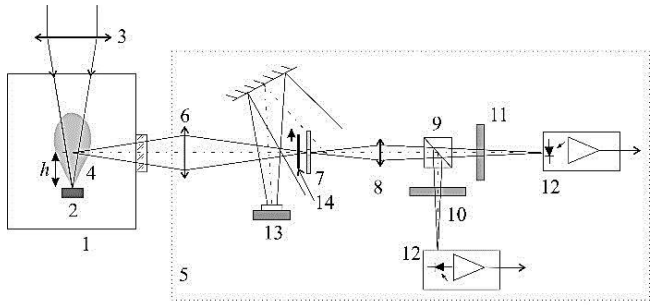

Fig. 2. Scheme of the color pyrometry method.

1 – vaporization chamber, *2* – vaporized Al_2O_3 sample, *3* – laser irradiation, *4* – condensing vapor torch, *5* – optic platform, *6*, *8* – lenses, *7* – input diaphragm, *9* – beam splitter cube, *10*, *11* – narrow band filters, *12* – photodiodes with amplifiers, *13* – video camera, *14* – gate.

Laser vaporization process was carried out inside chamber *1*, which was filled with an inert gas (Ar, He, N_2) up to a pressure of 0.025 MPa. Laser irradiation from a cw CO_2 laser with generation power up to 100 W focused by lens *3* was incident on the surface of alumina sample *2*. In both cases, temperature measurements were carried out along the axis of the condensing vapor torch *4* at various distances *h* from the sample surface. The selection of formed nanoparticles was carried out from the upper part of the condensing vapor torch; the selection system is not shown in the Fig. 1.

The radiation spectrum was recorded with an S-100 spectrometer through a light guide with a collimator *5*. The diameter of the region of the condensing vapor torch from which the radiation was collected was 2.5 mm. The spectrum registration time is up to 4 s. One of the features of the applied method for obtaining nanoparticles was the non-stationarity of the vapor torch, that is, during the recording of the spectrum, the torch could change its position and the brightness of the glow.

The temperature of the nanoparticles was calculated after calibrating the spectrometer S-100 with a light-measuring lamp and taking into account the spectral emissivity of tungsten. As a result, at a distance $h = 4$ mm from the surface of the vaporized Al_2O_3 sample, the measured temperature value was $T = 2920 \pm 50$ K. As h value increased, the temperature of the vapor torch decreased, so at $h = 6$ mm the temperature value was 2670 ± 50 K, and at $h = 8$ mm – $T = 2550 \pm 50$ K.

The scheme of the color pyrometer worked as follows. Objective *6* built the image of the condensing vapor torch on the input diaphragm *7*, through the hole in which the light fell on the lens *8*, which built the image of the hole through the beam splitter cube *9* and filters *10* (800 nm, $\Delta\lambda = 15$ nm) and *11* (925 nm, $\Delta\lambda = 20$ nm) at the input windows of the photodiodes. The amplified signal from the photodiodes was fed to the inputs of an oscilloscope set in the single trigger mode. Video camera *13* recorded the vapor torch configuration during the experiment. The launch was carried out at the moment of opening the shutter *14*. The change in the value of h was carried out by moving the platform *5*.

The temperature was calculated from the ratio of the radiation intensities in the indicated wavelength ranges using the Planck formula. In this case, the filters bandwidth and the dependence of the spectral sensitivity coefficient of the applied SFH-203 photodiodes on the wavelength were taken into account. The temperature values were measured with a time resolution of 20 μs and a recording time of 400 ms. The measurement error was 50 K.

Thus, summarizing the obtained results, the fundamental possibility of using the approaches of spectral and color pyrometry to study the temperature distribution along the h axis of the condensing vapor torch with a flow of nanoparticles, which arises in the process of laser vaporization of Al_2O_3 by a cw CO_2 laser irradiation, was demonstrated. From the data obtained by the color pyrometry method, it was shown that the change in the temperature of the vapor torch for various h is 1200 K. Cases of both the constancy of the temperature of nanoparticles localized in the vapor torch in the range from 1500 K to 2700 K (from measurement to measurement for various h) and dynamic processes when the temperature changed within 2050÷2700 K (maximum) during the measurement were registered. According to the results obtained by the spectral pyrometry method, it was found that the registered temperature maximum was observed at h=4 mm and amounted to 2920 ± 50 K. It was also shown that in the range $h = 4$–8 mm, the temperature of the condensing vapor torch decreases by about 400 K.

The work was financially supported by the Russian Science Foundation within Project No. 21-19-00429.

REFERENCES

1. **Kostyukov A., Snytnikov V., Yelisseyev A., Zhuzhgov A., Kostyukova N., Ishchenko A., Cherepanova S., Snytnikov V.** Synthesis, structure and optical properties of the laser synthesized Al_2O_3 nanopowders depending on the crystallite size and vaporization atmosphere // Advanced Powder Technology. 2021. Vol. 32, Iss. 8. P. 2733–2742.
2. **Chrzanowski K., Bielecki Z., Szulim M.** Comparison of temperature resolution of single-band, dual-band and multiband infrared systems // Applied Optics. 1999. Vol. 38, Iss. 13. P. 2820–2823.
3. **Gulyaev I.P., Ermakov K.A., Gulyaev P.Yu.** New high-speed combination of spectroscopic and brightness pyrometry for studying particles temperature distribution in plasma jets // European Researcher. 2014. Vol. 71, № 3-2. P. 564–570.

DOI: 10.53954/9785604788967_21

NUMERICAL STUDY OF OBLIQUE DETONATION FORMATION BY A FAST-MOVING BODY IN A HYDROGEN-AIR MIXTURE

I.A. Bedarev, V.M. Temerbekov

Khristianovich Institute of Theoretical and Applied Mechanics SB RAS
630090, Novosibirsk, Russia

Recently, various gaseous fuels have become widespread, which leads to great interest in studies of the combustion and detonation characteristics of such explosive substances. Hydrogen has a high calorific value and low flammability limits, as well as low harmfulness of oxidation products. This fuel is one of the most promising fuels in the world. This paper presents the results of numerical simulation of the oblique detonation waves various modes initiation by a fast-moving body in a stoichiometric hydrogen-air mixture depending on the initial pressure, velocity, and diameter of the body.

The mathematical model includes the Favre-averaged Navier – Stokes equations for a multicomponent gas mixture, taking into account chemical reactions. To simulate the chemical kinetics, the reduced kinetic scheme was used in this work, which includes one gross reaction of hydrogen combustion in the air. This kinetic scheme was previously verified using experimental data about ignition delay time and detonation velocity [1]. The ANSYS Fluent software package was used as a solver. For approximation in time, the second order implicit scheme is used, and for approximation in space, a splitting scheme for the AUSM flux vector with the second order upstream approximation is used. For the calculations, a structured tetragonal computational grid with the use of dynamic adaptation along the density gradient was used.

Additional verification and adaptation of the used kinetic scheme of chemical reactions in terms of the size of the detonation cell of the mixture at different initial pressures was carried out. As a result of calculating the problem of the motion of a fast-flying body in a hydrogen-air mixture, various combustion and detonation modes were obtained for a fixed diameter of a fast-flying body. The initial parameters of the mixture were varied for comparison with the results of previous calculations [2]. Also in this work the detonation initiation energy in a hydrogen-air mixture for the presented parameters was estimated according to the method described in [3].

The work was supported by Russian Science Foundation, project No. 22-29-00861, https://rscf.ru/project/22-29-00861/

REFERENCES

1. **Tropin D.A., Bedarev I.A.** Problems of detonation wave suppression in hydrogen-air mixtures by clouds of inert particles in one- and two-dimensional formulation // Combustion Science and Technology. 2021. Vol. 193, No. 2. P. 197−210.
2. **Bedarev I.A., Temerbekov V.M.** Estimation of the energy of detonation initiation in a hydrogen-oxygen mixture by a high velocity projectile // Thermal Science. 2021. Vol. 25, No. 5. P. 3889−3897.
3. **Vasil'ev A. A.** Detonation Combustion of Gas Mixtures Using a Hypervelocity Projectile // Combustion, Explosion, and Shock Waves. 1997. Vol. 33, No. 5. P. 583−597.

DOI: 10.53954/9785604788967_22

MOLECULAR DYNAMICS SIMULATION OF THE RHEOLOGY OF NANOFLUIDS WITH SPHERICAL PARTICLES

A.A. Belkin[1,2], T.A. Rafalskaya[1,2], V.Ya. Rudyak[1,2]

[1]State University of Architecture and Civil Engineering
630008, Novosibirsk, Russia

[2]Kutateladze Institute of Thermophysics SB RAS
630090, Novosibirsk, Russia

Nanofluids are systems with a complex internal structure and unique properties. In particular, many of them have non-Newtonian rheology [1]. The systematization of nanofluids according to their rheological properties and the study of the effect of shear rate on the mechanisms of momentum transfer in them are quite actual tasks today. They can be solved using the method of molecular dynamics, which has been repeatedly used to study the rheological properties of homogeneous liquids, in particular, polymers [2]. However, studies of the rheology of nanofluids by this method have practically not been carried out, only a few works are known [3]. This paper presents data on the rheological properties of nanofluids based on liquid argon and benzene with spherical nanoparticles.

The calculations were performed by means of LAMMPS [4] at a temperature T = 298 K and atmospheric pressure. The interaction of nanoparticles with the carrier liquid was described by a specially developed potential [5], and the interaction of molecules with each other was described by the Lennard-Jones low.

First, the rheological properties of the base fluids were investigated. If argon has a Newtonian rheology on the saturation line, then benzene is a non-Newtonian liquid at high shear rates. Up to a certain shear rate, the viscosity coefficient does not change; with a further increase in shear rate, it begins to decrease. Thus, this fluid is viscoplastic liquid from the point of view of rheological properties.

The addition of nanoparticles to both base liquids leads to a change in their rheology. Benzene-based nanofluids remain viscoplastic, but the critical shear rates at which the viscosity coefficient ceases to be constant decrease (see the figure and the table). The rheological properties of argon change qualitatively, nanofluids based on it become viscoplastic fluids. Approximations have been constructed that describe the dependence of the viscosity coefficient on the shear rate.

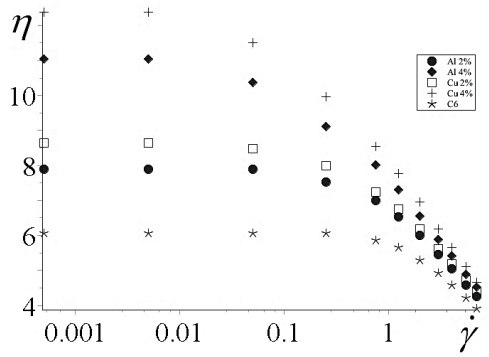

Dependences of the viscosity coefficients (mpoise) of nanofluids based on benzene with aluminum and copper particles of diameter 3 nm on the shear rate (10^{10} s^{-1}).

Values of viscosity coefficients η (mpoise) of nanofluids based on benzene with aluminum and copper particles of diameter 3 nm at different shear rates $\dot{\gamma}$ and volume fractions ϕ

ϕ, %	$\dot{\gamma} \cdot 10^{10}$ (s^{-1})							
	0.0005	0.005	0.25	1.25	2	4	5.5	7
2 (Cu)	7.90	7.90	7.53	6.54	6.01	5.05	4.58	4.25
2 (Al)	8.65	8.65	7.99	6.75	6.19	5.18	4.72	4.37
4 (Cu)	11.03	11.03	9.10	7.30	6.56	5.41	4.89	4.51
4 (Al)	12.39	12.39	9.96	7.76	6.95	5.65	5.10	4.66

The reasons for the change in rheology were studied. The radial distribution functions and density profiles calculated at different shear rates showed that high shear stresses destroy the structure (short-range order) in the studied fluids. This, of course, should lead to a decrease in viscosity.

It has been established that for adequate simulation of rheology, this simulation must be carried out in a nanochannel with a sufficiently large distance between the walls. This is due to the strong influence of the walls on the viscosity of the fluid located between them. Thus, the viscosity of water in a copper channel with a height of 15 nm is approximately 10% higher than the corresponding bulk value even at low shear rates. In this system, it is necessary to increase the distance between the channel walls to 25–30 nanometers. The results for very narrow channels are of independent importance, but they make it possible to study not the bulk rheological properties of various fluids, but their rheology in confined conditions.

The viscosity of nanofluids does not tend to the bulk value determined by the equilibrium MD method [6] as the shear rate tends to zero. However, this occurs when the diameter of the nanoparticles is 25–30% or more of the distance between the channel walls. Increasing the particle size affects the viscosity in two ways. On the one hand, the number of nanoparticles, which are centers of additional structuring, decreases, which should lead to a decrease in the viscosity coefficient. On the other hand, the viscosity increases in the regions between the coarse particle boundary and the wall surface.

If the channel walls begin to move rapidly, the shear flow significantly weakens the effects of structuring, and the rheological behavior of the nanofluid practically ceases to depend on the particle size; for shear rates above 10^{10} s^{-1}, the rheological dependences of the nanofluids practically do not differ from those for the corresponding base liquids.

This work was supported by the Russian Science Foundation under Grant 20-19-00043.

REFERENCES

1. **Minakov A.V., Rudyak V.Y., Pryazhnikov M.I.** Systematic experimental study of the viscosity of nanofluids // Heat Transfer Engineering. 2021. Vol. 42, No. 12. P. 1024–1040.
2. **Peng Y., et al.** Rheological and structural properties of associated polymer networks studied via non-equilibrium molecular dynamics simulation // Mol. Syst. Des. Eng. 2021. Vol. 6. P. 461–475.
3. **Devarajan D.S., Nourian P., McKenna G.B., Khare R.** Molecular simulation of nanocolloid rheology: Viscosity, viscoelasticity, and timeconcentration superposition // Journal of Rheology. 2020. Vol. 64. P. 529.
4. **Thompson A.P., et al.** LAMMPS – A flexible simulation tool for particle-based materials modelling at the atomic, meso, and continuum scales // Comp. Phys. Comm. 2022. Vol. 271. P. 108171.
5. **Rudyak V.Y., Krasnolutskii S.L.** The interaction potential of carrier gas molecules with dispersed particles. // Proc. of 21st Int. Symp. on Rarefied Gas Dynamics 21. Toulouse: Gépadués-Éditions. 1999. Vol. I. P. 263–270.
6. **Rudyak V.Y., Belkin A.A, Krasnolutskii S.L.** Molecular dynamics modeling transport processes of fluids and nanofluids in bulk and nanochannels // Advances in Molecular Dynamics Simulations Research / Ed. S. Köhler**.** Hauppauge, N.Y.: Nova Sci. Publ. Inc., 2021. Chap. 1. P. 1–86.

DOI: 10.53954/9785604788967_24

LOCATION OF THE LAMINAR-TURBULENT TRANSITION IN THREE-DIMENSIONAL BOUNDARY LAYERS

A.V. Boiko, V.I. Borodulin, K.V. Demyanko, A.V. Ivanov, C.V. Kirilovskiy, D.A. Mischenko, Yu.M. Nechepurenko, T.V. Poplavskaya

Khristianovich Institute of Theoretical and Applied Mechanics SB RAS
630090 Novosibirsk, Russia

It is known that the nature of the flow around aircraft (AC) affects its aerodynamic drag. The turbulent boundary layer dramatically increases the drag compared to the laminar one, which leads to high fuel consumption. Therefore, the position and extent of the laminar-turbulent transition (LTT) can be important in designing aircrafts.

In recent years, the co-authors of this report developed the LOTRAN software package for aerodynamic stability analysis and computation of LTT in boundary layers. To analyze the boundary layer stability, the package uses the full heat and mass transfer equations of the compressible medium linearized with respect to the laminar flow [1]. LOTRAN is based on the physically justified N-factors of the e^N-method, which is implemented for predicting the LTT in compressible (including incompressible) three-dimensional flows using original specialized matrix algorithms [2]. Meantime, various versions of this package are widely used for fundamental scientific and engineering computations (see, for example, [3–6]). In this paper, we summarize the practice of LOTRAN application in conjunction with ANSYS Fluent CFD software [7] for the computation of the transition positions in a number of aerodynamic flows of practical interest.

The results of a detailed systematic comparison of the computed and experimental data on the flows at a number of aerodynamic configurations are also presented. To this end, a series of unique experiments on the transition position determination in a three-dimensional boundary layer were carried out. One of the main goals of the conducted research is to create an experimental basis for the verification of LTT prediction methods within the framework of the developed LOTRAN software. To create such a database, along with detailed documentation of the flow parameters (velocity, degree of the freestream turbulence, etc.) and model parameters (geometry, degree of roughness, angle of attack), it is necessary to accurately and statistically reliably document the position of the LTT on the surface of the experimental model. Thus, the experiments were carried out in the low-turbulence wind tunnel T-324 of ITAM SB RAS. A swept-wing model with the sweep angle of 45° and a wing chord C = 700 mm was used. The experimental data were obtained by thermoanemometry, by pressure taps to measure static pressure on the surface, and by thermography.

In order to detect LTT, sequences of surface thermograms were recorded over time. A unique algorithm for determining the transition line was developed, the algorithm being based on the analysis of the wing surface cooling character, the key element of which is the transition from the analysis of a single frame of a thermal imaging camera to the consideration of a recorded sequence of thermograms [8]. It is shown that the proposed method makes it possible to determine the position of the boundaries of the transition region at both low and high degrees of turbulence of the incoming flow with high accuracy. In addition, this method, due to a high resolution of laminar and turbulent zones, makes it possible not only to determine the averaged position of the flow transition from laminar to turbulent state, but also to determine its extent, i.e. to detect the onsets of both the transition and the turbulence, which is also important for increasing the accuracy of engineering assessments.

The authors of this work have developed a method for calibrating the LOTRAN software, using the experimental data obtained for the transition position. To this end the experimental data are superimposed on the computed *N*-factor distributions to determine the values of critical *N*-factors [9]. As a result, diagrams of the critical *N*-factors of the onset of LTT as functions of the flow velocity, the relative roughness height, and the degree of turbulence of the incoming flow were obtained for Tollmien – Schlichting and crossflow types of instability.

This work was supported financially by the Russian Science Foundation (project No. 18-19-00460).

REFERENCES

1. **Boiko A.V., Demyanko K.V., Kirilovskiy S.V., Nechepurenko Y.M., Poplavskaya T.V.** Modeling of transonic transitional three-dimensional flows for aerodynamic applications // AIAA J. 2021. Vol. 59, No. 9. P. 3598–3610.
2. **Boiko A.V., Demyanko K.V., Nechepurenko Y.M.** On computing the location of laminar-turbulent transition in compressible boundary layers // Russ. J. Numer. Anal. Math. Modelling. 2017. Vol. 32, No. 1. P.1–12.
3. **Boiko A.V., Demyanko K.V., Inozemtsev A.A., Kirilovskiy S.V., Nechepurenko Yu.M., Paduchev A.P., Poplavskaya T.V.** Determination of the laminar-turbulent transition location in numerical simulations of subsonic and transonic flows past a flat plate // Thermophys. Aeromech. 2019. Vol. 26, No. 5. P. 629–637.
4. **Kirilovskiy S.V., Boiko A.V., Demyanko K.V., Nechepurenko Y.M., Poplavskaya T.V., Sidorenko A.A.** On integrating the LOTRAN 3.0 package into the ANSYS fluent CFD software // High-Energy Processes in Condensed Matter (HEPCM 2019): Proc. of the XXVI Conf. on High-Energy Processes in Condensed Matter, dedicated to the 150th anniv. of the birth of S.A. Chaplygin (Novosibirsk, April 3–5, 2019) : AIP Conf. Proc. 2019. Vol. 2125. Art. 030098 (6 p.) DOI: 10.1063/1.5117480
5. **Poplavskaya T.V., Boiko A.V., Demyanko K.V., Kirilovskiy S.V., Nechepurenko Y.M.** Numerical simulation of the transition to turbulence in subsonic and transonic flows // 4th All-Russian Sci. Conf. Thermophys. and Phys. Hydrodyn with the School for Young Scientists (Yalta, Crimea, September 15–22, 2019,): J. Phys.: Conf. Ser. 2019. Vol. 1359. Art. 012068. DOI:10.1088/1742-6596/1359/1/012068
6. **Kirilovskiy S.V., Boiko A.V., Demyanko K.V., Ivanov A.V., Nechepurenko Y.M., Poplavskaya T.V.** Numerical simulation of the laminar-turbulent transition on a swept wing in a subsonic flow // J. Phys.: Conf. Ser., 2019. Vol. 1359. Art. 012070. doi:10.1088/1742-6596/1359/1/012070
7. **Kirilovskiy S.V., Boiko A.V., Demyanko K.V., Nechepurenko Y.M., Poplavskaya T.V., Sidorenko A.A.** On integrating the LOTRAN 3.0 package into the ANSYS fluent CFD software. AIP Conf. Proc. 2019. Vol. 2125. 6 p. DOI:10.1063/1.5117480.
8. **Boiko A.V., Ivanov A.V., Borodulin V.I., Mischenko D.A.** Quantification technique of transition to turbulence in boundary layers using infrared thermography // Int. J. Heat Mass Transf. 2022. Vol. 183, Part A. Art. 122065. 11 p. DOI: 10.1016/j.ijheatmasstransfer.2021.122065.
9. **Boiko A.V., Demyanko K.V., Kirilovskiy S.V., Nechepurenko Yu.M., Poplavskaya T.V.** Determination of threshold N-factors of the laminar-turbulent transition in a subsonic boundary layer on a prolate spheroid // J. Appl. Mech. Tech. Phys. 2021. Vol. 62, No. 6. P. 3–7.

DOI: 10.53954/9785604788967_26

NUMERICAL SIMULATION OF A SWEPT WING FLOW AFFECTED BY BLOWING OR SUCTION AT A SECTION OF THE AIRFOIL

A.V. Boiko, I.R. Valiullin, K.V. Demyanko, S.V. Kirilovskiy, Y.M. Nechepurenko, T.V. Poplavskaya

Khristianovich Institute of Theoretical and Applied Mechanics SB RAS
630090, Novosibirsk, Russia

Boundary-layer control makes it possible to improve the efficiency of aircrafts, for example, by significantly reducing their drag due to delaying the laminar-turbulent transition (LTT) in the boundary layer. Among the control methods used are boundary layer suction blowing, as well as injection of gases with different viscosities or different temperatures. For subsonic flows, the actively studied control methods areblowing and suction of the flow through the flow-exposed surface [1], with numerical modeling allowing to build flow models and determine the main control parameters [2].

Numerical simulation of laminar-turbulent flow past a swept wing in a virtual wind tunnel (Fig. 1,*a*) based on the ANSYS Fluent package and LOTRAN 3 software package [3, 4] and calibration of numerical data on the basis of the extensive database of experimental data on LTT on a swept wing created within the framework of the Project were carried out within the Russian Science Foundation Project No. 18-19-00460. Numerical simulation of laminar-turbulent flow past a swept wing in a virtual wind tunnel (see Fig. 1,*a*) were carried out (within the Russian Science Foundation Project No. 18-19-00460) based on the ANSYS Fluent and LOTRAN 3 [3, 4] software packages. The obtained numerical data were calibrated using the extensive experimental database on LTT on a swept wing created within the Project. According to the experimental data, the threshold N-factors of LTT onset were determined for different flow regimes in the range of angles of attack from -5° to 5° and flow velocities from 10 m/s to 50 m/s.

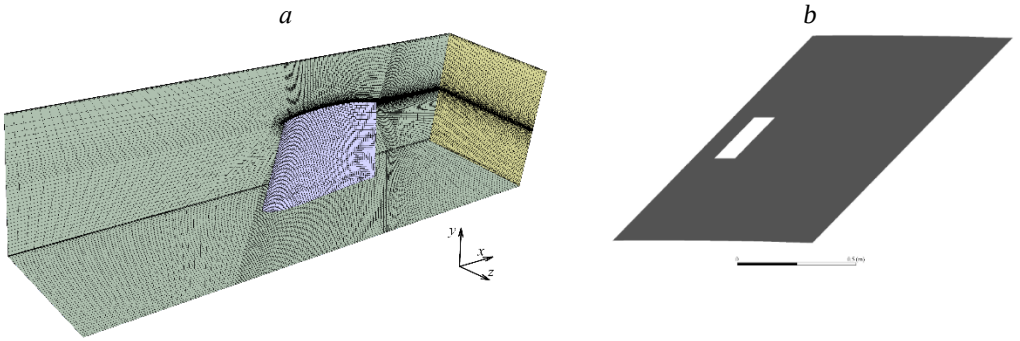

Fig. 1. The computational domain (virtual wind tunnel T-324 of the ITAM SB RAS) with the swept wing placed in it (*a*) and the upper surface of the swept wing with indication of the disturbance input surface (top view) (*b*).

In order to investigate the possibility of LTT control, numerical simulation of laminar-turbulent flow past a swept wing in the virtual wind tunnel under the influence of a local blowing or suction on the section of the wing surface was carried out in the present work. Such disturbance sources were simulated within the CFD package ANSYS Fluent in different ways:

1) by setting a non-zero velocity on the source section (boundary condition wall of the ANSYS Fluent package) using the created UDF module, embedded in the computational code;
2) by setting the source terms (in the continuity and momentum equations) in the first cell over the source section using the created UDF module embedded in the computation code;
3) the source section is allocated into a separate zone, where conditions for the velocity (velocity inlet) or pressure (pressure inlet), or mass-flow-rate were imposed.

These boundary conditions simulate the blowing or suction through a rectangular section of the wing surface (Fig. 1,*b*).

In the work, the influence of the source on the mean flow is investigated. It is shown that using the first and second approaches to the simulation of source lead to an intensive change of the flow velocity in the source section, but the impact does not extend beyond this section. For the third approach, an intense change in flow velocity is observed not only in the source region, but also downstream (Fig. 2).

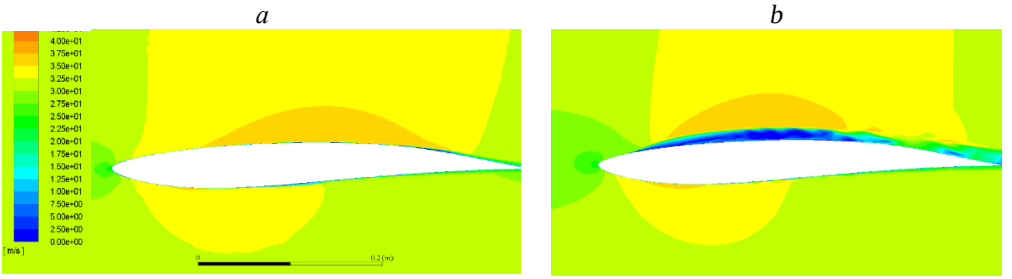

Fig. 2. Velocity in the central cross section of the swept wing without the influence of the source (*a*) and with the influence of the source (*b*).

In this work computations at different velocities of the source impact were performed to investigate the question about the value of velocity, at which a linear regime of disturbance evolution is formed (V = 0.3 m/s, which corresponds to 1% of the freestream velocity). Both the characteristics of the mean flow (CFD package ANSYS Fluent) and the LTT positions (software package LOTRAN 3) were obtained for such flow regimes.

This work was supported by the Russian Science Foundation (Project No. 18-19-00460).

REFERENCE

1. **Kornilov V.I., Boiko A.V.** Flat-plate drag reduction with streamwise noncontinuous microblowing // AIAA J. 2014. Vol. 52, No. 1, P. 93–103.
2. **Chung Y.M., Sung H.J., Boiko A.V.** Spatial simulation of the instability of channel flow with local suction/blowing // Phys. Fluids. 1997. Vol. 9, No. 11, P. 3258–3266.
3. **Boiko A.V., Kirilovskiy S.V., Maslov A.A., Poplavskaya T.V.** Engineering modeling of the laminar–turbulent transition: Achievements and problems (Review) // J. Appl. Mech. Techn. Phys. 2015. Vol. 56, No. 5, P. 761–776.
4. **Boiko A.V., Demyanko K.V., Kirilovskiy S.V., Nechepurenko Y.M., Poplavskaya T.V.** Modeling of transonic transitional 3D flows with a general-purpose CFD code using the eN-method // AIAA J. 2021. Vol. 59, № 9. P. 3598–3610.

DOI: 10.53954/9785604788967_28

SUPERSONIC FLOW AROUND WINGS TANDEM

V.E. Borisov, T.V. Konstantinovskaya, A.E. Lutsky

Keldysh Institute of Applied Mathematics RAS
125047, Moscow, Russia

The paper presents the numerical simulation results of supersonic flow around the wings tandem at $M_\infty = 3$ and $Re_{L=1m} = 10^7$, at which an interaction of the tip vortex from the front wing with the second (main) wing occurs. It is shown that several secondary vortices are formed as a result. Vortex influence on the main wing surface pressure was evaluated.

Configuration. The wings are rectangular in plan with sharp edges, installed one after the other in the direction of the flow, forming two configurations (Fig. 1) in such a way that the main part of the tip vortex descending from the wing-generator flows around the main wing from different sides. The angle of attack of the first wing is 10º, of the main one is 0º to the flow direction. The half-span of the main wing is l = 0.095, of the wing-generator is half of the main one. The computational domain is a parallelepiped with dimensions L_x = 0.33, L_y = 0.25, L_z = 0.15. The main wing has the same geometry as in [1].

A similar problem was previously investigated only for an incompressible fluid [2].

Mathematical and numerical models. The simulations were performed using the ARES code developed in Keldysh Institute of Applied Mathematics. A system of unsteady Reynolds-averaged Navier – Stokes equations (URANS) was used to describe three-dimensional turbulent flows of compressible fluid. The spatial approximation is performed using the finite volume method with a TVD reconstruction scheme of the 2nd order of accuracy. An implicit scheme based on the LU-SGS method was used for time approximation of the equations.

The Liutex criterion was used to identify vortex structures in the flow. It is free from shear and compressive components of the strain rate tensor by its construction [3], unlike methods of previous generations such as λ_2 or Q.

It is found that the vortex in both configurations is divided by the main wing first into two, and then into several vortices, while the secondary vortices decay quickly enough (Fig. 2). So, at a distance of 5 wing chords from the main wing axis, one main vortex remains.

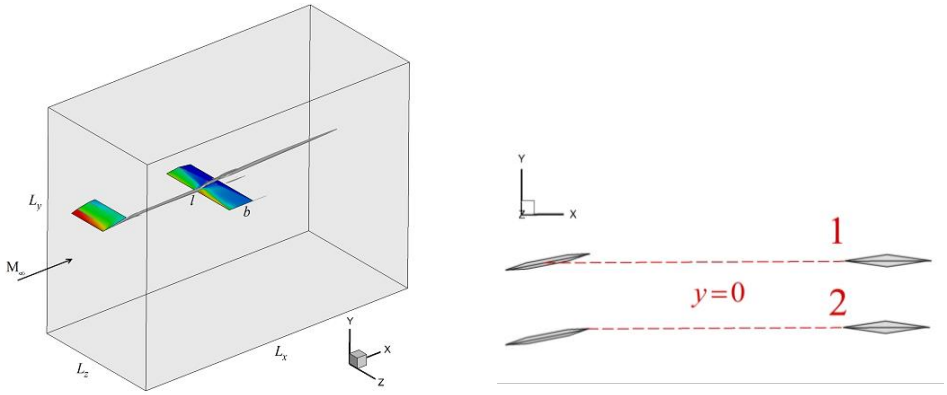

Fig. 1. Model setup.

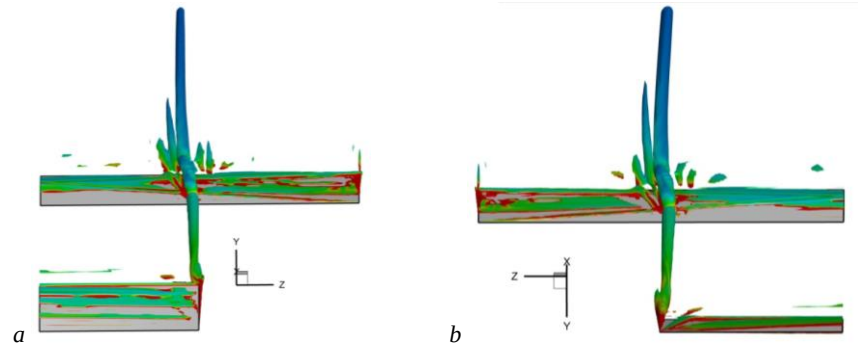

Fig. 2. Vorticity magnitude distribution on the iso-surfaces of Liutex criteria $\tilde{\Omega}_R = 0.45$.
a – configuration 1, *b* – configuration 2.

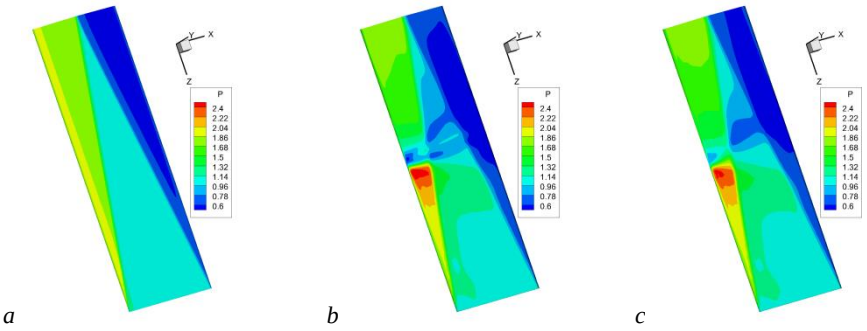

Fig. 3. Pressure distribution on the surface of the main wing for the different configurations.
a – one wing, *b* – configuration 1, *c* – configuration 2.

Pressure values on the main wing surface depending on configuration

Cases	P_{min}	P_{max}	P_{ave}
one wing	0.558665	1.96651	1.129081
Case 1	0.462011	2.6983	1.113758
Case 2	0.471492	2.54865	1.115363

A change in the pressure distribution on the main wing surface was obtained (Fig. 3, tab.). The local maximum pressure increases due to the fall of shock wave from the wing-generator. The minimum pressure value is noticeably reduced.

This work was supported by the Russian Science Foundation, project No. 22-21-00470.

REFERENCES

1. **Borisov V.E., Davydov A.A., Konstantinovskaya T.V., Lutsky A.E., Shevchenko A.M., Shmakov A.S.** Numerical and experimental investigation of a supersonic vortex wake at a wide distance from the wing // Proc. of 19 Int. Conf. on the Methods of Aerophys. Research (ICMAR2018): AIP Conference Proceedings. 2018. Vol. 2027. Art. 030120. 9 p. https://doi.org/10.1063/1.5065214
2. **Chen C., Wang Z., Gursul I.** Experiments on tip vortices interacting with downstream wings // Experiments in Fluids. 2018. Vol. 59(5). Art. 82. 24 p. https://doi.org/10.1007/s00348-018-2539-7
3. **Shrestha P., Nottage C., Yu Y., Alvarez O., Liu C.** Stretching and shearing contamination analysis for Liutex and other vortex identification methods // Adv. Aerodyn. 2021. Vol. 3. Art. 8. 20 p. https://doi.org/10.1186/s42774-020-00060-9

DOI: 10.53954/9785604788967_30

STUDY OF FUSELAGE INFLUENCE IN TASK OF AERODYNAMIC DESIGN OF COMPLEX LIFTING SYSTEMS WITH MINIMAL INDUCED DRAG

V. G. Borisova, V. A. Silantiev

Chaplygin Siberian Aeronautical Research Institute
630051, Novosibirsk, Russia

Despite the high level of excellence of the aerodynamic configurations of modern subsonic aircraft, the task of increasing their lift/drag ratio continues to be relevant. In particular, it is possible to achieve of this increase by reducing of the drag coefficient C_D at a given lift coefficient C_L. Therefore, in this study, we will talk about the decrease in the induced drag, which in the cruise of flight is about 40 % of the aircraft total drag. Approaches, aimed at reducing of the induced drag coefficient C_{D_i}, are often used in the design of new aircraft lifting systems and in the modernization of the existing aircraft fleet due to the installation of wingtip devices. However, at the stage of the numerical experiment, the use of methods based on the averaged Navier - Stokes equations does not provide a sufficient level of calculation accuracy of the minimum C_{D_i}. For such tasks, it is advisable to use methods based on the vortex theory.

The main methods aimed at minimizing induced drag were formulated in the papers of M. Mink, A. Betz, and L. Prandtl [1–3]. They are based on the idea of substitution of vortex system for aircraft lifting system. C_{D_i} is determined by the strength of vortex sheet in the Treftz plane, selected as a calculated plane and located at a considerable distance from the wing trailing edge across the free-stream flow.

Based on this relationship, the description and use of which are presented in [1–3] for a number of classic tasks, an approach was formed and a calculation program was developed for the aerodynamic design of complex lifting systems, taking into account the minimum of induced drag. The peculiarity of this approach consists in the optimization of airload (i.e. the strength of the bound vortex Γ), and not the vortex sheet strength of the lifting system spanwise. Circulation is approximated by a piecewise constant distribution spanwise of wing. Such the statement of the problem allows not only obtaining a comprehensive account of the optimal distribution of circulation intensity in spanwise direction, but also ensuring the convenience of including various limitations: on the lift coefficient, bending moment, etc.

The paper discusses two additional limitations: on the circulation value of the bound vortex in an arbitrary cross-section of the lifting system and on variation of the wing geometry part. The first of these allows you to optimize closed wing systems on spanwise, which makes it possible to investigate new complex aircraft configurations, and the second allows you to optimize the airload on the end elements of the lifting system (for example, on the winglet), where the base wing geometry will remain unchanged. This is necessary, in particular, for the modernization of the already-existing aircraft by installing of the winglets.

At the same time, the limitation on the change of the base wing geometry will have a fundamentally different theoretical approach, which allows it to be isolated as an independent calculation method. It is based on the idea of a separate accounting of the interaction of aerodynamic characteristics between the lifting system components (where, the fixed part is the base wing and the variable part is winglet). To meet the initial conditions of the task, the preliminary calculation of the flow around the initial configuration is performed using the panel method (Morino method), which has been realized in the AEROJET program [4]. Then, the load distribution on

the winglet is optimized by taking into account of the airload preservation on the base wing. Since the change in the winglet geometry due to optimization will lead to a certain change in the base wing airload, the optimization process must be repeated until the necessary convergence is reached.

However, the question arises about the way of fuselage modeling in the optimization calculation. Approximate accounting of the fuselage influence in the form of an infinite cylinder was conducted by I. Lennertz [5]. Quantitative estimate of this effect showed that the fuselage increases the induced drag coefficient by 2 %, 8 % and 17 % with the relative diameter $d/l = 0.1$; 0.2, and 0.3, respectively (where, d — fuselage diameter, l — wing span). The same results are demonstrated in [6].

In this paper, the effect of the longitudinal bending of the fuselage is considered. It is shown that this effect on the increase of the configuration induced drag can be significantly reduced.

The fuselages of modern long-range aircrafts have a segment in the form of a boat-tail body. The free vortex sheet is adjacent to the fuselage sidewalls and smoothly closes behind it, without causing any singularity in the symmetry plane. Estimate show that this leads to the induced drag decrease by 1% and 4% for the relative diameter of the fuselage $d/l = 0.1$; 0.2, respectively.

At the preliminary design stages, this enables the “wing-fuselage” configuration to submit in a form of an isolated gross wing.

REFERENCES

1. **Munk M. M.** The Minimum Inducted Drag of Airfoils: NACA Technical Report № 121, 1921. 16 p. URL: https://ntrs.nasa.gov/api/citations/19930091456/downloads/19930091456.pdf
2. **Betz A.** Behavior of Vortex Systems: NACA. Technical Memorandum № 713. Washington, 1933. 32 p. [Translated from “Zeitschrift für angewandte Mathematik und Mechanik”. 1932. Vol. 12, No. 3. P. 164–174, by the National Advisory Committee for Aeronautics].
3. **Prandtl L.** Applications of Modern Hydrodynamics to Aeronautics: in 2 parts / Translated by the Staff of the National Advisory Committee for Aeronautics, 1923. Rep. № 116. P. 157–215. URL: https://ntrs.nasa.gov/api/citations/19930091180/ downloads/ 19930091180.pdf.
4. **Silantiev V. A., Ryaguzov E. A.** Aerodynamic Analysis of Complex Aircraft Configurations with Engine Simulation Using The Potential Panel Method // Proceedings of the Fourth Sino-Russian Symposium on Aerodynamics. Chinese Aeronautical Establishment, 1995. P. 41–56.
5. **Karafoli E.** Aerodynamics of the aircraft wing: Incompressible fluid*. Moscow: Publ. House Academy of Sci. of the USSR, 1956. 479 p. [*Аэродинамика крыла самолёта: Несжимаемая жидкость*: Transl. from Romanian / Academy of Sciences of the USSR.]
6. **Teperin L. L., Pritulo T. M., Orfinezhad F. E., M'yo Tkheyn.** Resources of reducing the inducted drag of an aircraft wing* // Trudy MFTI. 2017. Vol. 9, No. 4. P. 94–105. [transl. from Russan: *Средства снижения индуктивного сопротивления крыла самолёта*.]

* The title translated by author of the article.

DOI: 10.53954/9785604788967_32

PARAMETRIC STUDY OF THE INFLUENCE OF TWO-DIMENSIONAL OBSTACLES ON PROCESSES IN THE BOUNDARY LAYER

D.A. Bountin, Yu.V. Gromyko

Khristianovich Institute of Theoretical and Applied Mechanics SB RAS
630090, Novosibirsk, Russia

Experiments were carried out in the wind tunnel "Tranzit-M". The experiments were carried out at Mach numbers M = 5, 6, and 8, stagnation temperature T_0 = 385 ÷ 499 K, and stagnation pressure P_0 = 2 ÷ 29 atm. The unit Reynolds number varied for M = 5 in the range $Re_1 = (3.46 \div 11.6) \times 10^6$ 1/m; for M = 6 in the range $Re_1 = (4 \div 13.4) \times 10^6$ 1/m; M = 8 in the range $Re_1 = (3.8 \div 13.8) \times 10^6$ 1/m.

To measure pressure fluctuations in the boundary layer and temperature and heat flux distributions on the surface, a model of a 5-degree pointed polyacital cone was designed and manufactured. The model was set at zero angle of attack. To measure pressure pulsations on the surface of the model, seven PCB 132A31 high-frequency pressure sensors were installed in the model. Heat fluxes on the model surface were measured using an InfraTec IR camera. The frame rate in the experiments was 491 Hz.

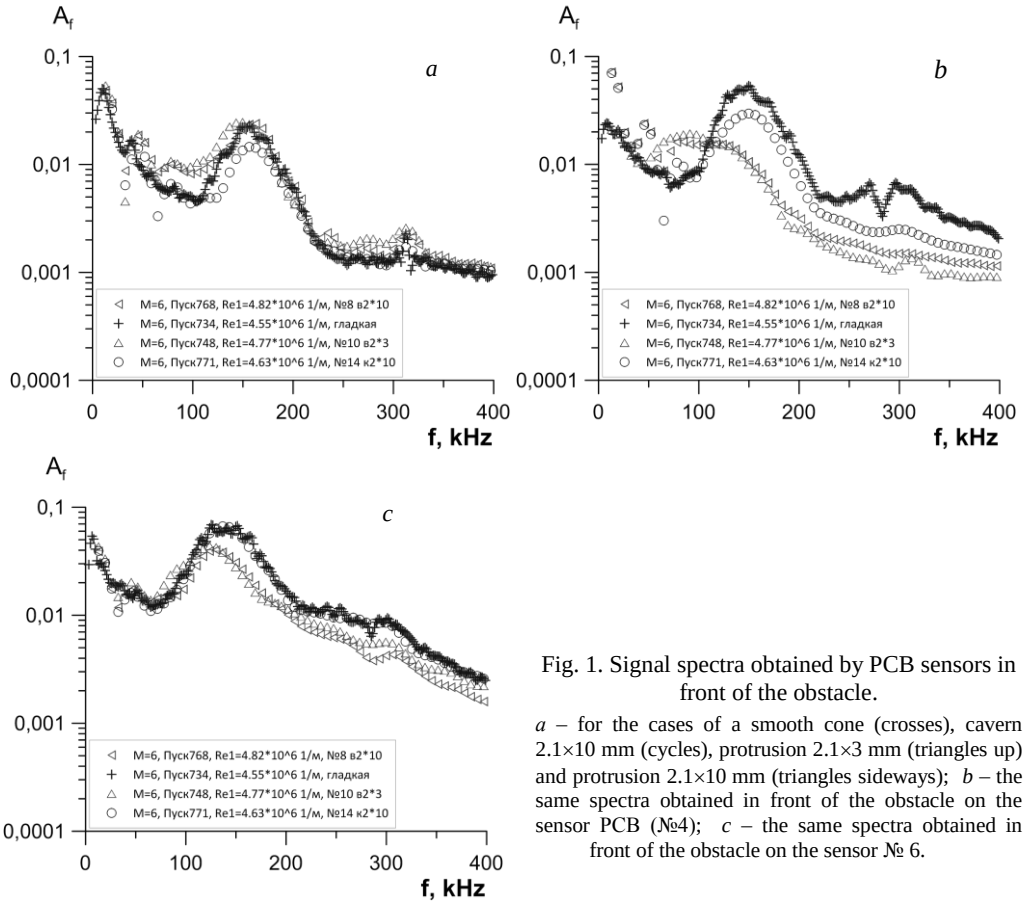

Fig. 1. Signal spectra obtained by PCB sensors in front of the obstacle.

a – for the cases of a smooth cone (crosses), cavern 2.1×10 mm (cycles), protrusion 2.1×3 mm (triangles up) and protrusion 2.1×10 mm (triangles sideways); *b* – the same spectra obtained in front of the obstacle on the sensor PCB (№4); *c* – the same spectra obtained in front of the obstacle on the sensor № 6.

The model was equipped with 14 interchangeable obstruction inserts (two-dimensional annular protrusions and caverns) made of polyacital. Two inserts made it possible to obtain a cone with a smooth wall and a cavity with a right angle. The rest of the inserts modeled a two-dimensional roughness with a ridge or a cavity, described by a profile proportional to $h \times \sin^2(f(x, w))$. The height/depth of the obstacle was h = 0.4, 1, 2.1 mm; width was w = 3 and 10 mm.

Distributions of heat fluxes along the generatrix of the cone and the spectra of pressure fluctuations on the surface were obtained in the experiments.

Figure 1 shows the spectra obtained for the case M = 6, $\mathrm{Re}_1 \approx 4.7 \times 10^6$ 1/m. The pulsations on the first two sensors coincide in all cases, however, on the sensor in front of the obstacle, one can see the effect, most likely, of the separation zone in front of the obstacle on waves in the range of 50–110 kHz (Fig. 1,*a*). Immediately behind the ridges, the amplitude of the waves of the second mode (peak around 150 kHz) drops significantly, like all other waves with higher frequencies. The increase in wave amplitudes in the frequency range of 50–110 kHz remains, due to the separation zone after the obstacle (Fig. 1,*b*). The influence of the cavity is noticeable, although much less than that of the protrusions. In contrast to the previous case, the influence of the protrusions on the waves of the second mode and the entire high-frequency part of the spectrum remains up to the last sensor (Fig. 1,*c*). The influence of the separation zone is no longer significant, the amplitude of waves with frequencies of 50–110 kHz returns to the case of a smooth wall. Behind the cavity, the flow completely relaxes and the spectra coincide with the case of a smooth wall. The influence of the width of the protrusion and the cavity is not traced.

Thus, it can be seen that for some regimes, two-dimensional obstacles locally suppressed pulsations in the high-frequency part of the spectrum, in particular, pulsations of the second disturbance mode. The roughness height is a key parameter affecting both the fluctuations and the distribution of heat fluxes in the boundary layer. At the same time, the width of the obstacles has practically no effect on the processes in the boundary layer.

This work was carried out partly within the framework of the Program of Fundamental Scientific Research of the State Academies of Sciences, Grant No. 121030500162-7 (measurement of the pressure pulsations) and partly supported by RSF project №22-21-20098 (heat flux measurement).

DOI: 10.53954/9785604788967_34

ALGORITHM FOR NUMERICAL INTEGRATION OF A SYSTEM OF EQUATIONS OF MULTIPHASE FLOWS WITH COMMON PRESSURE IN THE BAROTROPIC APPROXIMATION

S.V. Bulovich, I.A. Ignatiev

Peter the Great St. Petersburg Polytechnic University
195251, St. Petersburg, Russia

The mathematical model of the description of the environment within the framework of the multi-liquid approach is based on the concept of interpenetrating continuums, which was introduced by H. A. Rakhmatulin [1]. This model assumes the presence of several phases (liquids) at each point of space, each of which is characterized by the amount of the volume fraction of the substance. Balance rations are used to find the gas-dynamics functions of the state of multiphase flow and the interphase interaction is reflected by the source terms. In this paper, the system of equations is simplified using two approaches. Firstly, the pressures in all liquids are assumed to be equal, and the correctness of the Cauchy problem for the resulting system is restored by switching to a parabolic system due to the introduction of artificial viscosity [2]. Secondly, it is considering flows in which the thermodynamic process of energy exchange is not essential, which makes it possible to use the barotropic approximation. In this case, the law of conservation of energy is replaced by the expression of the relationship between density and pressure. So, the following system of equations is obtained:

$$\frac{\partial\left(A\alpha_k\rho_k\right)}{\partial t}+\frac{\partial\left(A\alpha_k\rho_k u_k\right)}{\partial x}=\frac{\partial}{\partial x}\left(A\nu_k\frac{\partial\left(\alpha_k\rho_k\right)}{\partial x}\right),$$

$$\frac{\partial\left(A\alpha_k\rho_k u_k\right)}{\partial t}+\frac{\partial\left(A\alpha_k\rho_k u_k^2\right)}{\partial x}+A\alpha_k\frac{\partial p}{\partial x}=\frac{\partial}{\partial x}\left(A\nu_k\frac{\partial\left(\alpha_k\rho_k u_k\right)}{\partial x}\right),$$

$$\sum_{k=1}^{N}\alpha_k=1,\qquad \rho_k=\rho_k\left(p\right),$$

where A – area of channel; α_k – volume fraction, ρ_k – density, u_k – velocity, ν_k – viscosity ratio of k's liquid; p – pressure; $k = 1\ldots N$ – number of liquid and total amount of liquids.

The numerical method is based on the use of the predictor-corrector scheme, which allows to achieve second-order accuracy in time. A finite-volume approach is used for space discretization, which require the formation of a convective and diffusive flow on the face of the calculated cell. At the predictor step, gas dynamic functions on the half-integer time layer n+1/2 determinates using an implicit scheme, which are used to calculate the flow through the cell face at the corrector step. The explicit procedure for generating the flow value on the cell face at the corrector step allows to use the TVD approach, which, depending on the template, provides an 2–5 order of accuracy in space on smooth solutions. In this paper, the second order of accuracy in space is achieved by replacing the piecewise-constant representation of the behavior of functions in a cell with a piecewise-linear one. The minmod limiter is used to determine the slope of the function in the cell. The functions involved in the formation of convective terms are extrapolated to the face along the flow, counterflow extrapolation is used for pressure.

To demonstrate the operation of the algorithm, the results of calculating the decay of a rupture in a shock tube in a three-fluid formulation are presented. The following input parameters are set: pressure in the left of the diaphragm: p = 8.5 MPa; pressure in the right of the dia-

phragm: p = 5.7 MPa; volume fractions of liquids: $\alpha_1 = 0.8000,\ \alpha_2 = 0.1999,\ \alpha_3 = 0.0001$; density of liquids: $\rho_1 = \left(\frac{p}{1.0e5}\right)^{0.714} \frac{\text{kg}}{\text{m}^3},\ \rho_2 = 1.0e3 \frac{\text{kg}}{\text{m}^3},\ \rho_3 = \left(\frac{p}{1.0e6}\right)^{7.7} \frac{\text{kg}}{\text{m}^3}$. Channel length – 1 m, number of cells – 1002.

The figure shows the pressure distributions and velocity of the fluid 2 along the channel, obtained using the algorithm described in this paper at the initial time, after 300 and 600 time steps. The time step is 5e-07. The figure shows that the algorithm proposed in this paper correctly displays the flow structure.

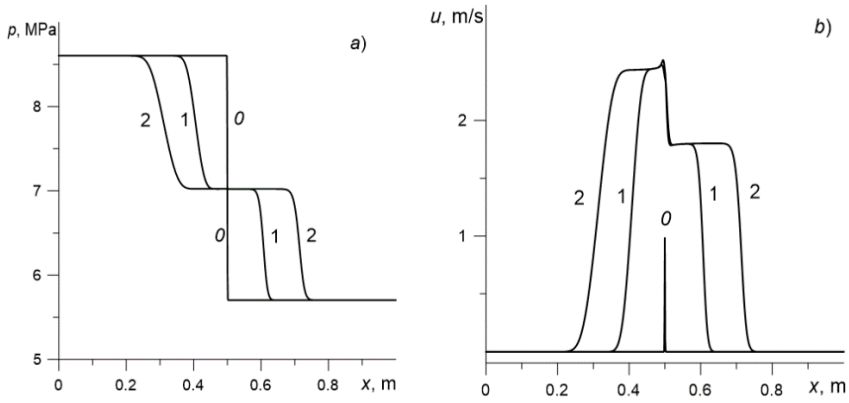

Distributions of pressure (*a*) and velocity for fluid 2 along the axis of the channel (*b*).

To sum up, in this paper a scheme of an increased order of accuracy is proposed for the numerical solution of a system of multiphase flows with a common pressure in the barotropic approximation. The second order of accuracy in time is achieved by using the predictor-corrector scheme. The corrector step, which uses an explicit scheme, allows to build a TVD scheme of 2–5 order of accuracy in space, which is shown in this paper by the example of a scheme of the 2nd order of accuracy.

REFERENCES

1. **Rakhmatulin Kh.A.** Gas-dynamics fundamentals of interpenetrating motions of compressible media // Journal of Applied Mathematics and Mechanics. 1956. Vol. 20, № 2. P. 184–195. (in Russian).
2. **Bulovich S.V., Smirnov E.M.**, Experience in using a numerical scheme with artificial viscosity at solving the Riemann problem for a multifluid model of multiphase flow // The Eighth Polyakhov's Reading: Proc. of the Int.l Sci. Conf. on Mechanics (Russia, Saint Petersburg, 29 January–2 February 2018): AIP Conference Proceedings. 2018. Vol. 1959 (1). Art. 050007. 8 p. DOI: 10.1063/1.5034635

DOI: 10.53954/9785604788967_36

THERMAL REGIMES OF QUARTZ DISCHARGE CHANNEL OF POWERFUL HIGH-FREQUENCY INDUCTION PLASMATRON IN PLASMA FLOWS OF MOLECULAR GASES

A.V. Chaplygin, S.A. Vasil'evskii, S.S. Galkin, A.F. Kolesnikov

Ishlinsky Institute for Problems in Mechanics RAS
119526, Moscow, Russia

The high-frequency induction plasmatrons of the IPMech RAS VGU-4 and VGU-3 are designed to study the heat exchange of materials under conditions simulating the full-scale thermochemical effect of a high-enthalpy gas flow over high-speed aircraft during re-entry in the atmosphere of Earth or Mars [1]. The swirling of gas flow at the entrance to the plasma formation region, first proposed by T. Reed [2], allows the use of uncooled quartz discharge channels in the design of these facilities. The operating envelope of a high-power HF-plasmatron with an uncooled discharge channel depends, among other things, on the thermal state of the discharge channel wall. Thermal regimes of the discharge channel wall of the 1 MW VGU-3 plasmatron were investigated in [3].

In this work, the thermal regimes of the quartz discharge channel of the 100 kW VGU-4 facility were studied.

The experiments were carried out in subsonic plasma jets of air, nitrogen and carbon dioxide of the VGU-4 HF-plasmatron, flowing from a quartz discharge channel with a diameter of 80 mm, at a pressure in the pressure chamber of the facility of 50 hPa, plasma forming gas mass flow from 1.8 to 3.6 g/s, for the power values of the HF-generator of the plasmatron according to the anode power supply of 45 and 70 kW. Using the thermal imager "Testo 890", temperature distributions on the outer surface of the uncooled quartz discharge channel of the HF-plasmatron VGU-4 were obtained depending on the composition and mass flow of the plasma forming gas and the supplied power. The maximum temperature of the discharge channel outer wall, depending on the plasma-forming gas mass flow at the HF-generator power of 70 kW is shown in the figure.

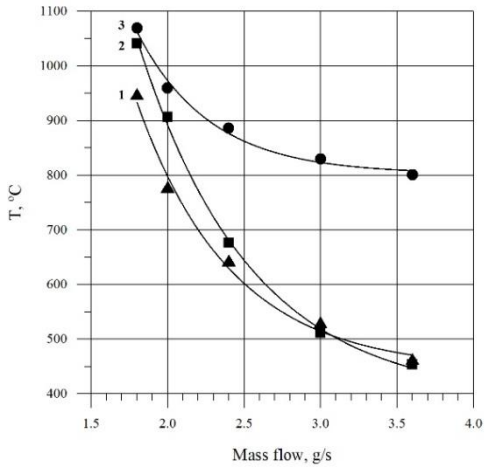

The maximum temperature of the discharge channel outer wall.
1 – nitrogen, *2* – air, *3* – carbon dioxide.

Numerical modeling. The calculation of chemically equilibrium plasma flow and the vortex electromagnetic field in the discharge channel of VGU-4 facility was carried out by the Alpha code developed in the Laboratory of Interaction of Plasma and Radiation with Materials of IPMech RAS. The Navier – Stokes equations were solved by the Patankar – Spalding finite volume method with non-uniform rectangular finite-difference grid, the source terms for these equations were determined by the tangential component of the electric field amplitude E_{teta}. To calculate the E_{teta}, an effective quasi-one-dimension model of Maxwell's equations was used, which is sufficiently accurate for a relatively thin channel of the VGU-4 plasmatron. The problem formulation and numerical method are described in details in [4]. Transport coefficients (viscosity, thermal conductivity, electrical conductivity) were determined by interpolation from tables that were calculated in advance for three gases – air, nitrogen and carbon dioxide – by the Chapman – Enskog method. Temperature fields and plasma streamlines of air, nitrogen and carbon dioxide in the discharge channel of the VGU-4 HF-plasmatron were obtained for the power values of 45 and 70 kW at a constant gas mass flow rate of 2.4 g/s and pressure in the pressure chamber of the facility of 50 hPa. The influence of the temperature of the inner wall of the discharge channel on calculation results was investigated. It was found that within the specified limits (300–960 K), the effect of wall temperature on plasma parameters (temperature, enthalpy and velocity) at the channel exit section is negligible.

Conclusion. Experimental and calculated data make it possible to predict the operability of the quartz discharge channel of the HF-plasmatron VGU-4 in a wide range of operating regimes of the facility for various gases. The lower limit of the plasma forming gas mass flow rate, at which a sharp increase in the maximum temperature of the discharge channel was observed, was 1.8 g/s. The highest temperatures of the discharge channel at constant power of the HF-generator were achieved in the carbon dioxide plasma, which is associated with a significant increase in the contribution of radiation to heat exchange.

The work was supported by the Ministry of Science and Higher Education within the framework of the Russian State Assignment under contract No. AAAA-A20-120011690135-5.

The experiments were carried out at HF-plasmatron VGU-4 (IPMech RAS Research Resource Center, https://ckp-rf.ru/usu/441568/).

REFERENCES

1. **Gordeev A.N.** Overview of Characteristics and Experiments in IPM Plasmatrons: NATO RTO EN-8, 2000. P 1A-1/1A-18 // Measurement Techniques for High Enthalpy and Plasma Flows [Techniques de mesure pour les ecoulements de plasma et les ecoulements a haute enthalpie Neuilly-Sur-Seine Cedex, France]. DTIC ADP010736: https://archive.org/details/DTIC_ADP010736 Publ. date 2000-04-01.
2. **Reed T.B.** Induction-Coupled Plasma Torch // Journal of Applied Physics. AIP Publishing. 1961. Vol. 32, Iss. 5. P. 821–824. DOI: 10.1063/1.1736112.
3. **Gordeev A.N., Pershin I.S., Yakushin M.I.** Heat Regimes of Quartz Discharge Channel of Powerful Induction Plasmatron IPG-3-200 // Environmental Testing for Space Programms: Proc. of the Third Int. Symp. (Noordwijk, the Netherlands, June 24–27, 1997) / Ed. T.-D. Guyenne. ESA SP-408. Paris: European Space Agency, 1997. Vol. 408. P. 189.
4. **Vasil'evskii S.A., Kolesnikov A.F.** Numerical simulation of equilibrium induction plasma flows in a cylindrical plasmatron channel // Fluid Dynamics. 2000. Vol. 35, No. 5. P. 769–777.

DOI: 10.53954/9785604788967_38

ENGINEERING MATHEMATICS FOUNDATIONS IN AEROHYDRODYNAMICS

Yu.D. Chashechkin

Ishlinsky Institute for Problems in Mechanics RAS
119574, Moscow, Russia

Treatises on fluid mechanics emphasize the division of a single subject into large sections (aerodynamics and hydrodynamics), processes (jets, waves, vortices, wakes ...), models (fundamental, reduced, constitutive...) and a large number of other irreducible gradations. [1]. Following the ideas of D.I. Mendeleev "not to separate the issue of air resistance from the issue of water resistance" [2], a unified approach is being developed. The basis is Engineering mathematics as an axiomatic science of the principles for choosing the symbol contents, operation rules and criteria accuracy control as well as Technical physics as the emprio-axiomatic science of nature as a whole, the properties and structure of matter, all types of state changes with control of errors. Physical quantities are selected that correspond in meaning to the symbols of engineering mathematics [3]. The mathematical description is based on the concepts of a real number, time, vector space, invariants and motion – a continuous orthogonal transformation of a metric space into itself with a parameter (time) while maintaining the distance and location of objects.

A matter, which is characterized by total energy and other properties, is being immersed in space. The main characteristic of the liquid matter is the internal energy, which is described by the Gibbs potential, and its derivatives, determining the thermodynamic quantities. In a medium consisting of atoms and molecules, supramolecular structures (voids, clusters, clathrates) are formed with their own internal energy and boundaries. The structures can be quickly destroyed with the transformation of a part of the Gibbs potential into other forms. An approach in which flows are defined as an inherent or forced transfer of momentum, total energy, matter, accompanied by self-consistent changes in physical quantities, allows to take into account all mechanisms of energy transfer – with a flow, waves, slow dissipative, fast in direct atomic-molecular interactions and structural transformations. Motion of the space and fluid flow are two independent entities that are identified in the approximation of constant density.

A matter, which is characterized by total energy and other properties, is being immersed in space. The main physical quantity of the liquid matter is the internal energy, which is described by the Gibbs potential, and its derivatives, determining the thermodynamic quantities. In a medium consisting of atoms and molecules, supramolecular structures (voids, clusters, clathrates) are formed with their own internal energy and boundaries. Structures can be quickly destroyed with the transformation of a part of the Gibbs potential into other forms. An approach in which flows are defined as an inherent or forced transfer of momentum, total energy, matter, accompanied by self-consistent changes in physical quantities, allows to take into account all mechanisms of energy transfer - with a flow, waves, slow dissipative as well as fast in direct atomic-molecular interactions and structural transformations . Motion of the space and fluid flow are two independent entities that are identified in the approximation of constant density.

Changes in the parameters of fluid flows that are momentum, total energy, density and constituent substances, are described by the axiomatically introduced system of fundamental equations, first fully presented in the treatise [1]. The system specifies a set of observable physical quantities, including the momentum of the medium or its components. "Fluid velocity" is a measure of the notion of space, not an observable quantity of a fluid flow. Complete solutions of the system of fundamental equations with initial and boundary conditions, constructed taking into account the compatibility condition, determine the basic classification of the flow structure components. Linear solutions include a family of ligaments – interfaces or fibers, and waves [3].

All flow components, both waves and ligaments, actively interact with each other [4]. Flows that include a large number of components with incommensurable parameters are unsteady.

Experimental studies of the pattern of air flow around bodies are carried out in TsAGI wind tunnels. Ligaments, or in terminology S.A. Khristianovich – "short waves", were first discovered at TsAGI in 1944 on schlieren photographs of the flow pattern around the wing at Mach numbers as thin elongated fibers with large density gradients located across the main flow. High-gradient structures were interpreted as a "flow-balanced shock waves", in which the losses of velocity and pressure drop create additional "wave drag" [5].

Experimental studies of the stratified fluid flow around the strip were carried out on the Unique Research Facility at the IPMech RAS stands. Numerical modeling of the flow around a plate with a stratified (strongly or weakly) and homogeneous (potentially or actually) fluid was carried out on the basis of a system of equations for the transfer of momentum, matter, continuity and incompressibility. Solutions were constructed in a single setting in a wide range of parameters, including creeping flows induced by diffusion on a fixed body [6] and non-stationary vortex regimes at the Reynolds number values, determined with the plate length of the order of $\mathrm{Re} \sim 10^5$ [7].

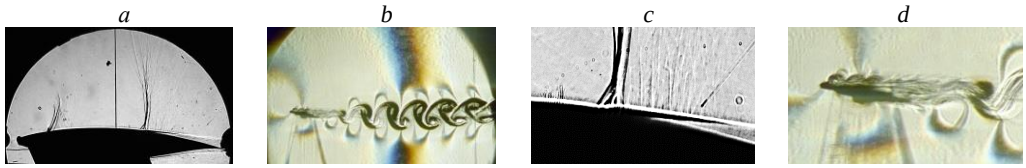

Schlieren images of the flow patterns.

a – wing at Ma = 0.77 (photo by V.G. Sudakov, TsAGI wind tunnel); *b* – plate in the stratified tank of the LMB IPMech RAS (buoyancy period T_b =7.55 s, plate length h = 2.5 cm, angle attack α = 12.5°, velocity U = 3.6 cm/s, Re = 900, Fr = 1.73); *c*, *d* – enlarged areas of patterns with fibers.

Presented data (see the figure) show that in the unsteady flow pattern near the plate in the entire range of parameters, all structural components are represented including slowly evolving internal waves, wake, vortices, as well as rapidly changing thin fibers (ligaments) and their sets that actively interact with each other, with waves and with the flow. Basic integral characteristics that are drag and lift coefficients weakly depend on stratification and strongly on the plate angle of attack.

Acknowledgments. The work was carried out on the topic of the state assignment (state registration number AAAA-A20-120011690131-7). The experiments were carried out on the test benches of the Institute of Institution "SPC IPMech RAS".

REFERENCES

1. **Landau L.D., Lifshitz, E.M.** Fluid Mechanics. Vol. 6. Course Theoret. Phys. Hydrodynamics. M.; L., Nauka, 1944. 646 p.
2. **Mendeleev D.I.** On Drag of Fluids and on Aeronautics. St. Petersburg: Typogr. V. Demakova,1880. 80 p.
3. **Chashechkin Y.D.** Foundations of engineering mathematics applied for fluid flows // Axioms. 2021. Vol. 10. No. 286. https://doi.org/10.3390/axioms10040286.
4. **Chashechkin Yuli D.** Conventional partial and new complete solutions of the fundamental equations of fluid mechanics in the problem of periodic internal waves with accompanying ligaments generation // Mathematics. 2021. Vol. 9. No. 586. https://doi.org/10.3390/math9060586
5. **Serebrisky Ya.M., Khristianovich S.A.** About wave resistance. Moscow, 1944. 18 p. (Proceedings / TsAGI; Iss. 550).
6. **Chashechkin Yu.D., Zagumennyi Ia.V.** Formation of waves, vortices and ligaments in 2D stratified flows around obstacles // Physica Scripta. 2019. Vol. 94, No. 5. Art. 054003. 17 p. DOI:10.1088/1402-4896/ab0066.
7. **Chashechkin Yu.D., Zagumennyi Ia.V.** 2D hydrodynamics of a plate: From Creeping Flow to Transient Vortex Regimes // Fluids. 2021. Vol. 6, Iss. 9. Art. 310. 28 p. DOI:10.3390/fluids6090310

DOI: 10.53954/9785604788967_40

ENERGETICS, HYDRODYNAMICS AND ACOUSTICS OF THE DROP IMPACT

Yu. D. Chashechkin

Ishlinsky Institute for Problems in Mechanics RAS
119574, Moscow, Russia

The drop impact that is a sequence of physical, hydrodynamic, acoustic processes that accompany the contact and merging of a drop with a target medium is of applied interest for a number of sections of aviation sciences including engine improvement, flight safety. The theory of drop flows is developed on the basis of the definition of a liquid as a continuous medium, which is characterized by internal energy. For the description, the Gibbs potential [1] was chosen, its derivatives which are thermodynamic quantities (density, pressure, temperature, surface tension, and others), kinetic and transfer coefficients for other quantities and fields.

Due to the natural structurization of the atomic-molecular medium (the existence of a free surface, associations of atoms into complexes, clathrates and voids separating them [2]), the internal energy is distributed non-homogeneously. The dynamics and structure of drop flows are affected by the transfer of all energy components (kinetic and potential, internal) and the rapid conversion of internal energy into other forms – perturbations of density, temperature, pressure and mechanical motion of thin layers and fibers of the liquid. The theory of flows is based on a system of fundamental equations for the transfer of momentum, energy, and matter, which are closed by the equations of state for the Gibbs potential and thermodynamic quantities. The system is supplemented by physically justified initial and boundary conditions, taking into account the conversion of surface energy [3]. The experimental technique was developed taking into account the properties of all components of the solutions of the fundamental system, and large-scale (flows, waves, vortices) and thin ligaments.

The experiments were carried out on the stands of the of Unique Research Facilities Complex “HPhC IPMech RAS” [4]. The dynamics and structure of processes at all stages of droplet dynamics were studied: during pinch off with the formation of satellites, free-fall eigenoscillations, primary contact with the formation of fast thin jets, and coalescence with the line and reticular pattern of substance distribution [5]. In the fluid layer under the cavern, the substance of miscible liquids of the drop propagates in the form of thin fibers and loops, both in inert and chemically reacting merging fluids [6]. The restructuring of the reaction products of solutions of ferric chloride and ammonium thiocyanate distribution during the collapse of the cavity patterns is shown in Fig. 1.

The drop substance, initially distributed in individual fibers, formed a grating on the crown as well as mesh in the cavity center gradually remove into nodes and is pressed into the target

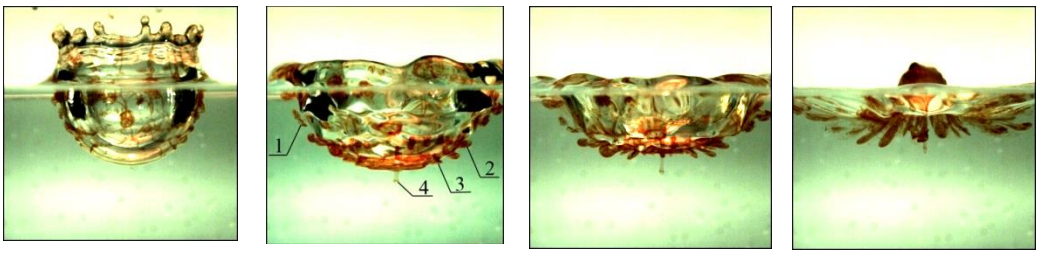

a *b* *c* *d*

Fig. 1. Evolution of inclined loops when merging a drop of 1% ferric chloride solution with a 20% solution of ammonium thiocyanate.
t = 10 (*a*), 35 (*b*), 41 (*c*), 52 (*d*) ms.

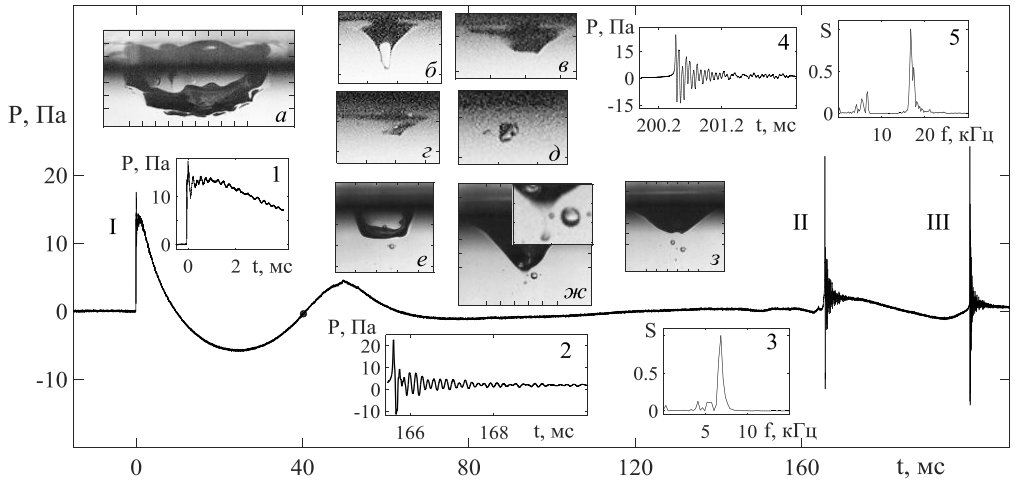

Fig. 2. Phonogram and the flow pattern photos.

Inserts 1 and 2 – extended shock pulse I and packet II, 3 – spectrum of packet II, 4 and 5 – extended packet III and its spectrum

fluid by singular fibers with a vortex head. The longest jetlet is formed in the primary contact point of the fluids under the center of the cavity. The fibers are extended by the flow and form the oblique loops under the collapsing cavity which are gradually drawn into the splash.

All active changes in the flow structure are accompanied by the generation of capillary and acoustic waves. Capillary waves start to radiate simultaneously with the formation of the cavity and the rise of the crown. External annular waves of maximum length and amplitude are formed in the crown decay phase. New groups of capillary waves arise during all changes in the flow structure – the formation of an ascending splash and its subsidence, the return of ejected secondary drops, the development of secondary caverns, the subsidence of a streamer and droplets. In a typical audiogram shown in Fig. 2, the high-frequency shock pulse is followed by low-frequency oscillations and, after a pause, two resonant packets, whose spectra are scanned in the insets [7].

A comparison of the patterns of flows and acoustic signals indicates that the processes of generation of resonant sound packets are synchronized with the detachment of gas cavities from the cavity formed when a drop immerses, or their rupture into fragments.

Acknowledgments The work was supported by the Russian Science Foundation (project no. 19-19-00598). The experiments were carried out on the stands of USF "HPC IPMech RAS".

REFERENCES

1. Feistel R., Harvey A. H., Pawlowicz R. Advisory Note No. 6: Relationship between various IAPWS documents and the International Thermodynamic Equation of Seawater-2010 (TEOS-10) / International Association for the Properties of Water and Steam. 2016. P. 1–5.

2. Eisenberg D., Kauzmann W. The Structure and Properties of Water. Oxford University Press, 2005. 308 p.

3. Chashechkin Y.D. Foundations of engineering mathematics applied for fluid flows // Axioms. 2021. Vol. 10. Art. 286. DOI: 10.3390/axioms10040286.

4. Hydrophysical complex of USF "HPC IPMech RAS": WebSite. URL: http://www.ipmnet.ru/uniqequip/gfk/#equip.

5. Chashechkin Yu. D., Ilinykh A. Yu. Drop decay into individual fibers at the boundary of the contact area with a target fluid // Doklady Physics. 2021. Vol. 66, No. 4. P. 101–105. DOI: 10.1134/S1028335821040078.

6. Chashechkin Yu. D., Ilinykh A. Yu. Visualization of media contact areas in drop impact flows with chemical reactions // Doklady Physics. 2021. Vol. 66, No. 10. P. 285–292. DOI: 10.1134/S1028335821100013.

7. Chashechkin Yu.D. Packets of capillary and acoustic waves of drop impact // Herald of the Bauman Moscow State Technical University. 2021. No. 1 (94). P. 73–92. DOI: 10.18698/1812-3368-2021-1-73-91.

DOI: 10.53954/9785604788967_42

COUNTERFLOWS IN A BOUNDARY LAYER AT A GIVEN PRESSURE GRADIENT

T. Chzhun, V.B. Zametaev

***Moscow Institute of Physics and Technology* (*National Research University*)**
141701, Dolgoprudny, Moscow region, Russia

Many articles have been devoted to the study of the interaction of a laminar boundary layer developing on a flat surface with a moving pressure perturbation. In particular, A.I. Ruban considered the case of a weak shock wave moving upstream [1], and in an article by Yapalparvi and Van Dommelen, a system of equations with a shock wave moving downstream was calculated [2]. This research is an addition to the analytical study [3] of the linear problem of the interaction of a dipole and a boundary layer on a plate moving upstream in a nonlinear mode with a given pressure gradient.

A two-dimensional laminar flow of a viscous incompressible fluid past a flat plate at high Reynolds numbers is considered as the basic flow in the study. At distance $\hat{L}$ from the leading edge of the plate and height $\hat{l}_d = \hat{L} \cdot l$ above the plate, a small body moves downstream with a given constant velocity $\hat{V}_d = \hat{V}_\infty u_W$, where $\hat{V}_\infty$ is the speed of the external flow (see the figure). For simplicity, a small body that creates a pressure perturbation in the flow and, accordingly, on the plate surface is modelled by a potential dipole with the momentum $\hat{d} = \hat{V}_\infty \hat{L}^2 m$.

On passing to the coordinate system moving downstream with the dipole, an observer moving with it will see a stationary flow with counterflows near the streamlined wall moving upstream. The viscous sublayer was artificially divided along a previously unknown curve $S(x)$, at each point of which the horizontal velocity turns to zero, into two subregions: region 1a, in which the flow is directed from right to left, and region 1b, in which the flow moves from left to right. As a result, in the case of a given pressure, we can formulate the correct parabolic problems in each introduced domain. After transformations of the vertical coordinate and the longitudinal velocity according to the formulas $y = S(x)Y$, $U = S(x)u$, the problem takes the following form:

$$U\frac{\partial U}{\partial x} + V\frac{\partial U}{\partial Y} = -S^2(x)\frac{dp_e}{dx} + \frac{1}{S(x)}\frac{\partial^2 U}{\partial Y^2} + \frac{S'(x)}{S(x)}U^2, \quad \frac{\partial U}{\partial x} + \frac{\partial V}{\partial Y} = 0, \quad p_e = M\frac{2(x^2-1)}{(x^2+1)^2}. \qquad (1)$$

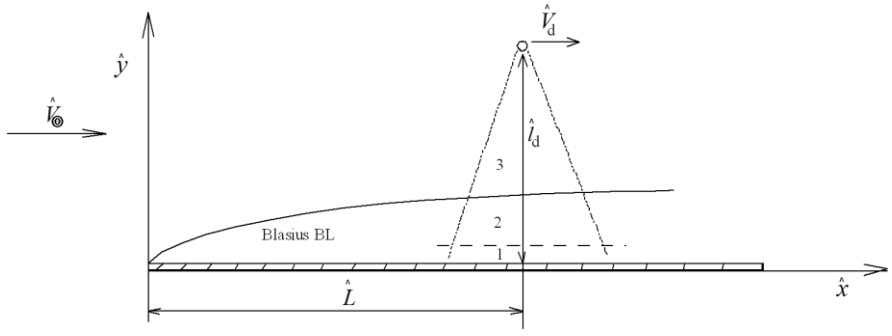

Basic flow.

1 – viscous sublayer, *2* – the main part of the boundary layer, *3* – external potential flow.

Initial and boundary conditions in region 1a:

$$Y = 0 : U = -S(x)U_W,\ V = 0;\ Y = 1 :\ U = 0;\ x \to +\infty :\ U = -U_W + Y + ...$$

Initial and boundary conditions in region 1b:

$$Y = 1 :\ U = 0,\ V_{1b}(x) = V_{1a}(x);\ Y \to +\infty :\ \frac{\partial U}{\partial Y} = S^2(x);\ x \to -\infty :\ U = -U_W + Y + ...$$

The unknown curve $S(x)$ was found using the condition of continuity of the tangential stress at the dividing line of the subregions:

$$Y = 1 :\quad \left.\frac{\partial U}{\partial Y}\right|_{1a} = \left.\frac{\partial U}{\partial Y}\right|_{1b}. \tag{2}$$

The numerical solution of problem (1) in a viscous sublayer for an arbitrary given function $S(x)$ was performed in two stages. At the first stage, the calculation was carried out by the right-to-left marching method in region 1a. Then, taking into account the boundary conditions for the vertical velocity on the curve $S(x)$ obtained from calculations in region 1a, the calculation was performed similarly from left to right in region 1b. As a result, the difference between the values of tangential stresses at a given boundary function $S(x)$ obtained from solutions in regions 1a and 1b was calculated. The true shape of the dividing line $S(x)$ was obtained by solving an implicit system of equations by Newton's method, consisting of the conditions of continuity of tangential stresses (2). Pictures of streamlines in a viscous sublayer were drawn, on which a closed vortex and two unclosed separated zones are visible near the zero-velocity line.

This work was performed with partial support of the Russian Science Foundation (project No. 20-11-20006) at the Moscow Institute of Physics and Technology.

REFERENCES

1. **Ruban A.I., Araki D., Yapalparvi R., Gajjar J.S.B.** On unsteady boundary-layer separation in supersonic flow. Part 1. Upstream moving separation point // J. Fluid Mech. 2011.Vol. 678. P. 124–155.
2. **Yapalparvi R. & Van Dommelen L.L.** Numerical solution of unsteady boundary-layer separation in supersonic flow: upstream moving wall // J. Fluid Mech. 2012. Vol. 706. P. 413–430.
3. **Chzhun T., Zametaev V.B.** Analytical solution of the linear problem of the interaction of a dipole and a boundary layer on a plate moving upstream // Proceedings of the 63rd All-Russian Scientific Conference (Moscow, November 23–29, 2020) // Aerospace Technologies. 2020. P. 246–247. [in Russian: **Чжун Т., Заметаев В.Б.** Аналитическое решение линейной задачи о взаимодействии диполя и пограничного слоя на пластине, движущейся вверх по потоку // Труды 63-й Всероссийской научной конференции (МФТИ 23–29 ноября 2020) // Аэрокосмические технологии. 2020. С. 246–247].

DOI: 10.53954/9785604788967_44

SUPERSONIC AND SUBSONIC INTERNAL FLOW DYNAMICS AFTER A PULSED LOCALIZED DISCHARGE NEAR AN OBSTACLE

D.I. Dolbnya, I.A. Znamenskaya, T.A. Kulizade, I.A. Doroshchenko

Lomonosov Moscow State University
119234, Moscow, Russia

The results of experimental studies on the pulsed volume discharge effect on subsonic and supersonic flow in the channel are presented. A single nanosecond volume discharge with pre-ionization from plasma electrodes [1, 2] was initiated at different stages of the flow behind the shock wave with Mach numbers M from 2.8 to 3.5 in the shock tube channel. The duration of the discharge electric current was 200 – 600 ns. The pulsed energy input was in a time (0.2–6.0) ms and velocity (900–300 m/s) ranges in the flow after SW passage. A dielectric ledge with dimensions of 6 mm × 2 mm × 48 mm mounted on the surface of the lower wall led to inhomogeneities in the discharge plasma distribution, and also served as an obstacle to the gas flow.

In recent years, among a wide variety of discharges types, discharges with a pulse duration from several to hundreds of nanoseconds have attracted increased interest. It was proposed to use them to intensify combustion [3]. The pulsed discharge is accompanied by a rapid increase in temperature, which is associated with the release of large energy in the local region [1]. The gas can be heated in less than 1 μs, the plasma zone generates a shock (explosive) wave; its configuration and intensity depend on the structure of the gas flow, the density distribution and, as a consequence, on the discharge energy localization.

In a supersonic flow around the obstacle a bow shock wave arises in front of it, a series of compression waves appear emanating from the shear layer, which form the oblique shock wave, and a recirculation region between the obstacle and a shear layer; an attachment shock is formed from the attachment point. The discharge at this stage is localized mainly in the leeward region of the obstacle (behind the obstacle relative to the oncoming flow) [2].

The absence of oblique shock waves and the appearance of a weak shock wave above the obstacle (in the local transonic region) indicate a subsonic flow. During the initiation of the dis-

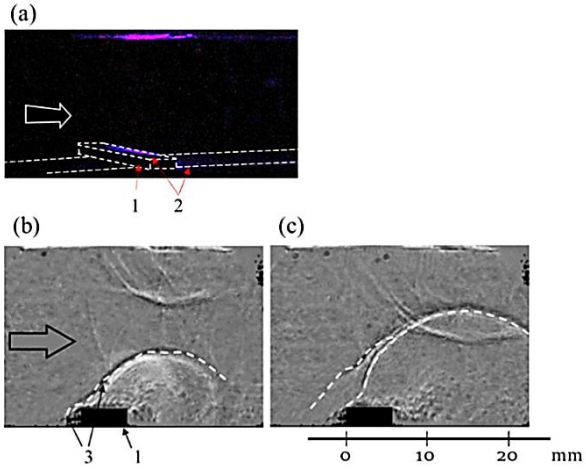

Fig. 1. Discharge initiation in a transonic flow, 3.03 ms after the passage of the SW front (M = 3.34).

a – discharge glow, *b*, *c* – successive shadow images of the evolution of disturbances from the pulsed energy input; *1* – the obstacle, *2* – glow of the self-localized pulsed discharge, *3* – explosive shock waves from the pulsed discharge energy input.

charge, the predominant fraction of the plasma is concentrated in the separation zone behind the obstacle, but part of it is located at the obstacle leading edge (Fig. 1). As a result of the pulsed energy input, the formation of explosive shock waves is observed (see Fig. 1), its lifetime depends on the flow velocity, and then on the local energy release intensity. The corresponding quantitative dependencies are obtained.

High-speed shadow imaging of the flow under consideration can contain several thousand frames, their processing and manuall analysis is a very hard work. To automate processing, two software tools were made and used for automatic detection and tracking of flow structures [4]. The first tool is our in-house code for shock wave detection based on the modified Canny edge detection and Hough transform algorithms for detecting straight shock wave segments and deriving their equations. The developed program allows tracking the position of gas-dynamic discontinuities, plotting the dependence of their positions on time, and velocity calculating using a polynomial approximation. The second tool is a convolutional neural network pre-trained on a large number of shadow frames, which allows tracking more complex flow structures – complex shock-wave configurations, the development of thermal plumes from discharge local energy release areas.

This study was carried out within the framework of the Development Program of the Interdisciplinary Scientific and Educational School of Moscow State University “Photonic and Quantum Technologies: Digital Medicine”. D. Dolbnya is a grant-aided student of the BASIS Theoretical Physics and Mathematics Advancement Foundation.

REFERENCES

1. **Mursenkova I., Znamenskaya I., Doroshchenko I., Ivanov I.** Flow analysis of a shock wave at pulse ionization: Riemann problem implementation // Phys. of Fluid. 2019. Vol. 31. Art. 116101. 11 p. DOI: 10.1063/1.5125884.
2. **Znamenskaya I.A., Tatarenkova D.I., Kuli-zade T.A.** Nanosecond ionization of an area of flowing around a rectangular ledge by a high-speed flow // Technical Physics Letters. 2020. Vol. 46, No. 1. 3 p. DOI:10.1134/s1063785020010149.
3. **Ju Y., Sun W.** Plasma assisted combustion: Dynamics and chemistry // Progress in Energy and Combustion Science. 2015. Vol. 48. P. 21–83.
4. **Doroshchenko I.A., Znamenskaya I.A., Sysoev N.N.** Animations analysis in experimental fluid dynamics // Scientific Visualization. 2021. Vol. 13, No. 4. P. 66–75.

DOI: 10.53954/9785604788967_46

CONSTANT VOLTAGE ANEMOMETER IN HIGH-SPEED FLOWS

A.D. Epikhin, D.S. Sboev, A.V. Liverko

Central Aerohydrodynamic Institute
140180, Zhukovsky, Moscow region, Russia

This work presents test results and their qualitive analysis for mockup of constant-voltage anemometer (CVA, developed in TsAGI) in the Ludwig's shock wave facility UT-1M (TsAGI) with Mach 6 chamber. The probe is Dantec 55R47 hot-film that is detached to the surface of canonic swept wing model in the area of flow's spreading behind the leading edge. The flow appears due to rupture of two membranes when the pressure difference between test chamber and high-pressure channel is enough. Operating time interval is 40 ms whereas whole flow's time is about 80 ms.

The data is the set of CVA output voltage oscillograms acquired for pressure from 20 to 100 atm in the high-pressure channel, for the set of probe's overheat ratio 1.0, 1.1, 1.2, 1.3 and for model's angle of attack 0 (Fig. 1) and –5 degree (Fig. 2). Overheat ratio was determined before the start (index 0) as the ratio of resistances of heated R_{w0} and unheated R_{a0} probe:

$$A_{w0} = R_{w0} / R_{a0} \,. \tag{1}$$

The qualitative analysis of results includes:

1) interpretation of flow's behavior near the probe by using the dependence of CVA output and current probe's resistance R_w :

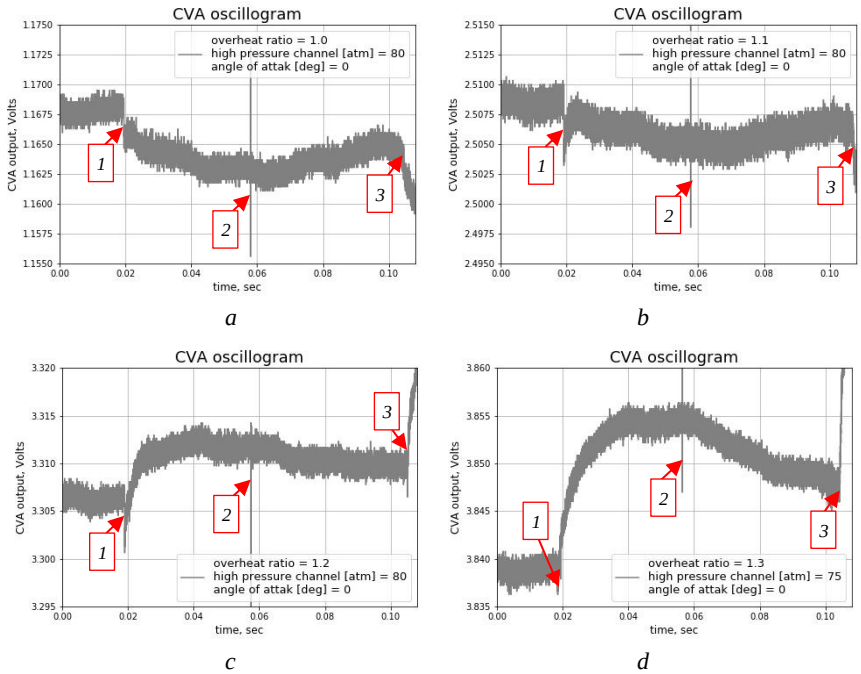

Fig. 1. Oscillograms of CVA output voltage.

Pressure in high-pressure channel is 80 atm, model's angle of attack and 0 degree for. Set of hot-film probe's of overheat ratios 1.0 (*a*), 1.1 (*b*), 1.2 (*c*), 1.3(*d*); *1* – start of income shock-wave, *2* – optic measure system spark, *3* – start of flow's destruction.

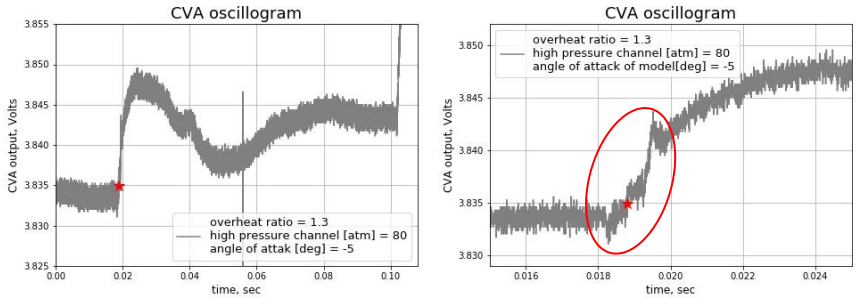

a *b*

Fig. 2. Oscillogram of CVA output voltage with pressure 80 atm in high-pressure channel and –5 degree for model's angle of attack.

Time scale 110 ms (*a*) and 10 ms (*b*); ★ – the same point, red oval – high-temperature area.

$$E_{out} = \left(1 + \frac{R_2}{R_1} + \frac{R_2}{R_w}\right) E_w \qquad (2)$$

where R_1, R_2 are parameters of the principal CVA scheme, E_w is probe's Voltage [1];

2) comparison of time scales for peculiar signal changes and already known time quantities;
3) comparison of peculiar signal changes with the results of numerical simulation for the Mach 8 flow in the Ludwig's shock wave facility UT-1M (TsAGI) (insight report);.
4) comparison with oscillograms acquired by constant-temperature anemometer CTA-2018 (CTA, developed in ITAM);
5) CVA and CTA output signal spectra comparison for steady-state flow from 20 ms to 40 ms since the shock-wave income.

Qualitative analysis has shown correct reaction of CVA to income flow and discovered high-temperature area in the forward of shock-wave that circled by red oval in the Fig. 2,*b*. Before, it was not taken into account during experiments in UT-1M facility, although it was predicted by numerical simulation. The quantitative analysis of results requires additional tests and measurements of additional parameters.

REFERENCE

1. **Kegerise M.A., Spina E.F.**, A comparative study of constant-voltage and constant-temperature hot-wire anemometers // Experiments in Fluids. 2000. № 29. P. 154–164.

DOI: 10.53954/9785604788967_48

AERODYNAMIC MODELS OF OUTFLOW OF PLANETARY ATMOSPHERES

N.V. Erkaev[1], K.D. Gorbunova[1,2]

[1]***Institute of Computational Modeling SB RAS***
660036, Krasnoyarsk, Russia

[2]***Siberian Federal University***
660041, Krasnoyarsk, Russia

The escape of atmospheric particles under the action of high-energy solar radiation is a key phenomenon that determines the structure and evolution of the atmospheres of the planets of the solar system, as well as exoplanets discovered in recent years. Therefore, the properties of the atmospheres of planets currently observed are closely related to the integral radiation flux received by the planet during its existence, and to the evolutionary path of its star. In the early stages of evolution, significant fluxes of extreme ultraviolet (EUV) and *X*-ray radiation from the host Star cause intense loss of planetary atmospheres. To study this process, a one-dimensional hydrodynamic model of the upper atmosphere is applied [1], based on solving the equations of conservation of mass, momentum, and energy flows for planets of various mass categories. The absorption of the EUV radiation leads to heating of the upper atmosphere, as well as to the dissociation and ionization of the atmospheric particles. As a result of heating, a radial outflow of atmospheric particles is formed. In this case, the most interesting and important process is that so called "blow-off" aerodynamic regime, in which the gas velocity monotonically increases to supersonic values with distance from the planet. In this formulation of the problem, there are three dimensionless similarity parameters $\lambda = G\, m\, M_p/(R_p\, kT_0)$, $a = \sigma_{\rm EUV}\, n_0\, R_p$, $q = \sigma_{EUV}\, J_{\rm EUV}\, R_{\rm p}\, m^{1/2}/(k\, T_0)^{3/2}$, where G is the gravitational constant, k is the Boltzmann constant, m is the mass of atmospheric particles, M_p and $R_{\rm p}$ are the mass and radius of the planet, T_0 and n_0 are the characteristic values of the temperature and density at the lower boundary of the atmosphere, $J_{\rm EUV}$ and $\sigma_{\rm EUV}$ are the intensity and absorption cross section for extreme ultraviolet radiation.

Numerical simulations were performed using a 4-th order compact MacCormack-type scheme [3]. Based on the calculations, the effect of similarity parameters on the mass flow rate was studied and the conditions for the blow-off flow regime were investigated. The gradients of the physical quantities (temperature, density, pressure) increase crucially with increasing parameter λ, which makes computational difficulties. The results were compared with those presented in [1, 2], which were obtained using the original MacCormack scheme. Our study reveals a significant advantage of the compact MacCormack-type scheme [3], which allows us to solve the problem considered above for large values of the parameter λ ($\lambda \geqslant 40$), while the scheme used in [1, 2] becomes unstable in this range of the parameter.

The figure shows the radial dependence of the temperature normalized to T_0 and the sonic Mach number for different λ parameters in the range from 30 to 80. The temperature typically has a non-monotonic variation with very steep rise in front of the maximum point, after which it decreases rapidly to the minimum value. The temperature peak is much higher for $\lambda = 80$ as compared to that for $\lambda = 30$.

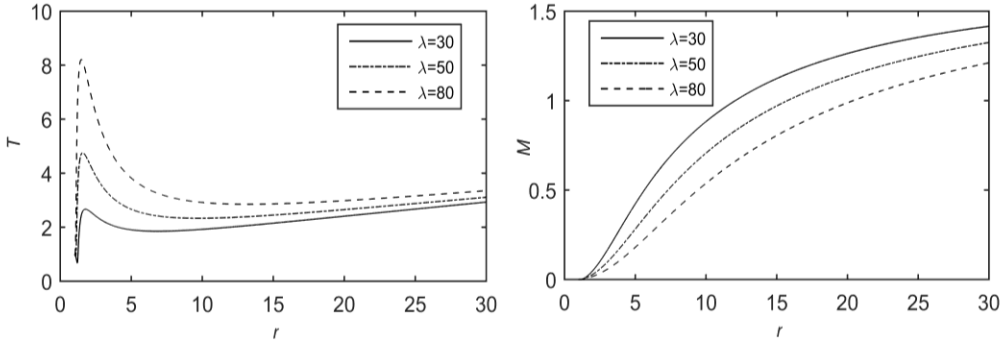

Temperature and Mach number as functions of the radial distance.

The temperature maximum, loss rate and sonic point radius for different values of the λ parameter

λ	20	30	40	50	60	70	80
T_{max}	2.84	2.93	3.69	4.76	5.88	7.04	8.21
L	3.53e-6	2.14e-6	1.50e-6	1.13e-6	7.63e-7	5.63e-7	4.19e-7
R_s	11	11.9	14	15.7	17.4	18.9	20.6

The Mach number is an increasing function of the radial distance, and the flow becomes supersonic at the upper boundary. But the critical sonic point, where M = 1, is located as farther, as larger the parameter λ.

The particular values for the maximum temperature (in units of T_0), the total loss rate (in units of $4\pi\ n_0\ (kT_0/m)^{1/2}\ R_p^2$) and the sonic point distance (in units of R_p) are presented in the table. The considered hydrodynamic escape model becomes inapplicable when the free path of the particles at the sonic point exceeds the characteristic length scale of the flow parameter. This can take place for very large λ parameters. In such cases the hydrodynamic solution has to be matched with the kinetic solution corresponding to the collisionless region at large distances.

REFERENCES

1. **Erkaev N.V., Lammer H., et al.** XUV exposed non-hydrostatic hydrogen-rich upper atmospheres of terrestrial planets. Part I: Atmospheric expansion and thermal escape // Astrobiology Journal. 2013. Vol. 13, No. 11. P. 1011–1029.
2. **Erkaev N.V., Lammer H., et al.** EUV-driven mass-loss of protoplanetary cores with hydrogendominated atmospheres: the influences of ionization and orbital distance // Monthly Notices of the Royal Astronomical Society. 2016. Vol. 460, No. 2. P. 1300–1309.
3. **Hixon R., Turkel E.**Compact Implicit MacCormack-Type Schemes with High Accuracy // Journal of Computational Physics. 2000. Vol. 158. P. 51–70.

DOI: 10.53954/9785604788967_50

MULTI-DISCHARGE ACTUATOR SYSTEM FOR SEPARATION CONTROL ON THE SWEPT WING MODEL

G.G. Gadzhimagomedov, A.P. Kuryachii, S.N. Tolkachev, D.S. Sboev

Central Aerohydrodynamic Institute
140180, Zhukovsky, Moscow region, Russia

The method of flow control in the boundary layer using volumetric forces caused by the action of an electric field on charged particles attracts quite a lot of attention from the scientific community [1–7]. This method provides high flexibility of parameter control and relative ease of integration into the structure of the aircraft.

TsAGI developed a design for a multi-discharge actuator system (MAS) operating on the principle of a dielectric barrier discharge (DBD), which makes it possible to generate a unidirectional air jet at a speed of up to 4 m/s in a resting environment when a voltage of 4.8 kV is applied. The electrode pitch was 6 mm. The high efficiency of pulse injection into the boundary layer makes it possible to consider MAS to suppress separation and, in the future, to improve the characteristics of aircraft flaps in takeoff and landing modes.

Experimental conditions. Separation control experiments were carried out in a subsonic wind tunnel equipped with an Eiffel chamber, TsAGI wind tunnel T-03. At the outlet of the nozzle, a jet core 580 mm wide and 370 mm high is formed. Several regimes were chosen according to the freestream velocity V_0: 8, 18 and 36 m/s. The turbulence level Tu was not measured, but 0.35% is typical for this setup.

A swept plate with a thickness of 15 mm was chosen as an experimental model. The leading and trailing edges of the model are cylindrical with a radius of 7.5 mm. The sweep angle of the plate is 35°.

To create a positive pressure gradient, a displacement body made of an Eppler E662 profile was used, set at a negative angle of attack of –12.4°. To stabilize the separation (so that separation occurs from the plate, and not from the displacement body), a slat was located in front of the displacement body. The model together with the displacement body and the slat were installed at a sweep angle of 35°.

Velocity distribution over the model surface and in the boundary layer was measured using particle image velocimetry (PIV). Using a pitot comb located at a distance of 30 mm from the trailing edge of the model, the distribution of the total pressure in the wake behind the model was measured and the integral pressure losses were estimated.

Results. In the study of regimes using an increased voltage (7–8 kV), a displacement of the separation point downstream was observed. Increasing the speed reduces the distance the separation point moves.

It was more convenient and clearer to track the integral effect of the MAS on the flow from the results obtained using the Pitot comb: the total pressure loss decreases simultaneously with a decrease in cross-section size of the wake behind the model. As the flow velocity increases, the relative contribution made by the actuator decreases. As an integral value characterizing the effect of the actuator on the flow, the specific force f (dimension N/m) is chosen, which is determined by the following formula (1):

$$f = \int_{-12.5}^{Y_s} (P - P_{\text{tot}})\ dY \tag{1}$$

where P is the pressure measured by the total pressure comb, P_{tot} is the total pressure in the control section of the WT outlet nozzle, Y_s is the position on the comb corresponding to the velocity defect created by the slat.

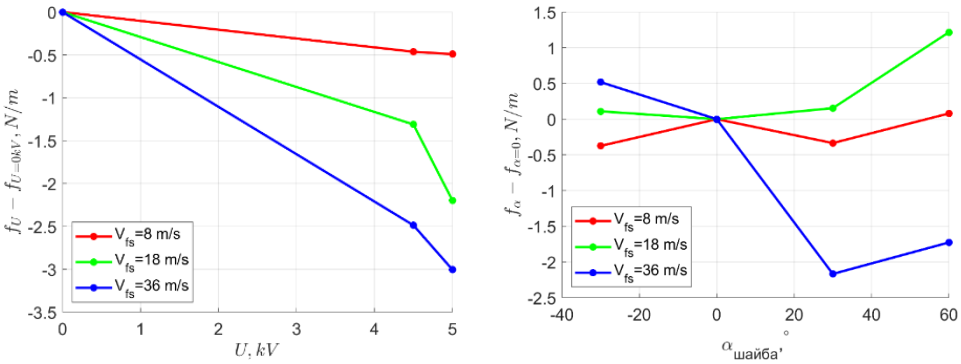

Fig. 1 Change in the specific force under the influence of MAS on the applied voltage (left) and on the angle of rotation of the insert with the actuator when a voltage of 5 kV is applied (right).

The results of measuring the average force depending on the applied voltage and on the rotation of the insert with the actuator are shown in Fig. 1. With an increase in the voltage across the actuator, the pressure loss decreases, and this is typical for the entire investigated range of speeds. In most of the modes, the maximum efficiency of the actuator is achieved when turning by +30°.

Acknowledgments. The work is prepared in the implementation of the program for the creation and development of the World-Class Research Center “Supersonic” for 2020-2025 funded by the Ministry of Science and Higher Education of the Russian Federation (Grant agreement of December, 8, 2020 № 075-11-2020-023).

REFERENCES

1. **Moreau E.** Airflow control by non-thermal plasma actuators // Journal of Physics D: Applied Physics. 2007. Vol. 40, № 3.
2. **Cattafesta L.N., Sheplak M.** Actuators for active flow control // Annual Review of Fluid Mechanics. 2011. Vol. 43.
3. **Corke T.C., Post M.L., Orlov D.M.** SDBD plasma enhanced aerodynamics: concepts, optimization and applications // Progress in Aerospace Sciences. 2007. Vol. 43, № 7–8.
4. **Wang J.J**. et al. Recent developments in DBD plasma flow control // Progress in Aerospace Sciences. 2013. Vol. 62.
5. **Benard N., Moreau E.** Electrical and mechanical characteristics of surface AC dielectric barrier discharge plasma actuators applied to airflow control // Experiments in Fluids. 2014. Vol. 55. Art. 1846. 43 p. DOI 10.1007/s00348-014-1846-x
6. **Kriegseis J., Simon B., Grundmann S.** Towards In-Flight Applications? A Review on Dielectric Barrier Discharge-Based Boundary-Layer Control // Applied Mechanics Reviews. 2016. Vol. 68, № 2.
7. **Corke T.C., Enloe C.L., Wilkinson S.P.** Dielectric barrier discharge plasma actuators for flow control // Annual Review of Fluid Mechanics. 2010. Vol. 42.

DOI: 10.53954/9785604788967_52

MODELING OF THE BOUNDARY LAYER STABILITY PROBLEM WITH A DIFFUSION FLAME

S.A. Gaponov

Khristianovich Institute of Theoretical and Applied Mechanics SB RAS
630090, Novosibirsk, Russia

Initial studies of the laminar flows stability in the presence of a diffusion flame were performed for fuel-oxidizer mixing layers or when a fuel jet was fed to the oxidizer, and the problem was solved in neglecting viscosity in the stability equations. Detailed information on such works can be found in the review [1]. To date, there are no studies on the stability of the boundary layer during combustion of fuel fed through a permeable surface and combusted in the oxidizer flow.

The presence of a diffusion flame leads to internal heat release and changes in the mixture composition, the density depends on both the temperature and the composition of the gas mixture. In addition, when fuel is fed through a porous wall streamlined with an oxidizer, an important factor affecting the stability of the boundary layer is related to gas injection.

In [2], by the example of the problem on the stability of the boundary layer of a dissociating gas, it was first shown that its stability weakly depends on perturbations of the heat source and the formation rates. The weak influence of these perturbations is related to the fact that their corresponding terms included in the stability equations are inversely proportional to the Reynolds number [3] and have the same influence as the terms related to the non-parallel flow in the boundary layer. In the parallel unperturbed flow approximation, the system of stability equations depends on the distributions of the basic velocity, concentrations of different substances, temperature, and density. In many cases, for example, during combustion of hydrocarbon fuels in an air flow, the gas density depends mainly on the temperature. The molecular mass of the mixture changes insignificantly along the boundary layer [4], its change can be neglected, and the density can be assumed to be inversely proportional to temperature, as it is often used in problems of stability of diffusion flames.

The paper shows that for a constant molecular mass of the gas mixture, the boundary layer stability problem with diffusion combustion is reduced to the standard boundary layer stability problem for a single-component gas with internal heat supply and blowing gas through a porous wall. Stability calculations have been performed for both subsonic and supersonic flow around the plate.

Rationale of the model. The formulation of the problem is based on the Dana – Lin equations, supplemented by equations for perturbations of concentrations of substances in the mixture. If diffusion coefficients of different gases are the same and molecular mass changes weakly along the boundary layer, the density perturbation does not depend on concentration perturbations and is determined only by pressure and temperature perturbations, as in the case of one-component gas. The stability problem is no different from the stability problem for the boundary layer of a one-component gas with internal heating and gas injection affecting the parameters of the unperturbed boundary layer.

If the diffusion coefficients of different gases are not identical, the problem is reduced to the problem about the stability of the boundary layer of a single-component gas up to terms of the order of $(\alpha \mathrm{Re})^{-2/3}$, where α — wave number of perturbation wave, Re — Reynolds number. Based on the experimental temperature distribution in the boundary layer with diffusion combustion, the law of internal heat input is proposed, $Q \sim \exp[-a(u-u_f)^2]$, and the amplification rates of perturbation growth depending on the intensity of gas injection are calculated.

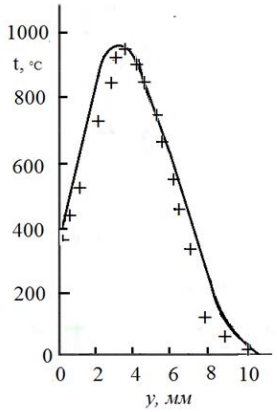

Fig. 1.

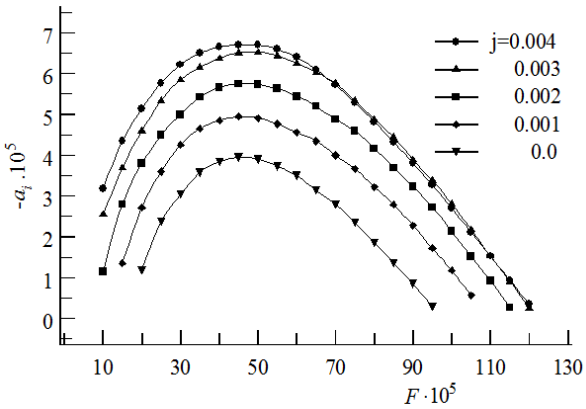

Fig. 2.

Figure 1 shows the experimental [5] (icons) and the temperature inside the boundary layer at subsonic velocity calculated using the necessary heat input into the one-component boundary layer.

Figure 2 shows the spatial rates amplification of disturbances depending on the frequency parameter $F = 2\pi f u_e^2 / \nu_e$, where f — frequency in Hz, u_e, ν_e — speed and kinematic viscosity outside the boundary layer at different values of mass flow, *j*, through the wall. .

The main conclusion of the research is to substantiate the possibility of reducing the stability problem of the boundary layer with diffusion combustion to the stability of the boundary layer of a single-component gas.

The study was supported by grant of Russian Science Foundation No. 22-21-00017, https://rscf.ru/project/22-21-00017/.

REFERENCES

1. **Jackson T.L.** Stability of Laminar Diffusion Flames in Compressible Mixing Layers // Major Research Topics in Combustion / Eds M.Y. Hussaini, A. Kumar, R.G. Voigt. ICASE/NASA LaRC Series. New York: Springer, 1992. P. 131–161. https://doi.org/10.1007/978-1-4612-2884-4_8 .
2. **Petrov G.V**. Dissociation Influence on Boundary Layer Stability // Development of Perturbations in the Boundary Layer. Novosibirs, 1979. P. 104–117.
3. **Gaponov S.A., Petrov G.V.** Stability of boundary layer of non-equilibrium dissociating gas. Novosibirsk: Nauka, 2013. 95 p.
4. **Lukashov V.V., Terekhov V.V., Terekhov V.I.** Near-Wall Flows of Chemical Reactants: A Review of the Current Status of the Problem // Combustion, Explosion, and Shock Waves. 2015. Vol. 51, No. 2. P. 160–172. http://dx.doi.org/10.1134/S0010508215020033
5. **Volchkov E.P., Lukashov V.V., Terekhov V.V., Hanjalic K.** Characterization of the flame blow-off conditions in a laminar boundary layer with hydrogen injection // Combustion and Flame. 2013. Vol. 160. P. 1999–2008. DOI:10.1016/j.combustflame.2013.04.004

DOI: 10.53954/9785604788967_54

DEVELOPMENT OF TURBULENCE MODELS FOR CHANNEL FLOWS USING TENSOR-BASIS MACHINE LEARNING TECHNIQUES

S.S. Garmaev[1,2], R.I. Mullyadzhanov[1], S.N. Yakovenko[1,2]

[1]*Novosibirsk State University*
Novosibirsk 630090, Russia

[2]*Khristianovich Institute of Theoretical and Applied Mechanics SB RAS*
Novosibirsk 630090, Russia

The Reynolds-averaged Navier – Stokes (RANS) equation models are widely used in industry to predict turbulent flows, due to its computational efficiency. However, these models are less accuracy in comparison to direct numerical simulation (DNS) or large eddy simulation (LES), which require huge computing resources so are still unsuitable for applications. As shown recently [1], machine-learning (ML) tools can be implemented to enhance the Reynolds-stress approximations using high-fidelity data of DNS, LES or measurement as a reference.

The present study compares ML methods for the Reynolds-stress anisotropy (RSA) prediction using the available DNS channel-flow data at various Reynolds numbers [2–4]. These techniques include tensor-basis neural network (TBNN) [5], tensor-basis random forest (TBRF) [6] proposed earlier, and the gradient boosting method with a similar tensor basis (TBGB) [7].

As the first case, a flow between parallel walls is considered at different Reynolds numbers $\mathrm{Re}_\tau = u_\tau d/\nu$ based on the skin friction velocity u_τ and the channel half-height d. In this case, the mean velocity U directed along x depends on wall-normal coordinate y only. Runs are done by OpenFOAM, with the simpleFoam solver, using the k-ω turbulence model. The first option for RSA is the Boussinesq model (BM) $b_{ij} = -(0.09/\omega)S_{ij}$ where $S_{ij} = (1/2)\cdot(\partial U_i/\partial x_j + \partial U_j/\partial x_i)$ is the strain tensor, U_i is the mean-velocity vector. The RSA tensor $b_{ij} \equiv a_{ij}/(2k) \equiv \tau_{ij}/(2k) - (1/3)\delta_{ij}$ includes the turbulent kinetic energy k and the Reynolds-stress tensor τ_{ij}. The second option is to predict the RSA tensor distribution after ML training, remove spurious oscillations by Gaussian filters and insert b_{ij} into the RANS solver to get the new fields of $U(y)$ and $k(y)$. The predicted profiles of $b_{ij}(y)$ allow us [7] to improve their behaviors to be closer to the reference DNS data.

Propagation of new b_{ij} into the RANS solver yields in fact under-estimation of the shear Reynolds stress $\tau_{12} = a_{12} = 2kb_{12}$ near the wall, and corresponding under-estimation of gradient $\partial U/\partial y$ and value $U(y)$ itself. This can occur due to under-estimation of k at $y/d < 0.5$ in runs by the k–ω model [8]. It is fixed using the dimensional tensor (a_{ij}) instead of the non-dimensional one (b_{ij}) for ML training. In such a case, the remaining under-estimation of k does not affect the velocity distribution. Another difficulty is deviation and spurios wiggles appearing if one inserts the only distribution $(a_{ij})^{\mathrm{ML}}$ from ML training into τ_{ij} in a RANS solver. Due to suggestion of [6], we avoid this by mutual insertion of $(a_{ij})^{\mathrm{ML}}$, adding the baseline BM distribution of $(a_{ij})^{\mathrm{BM}}$, as $\tau_{ij} = (2/3)\delta_{ij} + (1-\gamma)(a_{ij})^{\mathrm{BM}} + \gamma(a_{ij})^{\mathrm{ML}}$ where γ gradually grows from 0 to 0.8 with iterations.

The RSA components produced from DNS, baseline RANS and three ML techniques show (Fig. 1) that TBRF gives closer agreements to the benchmark DNS solution, so it is used for the further insertion into the RANS solver and called as RANS+ML. The resulting velocity distribution for RANS+ML in near-wall areas becomes closer to that for DNS than the baseline RANS solution (Fig. 2). For comparison, RANS+DNS results where the τ_{ij} values inserted into the solver are taken directly from the DNS data are shown too to be close to RANS+ML curves.

Next, we apply ML tools in 2D flows in square duct, channels with bumps, and for the turbulent-scalar-flux model enhancement in scalar (temperature, concentration) transfer cases.

The research was carried out within the state assignment of Ministry of Science and Higher Education of the Russian Federation (project No. 121030500149-8).

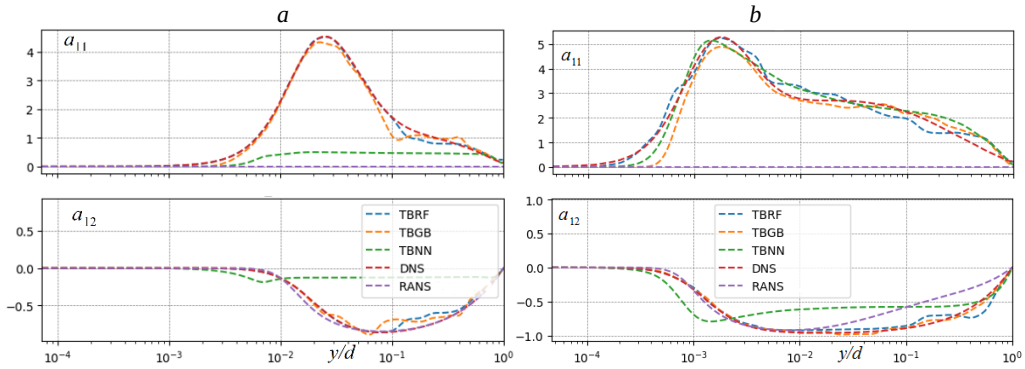

Fig. 1. Predicted RSA components a_{11} and a_{12} after training at Re_τ = 180, 395, 950, 1000, 2000 and 5200: interpolation and extrapolation abilities of the ML algorithms, respectively, at Re_τ = 550 (*a*) and 8000 (*b*).

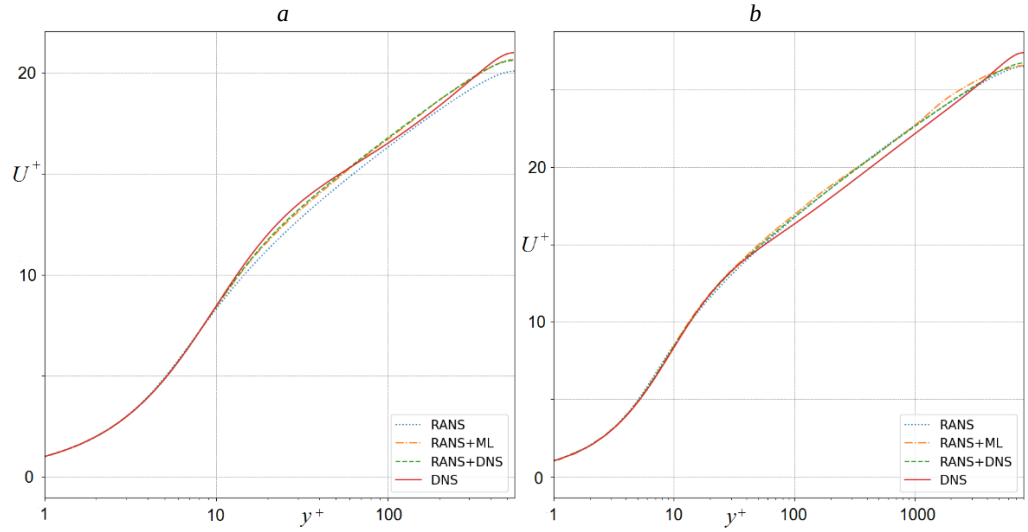

Fig. 2. Mean velocity profiles at Re_τ = 550 (*a*) and 8000 (*b*) where $U^+ = U/u_\tau$ and $y^+ = u_\tau y/\nu$.

REFERENCES

1. **Duraisamy K., Iaccarino G., Xiao H.** Turbulence modeling in the age of data // Annu. Rev. Fluid Mech. 2019. Vol. 51. P. 357–377.
2. **Kim J., Moin P., Moser R.** Turbulence statistics in fully developed channel flow at low Reynolds number // J. Fluid Mech. 1987. Vol. 177. P. 133–166.
3. **Lee M., Moser R.D.** Direct numerical simulation of turbulent channel flow up to $\mathrm{Re}_\tau \approx 5200$ // J. Fluid Mech. 2015. Vol. 774. P. 395–415.
4. **Yamamoto Y., Tsuji Y.** Numerical evidence of logarithmic regions in channel flow at Re_τ = 8000 // Phys. Rev. Fluids. 2018. Vol. 3. Art. 012602(R). 10 p. URL: https://journals.aps.org/prfluids/pdf/10.1103/PhysRevFluids.3.012602
5. **Ling J., Kurzawski A., Templeton J.** Reynolds averaged turbulence modelling using deep neural networks with embedded invariance // J. Fluid Mech. 2016. Vol. 807. P. 155–166.
6. **Kaandorp M., Dwight R.P.** Data-driven modelling of the Reynolds stress tensor using random forests with invariance // Comput. Fluids. 2020. Vol. 202. Art. 104497. P. 1–16.
7. **Garmaev S.S., Yakovenko S.N.** Enhancement of turbulence models using machine-learning methods // XXXVII Siberian Thermophysical Seminar (Novosibirsk, Russia, September 14–16, 2021): Abstracts. Novosibirsk, 2021. P. 9. (in Russian)
8. **Hedlund A.** Evaluation of RANS turbulence models for the simulation of channel flow: Technical report IT 14 072 / Uppsala Universitet. Uppsala, 2014. 26 p.

DOI: 10.53954/9785604788967_56

EQUIVALENCE CRITERION FOR A PROBLEM OF WAVE DRAG REDUCTION OF BODIES IN SUPERSONIC FLOW BY "THERMAL SPIKE"

P.Yu. Georgievskiy, V.A. Levin

Institute of Mechanics of Moscow State University
119192, Moscow, Russia

Previously, it was underlined [1] that the effect of wave drag reduction of bodies in the presence of an energy deposition region localized upstream is basically the result of formation of front separation zones due to the interaction of a high-temperature wake with a bow shock wave and a shock layer behind it. According to [2], the shape of isobaric separation zone is determined by the transverse distribution of local Mach numbers in the wake, whereas the pressure inside it is equal to a total pressure behind the normal shock in the wake. The effect does not depend on the thickness of the wake, which underlies the "thermal spike" conception [3].

In this paper we study the influence of Mach number of the supersonic flow M_0, the size of the energy deposition region, and the input power on the formation of front separation zones and the efficiency of wave drag reduction of bodies.

Euler equations were used in numerical simulation to describe unsteady flows of an ideal perfect gas with axial symmetry. The energy input was specified as a source on the right side of the energy equation with a Gaussian spatial distribution of specific power.

$$Q = Q_0(t)\exp(-(r/\Delta r(t))^2 - ((z - z_0)/\Delta z(t))^2)\,.$$

A physical equivalence criterion is formulated that provides an effective wave drag reduction of bodies: the intensity of the energy input Q_0 should be in inverse proportion to the longitudinal size of the energy source Δz and in direct proportion to the Mach number M_0 of the flow.

$$Q_0\Delta z/M_0 = \text{const.} \qquad (1)$$

The condition (1) means that every liquid particle during its movement through the energy deposition region receives approximately the same amount of heat. It has been established that when (1) is fulfilled, the power factor of the energy input $\xi = W/H$ (the ratio of the supplied power to the enthalpy flux of the incident flow through the cross section Δr of the energy deposition region) is preserved. In addition, despite the fact that at different Mach numbers of the incident flow, the flow regimes past energy sources differ significantly, the distributions in the transverse direction of the density and relative Mach number in the far high-temperature wake coincide not only qualitatively, but also quantitatively (Fig. 1).

This result is of significant importance from the point of view of wave drag reduction of bodies, since the geometry of the front separation zones is determined precisely by the transverse distribution of local Mach numbers in the wake [2]. To exclude the occurrence of flow pulsations of the front separation zones, which are typical for energy sources of very small size, the method of quasi-stationary transformation of the energy deposition region [3] was used (the energy source size decreased according to (1) in the simulation process). It is shown that, despite the significantly different flow patterns in general, at different Mach numbers of the upstream flow, quasi-stationary front separation zones of approximately the same geometric shape are formed (Fig. 2), so that $\Delta c_x = \text{const}$. In the share layer at the boundary of the separation zones, the Kelvin-Helmholtz instability develops, which manifests itself in the formation of vortex structures, but does not lead to the destruction of the separation zones.

A simple formula for the wave drag reduction efficiency coefficient $\eta = V_0\Delta F_x/W$ (defined as the ratio of saved and input power) has been proposed and verified in numerical simulation.

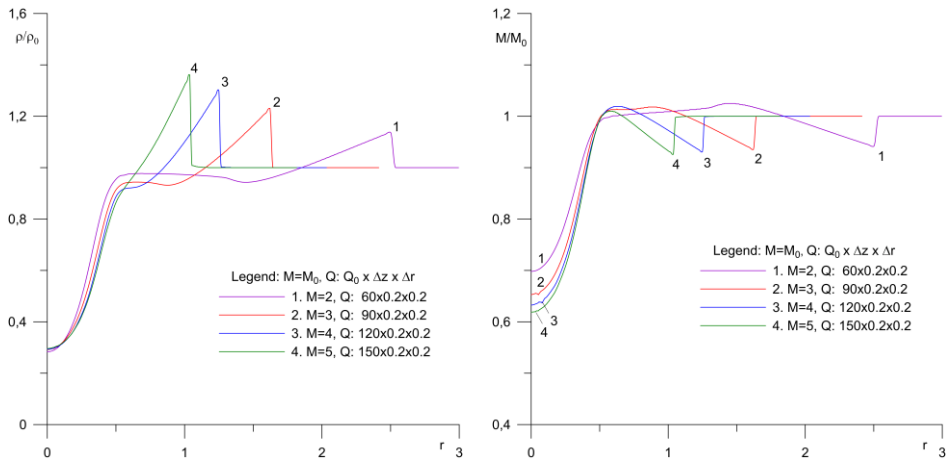

Fig. 1 Transverse distributions of density (left) and relative local Mach number (right) in the far high-temperature wake for various Mach numbers of the flow.

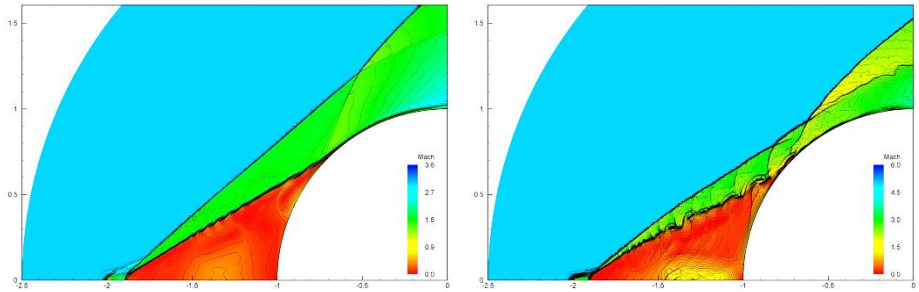

a) $M_0 = 3$ b) $M_0 = 5$

Fig. 2 Front separation zones at different Mach numbers of the incident flow for a spherical energy source $\Delta r = 0.02$ (distributions of local Mach numbers are shown).

$$\eta = (\gamma - 1)M_0^2\,\Delta c_x / 2\xi\Delta r^2. \qquad (2)$$

According to (2), since under condition (1) Δc_x and ξ do not change, the efficiency coefficient is proportional to the Mach number of the oncoming flow squared and the ratio of the mid-section areas of the body and the energy deposition region (that is $1/\Delta r$ squared). The calculations observed a decrease in the wave resistance of a blunt body (sphere) 35%, and the efficiency coefficient at a Mach number of 5 exceeded 1000 ("thermal spike" radius was $\Delta r = 0.02$).

The investigation was performed in accordance with the research plan of the Institute of Mechanics of Moscow State University with the financial support of the Russian Science Foundation (project 21-11-00307).

REFERENCES

1. **Georgievskii P.Yu., Levin V.A.** Control of the Flow past Bodies Using Localized Energy Addition to the Supersonic Oncoming Flow // Fluid Dynamics. 2003. Vol. 38, No. 5. P. 154–167.
2. **Guvernyuk S.V., Savinov K.G.** Isobaric Separation Structures in Supersonic Flows with a Localized Inhomogeneity // Doklady Physics. 2007. Vol. 52, No. 3. P. 151–155.
3. **Georgievskiy P.Yu., Levin V.A.** Front Separation Regions Control by the Upstream Energy Deposition // International Conference on Methods of Aerophysical Research: Proc. Pt. IV, Novosibirsk: Parallel, 2007. P. 35–42.

DOI: 10.53954/9785604788967_58

NUMERICAL SIMULATION OF THE GÖRTLER VORTEX DEVELOPMENT IN A COMPRESSIBLE BOUNDARY LAYER ON A CONE WITH CONCAVE SURFACE

T.A. Gimon, V.A. Kislovskiy, S.V. Lukashevich, S.O. Morozov, M.S. Nikolaev, A.N. Shiplyuk

Khristianovich Institute of Theoretical and Applied Mechanics SB RAS
630090, Novosibirsk, Russia

One of the most acute high-speed vehicles problems is the large heat presence fluxes to the surface leading to its destruction. In a turbulent boundary layer, heat fluxes are four or more times higher than in a laminar one; therefore, in order to create high-speed vehicles, it is necessary to be able to predict and control the position of the laminar-turbulent transition (LTT) of the boundary layer [1, 2]. At present, there are computational models that make it possible to predict with sufficient accuracy the magnitude of the heat flux, both in laminar and turbulent flows. However, the existing methods for predicting the position of the LTT do not have sufficient reliability. To develop methods for predicting the position of an LTT in a compressible boundary layer, a numerical simulation of the development of Görtler vortices on the surface of a cone with a concave surface was studied.

To test the introducing method artificial perturbations into a compressible boundary layer by periodic blowing/suction on the model surface, numerical simulations were carried out using the Fluent program of the ANSYS package. The calculation was carried out on a model with L_1 = 0.15 m; R = 1.5 m; a = 10°; b = 4° at M_∞ = 5.8; $Re_{1\infty} \approx 22 \cdot 10^6$ m^{-1}; T_0 = 386 K; T_w = 295 K. A three-dimensional computational domain was considered (Fig. 1).

In Fig. 2 shows the dependence of the disturbance amplitude in the boundary layer on the longitudinal coordinate of the model surface. For the calculations results in the framework of the stability linear theory, the perturbations amplitude was obtained as $A_{lst} = A_{dns}(x_w = 0.2\text{ m}) \cdot eN$.

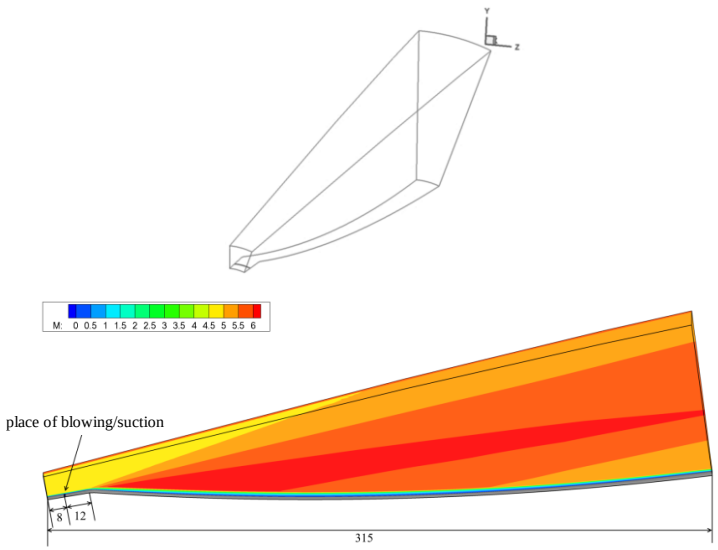

Fig. 1. Calculation area (top) and Mach number contours (bottom).
Dimensions: L_1 = 0.15 m; R = 1.5 m; a = 10°; b = 4°.

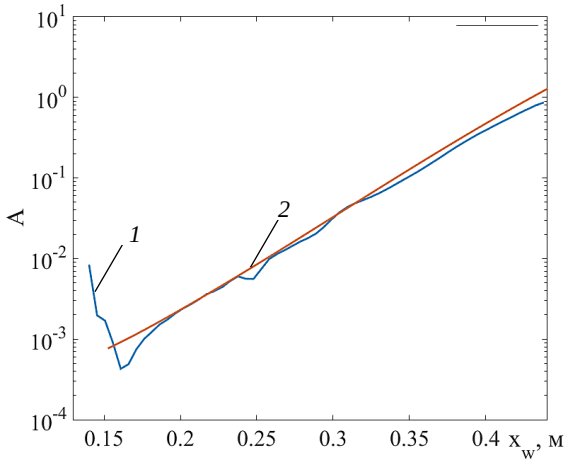

Fig. 2. Dependence of the amplitude of Görtler vortices with $n_\lambda = 36$ on the coordinate longitudinal to the surface.

1 – DNS, *2* – LST; $L_1 = 0.15$ m; $R = 1.5$ m; $a = 10°$; $b = 4°$.

It can be seen that in direct numerical simulation, the generated perturbation decays on the straight and convex parts of the model, while the perturbation grows on the concave part. The dependences of the perturbation amplitude obtained in the framework of the linear stability theory (LST) and those obtained by direct numerical simulation (DNS) on a concave surface practically coincide at $x_w > 0.2$ m. The amplit ude fluctuations obtained in DNS calculations at $x_w > 0.2$ m must be further analyzed. On a concave surface at $x_w < 0.2$ m, disturbances do not grow exponentially.

The work was supported by the RSF grant 21-19-00393.

REFERENCES

1. **Anderson B.P., Campbell C.H., Saucedo L.A., Kinder G.R., Berger K.T.** Boundary Layer Transition Flight Experiment overview and in-situ measurements // 48th AIAA Aerospace Sciences Meeting Including the New Horizons Forum and Aerospace Exposition (Orlando, Florida, USA, 4–7 January, 2010): AIAA 2010-240. 28 p. DOI:10.2514/6.2010-240.
2. **Gülhan A., Neeb D., Thiele T., Siebe F.** Aerothermal postflight analysis of the sharp edge flight experiment-II // Journal of Spacecraft and Rockets. 2016. Vol. 53, No. 1. P. 153–177.

DOI: 10.53954/9785604788967_60

INVESTIGATION OF THE EFFECT OF LIGHT GAS INJECTION ON THE LAMINAR-TURBULENT TRANSITION IN A BOUNDARY LAYER ON A CONE WITH CONCAVE SURFACE

T.A. Gimon, S.V. Lukashevich, S.O. Morozov, A.N. Shiplyuk

Khristianovich Institute of Theoretical and Applied Mechanics SB RAS
630090, Novosibirsk, Russia

The laminar-turbulent transition of a compressible boundary layer on concave surfaces can occur due to the growth of disturbances – Görtler vortices, the first and second Mack modes. It was shown within the framework of the linear stability theory that local surface heating [1] or local injection of a light gas [2] leads to a decrease in the growth rate of Görtler vortices and the first Mack mode on the concave nozzle surface. This work is devoted to an experimental study of the influence of local light gas injection on the laminar-turbulent transition of a compressible boundary layer on a concave surface.

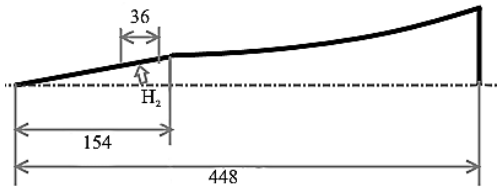

Fig. 1. Scheme of the experimental model. Dimensions in mm.

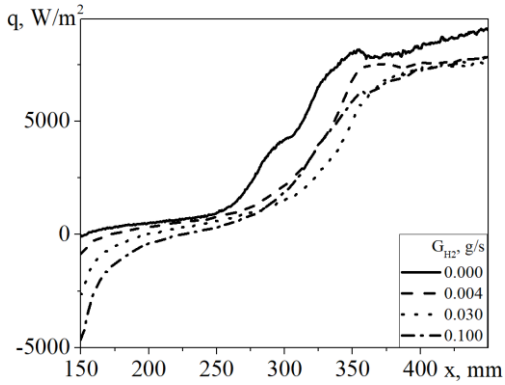

Fig. 2. The heat flux on the concave surface of the model vs. longitudinal coordinate x for various values of the mass flow rate of hydrogen.

The model for experimental studies is a cone, part of which has a concave surface (Fig. 1). The study was carried out at the free stream Mach number M = 5.8 and the stagnation temperature T_0 = 375–390 K. Hydrogen was used as a light gas at a flow rate G_{H2} = 0.004; 0.03; 0.11 g/s. It is shown that the local hydrogen injection leads to a shift in the laminar-turbulent transition position of the boundary layer downstream (Fig. 2). A non-monotonic dependence of the transition position on the mass flow rate of hydrogen is obtained. A comparison of the results of experiments and calculations within the framework of the linear theory of stability showed that, when a certain value of the hydrogen flow rate is exceeded, the transition is determined by the second mode of perturbations, and not by Görtler vortices, as in the case of the absence of injected gas.

The research was supported by the Russian Science Foundation (project No. 21-19-00393).

REFERENCES

1. **Morozov S.O., Shiplyuk A.N.** Investigation of the influence of a local change in surface temperature on the laminar boundary layer stability in a hypersonic nozzle // Thermophysics and Aeromechanics. 2020. Vol.27, No. 5. P. 633–642.
2. **Morozov S.O., Shiplyuk A.N.** Stability of the boundary layer of contoured M = 6 Nozzle with local foreign gas injection // XVII All-Russian Seminar with international participation “Dynamics of Multiphase Media” (Novosibirsk, 27 Aug. – 4 Sept. 2021): abstracts. Novosibirsk, 2021. P. 92 (in Russian)..

DOI: 10.53954/9785604788967_61

THE DEVELOPMENT OF A SMALL UNSTEADY DISTURBANCES SOURCE FOR INVESTIGATION OF GÖRTLER VORTICHES IN A COMPRESSIBLE BOUNDARY LAYER

T.A. Gimon[1], A.D. Zhelonkin[1,2], D.A. Elistratov[1,2], S.O. Morozov[1], S.V. Lukashevich[1]

[1]*Khristianovich Institute of Theoretical and Applied Mechanics SB RAS*
630090, Novosibirsk, Russia

[2]*Novosibirsk State Technical University*
630073, Novosibirsk, Russia

The study of the laminar-turbulent transition in the boundary layer is an urgent task [1]. For small initial disturbances, the laminar-turbulent transition consists of three stages: the receptivity of the boundary layer to various kinds of disturbances, linear growth, and nonlinear growth with a transition to turbulence [2]. In the case of the curvature of streamlines on concave surfaces, the boundary layers will be unstable with respect to Görtler vortices.

Generation of disturbances in experimental studies that, under conditions of Görtler instability, will lead to the appearance of Görtler vortices is major task. For this, various methods of generating stationary disturbances are used, such as surface roughness or the introduction of disturbances of flow parameters [3]. In [2], a method for generating non-stationary disturbances was developed, which consists in creating blowing/suction-type flow disturbances on a streamlined surface with a frequency not exceeding 10 Hz. To conduct research under conditions of a high-velocity boundary layer, a source of small non-stationary disturbances is required, which is capable of providing periodic blowing/suction on the model surface with a frequency of up to 1 kHz.

The source will be made in the form of a closed volume, connected by channels to the surface of the model, one of the walls of which is a flexible membrane with a piezoelectric element. When a sinusoidal voltage is applied to the piezoelectric element, the membrane begins to oscillate, periodically blowing and sucking in a certain amount of air through channels perpendicular to the surface of the model.

To estimate the realizable speed of the jets near the surface of the model, the amplitude of the oscillation of the piezoelectric element was measured and the volume flow rate of the displaced air was calculated. The measurements were carried out using an optoNCDT 1605 Micro-

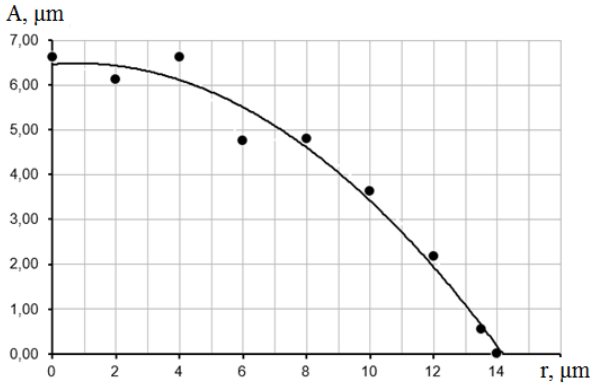

The distribution of the amplitude of the membrane vibrations vs the radius.

Epsilon laser sensor with a measurement range of ± 0.25 mm. An example of measuring the distribution of the oscillation amplitude along the membrane radius for a voltage amplitude of 2.2 V on the piezoelectric element is shown in the figure. For a voltage amplitude on the piezoelectric element of 10 V, an average air volume flow rate of 43.6 10^{-4} m^3/s was obtained, which, with a total area of all holes of 30 mm^2, will provide a jet velocity amplitude of 1.5 m/s at an oscillation frequency of 1 kHz.

The study was supported by the Russian Science Foundation grant No. 21-19-00393.

REFERENCES

1. **Boiko A.V., Ivanov A.V., Kachanov Y.S., Mischenko D.A.** Steady and unsteady Görtler boundary-layer instability on concave wall // Eur. J. Mech. B/Fluids. 2010. Vol. 29. P. 61–83.
2. **Boiko A.V., Ivanov A.V., Kachanov Y.S., Mischenko D.A.** Investigation of weakly-nonlinear development of unsteady Görtler vortices // Thermophysics and Aeromechanics. 2010. Vol. 17, No. 4. P. 455–481.
3. **Gimon T.A. Lukashevich S.V., Morozov S.O., Shiplyuk A.N.** Methods of experimental investigation of the Görtler instability in boundary layers: review // Thermophysics and Aeromechanics. 2022. Vol. 29, No. 2. P. 159–174.

DOI: 10.53954/9785604788967_63

OSCILLATINGLY-PULSATORY MODE OF THE FLOW OVER AN AIR INTAKE TESTED IN A HOT-SHOT WIND TUNNEL

Y.P. Gounko, I.N. Kavun

Khristianovich Institute of Theoretical and Applied Mechanics SB RAS
630090, Novosibirsk, Russia

The development of flow regimes around an axisymmetric internal-compression air intake tested in the electric-discharge impulse wind tunnel IT-301 [1, 2] is considered, the tunnel was arranged with a conical nozzle and designed for the operating flow Mach number M = 8. In [3, 4], there were studied numerically the unsteady flows forming in the joint processes of starting the wind tunnel and the air intake; the features of the formation of a pseudo-steady flow regime of the intake being in a started mode was determined. Now new numerical computations have been performed, they concern with changing in the flow regimes around the started air intake when the test lasting increased up to a subsequent destruction of the flow around the air intake and its transition to the flow mode corresponding to the un-started intake with a bow shock wave at the intake entrance. The numerical study was carried out similarly to [3, 4], the Reynolds-averaged Navier-Stokes equations and the SST *k*–ω turbulence model were used for calculations of the unsteady flows. The initiation of the flow in the wind tunnel was modeled as the disintegration of a gas-dynamic discontinuity corresponding to the diaphragm destruction at the exit from a forchamber, initial pressure and temperature $P_{ch} = 8.11 \cdot 10^7$ Pa, $T_{ch} = 1000$ K in it were accepted.

According to the data of [3, 4], the operating pseudo-steady flow regime at the nozzle outlet reached after its starting at $\tau > 787$ μs and is characterized by an almost constant Mach number $M_n = 7.45$ (±1%) therewith there are pressure fluctuations with an amplitude onto 25% and a frequency of about 300 Hz. The latter corresponds, with a time shift, to fluctuations in the gas parameters in the forchamber. The pseudo-steady flow around the air intake in the started flow mode in terms of the Mach number is achieved at $\tau > 950$ μs. At that time, the flow Mach number at the air intake entrance is $M_{inl} = 8.175$ (±0.1%), the unit Reynolds number decreases by 14 % (from $Re_1 = 2.19 \cdot 10^7$ [1/m] at $\tau = 1300$ μs up to $1.89 \cdot 10^7$ [1/m], $\tau = 5200$ μs). An example of such a flow picture is presented in Fig. 1,*a*, $\tau = 1302$ μs. In the inner duct of the air intake, a system of quasi-conical shock waves converging towards the axis and "illusory" regularly reflected from the axis is formed. Local separations of the boundary layer on the channel wall are not observed. The boundary layer in the outlet section occupies near the wall an annual area with a relative thickness $\delta/R \approx 0.5$.

Further evolution of the intake flow structure is related to development of the boundary layer and its separations with decreasing in the Reynolds numbers Re_1.

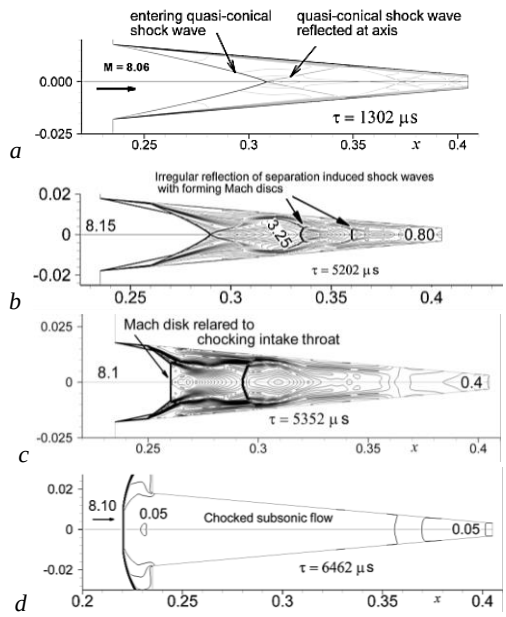

Fig. 1. Change in inlet flow pictures (in the form of Mach number isolines for a number time).

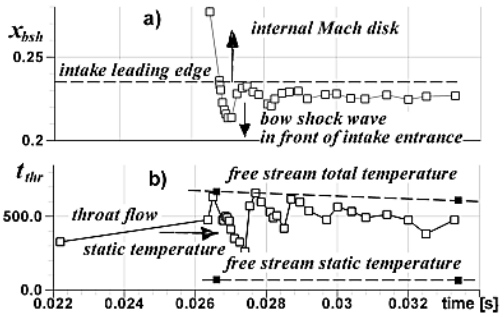

Fig. 2. Bow shock wave position (*a*), flow static temperature at the outlet throat (*b*).

Already at τ = 2000 μs, local small separations of the boundary layer appear on the duct wall at the point where the first internal shock wave reflected from the axis hit the wall and where that shock wave hit the wall which arises as latest reflected from the axis before the intake duct exit. Changes in the structure of the internal flow take place as shown in Fig. 1,*b*,*c*,*d* for a number of fixed times. The critical conditions for blocking the nonuniform flow are reached in a time interval τ = 4800–5300 μs at the outlet of the air intake duct – in the throat, as a result an internal Mach disk appears, it moves forward. Ultimately, when τ > 5472 μs, a flow regime occurs with a knocked-out head Mach disk. This is the regime with a bow shock wave before the intake duct entrance with subsonic velocity in the internal duct (see Fig 1,*d*).

Note that the experimental phenomenon of shock wave knocking out during the "breakdown" of the supersonic inflow into the internal duct of the air intake when testing air intakes in impulse wind tunnels is known, but, for example, in [2, 3], the appearance of this regime was considered as "instantaneous", and it was not studied in detail.

In the conducted numerical study, at τ > 6462 μs, the bow shock wave moves oscillatory (Fig. 2,*a*). Respectively, the parameters of the flow in the air intake vary oscillatory, as it shown for the static temperature of the flow at the axis in its outlet section Fig. 2,*b*. In an interval τ = 5800–8200 μs oscillation frequency is about 1180 Hz, amplitude rapidly decreases, so that at τ > 8200 μs the bow shock wave stabilizes at position $x_{\text{bsh}} \approx 0.227$ m, which corresponds to the regime of flow around an un-started intake with the bow shock wave in front of the intake entry. The main occasion for the oscillatory movement of the head bow shock wave during the "breakdown" of the flow around the air intake in the started mode is that when this shock wave begins to move against the flow from the intake duct exit, new shock waves appear in the duct along with the existing moving shock waves. Successive reflections of these waves occur at the intake entrance and an oscillatory-like process of the bow shock wave motion and changes in the parameters of the flow in the air intake is generated. The amplitude of fluctuations in the position of the head bow shock wave decreases with time, its position stabilizes at a certain distance from the leading edge of the air intake.

Essentially, the considered flow pattern around the air intake is a non-stationary process, transitional from the started-intake flow mode to the un-started intake flow mode with the head bow shock wave.

The research was supported by the Ministry of Science and Higher Education of the Russian Federation within the framework of the state assignment (project No.121030500158-0).

REFERENCES

1. **Korolev A.S., Boshenyatov B.V., Drouker I.G., Zatoloka V.V.** Hot-shot Wind Tunnels as a Hardware for Aerodynamic Investigations. Novosibirsk: Nauka, 1978. (in Russian)
2. **Boshenyatov B.V., Gilyazetdinov B.N., Zatoloka V.V.** Experimental investigations of hypersonic inlets // Aeromechanics: coll. of art. dedicated to the 60th anniv. of Acad. V.V. Struminsky. Moscow: Nauka, 1976. P. 87–98. (in Russian).
3. **Gounko Yu.P., Mazhul I.I., Kavun N.I.** An investigation of starting processes and flow patterns occurring in hypersonic axisymmetric inlets of internal compression // Proc. of the XXV Conf. on High-Energy Processes in Condensed Matter (HEPCM 2017) (Novosibirsk, Russia 5–9 June 2017): AIP Conference Proceedings. 2017. Vol. 1893, No. 1. S.l. Art. 030057. 15 p. DOI: 10.1063/1.5007515.
4. **Gounko Yu.P., Kavun N.I.:** Starting processes at testing inlets in impulse wind tunnels // Proc. International Conference on the Methods of Aerophysical Research (ICMAR 2018) (Novosibirsk, Russia 13–19 August 2018): AIP Conference Proceedings. 2018. Vol. 2027. Art. 030011 (12 p.). https://doi.org/10.1063/1.5065105.

DOI: 10.53954/9785604788967_65

CRITERIA OF INVISCID INSTABILITY OF A VIBRATIONALLY EXCITED DISSOCIATING GAS

Yu.N. Grigoriev[1], I.V. Ershov[2]

[1]Federal Research Center for Information and Computational Technologies
630090, Novosibirsk, Russia

[2]Novosibirsk State Agrarian University
630039, Novosibirsk, Russia

The problem of the evolution of inviscid disturbances is a part of the general problem of the linear stability of flows. From the spectrum of inviscid disturbances, the most growing modes are distinguished, which are reproduced in the viscous problem. For an ideal incompressible fluid, the necessary and sufficient condition of the existence of neutral (growing) perturbations is known as the Rayleigh criterion [1]. A compressible ideal gas has a similar condition of a "generalized" inflection point [2]. For a supersonic boundary layer at Mach numbers M > 2.2, the appearance of more unstable high-frequency modes was established [3]. Taking into account the real gas properties, such as vibrational excitation, dissociation-recombination, and other physical and chemical processes, from a mathematical point of view, leads to the appearance of source terms in the equations of continuity and energies of the initial stationary flow and the corresponding equations for disturbances of the linear stability theory. In this case, a consistent consideration of the conditions for the growth of inviscid disturbances should lead to further generalizations of the inviscid criterion.

In [4], an expression for the growth criterion of inviscid disturbances was obtained for a gas model with a simple first-order chemical reaction. However, when deriving, the term corresponding to the work of pressure forces during the medium dilatational strain in the energy equation was omitted. Such an unjustified simplification casts doubt on the adequacy of the result obtained, which especially not confirmed by numerical calculations.

In the report the necessary conditions of the existence of neutral (growth) inviscid disturbances in a vibrationally excited dissociating gas are obtained. The case of single-mode vibrational relaxation and dissociation-recombination of a two-atomic gas according to the scheme

$$A_2 + M \rightleftarrows A + A + M$$

is considered.

To avoid cumbersome calculations, we limited ourselves to some special cases that have a certain physical interpretation. The following specific cases are presented.

1. Vibrationally excited gas without taking into account the reaction of dissociation – recombination. This case is of independent interest and also corresponds to the initial stage of thermal dissociation, which is always preceded by vibrational excitation, when the concentration of atoms still is negligible and the gas remains single-component. The criterion is expressed by the formula

$$\frac{d}{dy}\left(\frac{1}{T_S}\frac{dU_S}{dy} + \max\left[\frac{\gamma_v(T_S' - T'_{vS})}{T_S(\gamma+\gamma_v)}\right]\frac{dU_S}{dy}\right) = 0. \qquad (1)$$

Here U_S, T_S, T_{vS} are the velocity, static and vibrational temperatures of the stationary flow, γ_v is the depth of excitation of the vibrational mode, the prime means the derivative with respect to the y coordinate.

2. “Frozen” reaction of dissociation-recombination taking into account vibrational excitation. In this case, it is assumed that the gas-phase dissociation-recombination reaction is “frozen” in the volume and a heterogeneous reaction remains on the solid surface only [5].

The criterion has the form

$$\frac{d}{dy}\left(\frac{1}{T_S}\frac{1+c_\infty}{1+c_S}\frac{dU_S}{dy}+\max\left[\frac{1+c_\infty}{1+c_S}\frac{\gamma_v(T_S'-T'_{vS})}{T_S(\gamma+\gamma_v)}\right]\frac{dU_S}{dy}\right)=0, \tag{2}$$

where c_S is the concentration of the atomic component in a steady flow.

3. A dissociating gas without taking into account vibrational excitation. The inviscid criterion is given by the expression

$$\frac{d}{dy}\left(\rho_S\frac{dU_S}{dy}\right)+\max\left\{\Re_{1S}\left[\rho_S\left(\frac{dc_S}{dy}h_a^0-\frac{de_{iS}}{dy}\right)+N\frac{d\rho_S}{dy}\right]\right\}\frac{dU_S}{dy}=0, \tag{3}$$

where

$$\Re_1=\frac{\rho_S}{(\rho_S N-\gamma M_\infty^2 p_S)},$$

$$N=(h_a^0-e_{iSc})(1+c_S)+[(h_a^0-e_{iS\,c})(1+c_S)+e_{iS\,T}T_S]\frac{\dot{w}_c(1+c_S)-\dot{w}_\rho\rho_S}{(1+c_S)\dot{w}_c-T_S\dot{w}_T},$$

ρ_S is a density, h_a^0 is an enthalpy of formation of atoms, f_p are derivatives of flow functions with respect to thermohydrodynamic variables.

If we neglect the effects of a real gas, all the obtained criteria turn into the “generalized” inflection point condition a for a one-component gas [2].

Numerical calculations performed for a vibrationally excited gas under the conditions considered in [6], at Mach numbers M ≤ 5, show that the wave numbers of I and II the inviscid modes obtained using criterion (1) differ by approximately 2–3% from those obtained from the condition of the “generalized” inflection point. At the same time, in a dissociating gas with almost complete dissociation on an absolutely noncatalytic adiabatic wall, the wave numbers of I and II inviscid modes calculated on the basis of criterion (3) are shifted by 15% to the region of longer wavelengths compared to the calculation by classical criterion

This work was supported by the Russian Foundation of Basic Researches (Grant No. 20-01-00168).

REFERENCES

2. **Lin C.C.** The Theory of Hydrodynamic Stability. Cambridge University Press, 1955. 155 p.
3. **Lees L.** The Stability of the Laminar Boundary Layer in a Compressible Fluid: NACA Technical Note. No. 1360. 1947. 144 p.
4. **Mack L.M**. Boundary Layer Stability Theory: Preprint of JPL Technical Report, Document 900-277, Rev. A. Pasadena: Caltech, 1969. 272p.
5. **Shen S.F.** Effect of chemical reaction on the Inviscid criterion for laminar stability of parallel flows // Proceedings of the 5th Midwestern Conference on Fluid Mechanics / Ed. A.M. Kuethe. Ann Arbor: The University of Michigan Press, 1957. P. 11–20.
6. **Gaponov S.A., Petrov G.V.** Stability of the Boundary Layer of a Nonequilibrium Dissociating Gas. Novosibirsk: Nauka, 2013. 95 p. [in Russian].
7. **Grigor’ev Yu.N., Ershov I.V.** Linear stability of the boundary layer of relaxing gas on a plate // Fluid Dynamics. 2019. Vol. 54, No. 3. P. 295–307.

DOI: 10.53954/9785604788967_67

FREQUENCY CHARACTERISTICS OF COLD PLASMA JET GENERATED BY UNIPOLAR POSITIVE PULSES

P.P. Gugin[1,2], E.V. Milakhina[1,2], D.E. Zakrevsky[1,2], I.V. Schweigert[1,2]

[1]*Rzhanov Institute of Semiconductor Physics SB RAS*
630090, Novosibirsk, Russia

[2]*Khristianovich Institute of Theoretical and Applied Mechanics SB RAS*
630090, Novosibirsk, Russia

Low temperature atmospheric plasma jet is a promising therapeutic tool in different fields of plasma medicine, such as sterilization, wound heating, denticity, tumor treatment.

In anticancer therapy, the effect of the cold atmospheric plasma jet on (CAPJ) treatment on cancer tissue is well known: it causes a decrease the proliferation rate of cancer cells. The CAPJ is a sequence of the cathode directed streamers initiated by periodic sinusoidal or pulsed voltage. There streamers deliver the high electric field, fluxes of electrons, ions and reactive species to a zone of plasma-target contact. The CAPJ is non-equilibrium plasma with high energy electrons and low energy ions. Therefore, the gas temperature in the zone of plasma-target contact does not exceed 40 degrees for the most cases of the treatment.

In the experimental and theoretical studies of CAPJ effect on biotargets the cold plasma jets are typically generated with a sinusoidal or pulsed voltage with amplitude of U = 2–6 kV and frequency *of* $f_U \approx$ 10–30 kHz. A variation of the values of U and f_U changes the picture of the periodic propagation of streamers, which affects the integral electric fields and the rates of chemical reactions in the zone of interaction between the CAPJ and the biological object during the treatment. Under certain conditions, the effect of a mismatch between the voltage frequency f_U and the frequency of touching the current of the target f_I was observed in the experiment and simulations [1]. In the CAPJ initiated by unipolar positive voltage pulses, we found that the coincidence of frequencies $f_U = f_I$ was observed in a wider range of parameters [2].

In this work, the generation of CAPJ excited by unipolar positive voltage pulses at a repetition rate f_U = 8–40 kHz is investigated experimentally and in numerical fluid model simulations. The effects of the voltage pulse duration τ, the rise rate of the voltage leading edge τ_f, and the magnitude of the negative bias voltage on the frequency ratio f_U, f_I were reported.

It was shown that a change of the duration of the leading edge of voltage pulses τ_f = 2.5–7.5 μs does not affect the frequency of the streamer touching the target, and a decrease in the duration of the voltage pulse extends the regime with $f_U = f_I$ to high frequency range. It is also shown that an increase in the negative bias voltage violates the condition $f_U = f_I$.

The research results were obtained with the financial support of the Russian Science Foundation, grant number 22-49-08003.

REFERENCES

1. **Schweigert I.V., Alexandrov A.L., Zakrevsky Dm.E.** Self-organization of touching-target current with AC voltage in atmospheric pressure plasma jet for medical application parameters // Plasma Sourc. Sci. Tech. 2020. Vol. 29. No. 12. Art. 12LT02. 6 p.
2. **Gugin P.P., Zakrevsky D.E., Milakhina E.V** Electrophysical and thermal parameters of an atmospheric pressure plasma jet in helium when excited by sinusoidal and pulsed voltages // Letters to the Journal of Technical Physics. 2021. Vol. 47, No. 22. P. 41–44. [in Russian: **Гугин П.П., Закревский Д.Э., Милахина Е.В.** Электрофизические и тепловые параметры плазменной струи атмосферного давления в гелии при возбуждении синусоидальным и импульсным напряжением // Письма в ЖТФ. 2021. Т. 47, вып. 22. С. 41–44. DOI: 10.21883/PJTF.2021.22.51726.18977].

DOI: 10.53954/9785604788967_68

CONTROL OF VORTEX STRUCTURES TO REDUCE THE DRAG OF BLUNTED BODIES AND TO INCREASE THE LIFT OF THICK CARRYING SURFACES

S.A. Isaev[1,3], V.A. Lebiga[2], A.G. Sudakov[1], D.V. Nikuschenko[3], K. Chung[4], V.N. Zinovyev[2]

[1]Saint Petersburg University of Civil Aviation
196210, Saint Petersburg, Russia

[2]Khristianovich Institute of Theoretical and Applied Mechanics SB RAS
630090, Novosibirsk, Russia

[3]Saint Petersburg State Naval Technical University
190121, Saint Petersburg, Russia

[4]National Cheng Kung University
70101, Tainan, Taiwan

Under consideration is the topical scientific field, the flow and structure. We analyze the flow around structured multi-scaled objects with controlling vortex and jet generators in the presence of wind disturbances; the purpose is to improve their aerodynamic characteristics (ADC). Under consideration are the objects presenting the ensembles of elements of different scales. Improvement of their ADCs is reached by 1) mutual bracing of elements, for example, the tandem combination; 2) with the aid of surface vortex generators, namely ordered concavities (holes, channels) and protuberances; 3) application of volume generators – screens and discs protruding ahead of the body; 4) application of energy-efficient vortex cells inside the thick profile with flow intensification in the captured vortex due to suction; 5) creation of construction channels implementing the throttling effect at the air bleeding-off from the flow stagnation area in the low-pressure zone in the near wake with the blow of a low-speed jet (the effect can be intensified by a fan installed in the offtake channel). The control of the flow around structured bodies results in the formation of intensive large-scale vortices integrated into the flow; these vortices permit reducing the profile drag of the bodies, increasing essentially the lift force and lift-drag ratio. It is also possible to create the effect of head stabilization of bodies with vortex generators associated with the appearance of the restoring moment at the angles of attack. Enhancement of aero-hydraulic characteristics of the structured objects with the aid of surface and volume vortex generators also stimulates intensified heat-exchange processes and enables to reach, for example, the considerable rise of the heat release from the surface structured by inclined oval-channel holes. The following most essential results should be noted.

1. In the numerical investigations of the external aerodynamics of the bodies with passive and active vortex cells, the stress is done on analysis of the compressibility effect. The packet VP2/3 (velocity, pressure, 2D/3D) based on multi-block technologies is applied; it was successfully applied in the calculations of stationary and non-stationary flows around bodies of different configurations. Sub- and transonic regimes of the axially symmetrical flow around the "disc – cylinder – disc" configuration are studied; the sizes of the front and aft discs are 0.63 and 0.9, with respective gaps between them and cylinder end-faces (elongation 4.5) 0.5 and 0.375 (in fractions of caliber) at $Re = 2\times10^5$ and Mach numbers varying from 0 to 0.95. Comparison of available experimental data and numerical predictions shows their qualitative and quantitative agreement. The model is good in describing the viscous-non-viscous interaction with the turbulence and generation of shock-wave structures. It is demonstrated that at transonic Mach numbers, approaching to 1, a shock-wave structure appears ahead of the disc – cylinder – disc configuration, with a weak shock near the cylinder leading edge, and a slightly oblique almost normal shock wave above the side surface.

2. The effect of compressibility on the flow at the zero angle of attack around the Goettingen profile with a circular vortex cell and suction control system by a fan with the fixed pressure drop in the offtake channel has shown that as the Mach number rises from 0.01 to 0.1, the lift-to-drag ratio remains 15, whereas from 0.15 we observe the dramatic drop to –0.4. In fact, the vortex cell stops operating, and the flow around the thick profile becomes separation at the separation point motions ahead of the cell.

3. The calculations by the compressible gas model have demonstrated that as two vortex cells are located on the backside of the semi-circular cylinder contour, at the zero angle of attack and M = 0, the almost separation-free flow around this cylinder is observed, as well as high lift force and lift-to-drag coefficients. As the Mach number rises to 0.3, the aerodynamic characteristics rise, and the lift-to-drag ratio increases by proximately 35%. At M = 0.4, the second vortex cell near the aft sharp edge stops operating and appears into the separation zone, whereas the first operating vortex cell permits preserving high aerodynamic characteristics. The lift-to-drag ratio reduces almost 6 times, but still remains at the level about 20.

4. The spatial model of the 37.5% thick profile with one slot vortex cell has been calculated; the 1.5 time increase of the lift-to-drag ratio is demonstrated.

5. Experimental investigation of the flow around a semi-circular cylinder with a slot has been carried out in the wind tunnel T-325M ITAM SB RAS; new information is gathered on the mean flow, intensity, and spectral composition of velocity fluctuations in the wake behind the semi-circular cylinder set at the angle of attack within the range ($\alpha = -20° \ldots 20°$) into the subsonic flow. It has been found that at small angles of attack, the slot results in the noticeable difference of the flow around the semicircular cylinder with the slot against the same cylinder without slot. At small angles of attack, the variations of the frequency and intensity of velocity fluctuations are especially intensive.

6. The performed parametric experimental researches have demonstrated that the deficit of the average velocity at small negative angles of attack for the semi-circular cylinder (SCC) with the slot is lower than it is in the case of the semicircular cylinder without slot. However, as the negative angle of attack rises, this deficit increases and at a certain moment, the deficit of the average velocity for the semi-circular cylinder with the slot becomes higher than it is for the semi-circular cylinder without slot.

The research are partially financially supported by the Russian Foundation for Basic Research (grant No. 21-58-52013).

REFERENCES

1. **Isaev S., Lebiga V., Sudakov A., Nikushchenko D., Miau J. J., Chung K. M., Zinovyev V.** Structures control with the use of the throttling effect, vortex cells and surface generators – inclined oval-trench dimples // Int.Conf. on The Methods of Aerophys. Research (ICMAR 2020) (Russia, Novosibirsk, November 1–7, 2020): AIP Conference Proceedings. 2021. Vol. 2351. Art. 020002 (6 p.). DOI:10.1063/5.0051715.
2. **Isaev S., Nikushchenko D., Sudakov A., Tryaskin N., Egorova A., Iunakov L., Usachov A., Kharchenko V.** Standard and modified SST models with the consideration of the streamline curvature for separated flow calculation in a narrow channel with a conical dimple on the heated wall // Energies. 2021. Vol. 14, Iss. 16. Art. 5038 (23 p.). DOI:10.3390/en14165038.
3. **Isaev S.A., Miau J.-J., Nikushchenko D.V., Sudakov A.G., Usachov A.E.** Modeling the effect of wind shear on reducing the drag of an energy-efficient high-rise structure using the throttle effect // Mathematical Models and Computer Simulations. 2022. Vol. 14. No. 1. P. 73–80.

DOI: 10.53954/9785604788967_70

SIMULATION OF THE TURBULENT FLOW BY SUBSEQUENT APPLICATION OF THE RANS METHOD AND THE MODEL OF THE IDEAL FLUID

P.S. Kalyasov, F.S. Peplin

National Research Lobachevsky State University of Nizhny Novgorod
603950, Nizhny Novgorod, Russia

Ability to simulate the unsteady characteristics of turbulent flows is essential to address different problems in aeroacoustics, aerodynamics, heat transfer and fluid-solid interaction in such diverse areas as shipbuilding industy, aerospace engineering and energy harvesting.

Simulation of turbulent flows currently is based on the physical simulation methods. In most engineering problems the reliable results may be obtained only with full-scale models. Mathematical methods of the unsteady turbulent characteristics are still in a formative phase of their development. They rely either on direct numerical simulation of the fluid flow (LES, DES, DNS) [1–4] or on the stochastic methods of the turbulent velocity fields generation [5– 7]. Vortex methods are also used to simulate unsteady flows, but the corresponding papers are sparse [8, 9].

The idea of the presented method is as follows. The simulation of the unsteady hydrodynamic processes in the area of the vortex (turbulent) flow is conducted using the inviscid fluid flow model using discrete pulsing vortices-generators along with arising according to Kelvin circulation theorem sheds of free vortices. Amplitudes and frequencies of the vortices-generators' pulsations are determined from the results of the RANS simulations. Positions and instantaneous circulations of free vortices are calculated according to the theorems of hydrodynamics. The vortex system determine the pulsating velocity terms. By ensuring the no-slip boundary conditions on the boundary of the body the unsteady hydrodynamic loads may be obtained. These forces may create the hydro acoustical noise, as well as cause and maintain high frequency hydroelastic vibrations of the structures etc.

The method was applied to the test problem of the turbulent boundary layer near the wall (Fig. 1).

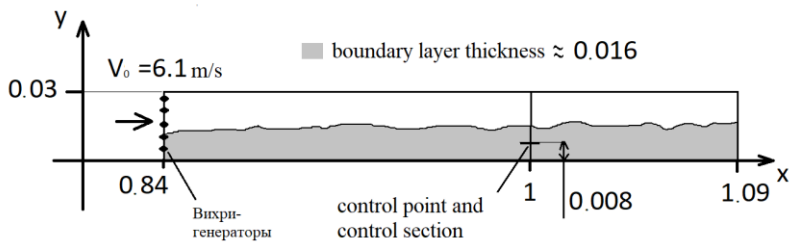

Fig. 1. Simulation domain.

The result of the simulation is the unsteady velocity field in the entire domain. The characteristics obtained with CFD simulation and with the presented method are compared. It is demonstrated that the averaged velocities, kinetic energy, correlation (spatial scale) obtained with LES method and with the presented approach are consistent with each other. The presented model predicts the beginning of the inertial interval of the turbulence kinetic energy spectra and allows to resolve an arbitrary frequency interval in this interval. The LES simulation for high frequencies tends to underestimate spectra, which is related to the coarse grid (Fig. 2).

The time required for the computation without parallelization is 30 minutes. Calculation with the LES model with parallelization into 4 threads took 24 hours.

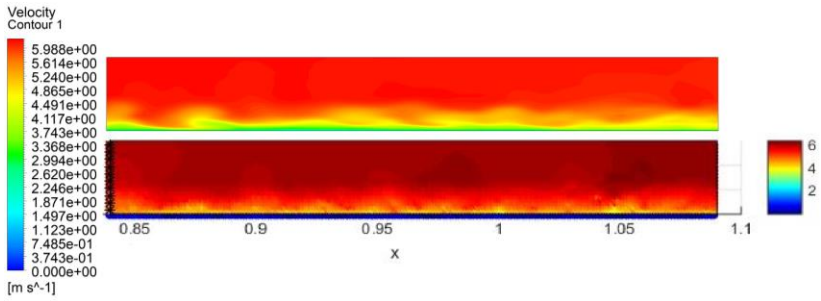

Fig. 2. Instantaneous velocity lengths according to the LES simulations (top) and the presented method (bottom).

The work was financially supported by the Strategic Academic Leadership Program "Priority 2030" (internal number H-496-99_2021-2023).

REFERENCES

1. **Garbaruk A.V.** Modern approaches to the turbulence simulation: textbook. St Petersburg: SPPU, 2016. 234 p [in Russian].
2. **Martin R., Soria M., Lehmkuhl O., Gorobets A., Canteand J., Vidal P.** Noise Radiated by An Open Cavity At Low Mach Number // Tenth International Conference on Computational Fluid Dynamics (ICCFD10) (Barcelona, Spain, July 9–13, 2018): ICCFD10-197. 18 p. DOI:10.1177/1475472X19871534
3. **Yokoyama H., Odawara H., Iida A.** Effect of freestream turbulence on cavity tone and sound source // International Journal of Aerospace Engeneering. 2016**.** Vol. 2016. Article ID 7347106. 16 p. http://dx.doi.org/10.1155/2016/7347106
4. **Alexandrov A.V., Dorodnitsin L.V., Duben A.P.** Generation of the 3D homogeneous isotropic turbulent velocity fields based on the randomized spectral method // Mathematical Modeling. 2019. Vol. 31, No. 10. P. 49–62 [in Russian]
5. **Siefert M., Ewert R.** Sweeping Sound Generationin Jets Realized with a Random Particle-Mesh Method // 15th AIAA/CEAS Aeroacoustics Conference (30th AIAA Aeroacoustics Conference), 2009: AIAA Pap. No. 2009-3369, 2009. DOI: 10.2514/6.2009-3369
6. **Ewert R., Dierke J., Appel C., Herr, M.** RANS/CAAbased prediction o fNACA 0012 broadband t0012 broadband trailing edge noise and experimental validation // 15th AIAA/CEAS Aeroacoustics Conference (30th AIAA Aeroacoustics Conference) 11–13 May 2009, Miami, Florida AIAA 2009-3269: AIAA Pap. 2009-3269, 2009. DOI: 10.2514/6.2009-3269
7. **Dergachev S.A., Marchevsky I.K., Shcheglov G.A.** Flow simulation around 3D bodies by using Lagrangian vortex loops method with boundary condition satisfaction with respect to tangential velocity components // Aerospace Science and Technology. 2019. Vol. 94. Art. 105374. 15 p. DOI:10.1016/j.ast.2019.105374
8. **Wu L., Jing X., Sun X.** Prediction of vortex-shedding noise from the blunt trailing edge of a flat plate // Journal of Sound and Vibration. 2017. Vol. 408, Iss. 10. P. 20–30 November 11

DOI: 10.53954/9785604788967_72

CALCULATION OF THE EFFICIENCY OF CAPTURE OF SUSPENDED PARTICLES BY A POROUS CYLINDER IN A PERIODIC CELL DUE TO INERTIA IMPACT AND INTERCEPTION

A.R. Khaziev, S.K. Zaripov, R.F. Mardanov

Kazan Federal University
420008, Kazan, Russia

During aerosols filtration through the porous medium of fibrous filters, suspended particles settle on the surface of the fibers due to inertial impaction, interception or diffusion mechanisms of settling. As a result of particle settling on the fibers, a porous layer is formed have a significant effect on the flow field around a single fiber, and hence on particle settling. Fibers surrounded by a porous layer can also be used as separate elements of fibrous filters [1]. The presence of an additional gas flow through a porous fiber also significantly affects the inertial capture and interception [2, 3].

A mathematical model of the hydrodynamic flow of an incompressible fluid in a circular and rectangular periodic cell with a single porous cylinder is presented. The flow field of the carrier medium outside and inside the region of the porous cylinder is described in the approximation of the Stokes – Brinkman model for an incompressible gas. For the model of a circular periodic Kuwabara cell [3], an analytical solution was obtained, in the case of a rectangular cell, the boundary value problem is numerically solved using the boundary element method.

On the base of the numerical solution of the Lagrangian equations of motion of suspended particles in the analytical and numerical fields of flow velocities, the trajectories of particles and the efficiency of particle settling due to inertial impact and the interception are calculated. A formula is derived for the efficiency of particle capture due to the interception by porous cylinder.

Parametrical studies of the efficiency E of capture of aerosol particles in dependence on the value of the Stokes number St for various values of the Darcy number Da of a porous cylinder, the density α of a periodic cell, and the interception parameter δ have been carried out. The dependencies of the efficiency $E(\mathrm{St})$ of capturing aerosol particles by a porous cylinder, taking into account both inertial impact and the interception effect for $= 0.1{,}0.5$ and $\mathrm{Da} = 0{,}0.1$ at $\alpha = 0.05$ are shown in the figure below. For comparison, the corresponding dependences for

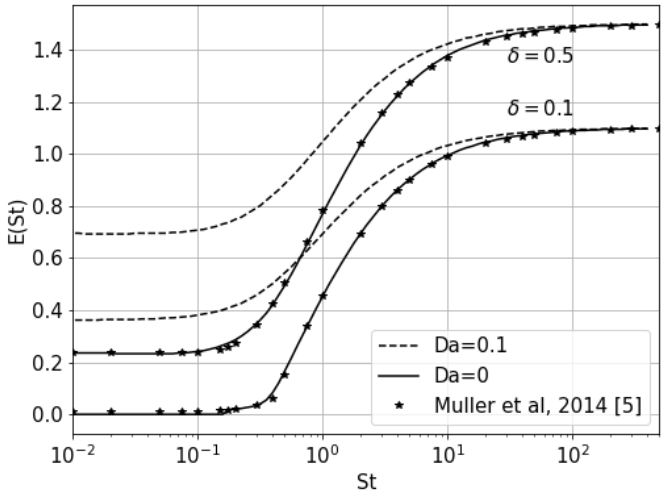

a solid cylinder ($\mathrm{Da} = 0$) from [4] are given, which practically coincide with the dependencies $E(\mathrm{St})$ obtained in this work. In the range of small Stokes numbers, the capture of aerosol particles is provided by both the interception and the flow through the porous cylinder. For large Stokes numbers, the value of $E(\mathrm{St})$ tends to $1 + \delta$ for both a solid and a porous cylinder.

The study was supported by the Russian Science Foundation grant No. 22-21-00176, https://rscf.ru/project/22-21-00176/

REFERENCES

1. **Kirsch V.A.** Aerosol filters made of porous fibers // Colloid Journal. 1996. Vol. 58, No. 6. C 737–740.
2. **Kirsch V.A.** Inertial deposition of aerosol particles in a model filter with dust-loaded fibres // The Journal of the Filtration Society / The Transactions of the Filtration Society. 2002, Vol. 2. No. 4. P. 109–113.
3. **Zaripov S.K., Solov'eva O.V., Solov'ev S.A.** Inertial Deposition of Aerosol Particles in a Periodic Row of Porous Cylinders // Aerosol Science and Technology. 2015. Vol. 49, No. 6. P. 400–408.
4. **Kuwabara S.** The forces experienced by randomly distributed parallel circular cylinders or spheres in a viscous flow at small Reynolds numbers // Journal of Physical Society of Japan. 1959. Vol. 14. P. 527–532.
5. **Muller T.K., Meyer J., Kasper G.** Low Reynolds number drag and particle collision efficiency of a cylindrical fiber within a parallel array // J. of Aerosol Science. 2014. Vol. 77. P. 50–66.

DOI: 10.53954/9785604788967_74

DEVELOPMENT OF A MODEL OF HYBRID DETONATION IN A MIXTURE OF OXYGEN-HYDROGEN-ARGON AND ALUMINUM PARTICLES

T.A. Khmel, S.A. Lavruk

Khristianovich Institute of Theoretical and Applied Mechanics SB RAS
630090, Novosibirsk, Russia

The study of hybrid detonation structures is connected both in terms of increasing the specific impulse of detonation engines, and in terms of explosion and fire safety. The fundamental task is to study the characteristics of cellular hybrid detonation. The aim of this study is to build a physical and mathematical model of hybrid detonation in oxygen-hydrogen-argon mixtures with the addition of aluminum particles.

The hybrid detonation model is based on the approaches of the mechanics of interpenetrating continuums [1]. Most of the gas suspensions that are of interest for studying the processes of heterogeneous and hybrid detonation are poor in composition or close to stoichiometric. In such mixtures, due to the large difference in the intrinsic densities of the material of particles and gas, the volume occupied by particles is very small (of the order of $10^{-4} \div 10^{-3}$) even in ρ-layers formed behind shock and detonation waves. Therefore, the approximation of a slightly dusty medium is justified.

To describe the reaction in a hydrogen-oxygen-argon gas mixture, a model of one-stage kinetics is used, developed and verified in [2] for various parameters. The combustion of finely dispersed (micron and submicron) aluminum particles is described within the framework of a single-stage reduced kinetics [3]. It is assumed that aluminum combustion occurs with the formation of solid aluminum oxide nanoparticles.

To test the hybrid detonation model, the following problem was solved. A channel is considered, consisting of two parts: high pressure chambers (HPC) and low pressure chambers (LPC), separated by a membrane. At the initial moment of time, the membrane breaks, and the gas from the high pressure chamber flows into the low pressure chamber. The aluminum particles were located together with the combustible mixture in the LPC.

Figure 1 shows the results of a comparison of gaseous detonation without the addition of aluminum particles in an oxygen-hydrogen-argon mixture with an excess of oxygen (Fig. 1,*a*) and the same mixture with a small addition of aluminum particles (0.003 kg/m^3) (Fig. 1,*b*).

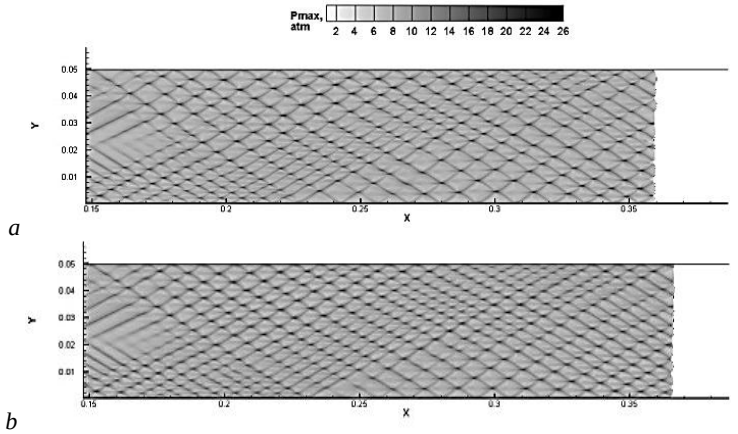

Fig. 1. Maximal pressure fields of for gas detonation (*a*) and hybrid detonation (*b*).

It can be seen from the figures that the propagation velocity of the hybrid detonation is higher than that of the gas detonation wave. It is also worth noting that in hybrid detonation the cell is more elongated in length.

As a result of calculations, it can be seen that the addition of combustible particles leads to a change in the flow structure. Thus, the addition of even a small amount of aluminum particles to the mixture of reacting gases makes it possible to control the detonation characteristics.

The work was supported by Russian Science Foundation, project No. 21-79-10083, https://rscf.ru/project/21-79-10083/

REFERENCES

1. **Nigmatulin R.I.** Dynamics of multiphase media. Part 1. Moscow: Nauka, 1987. 464 p.
2. **Bedarev I.A., Rylova K. V., Fedorov A. V.** Application of detailed and reduced kinetic schemes for the description of detonation of diluted hydrogen–air mixtures // Combust. Explos. Shock Waves. 2015. Vol. 51, № 5. P. 528–539.
3. **Khmel T., Lavruk S.** Detonation flows in aluminium particle gas suspensions, inhomogeneous in concentrations // J. of Loss Prevention in the Process Industries. 2021. Vol. 72. Art. 104522. 14 p. DOI:10.1016/J.JLP.2021.104522

DOI: 10.53954/9785604788967_76

NUMERICAL STUDY OF RECTANGULAR JET INSTABILITIES

D.V. Khotyanovsky, A.N. Kudryavtsev

Khristianovich Institute of Theoretical and Applied Mechanics SB RAS
630090, Novosibirsk, Russia

Numerical study of the development of instabilities in supersonic jets exhausting from rectangular nozzles has been performed on the basis of the Navier – Stokes simulations. Simulations are performed for an isobaric jet of monatomic gas (argon) exhausting into a co-flowing ambient stream from a square-section nozzle. Piecewise-monotonic (top-hat) jet profile is specified at the inflow cross-section with flow velocity $U = U_j$, $|y|, |z| \le h/2$ and $U = U_a$, $|y|, |z| > h/2$. Here U_j, U_a are respectively the velocities of the jet and the ambient stream, h is the size of the jet cross-section. The temperature and pressure of the two streams are assumed equal: $p_j = p_a$, $T_j = T_a$. Two cases are considered, one with a supersonic ambient stream, $M_j = 2.5$, $M_a = 1.5$, and the other with a subsonic ambient stream, $M_j = 1.5$, $M_a = 0.5$. Mach numbers are chosen so that the convective Mach number $M_c = (U_j - U_a)/(a_j + a_a) = 0.5$ is the same in both cases (a_j, a_a are the sound speeds). Calculations are carried out at two significantly different values of the Reynolds number $\mathrm{Re} = U_j h/\nu = 5000$ and 100,000.

Unsteady disturbances of the normal v and transverse w velocity components in the form of running waves are superimposed on the basic flow at the inflow cross-section. The shape functions of the disturbances are $\hat{v} = \hat{w} = 1/(\cosh(2y)\cdot\cosh(2z))$. The wave parameters of the disturbances are selected as follows. The wavelength of the main disturbance $\lambda = 2\pi/\alpha$ is assumed to be equal to the jet width $\lambda = h$, the phase velocity is set to the half-sum of the velocities of the jet and ambient stream $c = 0.5\,(U_j + U_a)$. In some simulations, in addition to the disturbance at the "fundamental" frequency $\omega = \alpha c$, its first harmonic with a frequency of 2ω and a subharmonic with a frequency of $\omega/2$ are also imposed. The initial amplitudes of the disturbances are sufficiently large, $A = 0.01$. Various phase shifts between disturbances of the two velocity components are considered.

The computational domain has the shape of a parallelepiped with a length $L_x = 40\,h$, and dimensions $L_y = 10\,h$, $L_z = 10\,h$ along normal axes. In some runs, an elongated domain with $L_x = 80\,h$ is used. The computational grid is condensed in the core and near field of the jet. Most of the test calculations are carried out on the grid with the number of cells $N_x = 768$, $N_y = 220$, $N_z = 220$. In some runs, more refined grid is used with $N_x = 1152$, $N_y = 330$, $N_z = 330$ (125 million). Computations are carried out using the HyCFS code on a hybrid computing server equipped with eight GPUs.

The numerical results show that in all considered cases, the instability rapidly develops at the jet boundary, and then spreads across the entire jet flow. Instability at a lower Reynolds number develops more slowly, but a particular difference is observed between the cases with supersonic and subsonic ambient streams. In the first case (Fig. 1,*a*) the disturbances maintain a fairly regular structure up to the output boundary, which is located at the distance of 40 h. In the case with a subsonic ambient stream (Fig. 1,*b*) instability develops noticeably faster, and, starting from a certain section, intensive eddy formation occurs, and mixing with the surrounding gas is intensified. The evolution of the flow in the jet core is illustrated at several cross-sections along the streamwise coordinate in Fig. 2. A notable feature of the jet flow is the intense emission of sound waves into the ambient stream, clearly visible in the density fields.

This work was supported by the Russian Science Foundation grant 18-11-00246.

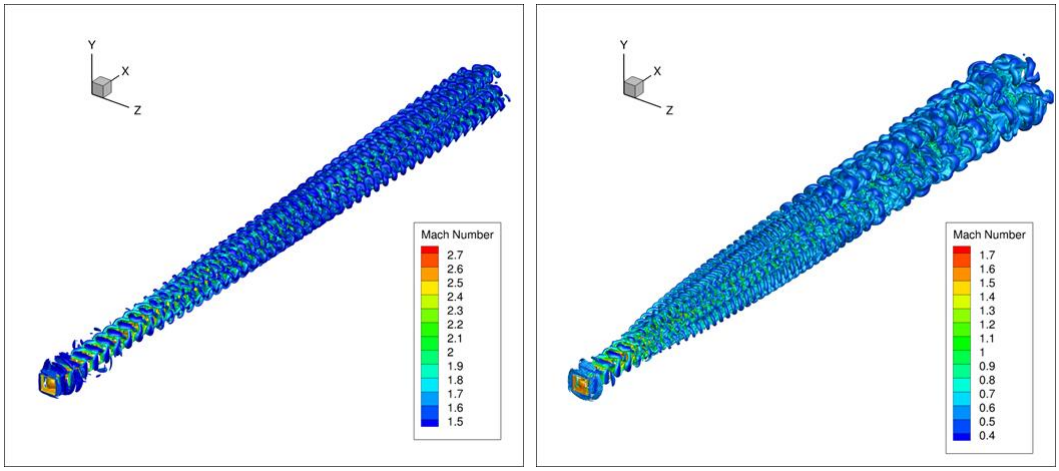

a *b*

Fig. 1. Q-criterion visualization of the instantaneous 3D flow field for $M_j = 2.5$, $M_a = 1.5$ (*a*) and $M_j = 1.5$, $M_a = 0.5$ (*b*).

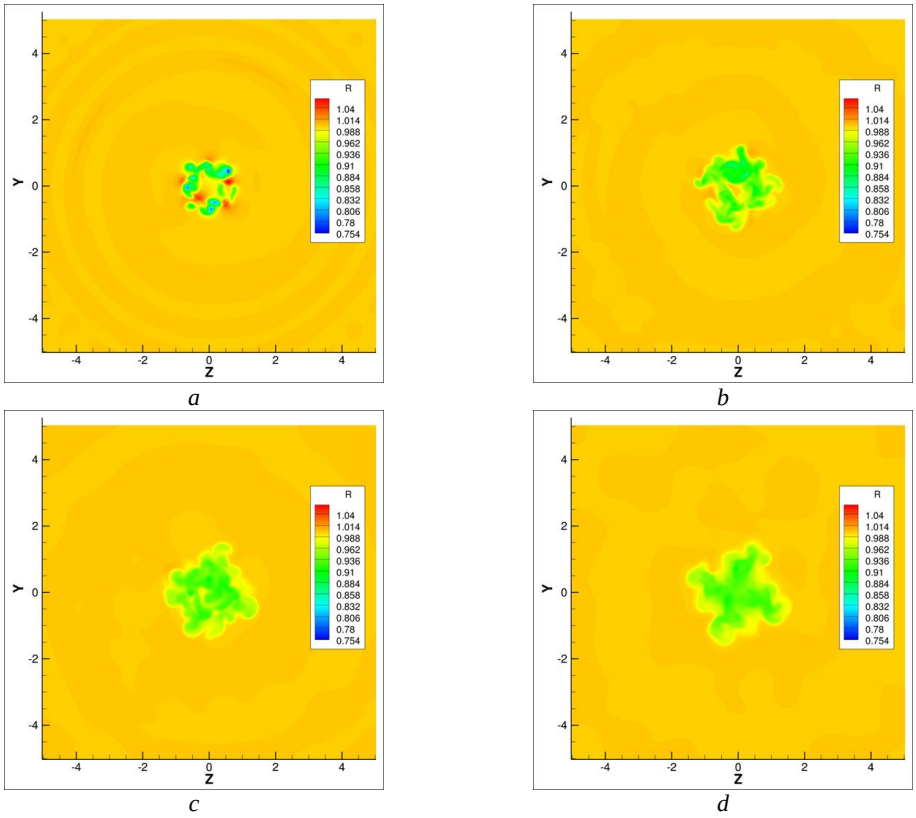

a *b*

c *d*

Fig. 2. Instantaneous density field at several cross sections for $M_j = 2.5$, $M_a = 1.5$. $x = 10$ (*a*), 20 (*b*), 30 (*c*), 40 (*d*).

DOI: 10.53954/9785604788967_78

NUMERICAL STUDY OF THE EFFECTS OF THE EXTERNAL PRESSURE GRADIENT ON LAMINAR-TURBULENT TRANSITION IN A SUPERSONIC BOUNDARY LAYER

D.V. Khotyanovsky, P.A. Polivanov, A.N. Kudryavtsev, A.A. Sidorenko

Khristianovich Institute of Theoretical and Applied Mechanics SB RAS
630090, Novosibirsk, Russia

The effects of the external pressure gradient on the laminar-turbulent transition in a flat-plate supersonic boundary layer are studied with the direct numerical simulation. The disturbed supersonic boundary layer on a flat plate interacts with the incident shock wave incoming from the upper boundary of the computational domain. The induced pressure gradient causes flow separation and significant amplification and transformation of the original boundary layer disturbances, which affects the laminar-turbulent transition.

The flow parameters correspond to the experiments performed at the T-325 wind tunnel of the Institute of Theoretical and Applied Mechanics (ITAM): flow Mach number M = 1.43, stagnation pressure $P_0 = 0.55 \cdot 10^5$ Pa, stagnation temperature $T_0 = 293$ K. The Reynolds number at the inflow cross-section based on the distance from the leading edge of the plate is $\mathrm{Re}_x = 4.9 \cdot 10^5$. The three-dimensional unstable waves of the linear stability theory (LST) are superimposed on the self-similar boundary layer profile at the inflow boundary. This approach for generation of the boundary layer disturbances was used in our previous studies [1, 2]. The wave parameters of the unstable disturbances and their eigenfunctions are obtained using the LST code VBLS3D developed at ITAM. The disturbances are excited at the fundamental LST frequency 25 kHz in a single-mode approach, or in the range of frequencies in the multi-mode approach.

The Navier – Stokes simulations are performed with the CFS3D numerical code developed at ITAM. This numerical code features modern high-order shock-capturing WENO scheme for spatial discretization of the convective fluxes. The code is parallelized using the domain decomposition technique and MPI communications. The results of the simulations with the shock-assisted boundary layer transition are compared with the DNS results of the laminar-turbulent transition on a flat plate without the external pressure gradient.

The 3D flow visualization and the distribution of the skin friction coefficient are shown in Fig. 1 in the presence of the incident shock wave. The numerical results show that the interaction

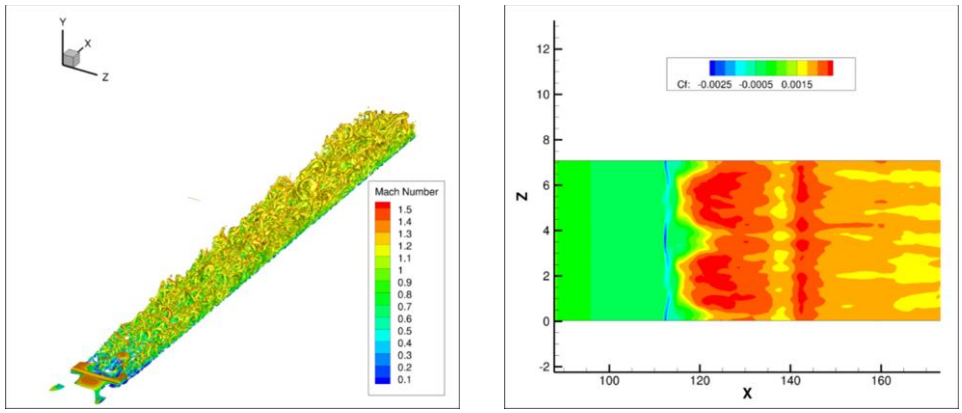

a *b*

Fig. 1. Q-criterion visualization of the instantaneous 3D flow field (*a*) and surface distribution of the time-averaged skin friction coefficient (*b*).

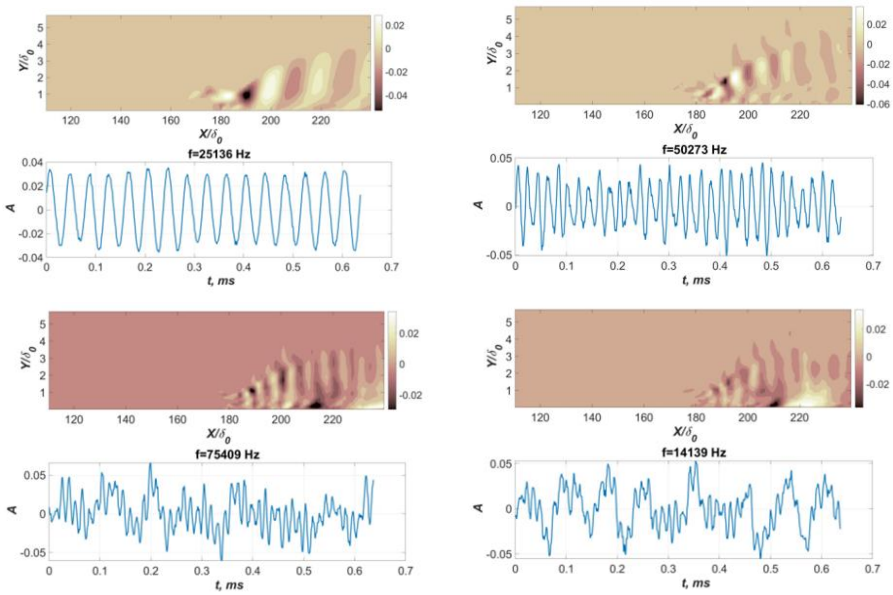

Fig. 2. Streamwise velocity distributions for different POD modes and their time evolution.

with the incident shock causes the induction of the adverse pressure gradient in the boundary layer and the formation of a separation zone, which leads to an increase in the boundary layer fluctuations followed by their rapid transition into nonlinear regime, which triggers the laminar-turbulent transition directly downstream from the interaction zone. The transition is accompanied by an increase of the skin friction.

The obtained unsteady DNS data are further processed with the advanced POD (Proper Orthogonal Decomposition) and DMD (Dynamic Mode Decomposition) techniques. These data processing algorithms can significantly reduce the dimensionality of the data matrices, which can improve the analysis of large amounts of the DNS data. The results of the POD analysis of the numerical data is shown in Fig. 2 for several POD modes corresponding to different frequencies in the presence of the incident shock wave.

This work was supported by the Russian Science Foundation grant 18-19-00547.

REFERENCES

1. **Polivanov P.A., Khotyanovsky D.V., Kutepova A.I., Sidorenko A.A.** Investigation of various approaches to the simulation of laminar–turbulent transition in compressible separated flows // Journal of Applied Mechanics and Technical Physics. 2020. Vol. 61, No. 5. P. 717–726.
2. **Khotyanovsky D.V., Kudryavtsev A.N**. Numerical study of the effects of upstream disturbances on shock wave/boundary layer interaction on a flat plate // Proc. of 20th Int. Conf. on the Methods of Aerophys. Research (ICMAR2020): AIP Conference Proceedings. 2021. Vol. 2351. Art. 030083. 6 p. doi.org/10.1063/5.0051695.

DOI: 10.53954/9785604788967_80

PHYSICAL EXPERIMENT IN PROBLEMS OF BUILDING AERODYNAMICS

E.F. Khrapunov, S.Yu. Solovev, V.V. Sokolov

Krylov State Research Centre
196158, St. Petersburg, Russia

The task of correctly determining and accounting for the wind loads becomes the key one in designing process of such unique architectural objects as high-rise buildings, stadiums, airports, large-span bridges, etc. [1]. It is important to note that the results of aerodynamic tests can be used not only to take into account the impact of wind on the facades or external railings of the object correctly, but also, for example, in the study of dynamic stability, or in determining the level of wind comfort in the pedestrian and viewing areas of the object. A physical experiment, which is also carried out in specialized wind tunnels (called ABL or Landscapes), is currently the most reliable source of information.

It is well known that the impact of natural wind on structures can be represented as a combination of steady and unsteady phenomena. The characteristics of a stationary effects can be determined during "typical" experimental studies, and in some cases, with an acceptable degree of accuracy, they can be calculated based on the results of numerical solutions of the three-dimensional equations [2]. The existence of unsteady processes, in turn, can lead to a loss of aerodynamic stability of the object (long-span bridge, high-rise building, flagpole etc.) or its part (for example, a protruding antenna, a spire, an overhanging visor). To determine the conditions for the occurrence and scenarios for the development of aerodynamic instability, it is necessary to perform experimental studies using models that allow reproducing the dynamic response of the structure to the air flow characteristics [3]. Such models are sectional models (simulate typical section of the real structure), and complete aeroelastic models with possibilities to study the dynamic response characteristics of the entire structure.

Experimental studies with sectional models are carried out usually in the study of the characteristics of the interaction of air flow and large-span bridges. Figure 1,*a* shows a photograph of the model in the test section of the wind tunnel. The model is suspended on a special stand on elastic elements, which reproduce the rigidity of a natural object. When exposed to air flow, the model can perform translational vibrations in the vertical plane, as well as torsional vibrations relative to the established center of rigidity. The model reproduces the main aerodynamically significant elements: protruding bridges, fences, etc. Figure 1,*b* shows the maximum amplitudes of oscillations in the vertical plane, obtained experimentally. It should be noted that the maximum value of the amplitude is determined on the basis of statistical analysis. It is clearly seen that in a certain range of flow velocities, a peak in the amplitude of oscillations is observed as

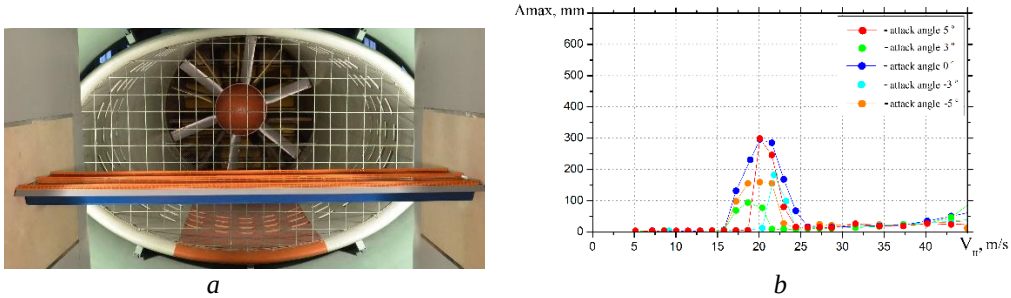

a *b*

Fig. 1. Simplified dynamically similar model in the working part of the wind tunnel (*a*) and experimental results (*b*).

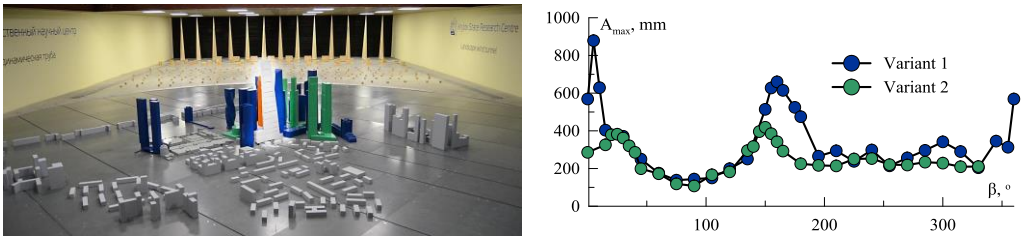

a *b*

Fig. 2. Full dynamically similar model in the working part of the wind tunnel (*a*) and experimental results (*b*).

a result of the development of the phenomenon of vortex excitation. A typical characteristic of vortex excitation is the growth of amplitudes in a narrow range of airflow velocities. Note that the natural frequency of oscillations, as well as the linear scale of the model, make it possible to unambiguously determine the velocity scale and transfer the experimental data to a full-scale object.

The use of full aeroelastic models is typical for the study of high-rise buildings and long-span bridges. Such tests performed in the special wind tunnels called atmospheric boundary layer wind tunnels (ABL) or Landscape wind tunnels [4]. An example of model in the test section of the Landscape Wind Tunnel of the Krylov Research Center is shown in Fig. 2,*a*. The model is a flexible rod on which contours are located, repeating the geometric shape of the building on a reduced scale. The calculation of the parameters of such a model can be carried out using the similarity criteria of Cauchy (in terms of stiffness), Newton (in terms of mass), Scruton (in terms of damping). Figure 2,*b* shows the maximum amplitudes of model oscillations for a fixed value of wind speed and different directions of its impact. Experimental studies have shown that model oscillations occur as a result of buffeting [5].

REFERENCES

1. **Simiu E., Yeo DH.** Wind effects on structures. John Wiley & Sons Ltd, 2019. 496 p.
2. **Blocken B.** 50 years of computational wind engineering: past, present and future // Journal of Wind Engineering and Industrial Aerodynamics. 2014. Vol. 12. P. 69–102.
3. **Moni M., Hwang Y., Kwon Y., Kim O., Jeong U.Y.** Real-time aeroelastic hybrid simulation of a base-pivoting building model in a wind tunnel // Frontiers in Built Environment. 2020. Vol. 6. P. 16.
4. **Solovev S., Khrapunov E.** Modeling of the mean wind loads on structures // Magazine of Civil Engineering. 2019. Vol. 88. P. 42–49
5. **Simiu E.** Buffeting and aerodynamic stability of suspension bridges in turbulent wind: Doctoral Dissertation. Princeton, 1971

DOI: 10.53954/9785604788967_82

PREDICTION OF THE POSITION OF THE LAMINAR-TURBULENT TRANSITION IN THE BOUNDARY LAYER OF AN AIRFOIL WITH A SEPARATION BUBBLE

S.V. Kirilovskiy, T.V. Poplavskaya, A.V. Boiko, A.A. Sidorenko

Khristianovich Institute of Theoretical and Applied Mechanics SB RAS
630090, Novosibirsk, Russia

It is known that the characteristics of aircraft can depend significantly on the position and length of the laminar-turbulent transition (LTT) region. When determining the position of the LTT in the boundary layer (BL), various specific features of the flow must be taken into account. For example, local separation bubbles may occur during flowing around an airfoil, which decrease the aerodynamic characteristics of the wing and whole aircraft. Such flows are usually arising in flow over laminarized profiles, where the LTT occurs due to the instability of the shear layer above this separation bubble.

In this paper, the numerical simulation of the LTT in the BL of an airfoil wing with a separation bubble was considered. To this end, the computation technology [1, 2] was used with the LOTRAN 3 software package [3, 4] integrated into the ANSYS Fluent CFD software. LOTRAN is based on the physically justified N-factor method (eN-method) implemented for predicting LTT in viscous compressible (including incompressible) flows using original specialized matrix algorithms [4]. The advantage of LOTRAN 3 is the possibility to analyze both the attached flows and the initial stage of laminar detachment of a BL.

In the framework of the Reynolds averaged Navier – Stokes equations (RANS), implemented in ANSYS Fluent, the flow over the airfoil was computed using the k–ω turbulence model. In addition, during steady-state computation of the main flow, a special user-defined functions (UDF) was used to partition preliminary the flow into laminar and known turbulent regions, which includes most of the separation area. Then, these computed data were transferred to the LOTRAN 3 module. In processing, LOTRAN 3 determines the BL characteristics (displacement and momentum loss thicknesses, etc.) to qualitatively evaluate the result of assimilating data obtained from ANSYS Fluent, performs flow stability analysis, draws the initial and final locations of temporal instability areas, N-factor curves, and their envelope.

Using ANSYS Fluent and LOTRAN 3 in numerical simulation of the problem considered in this work makes it possible to describe properly the presence of separation bubble in the flow, the length and thickness of the separation bubble, and their influence on the airfoil integral characteristics.

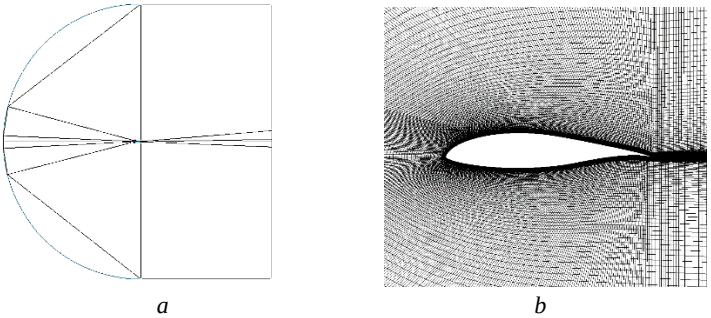

a *b*

Fig. 1. Computational domain with computational grid blocks (*a*) and a fragment of the computational grid near the airfoil (*b*).

In numerical simulation of subsonic flow over airfoil fx61168 (Fig. 1,*b*) with the chord length c = 1 m, the computational domain consisted of a semicircle of radius 20 m, combined with a rectangle of size 20 m by 40 m (Fig. 1,*a*). The computational domain was covered by a regular grid with C-topology around the wing.

In this paper, the flow around the airfoil fx61168 at different angles of attack (4°–7°) and Reynolds numbers Re from 10^5 to 2×10^6 was calculated. The results showed a weak dependence of the separation bubble position on the critical *N*-factor value (Fig. 2). At the same time, it can be seen that the change in the critical *N*-factor leads to a change in the length of separation bubble.

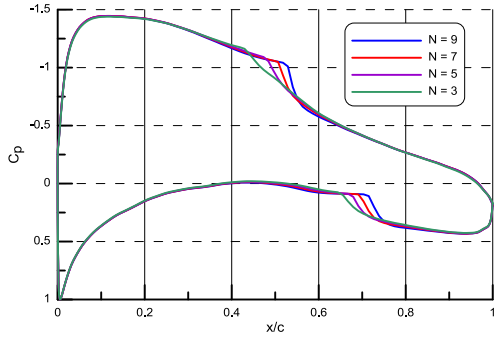

Fig. 2. Pressure distribution on the wing surface located under the angle of attack 4° for different N-factors, U_∞ = 7.3 m/s, Re = 10^5.

Thus, this study demonstrates the LOTRAN 3 software package capability to work in conjunction with the ANSYS Fluent package to compute the LTT positions in the BL of an airfoil with a separation bubble.

This work was carried out within the framework of the Program of Fundamental Scientific Research of the State Academies of Sciences (Grant No. 121030500162-7).

REFERENCES

1. **Boiko A.V., Demyanko K.V., Kirilovskiy S.V., Nechepurenko Y.M, Poplavskaya T.V.** Modeling of transonic transitional 3D flows with a general-purpose CFD code using the eN-method // AIAA J. 2021. Vol. 59, No. 9. P. 3598–3610.
2. **Kirilovskiy S.V., Boiko A.V., Demyanko K.V., Nechepurenko Y.M., Poplavskaya T.V., Sidorenko A.A.** On integrating the LOTRAN 3.0 package into the ANSYS fluent CFD software // Proc. of the XXVI Conf. on High-Energy Processes in Condensed Matter (HEPCM 2019) (Novosibirsk, Russia, 3–5 April 2019: AIP Conf. Proc. 2019. Vol. 2125 (6 p.). DOI: 10.1063/1.5117480
3. **Certificate** of state registration of a computer program № 2013660060 RF. Software package LOTRANxx for calculation of laminar-turbulent transition in boundary layers of viscous incompressible fluid flows over surfaces of small curvature / Y.M. Nechepurenko, A.V. Boiko. Federal Service for Intellectual Property: Appl. No. 2013617801 from 30.08.2013. Date of regist. 23.10.2013. Date of publ. 20.12.2013.
4. **Boiko A.V., Demyanko K.V., Nechepurenko Y.M.** On computing the location of laminar-turbulent transition in compressible boundary layers // Russ. J. Numer. Anal. Math. Modelling. 2017. Vol. 32, No. 1. P.1–12.

DOI: 10.53954/9785604788967_84

SUPERSONIC UNDEREXPANDED GAS – PARTICLES JET FLOWING INTO A SLOTTED FLOODED SPACE

S.P. Kiselev[1,2], V.P. Kiselev[1], V.N. Zaikovskii[1]

[1]Khristianovich Institute of Theoretical and Applied Mechanics SB RAS
630090, Novosibirsk, Russia

[2]Novosibirsk State Technical University
630092, Novosibirsk, Russia

In the paper [1] was shown the possibility of using a radial nozzle for coating the inner surface of pipers. The radial nozzle is formed by two parallel discs between which the gas is accelerated along with the particles. In [1], the structure of the gas flow between disks was studied without taking into account the influence of particles on the gas flow. In this paper, we study the flow of a two-phase gas – particles jet in the case when the influence of particles on the gas flow becomes significant. We consider two-phase gas – particles jet flowing from rectangular channel into slotted flooded space formed by two parallel disks. The continuum-discrete model is used to calculate the supersonic jet flow. In this model, the gas flow is described by the gas dynamic equations with right-hand sides, and the particles are described by a collisionless kinetic equation [2].

The rectangular channel was formed by a spacer with a rectangular cut provided in between the disks. For calculating the gas flow, the channel approximation was used. The stationary flow was calculated numerically by the relaxation technique. The problem statement and the solution method are described in detail in [3].

The results of the calculation of the flow in a jet of gas (air) – aluminum particles ($d_p = 10\ \mu$m) are shown in Fig. 1, *a*, *b*. The results of the calculation of the flow in a gas jet without particles are shown in Fig. 1, *c*. The radius of the disks is R = 35 mm, the distance between the disks is $h = 0{,}2$ mm, gas pressure and temperature in the prechamber are equal $p_0 = 1.0$ MPa and $T_0 = 300$ K. Aluminum particles were fed into the channel at the inlet, the mass flow rate of Al particles was equal to 0.7 of the gas flow rate.

It is seen from Fig. 1, that when gas flows out of rectangular channel into a slotted space, it accelerates to supersonic speed in a centered rarefaction wave emerging from a corner point. Particles decelerate the supersonic gas jet, so the maximum Mach number in a two-phase gas-

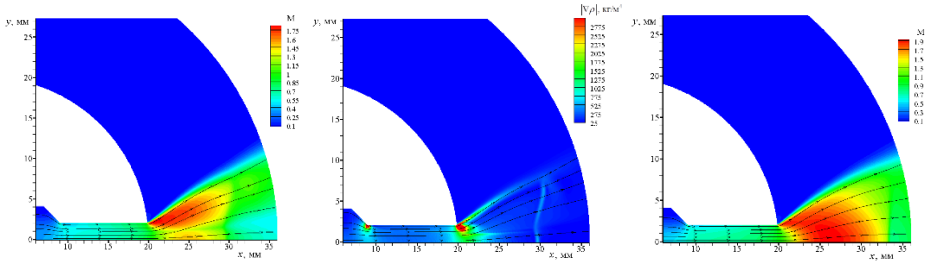

a *b* *c*

Fig. 1. Calculation results.

a – the Mach number $\mathrm{M}(x, y)$; *b* – the density gradient in gas $|\nabla\rho|(x, y)$; *c* – the Mach number $\mathrm{M}(x, y)$ in a jet without particles.

particles jet $M = 1.75$ (see Fig. 1, *a*). This value is less than in a gas jet without particles $M = 1.9$ (see Fig. 1, *c*). A curvilinear shock wave, which closes the supersonic flow, arises when the gas decelerated by particles and the walls of the disks. The inhomogeneity of the gas jet arises when the refraction wave interacts with the boundary of the particle jet, and then increases due to the deceleration of the gas by the particles. As a result, the closing shock wave in the two-phase jet becomes curvilinear as shown in Fig. 1, *b*.

Figure 2 shows the calculated volume concentration of particles in a two-phase flow.

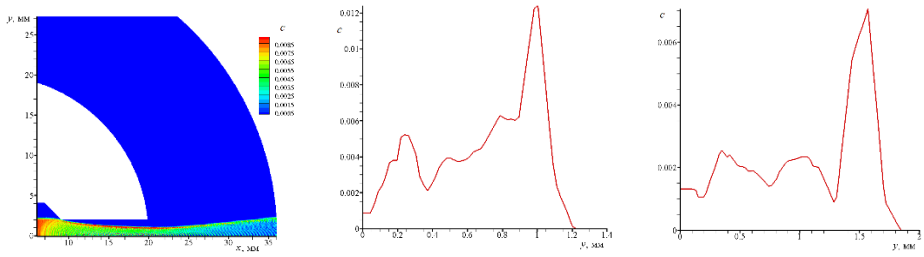

a *b* *c*

Fig. 2. Volume concentration of particles.

$a - c(x, y)$; $b - c(x_1, y)$ for $x_1 = 23\,\text{mm}$; $c - c(x_2, y)$ for $x_2 = 30\,\text{mm}$.

The jet of particles in the channel and slotted space is shown in Fig. 2. The jet of particles is compressed in a subsonic gas flow in the channel. On the contrary, the jet of particles expand in the slot space between the disks due to interaction with the supersonic gas jet. The distribution of particle volume concentration in in the cross section of the particle jet is substantially lopsided. The edge caustic is formed at the upper boundary of the particle jet. The density of particles increases on the caustic approximately two to three times. The concentration of particles on the caustic decreases with a downstream shift in the supersonic region, and the caustic shifts in the direction of the *y*-axis. The caustic is located at a distance $y_1 = 1\,\text{mm}$ from the axis (in the section $x_1 = 23\,\text{mm}$, see Fig. 2, *b*), and at a distance $y_2 = 1.6\,\text{mm}$ from the axis (in the section $x_2 = 30\,\text{mm}$, see Fig. 2, *c*).

REFERENCES

1. **Kiselev S.P., Kiselev V.P., Klinkov S.V., Kosarev V.F., Zaikovskii V.N.** Study of the gas-particle radial supersonic jet in the cold spraying // Surface & Coatings Technology. 2017. Vol. 313. P. 24–30.
2. **Kiselev S.P., Ruev G. A., Trunev A. P., Fomin V.M., Shavaliev M.S.** Shock-wave processes in two-component and two-phase media. Novosibirsk: Nauka, 1992. 260 p. (in Russian).
3. **Kiselev S.P., Kiselev V.P., Zaikovskii V.N.** Investigation of supersonic underexpanded jets exhausting into a slotted submerged space // Appl. Mech. Tech. Phys. 2020. Vol. 61, No. 2. P. 225–234.

DOI: 10.53954/9785604788967_86

FLOW STRUCTURE IN A HIGH-SPEED JET EXHAUSTING FROM A NOZZLE WITH CENTRAL BODY

N.P. Kiselev, V.I. Zapryagaev, I.N. Kavun, R.A. Styazhkin

Khristianovich Institute of Theoretical and Applied Mechanics SB RAS
630090, Novosibirsk, Russia

The relevance of the study is due to the fact that the internal tract of a two contour aircraft engine has internal structures, such as a central body, supporting pylons, etc. These elements of the nozzle design affect the flow structure and gas-dynamic parameters of the outflowing jet [1].Numerical work to determine the characteristics of the jet flow, as a rule, is carried out without taking into account the three-dimensional character of the flow in the internal contour [2]. The purpose of this work is to determine the influence of disturbances from supporting pylons when the geometric shape of the central body of the nozzle channel are changes.

In the present work, we study the stationary flow structure of a high-speed velocity jet flowing from an axisymmetric nozzle with a central body of variable cross section under several gas-dynamic flow regimes corresponding to transonic and supersonic flow regimes.

The experiments were carried out on the jet module of the T-326 periodical hypersonic wind tunnel at ITAM SB RAS. An axisymmetric convergent profiled nozzle with a central body (CB) was used (Fig. 1,*a*). The design feature of the nozzle is that there are supporting pylons (3 pcs.) at the nozzle inlet. Two types of central body were used, the internal contours of which are designed in such a way that a flow is realized in the nozzle channel at different speeds (Fig. 1,*c*).

a *b* *c*

Fig. 1. Nozzle model with CB: front view (*a*), rear view (*b*), CB (*c*).

The schlieren visualization of the jet flow was carried out for subsonic $N_{pr} = 1.7$ and supersonic $N_{pr} = 2.25$ regimes ($N_{pr} = P_0/P_e$, P_0, P_e – pressure in the prechamber of the facility and in the working chamber).

In the subsonic regime, when flowing around the conical part, a jet is formed with Mach number M = 0.9 at the exit, at some distance from the shear, the flow separates from the CB with the formation of a local supersonic zone with a shock wave in front of the separation region (Fig. 2,*a*).

At $N_{pr} = 2.25$, a weakly underexpanded jet is formed with $n = 1.18$, where $n = P_a/P_e$, P_a is the static pressure at the nozzle exit (see Fig. 2,*b*).

In the photograph, in addition to the boundary of the jet *3* flowing from the nozzle *1*, the separation trace *4*, due to the presence of the central body *2*, a shock-wave cell structure is visible, and a shock wave at the nozzle exit is visible. A shock *5* is formed in front of the separation

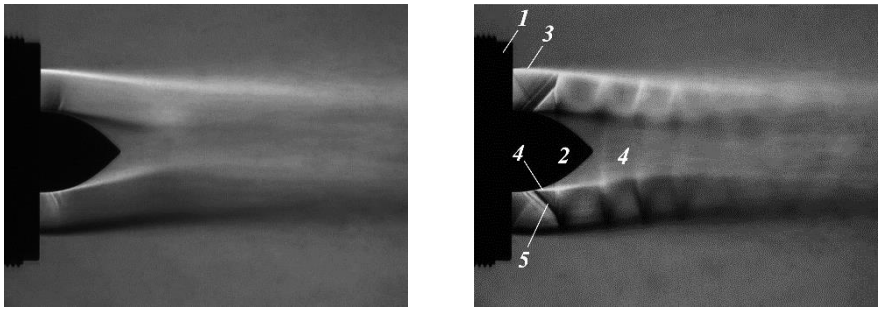

a *b*

Fig. 2. Schlieren image of the jet N_{pr}= 1.7 (*a*) and 2.25 (*b*), exposure 4 ms.

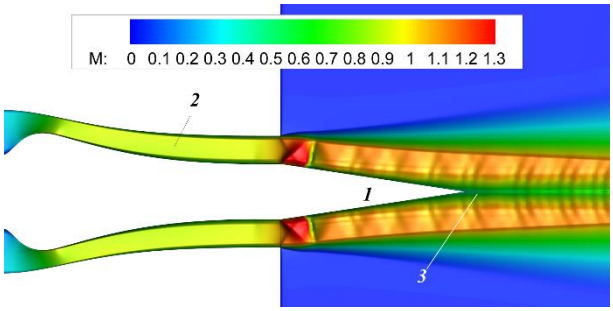

Fig. 3. The Mach number distribution, N_{pr} = 2.25.

line *4*. Further downstream, the jet narrows, and the intensity of the jumps decreases. Numerical calculation was performed using the Fluent program. Gasdynamic parameters: the jet working fluid is an ideal gas (cold air, T_0 = 300 K), P_0 = 1.7 and 2.25 bar, N_{pr} =1.7 and 2.25, M_a = 1, ambient pressure P_e = 1 bar. The Reynolds equations were solved in an axisymmetric formulation using the *k*–*w* SST turbulence model.

The results of the numerical calculation of the supersonic jet in the regime N_{pr}= 2.25 (Mach numbers) are shown in Fig. 3. In order to optimize the modeling process, reduce the intensity of flow pulsations and minimize the region of separated flow observed in the visualization with an ogival shape of the CB at the nozzle exit (pos. *2* in Fig. 2), the outlet part of the CB was modified (pos. *1*, Fig. 3).

It can be seen that inside the nozzle channel (pos. *2*, Fig. 3) a transonic flow with Mach number M = 0.9 is realized. A shock-wave flow structure is formed at the nozzle exit. In the first cell of the jet the flow accelerates to M = 1.3. The calculation data correspond to the experimental data. A subsonic wake is formed on the jet axis behind the CB cone, propagating downstream (pos. 3, Fig. 3). Experimental data on the three-dimensional structure of the flow in an exhausting jet are presented.

The research was carried out within the state assignment of Ministry of Science and Higher Education of the Russian Federation (project No. 121030500158-0).

REFERENCES

1. **Zapryagaev V.I., Kiselev N.P., Pivovarov A.A.** Formation of the three-dimensional structure of a high-speed jet exhausting from a model du-al-stream jet nozzle // Thermophysics and Aeromechanics. 2020. Vol. 27, No. 1. P. 23–33.
2. **Bosniakov S.M., Wolkov A.V., Duben A.P., Zapryagarev V.I., Kozubskaya T.K., Mikhaylov S.V., Troshin A.I., Tsvetkova V.O.** Comparison of two higher accuracy unstructured scale-resolving approaches applied to dual-stream nozzle jet simulation // Math. Models and Comp. Simulations. 2019. Vol. 31 No. 10. P. 130–144. DOI: 10.1134/S0234087919100101.

DOI: 10.53954/9785604788967_88

INVESTIGATION OF 2-D SUPERSONIC TRANSVERSE FLOW AROUND A CYLINDER WITH BLOWING FROM THIS CYLINDER SURFACE

V.A. Kislovskiy

Khristianovich Institute of Theoretical and Applied Mechanics SB RAS
630090, Novosibirsk, Russia

As a result of the oncoming flow interaction with the jet, significant changes in the flow occur on the streamlined body surface, as well as in the flow downstream from the interaction place. These flow changes are a combination of many complex gas-dynamic processes, including the formation of shocks and vortex structures, which significantly affect the redistribution of pressure on the streamlined body surface and heat transfer during the flow interaction with the streamlined body surface [1, 2].

In the study, we considered by numerical simulation the transverse flow around an infinite cylinder with a diameter D = 25 mm by a supersonic flow (M = 3, P_{st} = 16000 Pa, T_{st} = 106 K) in various cases blowing.

Several positions of the blowing hole along the streamlined cylinder circumference were considered: 0° (blowing against the oncoming flow); 45°; 90°; 135°; 180°. For all cases, the blowing parameters remained unchanged (b = 1 mm, M = 1, P_{st} = 1600000 Pa, T_{st} = 290 K).

The figure shows graphs of the static pressure distribution over the streamlined cylinder surface for all cases of blowing and for the case without blowing. The black line shows the value

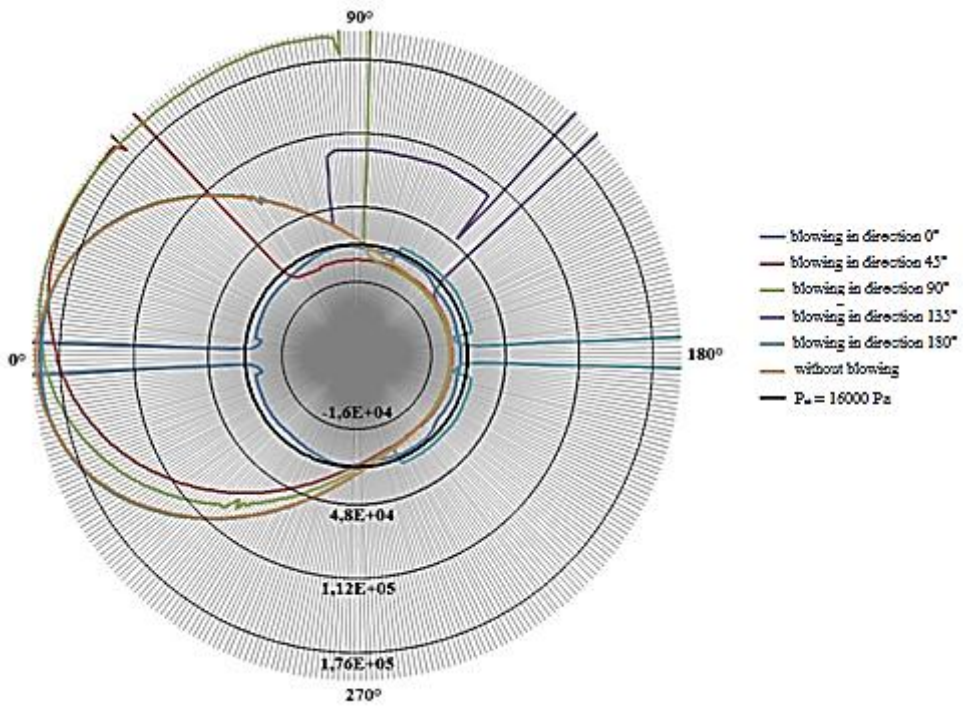

Distribution of static pressure on the streamlined cylinder surface in various cases of blowing.

of the static pressure in the oncoming flow. Thus, relative to this line, it becomes clear in which areas along the streamlined cylinder circumference the zones of high pressure or low pressure are formed as a result of the jet blowing. From the graphs presented, it becomes obvious that the pressure redistribution due to blowing has a significant effect on the integral value of the aerodynamic characteristics of the streamlined cylinder.

The work was carried out within the framework of the state task (state registration number 121030500154-2).

REFERENCES

1. **Bashkin V.A., Egorov I.V., Ezhov I.V.** Circular cylinder in a transonic flow at high Reynolds numbers: thermal problem // High Temperature. 2016. Vol. 54, No 4. P. 547–554.
2. **Kornilov V.I., Lysenko V.I.** Study of aerodynamic characteristics of cylindrical bodies in a supersonic flow // Bulletin of NSU. Series: Physics. 2011. Vol. 6, No. 4. P. 16–24.

DOI: 10.53954/9785604788967_90

EXPERIMENTAL STUDY OF IMPACT OF WEAK SHOCK WAVES ON A SUPERSONIC BOUNDARY LAYER OF THE SWEPT PLATE

V.L. Kocharin, A.A. Yatskikh, A.D. Kosinov, N.V. Semionov

Khristianovich Institute of Theoretical and Applied Mechanics SB RAS
630090, Novosibirsk, Russia

The process of laminar-turbulent transition in supersonic boundary layers substantially depends on the level of disturbances in the oncoming flow [1–4]. In wind tunnels the flow around the model can be affected by quasi-stationary disturbances in the form of weak shock waves generated by the surface roughness on the walls of the test section of the wind tunnel.

For flat plate models series of experimental [5–13] and numerical [14, 15] studies of the impact of weak shock waves on the flow in supersonic boundary layers were carried out. Works showed that the weak shock waves generate a longitudinal vortexes propagating in the boundary layer along the oncoming flow. In these regions, changes of pulsations and mean mass flow accompanied by changes in the amplitude-frequency spectra of mass flow pulsations in relation to the undisturbed boundary layer, both in the low-frequency and high-frequency ranges. At the same time, the weak shock wave can cause both a decrease and an increase in the boundary layer thickness. Experiments on visualization of heat flows [10, 11] showed that weak shock waves generate a longitudinal streak of temperature change in the form of two vortices that distribute downstream. Weak shock waves have different impact on the flow in the boundary layer, but they have a similar form.

The aforesaid studies of the effects of weak shock waves are performed for models with non-swept leading edge, however the case of an incident weak shock wave at a swept leading edge at a small angle, when the wave "catches up" the model is of fundamental and practical interest. In practice, this situation can occur when weak shock waves from the fuselage or other elements of the aircraft to get onto a wing. Experimental work [12] is devoted to the impact of weak shock waves on the boundary-layer of a flat plate at swept angles of the leading edge $\chi = 0 \div 25°$. It is showed that when the swept angle of the leading edge changed from 0 to 25 degrees under the impact of the catching-up weak shock wave, the widening of the vortex in the supersonic boundary layer occurred. In experiments [13], the influence of weak shock waves on the flow in the boundary layer of a swept plate was obtained at sweep angles of the leading edge $\chi = 35°$ and $\chi = 40°$. This work is continuation works [12, 13] and devoted to experimentally study of the impact of weak shock waves on the boundary layer of the swept flat blunt plate at the Mach number 2 and the leading edge swept angles from $\chi = 35°$ to $\chi = 50°$.

The experiments were carried out in the T-325 supersonic wind tunnel of ITAM SB RAS at Mach number M = 2 and unit Reynolds number $\mathrm{Re}_1 = (8 \pm 0.1) \cdot 10^6$ m^{-1}. In the experiments the model rotation mechanism was used which allowed changing the swept angle of the leading edge of the model directly during the experiment. The flat plate model had a bluntness radius of the leading edge $r = 2.5$ mm and was installed in the test section of the wind tunnel at the zero angle of attack. An adhesive PVC tape with a width (downstream) of 7 mm, a length (across the stream) of about 150 mm and a thickness of 0.13 mm was used as the roughness to generate weak shock waves. The measurements were performed along the z coordinate perpendicular to the oncoming flow at a fixed value of the transverse coordinate $y \approx 0.5$ mm. The measurements of the mean flow and mass flow pulsations were carried out by the constant temperature anemometer.

Experimental studies showed that when a weak shock waves were impact to the plate leading edge at swept angle $\chi = 35°$, longitudinal vortex in the boundary layer are generated and ac-

companied by an increase in the pulsation level and by a change in the pulsation's spectra. However, for a swept angle $\chi = 50°$, the level of rms pulsations and mean mass-flow for the case with two-dimensional roughness on the wall of the test section of the wind tunnel corresponds to the case of free oncoming flow around the model (without weak shock waves), i.e., weak shock waves do not impact on the boundary layer at $\chi = 50°$.

The research was carried out within the state assignment of Ministry of Science and Higher Education of the Russian Federation (project No. 121030500161-0). The study was conducted at the Equipment Sharing Center "Mechanics" of ITAM SB RAS.

REFERENCES

1. **Gaponov S.A., Maslov A.A**. Development of disturbances in compressible flows. Novosibirsk: Nauka, 1980.
2. **Lebiga V.A., Maslov A.A., Pridanov V.G.** Experimental investigation of the stability of supersonic boundary layer on a flat insulated plate // Archives Mech. 1979. Vol. 31, No. 3. P. 397–405.
3. **Laufer J.** Aerodynamic noise in supersonic wind tunnels // J. Aerospace Sci. Vol. 28, No. 9. P. 685–692.
4. **Kendall J.M.** Wind tunnel experiments relating to supersonic and hypersonic boundary layer transition // AIAA Journal. 1975. Vol. 13. P. 290–299.
5. **Kocharin V.L., Semionov N.V., Kosinov A.D., Yermolaev Yu.G., Yatskikh A.A.** Experimental study of effect of a couple of weak shock waves on boundary layer of the blunt flat plate // Proc. of the XIX International Conference on the Methods of Aerophysical Research (ICMAR 2018): AIP Conference Proceedings. 2018. Vol. 2027, No. 1. Art. 040026. 5 p. DOI:10.1063/1.5065300
6. **Yermolaev Yu.G., Kosinov A.D., Kocharin V.L., Semionov N.V., Yatskih A.A.** Experimental investigation of the weak shock wave influence on the boundary layer of a flat blunt plate at Mach number 2.5 // Fluid Dynamics. 2019. Vol. 54, No. 2. P. 257–263.
7. **Kocharin V.L., Afanasev L.V., Kosinov A.D., Yatskikh A.A., Semionov N.V., Yermolaev Yu.G.** Experimental investigation of effect of an external wave on supersonic boundary layer of the blunt flat plate // Proc. of the XXVI Conf. on High-Energy Processes in Condensed Matter, dedicated to the 150th anniversary of the birth of S.A. Chaplygin: AIP Conference Proceedings. 2019. Vol. 2125. Art. 030104. 6 p. DOI:10.1063/1.5117486
8. **Kocharin V.L., Yatskikh A.A., Kosinov A.D., Yermolaev Yu.G., Semionov N.V.** Experimental study of the weak shock wave action on the boundary layer of a plate at the Mach number 2.5 // Siberian J. of Physics. 2019. Vol. 14, No. 2. P. 46–55.
9. **Piterimova M.V., Kosinov A.D., Semionov N.V., Yatskikh A.A., Yermolaev Yu.G., Kocharin V.L.** Experimental study of excitation and evolution of contrarotating longitudinal vortices in a boundary layer of a flat plate at M = 2 // Proc. of the XXVII Conf. on High-Energy Processes in Condensed Matter, dedicated to the 90th anniversary of the birth of R.I. Soloukhin: AIP Conference Proceedings. 2020. Vol. 2288. Art. 030034. 5 p. DOI:10.1063/5.0028327
10. **Kocharin V.L., Yatskikh A.A., Prishchepova D.S., Panina A.V., Yermolaev Yu.G., Kosinov A.D., Semionov N.V., Afanasev L.V.** Experimental study of heat transfer in the boundary layer of a flat plate with the impact of weak shock waves on the leading edge // Proc. of the XXVII Conf. on High-Energy Processes in Condensed Matter, dedicated to the 90th anniversary of the birth of R.I. Soloukhin: AIP Conference Proceedings. 2020. Vol. 2288. Art. 030014. 4 p. DOI:10.1063/5.0028302.
11. **Kocharin V.L., Yatskikh A.A., Prishchepova D.S., Panina A.V., Yermolaev Yu.G., Kosinov A.D., Semionov N.V., Afanasev L. V.** Experimental study of the impact of N-wave on heat transfer in a boundary layer of a flat plate at the Mach number 2 // Proc. of the XX International Conf. on the Methods of Aerophysical Research (ICMAR – 2020): AIP Conference Proceedings. 2021. Vol. 2351, No. 1. Art. 040036. 4 p. DOI:10.1063/5.0051930
12. **Kocharin V.L., Kosinov A.D., Yatskikh A.A., Ermolaev Yu.G., Semionov N.V., Piterimova M.V., Shevelkov S.G., Minin O.P.** The impact of weak shock waves on the flow in the boundary layer of a flat plate with a variable sweep angle of the leading edge // Thermophysics and Aeromechanics. 2019. Vol. 26, No. 6. P 803–809.
13. **Kocharin V.L., Kosinov A.D., Yatskikh A.A., Afanasev L.V., Ermolaev Yu.G., Semionov N.V.** The experimental study of the weak shock wave action on the boundary layer of the sweep flat plate // J. Phys.: Conf. Ser. 2019. 1404. Art. 012083 4 p. DOI:10.1088/1742-6596/1404/1/012083.
14. **Din Q.H., Egorov I.V., Fedorov A.V.** Interaction between Mach waves and the boundary layer in supersonic flow past a plate with a sharp leading edge // Uch. Zap. TsAGI. 2017. Vol. 48, No. 4. 317–329.
15. **Din Q.H., Egorov I.V., Fedorov A.V.** Mach wave effect on laminar-turbulent transition in supersonic flow over a flat plate // Fluid Dynamics. 2018. Vol. 53, No. 5. P. 690–701.

DOI: 10.53954/9785604788967_92

CLOGGING EFFECT ON THERMOSOLUTAL CONVECTION IN A LAYERED POROUS MEDIUM

N.V. Kolchanov, E.A. Kolchanova

Institute of Continuous Media Mechanics UB RAS
614013, Perm, Russia

The paper is devoted to the study concerning the adsorption and desorption effects on the onset of thermosolutal convection (or double-diffusive convection) in an anisotropic porous medium saturated with a binary mixture in the gravitational field (Fig. 1). The medium consists of the two composite homogeneous porous sublayers with the different permeabilities of K_1 and K_2. The mixture includes a light carrier fluid and an active heavy solute that can interact with the solid matrix of the porous medium. The solute particles can stick to the matrix and be immobile for some time. So, the mixture transport within the porous medium is accompanied by immobilization. The system of porous sublayers is in the non-isothermal conditions. It is heated either from below or from above (Fig. 1).

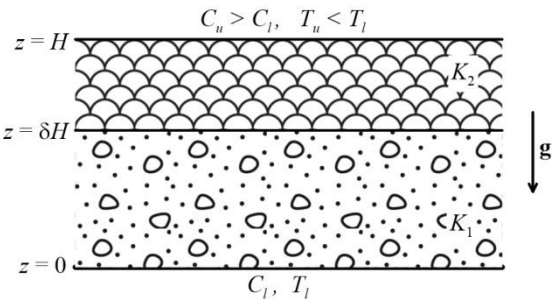

Fig. 1. A non-isothermal system of the two mixture-saturated porous sublayers with different permeability in the presence of sorption in the gravitational field.

Our study continues the recent works of [1–3] where solutal convection in a separately located porous layer [1, 2] or in a system of two porous sublayers [3] was considered under the isothermal conditions. The equations for thermosolutal convection, which take into account pore clogging, are presented on the basis of the Boussinesq approximation and Darcy model [4]. Numerical simulation of the boundary value problem is performed by the method of constructing a fundamental system of solutions. The main governing parameters of the problem are a ratio of the adsorption and desorption coefficients ω, clogging coefficient ζ of the porous medium, ratio of permeabilities $K_r = K_2/K_1$, buoyancy ratio $N = (\beta_T \Delta T)/(\beta_C \Delta C)$, solutal Rayleigh – Darcy number $\mathrm{R}_m = \rho_f \beta_C g H K_m \Delta C/(\eta D \phi_m)$, where $K_m = \delta + (1-\delta)K_r$ is an average permeability of the sublayers and $\phi_m = \delta + (1-\delta)\phi_r$ is an average porosity of the sublayers.

One has found the threshold value of R_{m*} for the stability of a mechanical equilibrium state of the mixture with respect to small disturbances with the wave number of k_* at $\omega = 1$ and different values of the clogging coefficient of ζ. Figure 2 demonstrates stability maps for a two-layered system with a highly permeable upper sublayer at the two values of the permeability ratio of $K_r = 10$ (lines *1*) and $K_r = 40$ (lines *2*) and different positions of their interface of $\delta = 0.5$ (lines *1*) and $\delta = 0.8$ (lines *2*) (Fig. 2, *a*, *b*). It has been shown that the onset value of thermosolutal convection decreases with increasing the positive buoyancy ratio (the system is heated from below), and in the opposite case of an increase in the absolute negative buoyancy ratio (the sys-

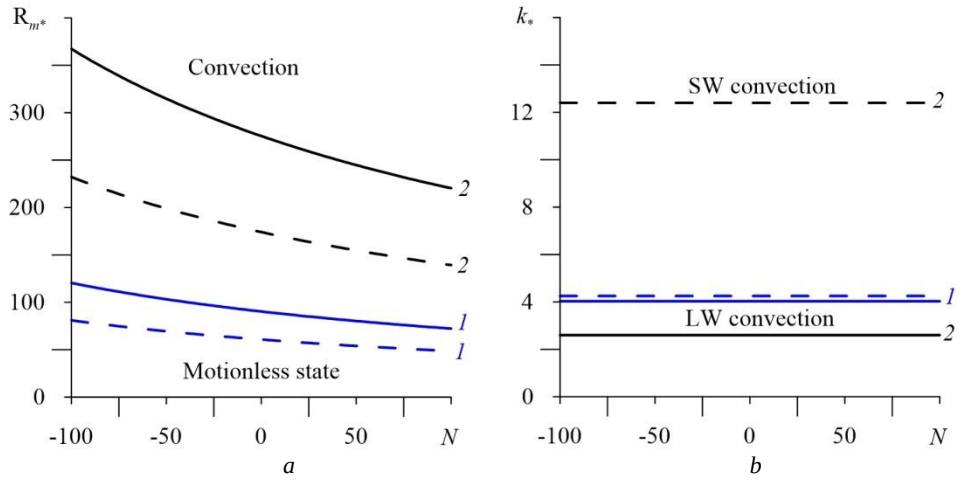

Fig. 2. The critical solutal Rayleigh-Darcy number (*a*) and critical wave number of convective patterns (*b*) versus the buoyancy ratio N at $\omega = 1$ and different values of the clogging coefficient ζ: 0 (dashed lines), 0.3 (solid lines). The denotation of SW is for the short-wave convection and that of LW is for the long-wave convection.

1 – $K_r = 10$, $\delta = 0.5$, *2* – $K_r = 40$, $\delta = 0.8$.

tem is heated from above) the threshold Rayleigh – Darcy number grows (Fig. 2 *a*). This is due to the fact that in the first case when $N > 0$, both density gradients caused by the temperature and concentration drops are directed upward. It means that a heavier mixture component accumulates near the upper boundary of the system and causes the unstable density stratification. In the second case when $N < 0$, the thermal and solutal density gradients are directed opposite to each other, so the equilibrium state of mixture stabilizes as the temperature difference at external boundaries of the system increases.

With increasing the clogging coefficient of ζ both in the isothermal [3] and non-isothermal conditions, it becomes possible to change the scale of a convective roll pattern from the local short-wave to large-scale long-wave convection (Fig. 2,*b*). At the same time, this situation manifests itself for all heating directions considered (they are heating from below and above).

The work was supported by the Russian Science Foundation (Grant No. 20-11-20125).

REFERENCES

1. **Maryshev B.S., Klimenko L.S.** Solutal convection in a horizontal porous layer with clogging at a high solute concentration // VII Perm Hydrodynamical Forum (PHD-Forum 2020) (Perm, Russia, 22–24 October 2020): [Proc.]; Journal of Physics: Conference Series. 2021. Vol. 1809. Art. 012009. (7 p.). https://doi.org/10.1088/1742-6596/1809/1/012009.
2. **Maryshev B.S., Klimenko L.S.** Convective stability of a net mass flow through a horizontal porous layer with immobilization and clogging // Transport in Porous Media. 2021. Vol. 137. P. 667–682.
3. **Kolchanova E.A., Kolchanov N.V.** Onset of solutal convection in layered sorbing porous media with clogging // International Journal of Heat and Mass Transfer. 2022. Vol. 183. Part A, Art. 122110. 14 p. https://doi.org/10.1016/j.ijheatmasstransfer.2021.122110
4. **Nield D.A., Bejan A.** Convection in Porous Media. Switzerland: Springer International Publishing, 2017. 988 p.

DOI: 10.53954/9785604788967_94

THE EFFECT OF THIN AIR INTERLAYER ON CONVECTION INDUCED BY INTERNAL HEATING IN LAYERED POROUS MEDIUM

E.A. Kolchanova, N.V. Kolchanov

Perm State University
614990, Perm, Russia

The work is devoted to the investigation of a threshold-like excitation of thermal convection in a three-layered system consisting of the two heat-generating porous layers separated by a thin air interlayer (Fig. 1). The heat source strength in each of the air-saturated porous layers is the same and linearly depends on the solid volume fraction. The ratio of permeabilities of the upper and lower porous layers is equal to $K_r = 10$. The external boundaries of the three-layered system have constant equal temperatures and are impermeable to air. The basic temperature profile which establishes in the absence of convection is a quadratic dependence on the transverse z-coordinate. Thus, in the presence of internal heat generation there are favorable conditions for the threshold-like onset of the convective flow in the layers under the gravitational field.

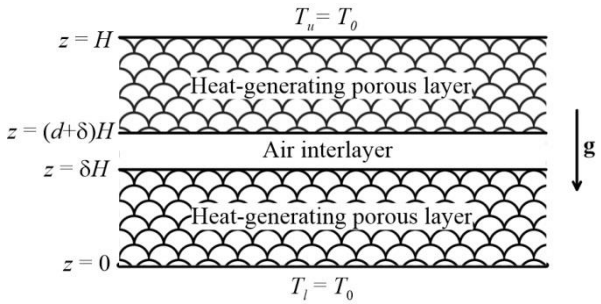

Fig. 1. A three-layered convective system consisting of the two heat-generating porous layers which are separated by an air interlayer in the gravitational field.

Heat release makes some parts of the porous medium overheat. Convective air ventilation allows one to effectively remove heat from these areas. This is relevant, for example, in the biologically active heat-generating media (the bulk agricultural raw materials), where it is necessary to maintain optimal thermal storage conditions. Applying an air interlayer of a given depth between the layers of the medium, one can control the convective heat transfer and, therefore, prevent the medium parts from overheating.

The purpose of our work is to analyze the effect of a thin air interlayer on the onset of convection driven by internal heat generation. The internal Rayleigh-Darcy number of $\mathrm{Ra}_{m*} = \phi R_{I*}(\delta + K_r(1-\delta))$ is determined through the average permeability of the upper and lower porous layers, where $\mathrm{R}_{I*} = (\rho C)_a g\beta Q_s K_1 H^3/(2\nu\kappa_p^2)$ is the internal Rayleigh – Darcy number normalized by the solid fraction ϕ and expressed through the parameters of the lower porous layer. The thermal conductivity κ_p of the saturated porous medium is found though thermal conductivities of the air and solid elements having water in their composition.

Figure 2 shows the threshold Rayleigh – Darcy number Ra_{m*} and critical wave number k^* of the convective patterns which initiate near the stability threshold of the air motionless state versus the interlayer parameter $\varepsilon = d^3/(12\mathrm{Da})$ at various values of the parameter δ. Here, Da is the Darcy number. The interlayer parameter is obtained within the approximation of a small depth d of the air interlayer. Convection in this interlayer is a throughflow with a simple pattern. The three-layered system reduces to a system of two porous layers with effective interface conditions at $z = \delta$. It can be seen that the presence of the interlayer speeds up the onset of convec-

tion at any value of the parameter δ (Fig. 3,*a*). Note that curve *3* in Fig. 3,*a* has a kink in the region of small values of the parameter ε. This kink is associated with an abrupt, jump-like transition from the large-scale long-wave convection in both porous layers to local short-wave convection in the upper highly permeable porous layer ($K_r = 10$) (curve *3* in Fig. 3,*b*). The rest threshold curves *1*, *2*, and *4* in Fig. 3,*a* do not have any characteristic kinks. In this case, the critical wave number of convective patterns monotonically decreases with increasing the parameter ε. A similar competition of local and large-scale convection has been studied in the two- and three-layered systems in the absence of internal heat heating in [1–3] and in its presence in a three-layered system consisting of the two fluid layers separated by a porous medium in [4]. Our study presents new results for a three-layered heat-generating porous-air-porous system.

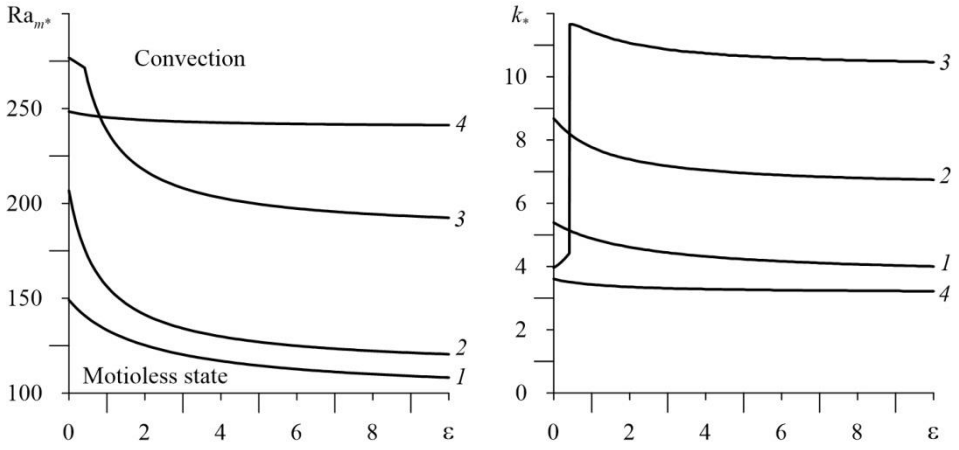

a *b*

Fig. 2. The threshold internal Rayleigh – Darcy number (*a*) and critical wave number (*b*) of convective patterns versus the interlayer parameter ε for the ratio of the layer permeabilities of $K_r = 10$ and different values of the parameter δ.

δ = 0.50 (*1*), 0.75 (*2*), 0.85 (*3*), 0.90 (*4*).

The work was supported by the Russian Science Foundation (Grant No. 21-71-10045), https://rscf.ru/en/project/21-71-10045/.

REFERENCES

1. **Kolchanova E.A., Lyubimov D.V., Lyubimova T.P.** The onset and nonlinear regimes of convection in a two-layer system of fluid and porous medium saturated by the fluid // Transport in Porous Media. 2013. Vol. 97, No. 1. P. 25–42.
2. **Tsiberkin K.** Porosity effect on the linear stability of flow overlying a porous medium // European Physical Journal E. 2020. Vol. 43, No. 34. https://doi.org/10.1140/epje/i2020-11959-6
3. **Lyubimova T.P., Muratov I.D**. Interaction of the longwave and finite-wavelength instability modes of convection in a horizontal fluid layer confined between two fluid-saturated porous layers // Fluids. 2017. Vol. 2, No. 39. (8 p.) DOI:10.3390/fluids2030039
4. **Shalbaf S., Noghrehabadi A., Assari M.R., Dezfuli A.D.** Linear stability of natural convection in a multilayer system of fluid and porous layers with internal heat sources // Acta Mechanica. 2013. Vol. 224. P. 1103–1114.

DOI: 10.53954/9785604788967_96

EFFECT OF THE BLUNT-FIN SWEEP ANGLE ON 3D STRUCTURE OF A LAMINAR SUPERSONIC JUNCTION FLOW

E.V. Kolesnik, E.V. Babich, A.A. Smirnovsky, E.M. Smirnov

Peter the Great St. Petersburg Polytechnic University
195251, St. Petersburg, Russia

A laminar supersonic flow past a blunt fin mounted on a plate along which the boundary layer evolves is considered for different values of sweep angle (Fig. 1,*a*). The main components of the problem definition are based on [1], where the flow past an unsweep fin with the freestream Mach number of 6.7 was studied in the range of Reynolds numbers, Re_D, from $1.25\cdot10^4$ to $3.75\cdot10^4$, if evaluated on the fin diameter, D. In [1], the results of both experiments and numerical simulations were reported, and the authors interpreted the obtained numerical solutions as stationary and unique for all Re_D-values considered. However, it was shown later, [2], that the flow simulated at $\mathrm{Re}_D = 2.5\cdot10^4$ is unsteady. In our recent paper [3], it was shown that at $\mathrm{Re}_D = 1.25\cdot10^4$ there are two stable stationary solutions that correspond to two metastable flow states with different configurations of the vortex structure. As well, in [4, 5] results at different Reynolds numbers for the same configuration were studied and the branch point of the solutions was determined. It is well known also, that one of the most dominant parameters on the shock-wave-boundary-layer interaction in such configurations is the sweep angle of the fin relative to the plate [2]. The objective of present research is to investigate numerically the effects of the blunt fin sweep angle on the shock wave boundary layer interaction, on local heat transfer, and on the existence of dual solutions as well. Cases with negative and positive values of the sweep angle (Ω, varied from -10° to 10°) are calculated.

The computational domain is shown in Fig. 1,*a* (dashed lines). The flow in this configuration can be treated as symmetric [3], therefore only half of the configuration is considered. The flow structure and heat transfer are determined by the following dimensionless parameters: geometric factor L/D, freestream Mach number $\mathrm{M} = U_\infty/a_\infty$, Reynolds number $\mathrm{Re}_D = U_\infty D/\nu_\infty$, Prandtl number Pr, temperature factor T_∞/T_w, and the ratio of the specific heats γ. According to [1], the following set of unchanged parameters is considered: M = 6.7, $T_w/T_\infty = 4.75$, Pr = 0.7, γ = 1.4. The simulation has been performed for $\mathrm{Re}_D = 1.25\cdot10^4$ (D = 2.5 mm). The distance L between the leading edge of the plate and the body was fixed and equal to 145 mm; thus, the boundary layer evolves on the plate in the same manner for all considered cases. At the inlet boundary of the computational domain, a uniform flow is specified; the no-slip boundary conditions are specified at the fin surface and at the plate. At the lateral and upper boundaries, the non-reflecting boundary conditions are

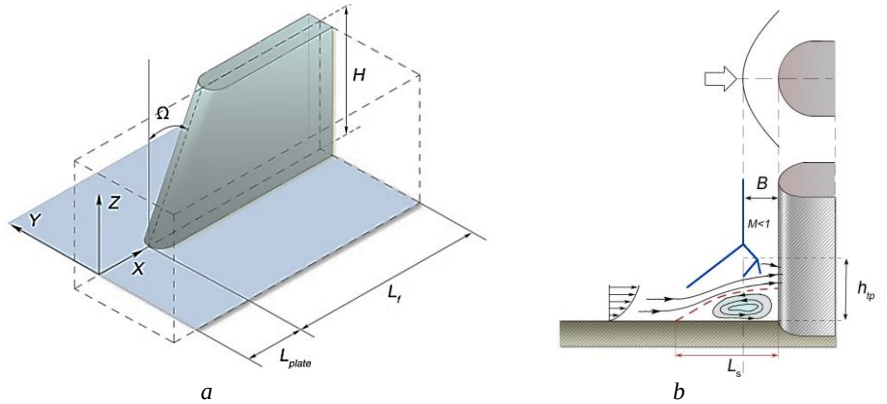

a *b*

Fig. 1. Computational domain (*a*) and general flow structure in a symmetry plane for Ω = 0° (*b*).

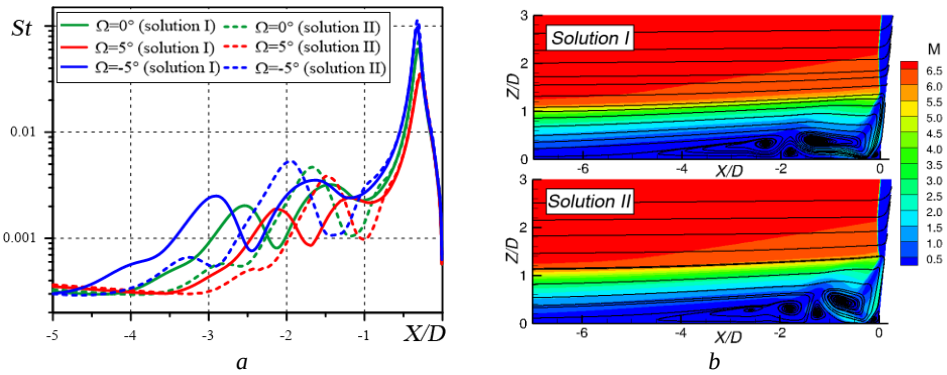

Fig. 2. Stanton number distribution over the plate for three values of sweep angle(*a*) and Mach number map in symmetry plane computed in case Ω = 5° (*b*).
Data obtained for two solutions are shown.

prescribed, while the zero-gradient condition is specified at the outlet. The fin and plate surfaces are maintained at constant temperature T_w. Numerical solutions were obtained using the finite-volume unstructured code SINF/Flag-S developed at the Peter the Great St. Petersburg Polytechnic University. The calculations were performed using quasi-structured grids consisting of 10 mln cells.

General structure of the flow in the symmetry plane is illustrated in Fig. 1,*b*, where an extended separation region in front of the body, as well as oblique compression waves induced by supersonic flow interaction with the separation zone are observed. Vortex structure in the separation zone determines a peculiar heat flux distribution with multiple local maxima. As shown in [3–5], in case of $Re_D = 1.25 \cdot 10^4$ and Ω = 0°, calculations starting from considerably different initial conditions had resulted in two different stable stationary solutions corresponding to metastable flow states with different configurations of the vortex structure. These solutions were used as initial data for calculations with different sweep angles. Figure 2,*b* illustrates Mach number maps obtained in case of Ω = 5° for two solutions. The distinctive features of these solutions are similar to those reported in [4] for Ω = 0°: the separation zone in Solution I is more extended, and the main vortex center is located about twice further from the fin leading edge, as compared to Solution II. Stanton number distributions over the plate are shown in Fig. 2,*a* (green lines indicate the Ω = 0° case). In addition to the global maximum, Stanton number distributions related to Solution II contains one more, well pronounced, local maximum, whereas in Solution I two local maxima of a lower level are predicted. In Fig. 2,*a*, one can see clearly that even a relatively small positive value of sweep angle leads to a considerable reduction of the separation region, to a shift of local maxima towards the fin leading edge and to a decrease in the peak value of global maximum. Opposite trends are observed in case of negative sweep angle values.

It was revealed also that in case of negative sweep angle, an increase in its module leads to more pronounced distinctions between Solution I and Solution II, with no specific issues of obtaining a dual solution. Contrary to that, our preliminary calculations have shown that in case of positive sweep angles, the possibility of obtaining a dual solution is reduced: in particular, in case of Ω = 10° only a solution of the second type (Solution II) was obtained.

REFERENCES

1. **Tutty O. R., Roberts G. T., Schuricht P. H.** High-speed laminar flow past a fin-body junction // J. Fluid Mech. 2013. Vol. 737. P. 19–55.
2. **Mortazavi M., Knight D.** Simulation of Hypersonic-Shock-Wave – Laminar-Boundary-Layer Interaction over Blunt Fin // AIAA Journal. 2019. Vol. 57. № 8. P. 3506-3523.
3. **Kolesnik E. V., Smirnovsky A. A., Smirnov E. M.** Duality of the Vortex Structure Arising in a Supersonic Viscous Gas Flow Past a Plate and a Blunt-Fin Body Junction // Tech. Phys. Lett. 2020. Vol. 46. № 6. P. 579–582.
4. **Kolesnik E. V., Smirnov E. M.** Dual numerical solutions for a supersonic laminar flow past a plate and a blunt-fin body junction // AIP Conference Proceedings. 2021. Vol. 2351. P 040030.
5. **Kolesnik E. V., Smirnov E. M.** Supersonic Laminar Flow Past a Blunt Fin: Duality of the Numerical Solution // Technical Physics. 2021. Vol. 66. № 6. P. 741–748.

DOI: 10.53954/9785604788967_98

NEW POSSIBILITIES FOR LOCAL SIMULATION OF AERODYNAMIC HEATING IN SUBSONIC HIGH-ENTHALPY AIR JETS IN POWERFUL HF-PLASMATRONS

A.F. Kolesnikov, S.A. Vasil'evskii, A.V. Chaplygin, S.L. Shchelokov

Ishlinsky Institute for Problems in Mechanics SB RAS
119526, Moscow, Russia

Induction HF-plasmatrons VGU-3 and VGU-4 (IPMech RAS) are included in the "List of Unique Research Facilities of the Russian Federation": https://ckp-rf.ru/usu/441568/. These facilities [1] are exploited for basic and applied aerophysical research including aerothermodynamics of plasmas and high-enthalpy gas flows, heat transfer in equilibrium and nonequilibrium chemically reacting gas flows, aerothermal testing high-temperature materials in order to estimate thermochemical stability and resource.

This paper continues approach [2] in order to analyze capabilities of the 1-MW power VGU-3 plasmatron for direct local simulation of aerodynamic heating in high-enthalpy subsonic air jets. To duplicate stagnation point heat flux for a blunt body re-entry conditions in HF-plasmatron, three requirements should be provided [3]: 1) enthalpy at the outer edge of the boundary layer near stagnation point of the test model equals the total enthalpy for re-entry conditions; 2) stagnation pressures in HF-plasmatron jet and on re-entry blunt body are equal; 3) equality of velocity gradients at the outer edge of boundary layers near the stagnation points in experiment and re-entry conditions. As input data for analysis, computed distributions of velocity and enthalpy in subsonic air jets for the VGU-3 tests conditions are used. In Fig. 1 enthalpy profiles at the exit of the VGU-3 discharge channel are shown.

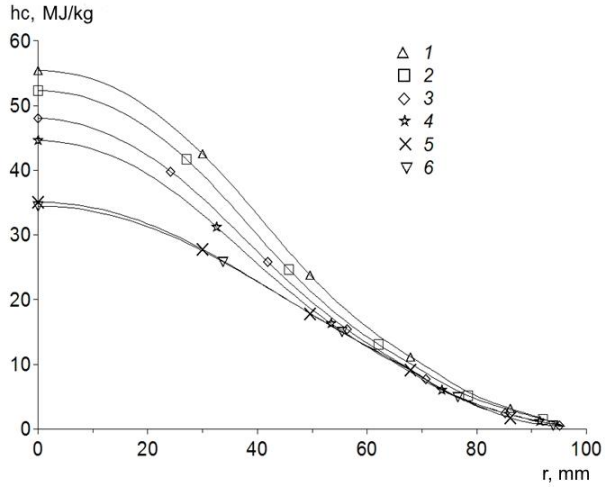

Fig. 1. Radial profiles of enthalpy at the discharge channel exit section for the VGU-3 plasmatron regimes at different pressure P, mbar, and anode power N_{ap}, kW.
1 – 200, 300; *2* – 300, 300; *3* – 200, 200; *4* – 300, 200; *5* – 200, 100; *6* – 300, 100.

As a result of analysis of large numerical data for VGU-3 plasmatron the universal correlation for velocity at the center of the plasmatron exit section is proposed as multi-parameter function of enthalpy and pressure in subsonic air jet. Using this universal correlation, conditions of the local heat transfer simulation [3] and results from [2], the domains in terms "total enthalpy –

stagnation pressure" and corresponding "flight velocity – re-entry altitude" are built in order to show where local simulation of the stagnation point heat fluxes is possible for nose radius range 0.1–1.0 m using VGU-3 and VGU-4 facilities. For both HF-plasmatrons analytical approximations for effective radii of models intended for heat transfer simulation are established as functions of re-entry velocity and atmospheric air density.

Experiments have been carried out to determine heat fluxes in the stagnation point area of a water-cooled copper surface of a model with a diameter of 50 mm with a flat nose and a rounded side edge (standard ESA model) in subsonic jets of air plasma of HF-plasmatrons VGU-4 and VGU-3. In the VGU-4 facility standard configuration of a discharge channel with a diameter of 80 mm was used. Heat flux measurements in the VGU-3 facility were carried out in jets flowing from a conical nozzle with a 60-mm diameter. Experimental results are shown in Fig. 2. The use of two facilities of different power in experiments substantially expanded the range of heat fluxes realized on the model of the same geometry and capabilities for local aerodynamic heating simulation in wide ranges of total enthalpy and stagnation pressure.

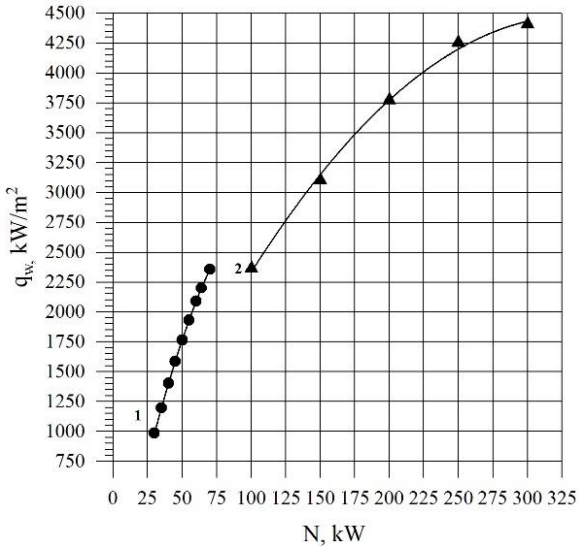

Fig. 2. Heat fluxes to the cold copper surface at the stagnation point of the ESA standard model in subsonic jets of high-enthalpy air obtained by the two facilities of different power.
1 – VGU-4 (100 kW), *2* – VGU-3 (1 MW).

This work was supported by the Ministry of Science and Higher Education within the framework of the Russian State Assignment under contract No. AAAA-A20-120011690135-5.

REFERENCES

1. **Gordeev A.N., Kolesnikov A.F.** High-frequency induction plasmatrons of the VGU series // Topical Problems in Mechanics. Physical and Chemical Mechanics of Liquids and Gases. Moscow: Nauka, 2010. P. 151–177 [in Russian].
2. **Kolesnikov A.F., Shchelokov S.L.** Analysis of the simulation conditions of the aerodynamic heating in subsonic high-enthalpy air jets from the VGU-4 HF plasmatron // Fluid Dynamics. 2021. Vol. 56, No. 2. P. 236–241.
3. **Kolesnikov A.F.** Conditions of simulation of stagnation point heat transfer from a high-enthalpy flow // Fluid Dynamics. 1993. Vol.2 8, No. 1. P.131-137.

DOI: 10.53954/9785604788967_100

APPLICATION EXPERIENCE OF AIR BLOWING TECHNOLOGY IN A FLOW AROUND A BODY OF REVOLUTION

V.I. Kornilov, A.N. Popkov

Khristianovich Institute of Theoretical and Applied Mechanics SB RAS
630090, Novosibirsk, Russia

To the current, a number of artificial methods for passive and active control by turbulent shear flows have been developed [1, 2]. Studies on this problem have been undertaken both on a plan surfaces and on those curved in the streamwise direction. They cover a wide range of applied control methods, such as uniform blowing or suction, periodic blowing/suction, etc. not only in subsonic gas flow, but also in high-velocity compressible flows. One of the methods which was not properly evaluated and logically concluded is the gas blowing or injection into a turbulent boundary layer of bodies of revolution (TB). On the whole, as applied to aerodynamic elements of the type of fuselage or rocket body, the technology of distributed f blowing under the conditions of developed turbulent flow turned out to be unstudied even on schematized constructions of flying vehicles. In fact, such studies are limited to one or two papers (see, for example, [3]) in which this problem is touched upon in one way or another. Moreover, even uncontrolled axisymmetric boundary layers have not been investigated thoroughly in the same way as plane due to the difficulties in providing coaxial flow around the body and the absence of its deflection.

At the same time, the development of modern blowing technology on the BR is a rather difficult multi-parameter task associated with the need to study the effect of a number of major parameters that determine the effectiveness of the control method.

In the present paper, the concept of controlling the turbulent boundary layer on the BR of a large aspect ratio via distributed air blowing through a finely-perforated section, which is a part of the idealized fuselage of the subsonic transport aircraft is formulated; this concept is numerically and experimentally verified. The studies of the mean flow parameters and turbulent characteristics of the boundary layer, the pressure distribution on the BR surface, as well as the aerodynamic drag of the BR were carried out. The mechanism responsible for changing the physical properties of the flow and aerodynamic characteristics of the BR with both a distributed air blowing of various intensity and changing the relative length of the perforated section is discussed.

The performed studies give grounds for the following brief conclusion:

– forced blowing through the permeable surface with a lenght $\Delta l/L = 0.0474$ provides a significant gain in the skin friction of the BR in comparison with similar magnitude on the baseline. Beginning from the leading edge of the perforated insert and further downstream, up to a distance $x \approx 600\delta^{**}$, where δ^{**} is the boundary-layer momentum thickness, there is a steady decrease in local friction, the value of which reaches more than 56% directly in the blowing region at its maximum intensity C_b (Fig. 1);

– spontaneous blowing that can be attributed to the natural difference between barometric pressure and static pressure in the wind-tunnel test section also reduces the skin friction coefficient, the value of which at the basic freestream mode is about 28%. It has been found that increase of freestream velocity contributes to further decrease in skin friction, confirming, thereby, the main mechanism of this phenomenon;

– numerical simulation of the flow around both the baseline and the BR with a blowing of variable intensity on the whole demonstrates adequate to the physical representations and obtained experimental data the reproduction of the main flow characteristics on the basis of turbulence model used here;

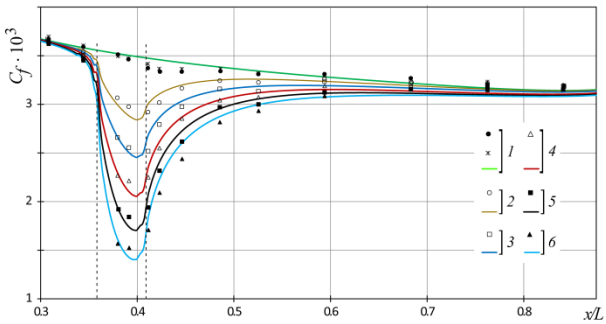

Fig. 1. Variation of local skin-friction coefficient along the body of revolution.

C_b = 0 (*1*), 0.00186 (*2*), 0.00354 (*3*), 0.00531 (*4*), 0.00708 (*5*), 0.00885 (*6*). Points are experiment (measurements with Preston tubes of different diameter); solid line is numerical calculation.

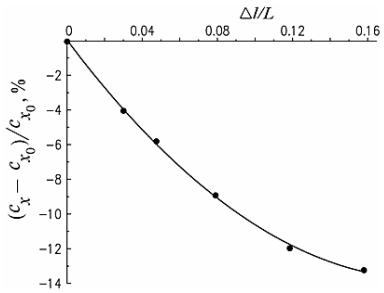

Fig. 2. Percentage decrease in total aerodynamic drag of the body ofrevolution with increase of perforated section length.

C_b = 0.00885.

– a significant interference effect between the flow on the BR and the wind tunnel walls has been found, which requires taking into account this effect on the aerodynamic performances of the BR;

– the data of numerical calculations show that due to an increase in the length of the perforated section up to the value $\Delta l/L$ = 0.158, the total aerodynamic drag of the BR can be reduced by 13% (Fig. 2). However, the final conclusion about the effectiveness of the use of the control method can be drawn after experimental verification and additional calculations with variation of the most important parameters of the main and secondary flows.

This work was carried out at the Khristianovich Institute of Theoretical and Applied Mechanics SB RAS with the support by the Russian Scientific Foundation (Grant No. 22-29-00003). The experiments were performed on the equipment of the Collective Use Center “Mekhanika” (Mechanics).

REFERENCES

1. **Abbas A., de Vicente J., Valero E.** Aerodynamic technologies to improve aircraft performance // Aerospace Science and Technology. 2013. Vol. 28. P. 100–132.
2. **Kornilov V.I.** Current state and prospects of researches on the control of turbulent boundary layer by air blowing // Progress in Aerospace Sciences. 2015. Vol. 76. P. 1–23.
3. **Schetz J.A., Nerney B.** Turbulent boundary layer with injection and surface roughness // AIAA J. 1977. Vol. 15, No. 9. P. 1288–1294.

DOI: 10.53954/9785604788967_102

INVESTIGATION OF ICE GROWTH ON A SWEPT WING WITH CONSIDERING THE MODEL OF UNIFORM ROUGHNESS

K.B. Koshelev, A.V. Ivanov, S. V. Strijhak

Ivannikov Institute for System Programming RAS
109004, Moscow, Russia

The problem of studying the icing of regional aircraft elements (slats, flaps, wing, pressure receiver) is relevant due to an increase in the number of flights through the northern territories of the Russian Federation and ensuring flight safety in difficult climatic conditions.

The study and testing of computational algorithms, numerical schemes and physical and mathematical models of icing presented in the work is carried out on the problem of a gas-droplet flow around a swept wing.

In open access publications, there are experimental data for a model swept wing with a GLC-305 airfoil and a large wing in wind tunnels [1, 2]. At the same time, the calculation data on the thickness of ice and the aerodynamic characteristic of the wing are also available based on the results of mathematical modeling. The example for the case of a flow around a wing with a flow corresponding to the "rime ice" regime is the simplest in terms of ice accretion modeling.

ISP RAS previously developed the iceFoam solver based on the OpenFOAM v1912 library [3]. The solver was tested on problems with the flow around the cylinder and NACA 0012 airfoil. The solver uses the URANS method and the Spalart – Allmaras turbulence model, the thermodynamic model of the liquid film, and the bisector method for rebuilding the body geometry.

Accounting for the influence of surface roughness can be done through the use of the Spalart – Allmaras turbulence model and the wall function model. The effect of roughness is taken into account by setting the equivalent roughness parameter.

In this work, the computational domain and two variants of computational grids were prepared: unstructured and block-structured. The wing dimensions were chosen as in the experiment of prof. M. Papadakis [1].

The block-structured grid has certain advantages. For example, it is possible to build a high-quality mesh at the leading edge and at the tail of the wing. The number of computational blocks was chosen to be 18. The preparation of the computational domain and mesh were carried out in the open source Salome software package. The number of computational cells in the unstructured grid was about $2.5 \cdot 10^6$.

The simulation case included setting the initial and boundary conditions. The values for the parameters of flow velocity, median droplet diameter, liquid water content, air temperature, and icing time were set in accordance with the case of rime ice regime from [1]. The assignment of the roughness value was carried out based on the data of [4].

The fields of velocity, pressure, ice thickness, drag coefficient were calculated. The problem statement was corresponded to the rime ice regime of icing: flow velocity was 90 m/s, angle of attack was 6°, air temperature was 261.87 K, liquid water content was 0.51 g/m^3, particle diameter was 14.5 μm, icing time was 5 min. The time step was set equal to $6 \cdot 10^{-5}$ seconds. One case simulation using HPC4 computing cluster of the National Research Center "Kurchatov Institute" took 33 hours on 24 computing cores. A comparison with experimental data for the case of a smooth and rough surface is made.

Figure 1 shows the computational area and the droplets movement calculating results. Figure 2 shows the ice surface shape from below on the wing. One can see the 3D position of the ice surface and the ability of the solver to model essentially 3D icing processes. The averaged

only 2D graphs of the ice surface are given in [1]. At the same time, it can be noted that the results of this work are close in terms of the maximum ice thickness (about 3 mm) to the experimental data; in terms of the ice shape, the results also qualitatively coincide.

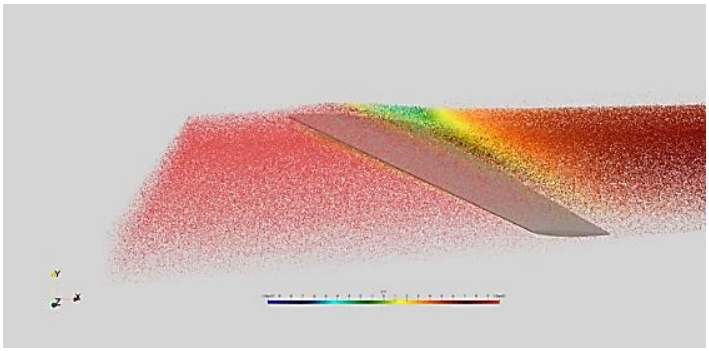

Fig. 1. Computational area.

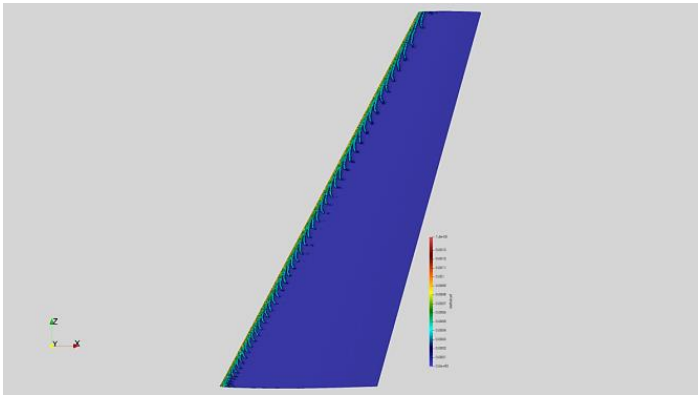

Fig. 2. Wing with ice on the leading edge.

The calculations were carried out on 12, 24, 36 cores in parallel mode using high-performance clusters of the ISP RAS and the National Research Center "Kurchatov Institute".

The reported study was funded by Russian Foundation for Basic Research, project number 19-29-13016.

REFERENCES

1. **Papadakis M., Yeong H-W., Wong S-C.,** Vargas M., Potapczuk M. Experimental investigation of ice accretion effects on a swept wing: Final Report No. DOT/FAA/AR-05/39. Department of Aerospace Engineering Wichita State University, Wichita; NASA John H. Glenn Research Center at Lewis Field Cleveland, OH. 2005, 210 p. URL: http://www.tc.faa.gov/its/worldpac/techrpt/ar05-39.pdf
2. **Fujiwara G.E., Bragg M.B.** Method for Designing Hybrid Airfoils for Icing Wind-Tunnel Tests // Journal of Aircraft, 2019. Vol. 56, No. 1. P. 137–149.
3. **Koshelev K.B., Melnikova V.G., Strijhak S.V.** Development of iceFoam solver for modeling ice accretion // Proceedings of the Institute for System Programming of the RAS (Proceedings of ISP RAS). 2020 Vol. 32, No. 4. P. 217–234. (In Russ.) https://doi.org/10.15514/ISPRAS-2020-32(4)-16
4. **Aupoix B., Spalart P.** Extensions of the Spalart – Allmaras turbulence model to account for wall roughness // International Journal of Heat and Fluid Flow. 2003. No. 24. P. 454–462.

DOI: 10.53954/9785604788967_104

A MODEL OF THE BIG BANG AND UNIVERSE EXPANSION IN GENERAL RELATIVITY WITH SPREAD OF A HOT START SINGULARITY TO EMPTY SPACE

A.N. Kraiko

Baranov Central Institute of Aviation Motors
111116, Moscow, Russia

In 1929, Hubble discovered a law ("Hubble's law") based on measurements of the Doppler shift of light, according to which distant galaxies are moving away from us at a speed: $\mathbf{u} = H(t)\mathbf{r}$ with a radius-vector $\mathbf{r}$ to them and a function of time $H = H(t)$, called the "Hubble constant". If there is a solution describing such a spread, it is possible to determine when the gas that formed the galaxies began to disperse. After the discovery of Hubble, the expansion of the Universe began to be described by the decision of A. Friedman in 1922. In it, the scalar parameters of the gas are functions of only time t, the distances between material points grow with the growth of t, and the moment of singularity of its scalar parameters is taken as the beginning of the expansion of the always boundless Universe. The time t_0, counted from this moment, is the time of the "life" of the Universe. The description of the expansion of the Universe by this solution did not cause any consensus until 1998, when two groups of US astronomers discovered its inconsistency with observational data. To eliminate this discrepancy, A. Friedman's solution was generalized to non-zero "cosmological constants" Λ, introduced by A. Einstein tried to describe the Universe, which until 1929 was considered stationary. The sub-selection of the value of Λ allows us to coordinate observations with this solution. The found values Λ, like those of A. Einstein, lead to the effect of antigravity. So far, an undetected carrier of antigravity with very unusual properties is called "dark energy".

It would seem more natural to solve the problem of the expansion from a point into the void of a finite mass of gas. However, until 2015, there was no such solution even in the classical setting. In 2015, in [1], in this formulation, the problem of the expansion of a finite mass m_0 of an inviscid gas with a specific entropy s_0 from a point into the void was solved. According to its solution, a gas compressed to a point and, because of this, having infinite total E_0 and specific (volume units) energy ε_0, temperature T_0, pressure p_0, density ρ_0 and sound velocity a_0 at finite m_0 and s_0, scatters into the entire space so that a, T, p and ρ become zeros and

$$t > 0,\ 0 \le r \le \infty:\ \mathbf{u} = \mathbf{r}/t,\ \rho = p = T = a = 0,\ s = s_0. \qquad (1)$$

Thus, gas particles fly away from a point with arbitrarily high velocities, which contradicts SR and GR, according to which the velocity of particles cannot exceed the speed of light c. Solutions [1–4] within SR satisfied this restriction, with the same formula for $\mathbf{u}$ as in (1), but with restrictions: $r \le ct$ and $u \le c$. Comparison of this surprisingly simple solution for $\mathbf{u}$ with $H = 1/t$ and observational data showed that it describes them no worse than any modern cosmological theory with dark energy and matter. This is confirmed by the figure from [1–4] with more than 200 variants of processing by modern cosmological theories of the most reliable observational data [5], forming a zone of crosses (errors in determining H and t_0). Curve *1* passes through it, defined by consequence (1) – formula: $H = 978/t_0$. Curve *2*: $H = 652/t_0$ is a consequence of A. Friedman's solution with $\Lambda = 0$ for a monatomic gas with $H = 2/(3t)$. A comparison of the cross zone with curve *1*, obtained without a single empirical constant, is evidence that dark energy is superfluous.

In [6, 7], the expansion into the void of the hot start singularity (HSS) of a gas of baryons inside its gravitational radius ($r \le r_g = 2E_0G/c^4$, G is the gravitational constant) is considered in

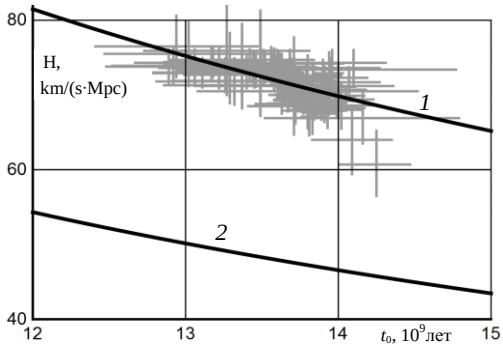

Dependence of the "Hubble constant" on the lifetime of the Universe.

the framework of GR. The degree of heating of the HSS determines the ratio of its total energy E_0 to the rest energy of all its N_0 baryons: $\sigma = E_0/(N_0 m_B c^2)$, where m_B is the rest mass of the cold baryon. At first glance, such a spread, like the spread of the singularity of a black hole, is impossible. The fundamental difference, however, is that a black hole is the result of a collapse after burning out thermonuclear fuel in a star. Therefore, during collapse, the growth of T, p and ρ is such that in the process of compression, the gravitational forces are always greater than the pressure drop opposing them. When expansion of the HSS, the opposite is true due to the enormous pressure at the beginning of the spread of all massless (with zero rest mass) and mass particles and antiparticlies with a negligible contribution of excess (over anti-baryons and positrons) barions and electrons. When the expansion is realized, the density in its center immediately becomes finite, decreasing with the growth of t. Due to this, an area arises and grows in the center of the expansion, in which the metric is close to the Galilean one and three equations of SR without gravity and their solutions for velocity: $\mathbf{u} = \mathbf{r}/t$ and pressure: $p = 0$ follow from the GR equations. It is noteworthy that, unlike [1–4], the last equality turned out without a boundary condition: $p(t, r = ct) = 0$. This is essential, because the region of the almost Galilean metric with the found solution separates the spherical layer described by the GR equations from the void. It is shown that for an arbitrarily large σ, the expanding HSS remains inside the gravitational radius.

The work is made with support of RFFR (project 20-01-00100).

REFERENCES

1. **Valiyev Kh.F., Kraiko A.N.** The dispersion of an ideal gas from a point into a void. A new model of the Big Bang and the expansion of the Universe // J. of Applied Mathematics and Mechanics. 2015. Vol. 79. No. 6. P. 556–565.
2. **Valiyev Kh.F., Kraiko A.N.** Compression of Ideal Gas into a Point, its Finite Mass dispersing from the Point into the Vacuum, the Big Bang and the Universe Expansion // Proceedings of International Conference XVII Khariton's Topical Scientific Readings / Ed. A.L. Mikhaylov. Sarov: RFNC-ARRIEP, 2015. P. 621–626.
3. **Kraiko A.N., Valiyev Kh.F.** The new model of the Big Bang and the Universe expansion. A comparison with modern observational data and cosmological theories // Proceedings of the 18th International Conference on the Methods of Aerophysical Research (ICMAR 2016) / Ed. Vasily Fomin. AIP Conference Proceedings. 2016. Vol. 1770. Art. 020002 (11 p.) DOI:10.1063/1.4963925.
4. **Kraiko A.N., Valiyev Kh.F.** A Model of the Big Bang and the Universe Expansion with the Dispersion to the Void a Gas, Compressed "Almost in a Point". A Comparison with Observational Data and Modern Cosmological Theories // Proceedings of International Conference XIX Khariton's Topical Scientific Readings / Ed. A.L. Mikhaylov. Sarov: RFNC-ARRIEP, 2017. P. 12–19.
5. **WMAP** Cosmological parameters Model/Data Set Matrix. NASA. URL: http://lambda.gsfc.nasa.gov/product/map/current /parameters.cfm.
6. **Kraiko A.N.** A Model of the Big Bang and Universe Expansion in General Relativity with Spread of a Gas Mass from a Point to Empty Space // Grav. Cosmol. 2020. Vol. 26, No. 4. P. 399–407.
7. **Kraiko A.N.** Erratum to: A Model of the Big Bang and Universe Expansion in General Relativity with Spread of a Gas Mass from a Point to Empty Space // Grav. Cosmol. 2022. Vol. 28, No. 1. P. 96.

DOI: 10.53954/9785604788967_106

VALIDATION OF KINETIC MODELS BASED ON STATE-TO-STATE SIMULATION OF OXYGEN RELAXATION BEHIND REFLECTED SHOCK WAVES

D.S. Kravchenko, E.V. Kustova, M.Yu. Melnik

St. Petersburg University
199034, St. Petersburg, Russia

Simulations of high-temperature flows are of vital importance for aerospace applications. One of the most suitable continuum approaches for modeling vibrational relaxation and chemical reactions under nonequilibrium conditions is a state-to-state approach based on solving fluid-dynamic equations fully coupled to the master equations for the populations of each molecular vibrational level [1]. However, while being rather accurate, this approach is computationally expensive; therefore it has to be validated first on simple test cases.

The objectives of this work are: state-to-state simulations of oxygen flows behind the reflected shock wave (SW) under conditions of the experiment [4], comparison with experimental data, analysis of the effect of relaxation behind the incident shock wave on the flow parameters behind the reflected wave, and recommendation of a model that provides the best agreement with the experiment.

The key difference in the formulation of the present problem from the previous works [2, 3] is that modeling is carried out not only for an incident, but also for a reflected shock wave. The advantage of experiments with reflected SW is that the gas is heated up to significantly higher temperatures than in experiments with only incident shock waves; therefore, they allow validation of theoretical models at higher temperatures. However, the theoretical description of such flows causes some difficulties. The reflected SW passes through a nonequilibrium gas which is already heated by the incident SW, and therefore, the relaxation processes are not completed in the gas. In this work, we start with preliminary modeling of partial relaxation ("partial" relaxation means incomplete relaxation process) behind the incident SW during the time interval t_r between the passage of the incident and reflected SW. Based on this solution, we then compute the parameters behind the reflected SW and simulate the main relaxation problem. It is worth noting that the authors of the experiment [4], in order to extract fluid-dynamic variables from the absorbance time-histories, use the assumption that all relaxation processes behind the incident SW are frozen. In the present work, modeling is carried out in both cases of partial and frozen relaxation.

Relaxation was modeled on the basis of the zeroth-order approximation of the Chapman-Enskog method in the accurate state-to-state formulation [1], which makes it possible to describe in detail the strongly nonequilibrium physicochemical kinetics. Vibrational energy exchanges were described using the generalized Schwartz – Slawsky – Herzfeld theory (SSH-theory) [5] and the forced harmonic oscillator (FHO) model [6]; only single-quantum transitions were considered. The dissociation process was described using the Marrone – Treanor model [7] with the most common in literature [2, 4] values of the parameter U and the parameters proposed in [8, 9]. In general, the most satisfactory agreement with experimental data for all fluid-dynamic parameters is obtained for the SSH model in conjunction with the Marrone-Treanor model with the parameter $U = 3T$.

The effect of relaxation processes behind the incident SW on the macroparameters of the mixture behind the reflected SW is discussed. Comparison with experimental data was carried out for the cases with and without relaxation behind the incident shock wave. The values of p^0 (the initial pressure immediately behind the reflected SW) and t_r are given in the table below; the number in the left column of the table represents the experimental case from [4]. The data are presented for the translational temperature range from 6230 K to 9560 K and incident wave

Initial pressure p^0 behind the reflected SW and time t_r

No.	Without relaxation		With relaxation		[4] p^0, Torr	Time between the passage of the waves t_r, μs
	p^0, Torr	Deviation from [4], %	p^0, Torr	Deviation from [4], %		
1	50	12	56	2	57	47
2	72	19	85	5	89	48
3	55	13	64	2	63	46
4	34	10	39	5	37	45
5	23	23	25	17	30	44
6	35	15	41	0	41	43
7	22	15	26	0	26	41
8	31	9	37	9	34	40

velocity range from 2220 m/s to 2760 m/s. One can see that the values of pressure p^0 obtained in the case with relaxation are much closer to the experimental data than the values obtained in the case without relaxation. The same result is obtained for the initial values of number density of oxygen molecules. On the contrary, for the vibrational temperature the reverse tendency is observed: the initial values are in better agreement in the case with frozen relaxation behind the incident SW. Such a contradiction emphasizes two aspects: 1) the important role of relaxation processes behind an incident SW; 2) the need in refining the methodology for recalculating the fluid-dynamic variables from experimental spectroscopic data.

The work was supported by St Petersburg University (Project No 93022273).

REFERENCES

1. **Nagnibeda E.A., Kustova E.V.** Nonequilibrium Reacting Gas Flows. Kinetic Theory of Transport and Relaxation Processes. Berlin, Heidelberg: Springer-Verlag, 2009.
2. **Campoli L., Kunova O., Kustova E., Melnik M.** Models validation and code profiling in state-to-state simulations of shock heated air flows // Acta Astronautica 2020. Vol. 175. P. 493–509. https://doi.org/10.1016/j.actaastro.2020.06.008
3. **Kunova O.V., Kustova E.V., Melnik M.Yu., Savelev A.S.** Validation of models of state-to-state oxygen kinetics behind shock waves // Phys. Chem. Kinetics Gas Dynam. 2018. Vol. 19, Iss. 3. 8 p. http://doi.org/10.33257/PhChGD.19.3.765/
4. **Streicher J.W., Krish A., Hanson R.K.** Coupled vibration-dissociation time-histories and rate measurements in shock-heated, nondilute O_2 and O_2 – Ar mixtures from 6000 to 14000 K // Phys. Fluids. 2021. Vol. 33. Art. 056107. https://doi.org/10.1063/5.0048059
5. **Schwartz R.N., Slawsky Z.I., Herzfeld K.F.** Calculation of vibrational relaxation times in gases // J. Chem. Phys. 1952. Vol. 20, No. 10. P. 1591–1599. https://doi.org/10.1063/1.1700221
6. **Adamovich I., Macheret S., Rich J., Treanor C.** Vibrational energy transfer rates using a forced harmonic oscillator model // J. Thermophys. Heat Transf. 1998. Vol. 12, No. 1. P. 57–65. https://doi.org/10.2514/2.6302
7. **Marrone P., Treanor C.** Chemical relaxation with preferential dissociation from excited vibrational levels // Phys. Fluids. 1963. Vol. 6, No. 9. P. 1215–1221. https://doi.org/10.1063/1.1706888
8. **Kunova O., Kustova E., Savelev A**. Generalized Treanor–Marrone model for state-specific dissociation rate coefficients // Chemical Physics Letter. 2016. Vol. 659. P. 80–87. http://dx.doi.org/10.1016/j.cplett.2016.07.006
9. **Pogosbekyan M., Sergievskaya A.** Simulation of the oxygen dissociation reaction under thermally nonequilibrium conditions: models, trajectory calculations, and the experiment // Russ. J. Phys. Chem. B 2018. Vol. 12. P. 208–218. https://doi.org/10.1134/S1990793118020239

DOI: 10.53954/9785604788967_108

FEATURES OF TURBULENT TRANSPORT IN THE STABLY STRATIFIED BOUNDARY LAYER ATMOSPHERE

L.I. Kurbatskaya

Institute of Computational Mathematics and Mathematical Geophysics SB RAS
630090, Novosibirsk, Russia

The RANS turbulence scheme [1], including the effect of internal gravitational waves, was applied to the analysis of the flow structure and turbulence statistics of a stably stratified atmospheric boundary layer. The inclusion of the effect of internal waves on the transfer of momentum and heat into the three-parameter $E-\varepsilon-\overline{\theta^2}$ RANS scheme of stratified turbulence makes it possible over allows correctly reproducing some features of eddy mixing in a stably stratified atmospheric boundary layer. Numerical simulation results are consistent with LES simulation results and atmospheric observational data.

RANS model of atmospheric turbulence: Eddy fluxes of momentum and heat. In stably stratified flows on environment, turbulence can be generated through shear and be destroyed via impact of negative buoyancy and viscosity. The opposite directions for buoyancy and shear effect induce a decline in turbulence intensity for the situation of stable stratification as compared with neutral stratification and convective mixing. However, this increases the activity of internal gravitational waves, which can transport momentum, but not heat. A dimensionless relation, the so-called gradient Richardson number, characterizes the relative importance of differently directed effects of the shear and stratification

$$\mathrm{Ri} = N^2 / S^2,$$

where $N = \left[\left(g/T_0 \right) \left(\partial\Theta/\partial z \right) \right]^{1/2}$ is the frequency of internal gravitation waves or the Väisälä–Brünt frequency, S is the vertical shear of the horizontal velocity.

Including into the three-parametric $E-\varepsilon-\langle\theta^2\rangle$ RANS -scheme for the stratified turbulence [1, 2] of internal waves effect on momentum and heat transport over allows reproducing correctly behavior of eddy diffusivities of momentum and heat in the consent with of measurements data in an atmosphere [1, 2]. The prognostic equations of the model obtained from the Reynolds-averaged Navier-Stokes equations, in which the decomposition of variables into the mean and fluctuation parts is used. The equations for average speed $\mathbf{U} = (U, V, W)$ and average potential temperature Θ are the starting point. A significant feature of the model, unlike the standard models of eddy viscosity, is its capability of accounting for the anisotropic distribution of the turbulent kinetic energy components. This is extremely important for stratified flows on the whole and for the ABL in particular because they may manifest a high degree of anisotropy.

Numerical realization of the explicit algebraic model of turbulence in a stable ABL for the case with a constant surface forcing. Consider the formation of a stable ABL according to the GABLS1 scenario [3] when a purely stable ABL is initiated by the superposition of a geostrophic wind of constant velocity at the surface cooling also with a constant velocity. Of the main interest is here in the investigation of to which extent the model works well at the prediction of a stably stratified turbulence in atmosphere by comparing with the accessible LES data obtained for the GABLS1 case (see, for example, [4]). The constant velocity of the geostrophic wind is equal in this case to $U_g = 8$ ms^{-1}, the wind vector is directed along the X axis.

The figure shows the results for the turbulent fluxes of the momentum and heat, for profiles of the TKE, the wind mean velocity and the mean potential temperature. For all profiles,

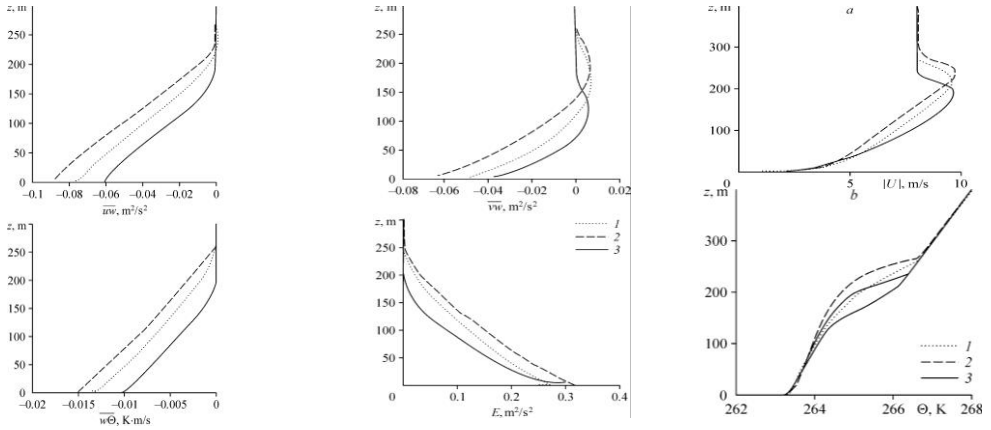

Profiles of turbulent fluxes of the momentum $\overline{uw}$, $\overline{vw}$, heat $\overline{w\theta}$, TKE, wind velocity $|U|$ and the potential temperature Θ for the GABLS1 case.

1 — present computations, *2* — the data of the Meteo-France ARPEGE model [5], *3* — LES data [4].

the results of the present model are close to LES data [4], whereas other approaches give a smaller turbulent layer. This reflects the capability of the model to good predictions of the characteristics of stably stratified flow. One can see that model [5] demonstrates the profiles similar to the results of the present model, and although these models rely on different principles, they give a good description of turbulence in the present test. However, one should note that the standard TKE-scheme of model [5] overestimates the boundary layer height.

The work was carried out within the framework of the state order of the Institute of Computational Mathematics and Mathematical Geophysics of the Siberian Branch of the Russian Academy of Sciences No. 0251-2021-0003 and with partial financial support from the Russian Foundation for Basic Research within the framework of the scientific project 20-01-00560 A.

REFERENCES

1. **Kurbatskii A.F., Kurbatskaya L.I.** Investigation of a stable boundary layer using an explicit algebraic model of turbulence. // Thermophysics and Aeromechanics. 2019. Vol. 26, No. 3. P. 335–350.
2. **Kurbatskii A.F., Kurbatskaya L.I.** An explicit algebraic model of planetary boundary layer turbulence: test computation of the neutrally stratified atmospheric boundary layer // Thermophysics and Aeromechanics. 2017. Vol. 24, No. 5. P. 705–717.
3. **Cuxart I.J., Holtslag A.A.M., Beare R.J., Bazile E., Beljaars A., Cheng A., Conangla L., Ek M., Freedman F., Hamdi R., Kerstein A., Kitagawa H., Lenderink G., Lewellen D., Mailhot J., Mauritsen T., Perov V., Schayes G., Steeneveld G.-J., Svensson G., Taylor P., Weng W., Wunsch S., Xu K.-M.** A single-column model intercomparison for a stably stratified atmospheric boundary layer // Boundary-Layer Meteorology. 2006. Vol. 118, No. 2. P. 273–303.
4. **Beare R.J., MacVean M.K., Holtslag A.A.M., Cuxart J., Esau I., Golaz J.C., Jimenez M.A., Khairoutdinov M., Kosovic B., Lewellen D., Lund T.S., Lundquist J.K., McCabe A., Moene A.F., Noh Y., Raasch S., Sullivan P.** An intercomparison of large-eddy simulations of the stable boundary layer // Boundary-Layer Meteorology. 2006. Vol. 118. P. 247–272.
5. **Bazile E., Marquet P., Bouteloup Y., Bouyssel F.** The turbulent kinetic energy (TKE) scheme in the NWP models at Météo-France // Proceedings of the Workshop on Diurnal Cycles and the Stable Boundary Layer (Reading, Berkshire, England, 7–10 November, 2011). Reading: ECMWF, 2012. P. 127–136.

DOI: 10.53954/9785604788967_110

NUMERICAL SIMULATION OF THE DEVELOPMENT OF DISTURBANCES IN A SUPERSONIC BOUNDARY LAYER EXCITED BY A PERIODIC HEAT SOURCE

A.I. Kutepova, D.V. Khotyanovsky, A.A. Sidorenko

Khristianovich Institute of Theoretical and Applied Mechanics SB RAS
630090, Novosibirsk, Russia

The development of pulsed disturbances from a localized heat source and the physical mechanisms of the laminar-turbulent transition in the flat-plate supersonic boundary layer are studied with the direct numerical simulation. Numerical simulations on the basis of the unsteady three-dimensional Navier – Stokes equations are performed with the HyCFS-R hybrid parallel code developed at the Institute of Theoretical and Applied Mechanics (ITAM).

The flow parameters correspond to the experiments performed at ITAM for a transitional supersonic boundary layer on a flat plate: flow Mach number M = 1.45, stagnation pressure $P_0 = 5.5 \cdot 10^4$ Pa, stagnation temperature T_0 = 290 K, and the plate temperature T_w = 290 K. The calculation parameters also corresponded to the conditions of the earlier numerical study [1] using two different approaches: direct numerical simulation and solution of the Reynolds-averaged Navier – Stokes equations. The numerical simulations are performed in the computational domain with the shape of a parallelepiped whose lower face matches with the plane of the plate. The computational grid was condensed along the normal coordinate in the region of the boundary layer. The calculations used a rectangular structured computational grid with the number of cells along the coordinates N_x = 768, N_y = 200 and N_z = 46, respectively. The total number of cells was about 7 million. The boundary layer at the inflow cross-section is assumed to be laminar and self-similar. The inflow Reynolds number based on the distance from the leading edge of the plate is $\mathrm{Re}_x = 4.9 \cdot 10^5$. Thermal disturbances are excited as rectangular periodic pulses of the plate temperature across the rectangular wall element with the sizes of 3 mm in streamwise and 2 mm in spanwise directions. The pulse frequency is 25 kHz with the duty cycle ½ and the pulse temperature of 500 K. The chosen pulse frequency is close to the frequency of the fundamental three-dimensional instability wave obtained in the linear stability analysis of the boundary layer at the inflow cross-section.

The effects of the pulsed heat source introduced into the boundary layer have been studied in detail with the numerical simulation. The development of a thermal disturbance in the boundary layer rather quickly leads to an increase in fluctuations as shown by the results of numerical calculations. The introduction of thermal disturbances is accompanied by a change (Fig. 1) in the average and pulsation characteristics.

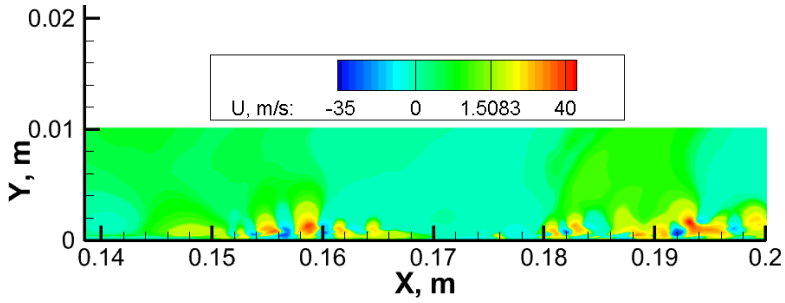

Fig. 1. Velocity field in section $z = 0$.

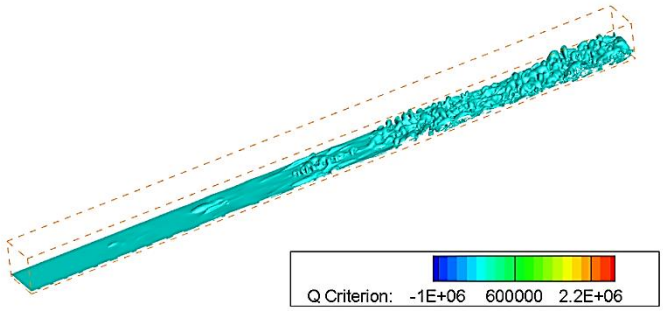

Fig. 2. Visualization of the Q-criterion.

The results of the simulations show that the excited periodic temperature disturbances transform into the boundary layer instability waves growing in the streamwise direction. The development of these growing disturbances is attained by the formation of three-dimensional longitudinal vortex structures and leads to the onset of the laminar-turbulent transition, which manifests in highly chaotic flow behavior and significant changes in the mean flow characteristics (Fig. 2).

The work was supported by the the Russian Scientific Foundation (grant 18-19-00547).

REFERENCE

1. Polivanov P.A., Khotyanovsky D.V., Kutepova A.I., Sidorenko A.A. Investigation of various approaches to the simulation of laminar-turbulent transition in compressible separated flows // Journal of Applied Mechanics and Technical Physics. 2020. Vol. 61, No. 5. P. 717–726.

DOI: 10.53954/9785604788967_112

GAS FLOW MIXING CONTROL

A.F. Latypov

Khristianovich Institute of Theoretical and Applied Mechanics SB RAS
630090 Novosibirsk, Russia

In 1961, Academician S.A. Khristianovich, as applied to gas ejectors, proposed a method of distributed high-pressure gas along the length of the injection channel. Using this idea, B.A. Uryukov developed a theory of gas ejectors called differential. The calculations showed an increase in the stagnation pressure at the end of the mixing chamber of such a scheme compared to a single-stage ejector [1]. In order to find out the reason for the possible efficiency of distributed mixing, this work was undertaken. Let us first write down the necessary formulas and relations for the gas flows in the channel. Accepted assumptions: gases are perfect, flow parameters in each section are uniform.

1. Let us introduce the function of the specific total impulse $r = (mV + pF)/m = V + RT/V$. At the Mach number $\mathrm{M} = 1$ the specific total impulse takes the minimum value $r_{\min} = a_* (\gamma + 1)/\gamma$ (a_* – is the critical speed of sound).

2. To determine the values of the gas flow parameters T, p, V, ρ in any section of the channel for given values $h_0, r, m/F$ we have a system of equations consisting of the equations of energy, momentum, continuity, state

$$h + \frac{V^2}{2} = g_1 = h_0, V + \frac{RT}{V} = g_2 = r, \rho V = g_3 = m/F, p = \rho RT. \tag{1}$$

The system of equations (2) has an analytical solution.

$$V = \frac{\gamma}{\gamma + 1} r \left(1 \pm \sqrt{1 - \left(\frac{r_{\min}}{r} \right)^2} \right), T = T_0 - \frac{V^2}{2c_p}, \quad p = \frac{RT}{V} \frac{m}{F} \tag{2}$$

The upper sign in "±" corresponds to the supersonic flow, the lower one – to the subsonic one.

3. Let us consider the mixing of two flows of a perfect gas, the parameters of which are marked with indices *W* (high-pressure flow) and *G* (low-pressure flow), the parameters of the mixture are marked with the index *S*. Flows are considered in which the gas pressure *W* is greater than the gas pressure in the flow *G*. Before mixing, the cross section of the high-pressure flow can change by δf.

4. Let us compare the mixture parameters of two mixing options: 1) $\delta f = 0$, 2) $\delta f \neq 0, |\delta f / F_{W0}| \ll 1$. Let us denote $\bar{m}_W = m_W / m_G, \bar{F}_W = F_W / F_G, m_S = m_G + m_W$. The mixing equations have the form (1), where, using the accepted markings, the parameters on the left side and the state equation are supplied with the index *S*, and the right parts for the 1st option

$$g_1 = h_{0S} = \frac{m_W h_{0W} + m_G h_{0G}}{m_S} = \frac{\bar{m}_W h_{0W} + h_{0G}}{1 + \bar{m}_W},$$

$$g_2 = r_S = \frac{m_W r_W + m_G r_G}{m_S} = \frac{\bar{m}_W r_W + r_G}{1 + \bar{m}_W}, g_3 = \frac{m_S}{F_S} = \frac{m_W + m_G}{F_W + F_G} = \frac{1 + \bar{m}_W}{1 + \bar{F}_W} \frac{p_G V_G}{R_G T_G}.$$

For the second option, the difference will be only in the second equation

$$g_2 = r_S = \frac{m_W r_W + m_G r_G + p_W \delta f}{m_S} = \frac{1}{1+\bar{m}_W}\left[\bar{m}_W\left(r_W + \frac{R_W T_W}{V_W}\frac{\delta f}{F_W}\right) + r_G\right].$$

Let us subtract from the equations of the second variant the corresponding equations of the first variant. We will obtain equations in variations to determine the differences in the values of parameters and entropies

$$\frac{\delta T_S}{T_S} + (\gamma_S - 1)\mathrm{M}_S^2 \frac{\delta V_S}{V_S} = 0,\ \frac{\delta T_S}{T_S} + \left(\gamma_S \mathrm{M}_S^2 - 1\right)\frac{\delta V_S}{V_S} = \gamma_S \mathrm{M}_S^2 \frac{\delta r_S}{V_S},\ F_S = F_W + F_G,\ \delta F_S = \delta f,$$
$$\frac{\delta p_S}{p_S} = \frac{\delta T_S}{T_S} - \frac{\delta V_S}{V_S} - \frac{\delta F_S}{F_S},\ \delta r_S = \frac{p_W \delta f}{m_S} = \frac{R_S T_S}{V_S}\frac{p_W}{p_S}\frac{\delta f}{F_S},\ \delta\bar{s} = \left[1 - \frac{p_W}{p_S}\right]\frac{\delta f}{F_S}. \quad (3)$$

It follows from solution (3) that in order to increase the mixing efficiency (increase in the total pressure of the mixture), it is expedient to pre-expand the high-pressure gas flow, since $p_G < p_S < p_W$ and $d\bar{s} < 0$.

5. Let us consider two limiting cases: the first is when infinitely small portions of a high-pressure gas flow are mixed into the gas in the channel (distributed mixing), and the second is when the gases are mixed in a single-stage mode. To determine the parameters of gas mixing in the first case, we write the equations of conservation laws in differential form. Let us introduce the parameter $x \in [0,1]$ – analogue of the longitudinal coordinate of the channel, and we assume that the gas is injected into the channel uniformly along the length. We obtain a system of ordinary differential equations, integrating which at initial values $x = 0,\ T_S = T_W,$ $p_S = p_W, V_S = V_W, r_S = r_W$ we get the values of the mixture parameters $T_{S1}, p_{S1}, V_{S1}, r_{S1}, F_{S1}$. In the second case, the high-pressure gas flow first expands to the value of the total specific impulse r_{W2}, satisfying the condition

$$r_{S2} = \frac{\bar{m}_{W0} r_{W2} + r_G}{1 + \bar{m}_{W0}} = r_{S1}.$$

Thus, the values of the right parts of the system of equations (1) are equal for both cases, and therefore the solutions are identical. Distributed mixing and single-stage mixing give the same result. However, it is necessary to implement distributed (multi-stage – finite-dimensional analogue) mixing, because in this case, flow control is available to comply with the conditions for the existence of a stationary flow in channels [2].

Designations: T – temperature, p – pressure, ρ – density, V – velocity, M – Mach number, m – mass flow, F – flow cross-sectional area, h – enthalpy, R – gas constant, c_p – heat capacity at constant pressure, γ – adiabatic exponent, $\bar{s} = s/R$ – normalized entropy, m_{W0}, F_{W0} – initial flow and the initial cross-sectional area of the high-pressure flow; *indices:* 0 – deceleration parameters, G – low-pressure flow, W – high-pressure flow, $\bar{m} = m/m_G$.

REFERENCES

1. **Uryukov B.A.** Theory of differential ejector // Applied Mechanics and Technical Physics. 1963, No. 5. P. 41–47.
2. **Latypov A.F.** The condition for the existence of a stationary flow in a channel of variable cross section with heat supply and dissipation of kinetic energy // Letters to the Journal of Technical Physics. 2012. Vol. 38, No. 22. P. 21–27.

DOI: 10.53954/9785604788967_114

SIMULATION OF THE INTERACTION OF A DETONATION WAVE WITH A POROUS INSERT WITH DIFFERENT GEOMETRY

S.A. Lavruk, D.A. Tropin

Khristianovich Institute of Theoretical and Applied Mechanics SB RAS
630090, Novosibirsk, Russia

The prevention and suppression of detonation combustion is one of the priority areas of environment pollution.

The aim of this work is to study the interaction of heterogeneous detonation waves (DW) with a porous insert, which consists of an inert filter, and to determine the critical conditions for suppressing or sufficiently attenuation the detonation. During the simulation, the amount of inert cylinders, the volume concentration of the solid phase in the porous body, and the diameter of the cylinders in the porous body vary. The main feature of this study is that the porous insert is modeled implicitly: it is assumed that the porous body is a set of cylinders, for which an additional energy equation is given, simulating the impact introduced by this body.

The following problem was considered: along a flat channel filled with a stoichiometric mixture of aluminum particles in oxygen, a cellular heterogeneous detonation wave propagates, and then interacts with a porous media occupying a certain part of the channel (Fig. 1). In this case, the size of the inert inserts was varied, as well as the volume concentration of the cylinders. In this simulation, a channel wide varies from 5 to 10 cm. Width of the open space without porous inserts varies from 0.5cm to 9 cm.

The results for micron particles are shown in Figs. 1, fields of maximum pressure for one (Fig. 1,*a*) and two holes (Fig. 1,*b*) in a porous element. It can be seen that for both cases, in the region without a porous insert, plane detonation waves propagate at about 1.5 km/s. In the case of two holes (Fig. 1,*b*), an area with increased pressure is formed in the porous insert, which is caused by the intersection of two oblique shock waves in the porous element.

As a result of calculations, the critical width of the channel was determined, along which the propagation of heterogeneous detonation is possible.

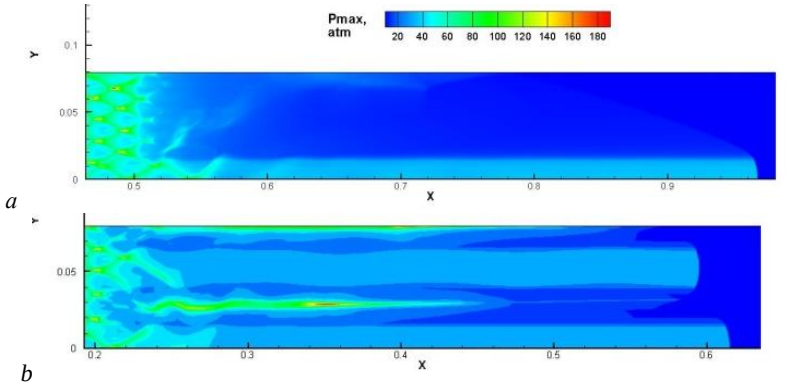

Fig. 1. Maximal pressure fields of one (*a*) and two holes (*b*) in a porous element.

The work was supported by Russian Science Foundation, project No. 21-79-10083, https://rscf.ru/project/21-79-10083/

DOI: 10.53954/9785604788967_115

MEASUREMENT OF GAS-DYNAMIC PARAMETERS OF A TWO-PHASE FLOW USING PROBE AND LASER-OPTICAL METHODS

I.A. Lepeshinsky, V.A. Reshetnikov, A.V. Tsipenko, N.A. Kucherov, P.V. Zotikova

***Moscow Aviation Institute* (*National Research University*)**
125993, A-80, GSP-3, Moscow, Russia

In the experimental study of two-phase flows, it is often necessary to measure the local values of the phase parameters. These parameters can be measured both by laser-optical and probe methods. Laser-optical methods previously did not allow us to study flows with a high concentration of the dispersed phase, as well as to determine the parameters of the gas phase in a two-phase flow.

Probe methods have long been used to measure the parameters of a two-phase flow [1–9]. They are one of the few with which it is possible to measure local phase costs. However, when using them, a number of problems arise. This is the problem of isokinetics in sampling and the value of the impact elasticity coefficient. Using some design improvements and applying the probe method in compilation with the PIV method [10], it is possible to solve these problems and determine all the parameters of a two-phase flow at high concentrations.

Consider the schematic diagram of the probe method shown below [2].

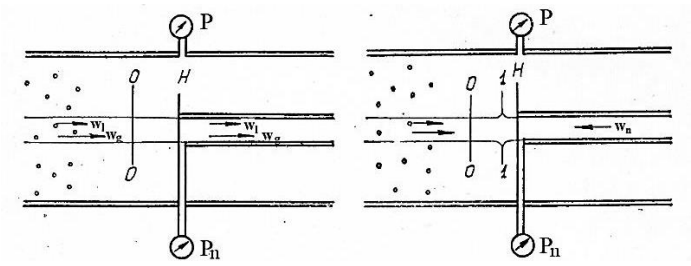

a *b*

Schematic diagram of the probe method operation.

A cylindrical probe with an inlet d_n is inserted into the flow. When determining the flow rate and phase concentration, the probe is connected to the suction system (position a) and operates in the isokinetic sampling mode, in which the static pressure inside the probe (in the p_n figure) is maintained equal to the static pressure in the working chamber or the environment. In this case, there is no deformation of the current lines during sampling. The selected sample is divided into phases using a separator. By measuring the flow rate of each phase, you can find the consumable mass concentration of the phases $\psi = \frac{G_l}{G_g}$.

When measuring the braking pressure of the mixture P^*, the channel for phase selection is blocked, and the probe operates in the Pitot tube mode. The formula for calculating P^* has the form

$$P^* = P + \frac{\rho_g w_g^2 (1-\alpha_l)}{2} + K_e \frac{\rho_l w_l^2 \alpha_l}{2}.$$

The value of K_e plays the role of the impact elasticity coefficient [11], which varies in the range from 1 to 2. We assume that at $K_e = 1$ the impact is elastic, at $K_e = 2$ the impact is inelas-

tic. Let us add the phase expense equations: $G_g = \alpha_g \cdot \rho_g \cdot w_g \cdot S$; $G_l = \alpha_l \cdot \rho_l \cdot w_l \cdot S$; gas equation of state $\rho_g = \frac{P_g}{R \cdot T_g}$; equation of volume concentrations $\alpha_g + \alpha_l = 1$. Here w_g is the velocity of gas, w_l is the velocity of droplets, α_g is the volume concentration of gas, α_l is the volume concentration of liquid (droplets), ρ_g is the density of gas, ρ_l is the density of liquid. By measuring the temperature of the liquid T_l and assuming $T_l = T_g$. We get the value of one of the variables involved in the model. If we measure the total pressure of the two-phase flow and the mass flow rates of the phases, we get a system of five equations containing six unknowns: and if the flow parameters are determined at two adjacent points, it is possible to determine the average mass size of the droplet based on the equation of motion of the droplet relative to the gas:

$$M_k \frac{dw_l}{dt} = C_x \frac{\rho_g \cdot (w_g - w_l)\left|w_g - w_l\right|}{2} f_k ,$$

where $M_k = \rho_l \frac{\pi D_k^2}{4}$ – the mass of the drop, D_k – the diameter of the drop, f_k – the cross-sectional area of the drop, C_x – the drop resistance coefficient, assuming a spherical drop, you can determine their diameter.

The proposed method of joint use of probe and laser-optical measurement methods and design changes of the probe, made it possible for the first time to measure all the necessary parameters of a two-phase highly concentrated two-phase gas droplet flow and improve the accuracy of their measurement. For the first time, the coefficient of elasticity of the impact of a drop was determined, which made it possible to measure the parameters of the gas phase of a two-phase highly concentrated flow: speeds and consumption.

REFERENCES

1. **Mokeev Yu.G.** Experimental study of a gas-liquid jet propulsion model with thrust forcing by ballasting // Hydromechanics. 1973. Iss. 24. P. 73–77.
2. **Zuev Yu.V., Lepeshinsky I.A., Tsarenko P.B.** Probe method for measuring parameters of a two-phase highly concentrated flow // Jet, Tear-off and Unsteady Flows: Abstracts of the XXI All-Russian seminar. Novosibirsk, 2007. P. 128–130.
3. **Lepeshinsky I.A., Zuev Yu.V., Bazhanov V.I.** Probe method for measuring phase parameters of a two-phase two-component gas flow // Gas Thermodynamics of Multiphase Flows in Power Plants. Iss. 1. Kharkiv: KHAI, 1978. P. 123–128.
4. **Vasiliev Yu.V. Galnbek A.A., Kitanin E.L.** The use of tubular probes in the study of hydrodynamics of gas-liquid flows // Gas Thermodynamics of Multiphase Flows in Power Plants. Iss. 1. Kharkiv: KhAI, 1978. P. 117–123.
5. **Buzov A.A.** Some results of an experimental study of an isokinetic probe for measuring phase velocities and concentrations in a two-phase flow // TVT. 1981. Vol. 19, No. 5. P. 1117. [№ 2251-81, деп. в ВИНИТИ от 14.V.81]
6. **Pchelkin I.M., Kalakutskaya N.A., Parfentieva I.F.** Investigation of local characteristics of a two-phase flow on a nozzle slice // Research on Mechanics and Heat Exchange of Two-phase Media. Iss. 25. Moscow, 1974, P. 63–78.
7. **Petukhov I.I., Frolov S.D.** On the measurement of local parameters of a bubble gas-liquid flow by tubular probes. Gas thermodynamics of multiphase flows in power plants. Kharkiv: KhAI, 1980. P. 121–126.
8. **Hewitt G.F.** Measurement of two-phase flow parameters. New York et al.: Academic Press, 1978. 287 p.
9. **Anderson G.H., Mantsuurania D.G.** Two-phase (gas/liquid) flow phenomena – II: Liquid entrainment // Chemical Engineering Science. 1960. Vol. 12, Iss. 4. P. 233–242.
10. **Tsipenko A.V.** Theoretical foundations and practical methods for studying nonequilibrium gas-drop flow with a large proportion of liquid in the development of fire extinguishing systems for emergency situations: Diss. … Doctor of Tech. Sci. / Res. Inst. of Low Temp. at the Moscow Aviation Inst. Moscow, 2006.
11. **Savelyev I.V.** Mechanics of molecular physics. Vol. 1. Moscow: Nauka, 1959.

DOI: 10.53954/9785604788967_117

MODELING OF RAREFIED GAS TRANSFER PROCESSES IN NANOCHANNELS

E.V. Lezhnev, V.Ya. Rudyak

[1]*Novosibirsk State University of Architecture and Civil Engineering*
630008, Novosibirsk, Russia
[2] *Kutateladze Institute of Thermophysics*
630090, Novosibirsk, Russia

Microsystem technology has been actively developing for the last four decades. Recently, we can already talk about nanosystem technology. In corresponding devices, flows usually take place in channels, the dimensions of which vary from tens of nanometers to hundreds of micrometers. The flows in such channels are controlled by the transfer processes occurring in them. It is practically impossible to study them experimentally under such conditions. In addition, if it is possible to obtain the necessary information, then its interpretation requires extremely accuracy and appropriate tools. In this regard, there is a need for correct modeling of transport processes in such cramped conditions. One of the main tasks in this regard is the modeling and calculation of transfer coefficients. The latter, as is known, have a molecular nature, and their description should be based on the molecular description of the fluid [1].

A widely used method for modeling transfer coefficients is the well-known method of molecular dynamics [2]. In the case of a rarefied gas, it is practically not applicable, since a huge number of particles are required for correct modeling. The computational cell in this case should have a characteristic size exceeding the mean free path of the molecules. In addition, the molecular dynamics method, due to the presence of dynamic chaos in the systems under consideration, does not give true phase trajectories [3, 4]. Adequate values of observables by this method are obtained only by averaging over a large number of independent phase trajectories. With these considerations in mind, in our works [5–7] we developed a method of stochastic molecular modeling (SMM) of rarefied gas transport coefficients. It was found that the transfer coefficients in the volume are modeled with the accuracy of obtaining experimental data. The purpose of this work is to model and study the viscosity and thermal conductivity of rarefied gases in nanochannels with a square cross section. To do this, the SMM method is preliminarily generalized to describe the transfer coefficients in constrained conditions [8, 9].

The height of the channels varied from 8.5 to 1000 nanometers. The interaction of gas molecules with the boundary is described by mirror or mirror-diffuse laws, and the molecules between themselves are described by the Lennard-Jones potential. The algorithm's efficiency is demonstrated by calculating the argon self-diffusion coefficient in the nanochannel. The accuracy of modeling, its dependence on the number of particles and phase trajectories used for averaging is investigated. Transfer coefficients are generally determined by fluctuation-dissipation theorems that relate the values of transfer coefficients to two-time correlation functions of the corresponding dynamic variables. The viscosity and thermal conductivity coefficients were calculated for several monatomic and polyatomic gases (Ar, Kr, Ne, Xe, O_2, CH_4). Previously, in all cases, modeling of the transfer coefficients of these gases in the volume was performed.

When studying thermal conductivity, it is shown that it is anisotropic in nanochannels, that is, it is different along and across the channel. The thermal conductivity coefficients along and across the channel can differ by three orders of magnitude. This, in particular, means that the total coefficient of thermal conductivity is almost three times lower than in volume. The observed anisotropy of thermal conductivity is due to the interaction of gas molecules with the channel walls. Therefore, by changing the material of the walls (the law of interaction of gas

molecules with the walls), it is possible to control the thermal conductivity of the gas in the channel. It should also be noted that this anisotropy persists in micron-sized channels, although it decreases with increasing channel height.

It is necessary to note one more important circumstance. In cramped conditions, due to the intense interaction of gas molecules with the walls of the channel, a fluctuating movement of its center of mass occurs. The average velocity of the center of mass of the gas is, of course, zero, since the equilibrium state is modeled. The presence of this fluctuating motion changes the energy transfer in the system. To calculate the true thermal conductivity of a gas, this contribution, generally speaking, should be excluded. However, there are no experimental methods to separate these two contributions. Therefore, the thermal conductivity of the gas in the nanochannel is a property of the entire gas+channel wall system.

The next important conclusion concerns the viscosity of gas in nanochannels, which has also been systematically studied. It is shown that it is non-isotropic, and its difference along and across the channel is determined by the interaction of gas molecules with the channel walls. By changing the material of the walls, it is possible to significantly change the viscosity of the gas, and it can be both several times more than in volume, and less. The indicated nonisotropy of viscosity is fixed not only in nano-, but also in microchannels. Naturally, as the height of the channel increases, the anisotropy decreases.

Real channels usually have roughness. Their presence leads to an increase in the surface area of the channel. This means that the nonisotropy of momentum transfer in gas in such channels will be more pronounced than in a channel with smooth walls. Therefore, the presence of roughness can lead to both an increase in viscosity and a decrease in it. It all depends on the nature of the interaction of gas molecules with the surface.

The work was supported by the Russian Foundation for Basic Research (grant No. 20-01-00041) and a megagrant of the Ministry of Science and Higher Education of the Russian Federation (Agreement No. 075-15-2021-575).

REFERENCES

1. **Rudyak V.Ya**. Statistical aerohydromechanics of homogeneous and heterogeneous and heterogeneous media. Vol. 1. Kinetic theory. Novosibirsk, 2004. 320 p.
2. **Rapaport D.C.** The art of molecular dynamics simulation. Cambridge, 2004. 549 p.
3. **Norman G.E., Stegailov V.V.** Stochastic theory of the method of classical molecular dynamics // Math. modeling. 2012. Vol. 24. No. 3. S. 305–333.
4. **Rudyak V.Ya.** Statistical aerohydromechanics of homogeneous and heterogeneous and heterogeneous media. Vol. 2. Hydromechanics. Novosibirsk, 2005. 470 p.
5. **Rudyak V.Ya., Lezhnev E.V.** Stochastic method for modeling rarefied gas transport coefficients // Math. modeling. 2017. Vol. 29. No. 3. P. 113–122.
6. **Rudyak V.Ya., Lezhnev E.V.** Stochastic algorithm for simulating gas transport coefficients // J. Comp. Physics. 2018. Vol. 355. P. 95–103.
7. **Rudyak V.Ya., Lezhnev E.V.** Stochastic molecular modeling the transport coefficients of rarefied gas and gas nanosuspensions // Nanosystems: Physics, Chemystry, Mathematics. 2020. Vol. 11, No. 3. P. 285–293.
8. **Rudyak V.Ya., Lezhnev E.V.** Viscosity of gases in nanochannels // JTF Letters. 2020. Vol. 46, No. 20. P. 51–54.
9. **Rudyak V.Ya., Lezhnev E.V., Lyubimov D.N.** On the anisotropy of gas transfer processes in nano- and microchannels // Bulletin of St. Petersburg State University. Mathematics, Mechanics, Astronomy. 2022. Vol. 9, No. 1. P. 152–163.

DOI: 10.53954/9785604788967_119

HOT-FILM MEASUREMENTS IN THE BOUNDARY LAYER OVER AIRFOIL IN COMPRESSIBLE FLOW

A.V. Liverko, D.S. Sboev, V.G. Soudakov, A.O. Obraz

Central Aerohydrodynamic Institute
140180, Zhukovsky, Moscow region, Russia

Data on shear stresses are an important parameter in the study of boundary layers. It is, however, quite difficult to obtain reliable data experimentally. There are several methods for measuring skin friction (pneumometric methods, direct measurements of friction forces using a floating element *etc*), but many of them have certain disadvantages. In addition, these methods are not sufficiently suitable for measuring shear stress pulsations (insufficient frequency responses). One of the most suitable method for high-frequency measurements using hot-film sensors with a constant temperature anemometer will be considered in this contribution. The basis of the technique is the ratio between the heat released by the heated surface area and the shear stress on it (the power required to keep the element warm compensates for the heat that is wasted by convection in the flow).

The main goal of the work is mastering the measurements by hot-film sensors in the boundary layer on a straight wing model at high Re and M numbers, as well as to compare experimental data with the linear stability calculations in a wide range of velocities.

Results. The experiment was carried out on a large-scale model of a straight wing with a transonic airfoil OSPB-77, which was installed from one side wall to another in the TsAGI wind tunnel T-128 in test section No. 3 (section 2.75×2.75 m). The chord length was C = 0.5 m. During the experiment, the Mach number of the flow was varied as M = 0.2–0.79; the measurements were carried out in a wide range of the angle of attack from α = –0.25° to 3°. Experiments were carried out at several unit-Reynolds numbers. The pressure distributions on the model were characterized by their evolution from the distributions with a suction peak in the region up to X/C = 0.25 at low M and off-design regimes to the flat distributions that typical to transonic airfoils in cruise regimes at M more than 0.7 (Fig. 1). The five Dantek 55R47 glue-on sensors were used, placed on the all-metal model at the distances from the leading edge of 5, 15, 25, 35 and 57% of the chord. The measurements were carried out with a CTA2018 multichannel constant temperature anemometer manufactured by ITAM SB RAS.

For this short paper the two sets of data were chosen for comparison of the experimental data and calculations: the one with α = 0.125°, M = 0.31, as well as a regime with α = 0°, M = 0.77. In the α = 0°, M = 0.77 case the CTA signals and spectra obtained (Fig. 2) shows that the laminar-turbulent transition occurred between positions of 25 and 35% of the chord. At the

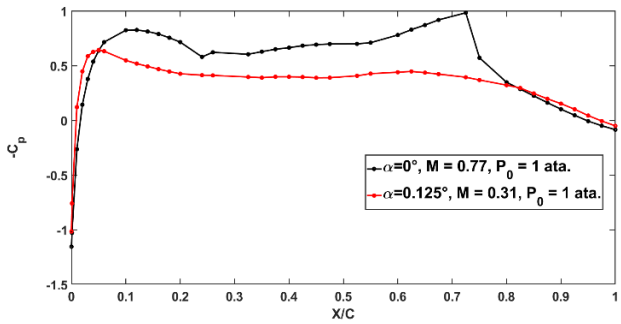

Fig. 1. The examples of pressure distributions.

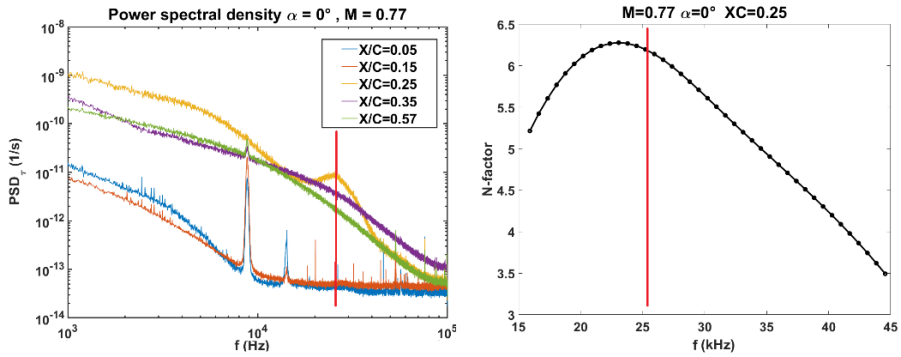

Fig. 2. Spectra of dimensionless shear stress pulsations α = 0° and M = 0.77 (left) and dependence of the *N*-factor on the frequency of TS-waves at *X*/*C* = 0.25 (right).

The vertical line shows the peak frequency of the wave packet in experiment.

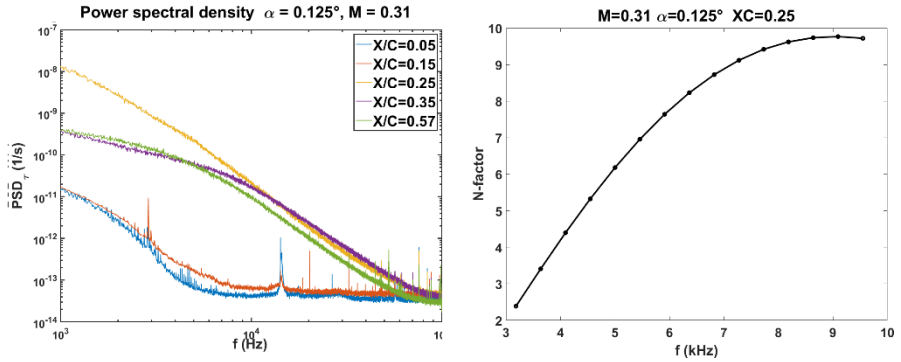

Fig. 3. Spectra of dimensionless shear stress pulsations α = 0.125°, M = 0.31 (left) and dependence of the *N*-factor on the frequency at *X*/*C* = 0.25 (right).

X/*C* = 25% location a wave packet was observed in the range from about 20 to 40 kHz with the central frequency about 25.4 kHz. This correlates well with the calculations, which show that all this frequency range is unstable in this regime with the most amplified wave at 23 kHz. The α = 0.125°, M = 0.31 case has demonstrated that, due to the discrete location of the sensors on the model, it was not possible to find a distinct wave packet of unstable disturbances. The laminar-turbulent transition occurred also between *X*/*C* = 0.25 and 0.35. However, from the spectra in Fig. 3, it can be seen that at least there is an increase of the disturbances energy in the band 3–10 kHz from the *X*/*C* = 0.05 to 0.15, which is confirmed by the calculations. The spectrum at *X*/*C* = 0.25 (Fig. 3) corresponds to the very late stages of transition.

From the results of the experiments and on the basis of the calculations, it can be concluded that the hot-film sensors makes it possible to reliably diagnose the state of the boundary layer and to trace the development of boundary layer disturbances during measurements in high-speed flows in industrial wind tunnels, which were not originally intended to such studies. The frequency range of the Dantek 55R47/CTA2018 combination in experiments was about 80–100 kHz at the late stages of transition and in the turbulent regimes.

DOI: 10.53954/9785604788967_121

ANALYSIS OF FACTORS DETERMINING THE FLOW STRUCTURE IN COMPUTATION OF FLOW IN THE ONERA LAPCAT II EXPERIMENTAL MODEL

W. Liu

***Moscow Institute of Physics and Technology* (*National Research University*)**
141701, Dolgoprudny, Moscow region, Russia

Research of combustion in a duct with supersonic flow at the entrance has been one of the top interests since the emergence of high-speed flight vehicle concept. A series of experiments for modeling high-speed combustion were performed by the French Aerospace Lab (ONERA) within the framework of the European project LAPCAT II at the ONERA-LAERTE facility [1]. The experimental setup consisted of preheater, Laval nozzle and the experimental model (an expanding duct with hydrogen injection from the walls) (see the figure).

Previously, two variants of chemical kinetics [2] have been prepared by author for the implementation in the TsAGI in-house code zFlare [3]. Simulation of LAPCAT II experimental model using these kinetic schemes [4] has shown that the distributions of the active radical mass fractions at the entrance to the experimental model depend significantly upon the kinetic scheme. It was also found that the heat transfer on walls of the duct has a significant effect on the flow structure and combustion characteristics. Later, numerical simulations with taking into

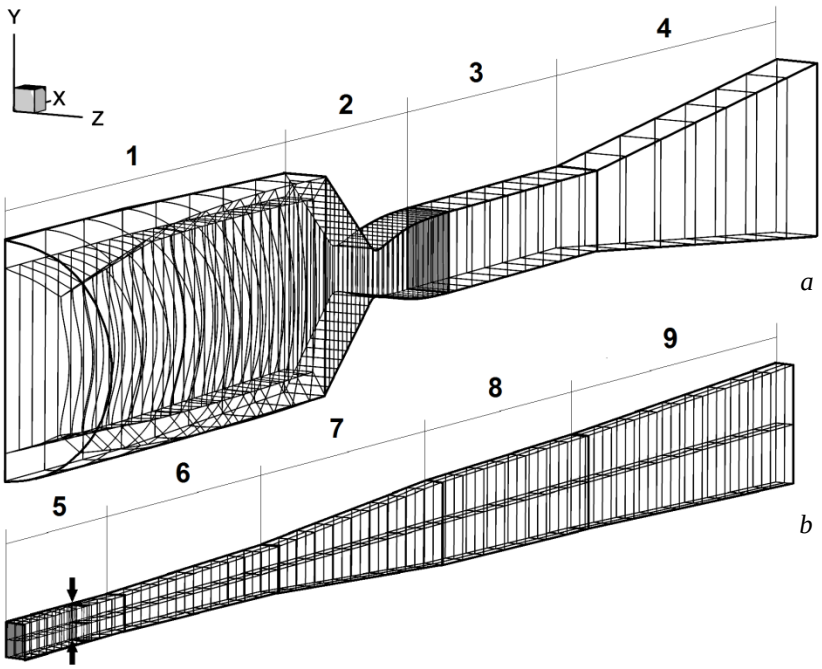

Geometry of the experimental setup and the block structure of the grid for computations of the heater and Laval nozzle (*a*) and the experimental model (*b*).

Arrows – fuel supply; gray color – cross-section of the Laval nozzle docking with the experimental model. *1* – heater; *2* – Laval nozzle; *3* – buffer section of constant area with no-slip condition on the walls; *4* – expanding buffer sections with slipping walls; *5* – constant-area section; *6* – a section with an extension of 2°; *7* – a section with an extension of 6°; *8* – a section with an extension of 2°; *9* – an expanding buffer section with slipping walls.

account the roughness of the duct walls were performed [5, 6]. With a modified wall temperature 1413K, a good accordance of experiment and simulation data is reached.

Recently, numerical simulations using ANSYS Fluent were performed for research of the physical factors determining the flow structure in the LAPCAT II experimental model. The computations were based on numerical solution of RANS equations for a multicomponent gas with finite-rate chemical reactions. The SST k–ω turbulence model [7] and the roughness model proposed by Aupoix [8] were used. The flow regime corresponding to "Case B" from [5] was considered. Computations on the basis of FLUENT code were compared with analogous numerical results from [5, 6] and with the experimental data [1].

Influence of computational grid and of boundary condition on the duct walls is analyzed. Importance of such physical factors as the penetration capability of the fuel jets, heat exchange on the duct walls, different treatments of molecular transport of heat and mass is studied.

Special attention is paid to the influence of chemical kinetics scheme on the results of computations. Considering the combustion process is mainly controlled by the heat release, chemical kinetics plays an important role in determining the flow structure in the duct of the experimental model. Several kinetic schemes are compared: different variants of Jachimowski scheme [2], ONERA kinetics [9] and model from the work [10]. Since different kinetics gives different intermedia distribution in preheater and Laval nozzle, those influence on the calculation of flow in the experimental model duct is demonstrated. The influence of NOx on flow structure in LAPCAT II experimental model is also evaluated.

REFERENCES

1. **Vincent-Randonnier A., Moule Y., Ferrier M.** Combustion of hydrogen in hot air flows within LAPCAT-II Dual Mode Ramjet combustor at ONERA-LAERTE facility — experimental and numerical investigation: AIAA Paper No. 2014-2932, 2014.
2. **Jachimowski C.J.,** An analytical study of the hydrogen-air reaction mechanism with application to scramjet combustion: NASA TP-2791, 1988.
3. **Vlasenko V.V., Mikhailov S.V., Molev S.S., Troshin A. I., Shiryaeva A.A.** Software for numerical simulation of three-dimensional flows with combustion in the channels of ramjet engines in the framework of URANS and DES approaches with the use of models of turbulence–combustion interaction, fractional time stepping technology, and the method of wall functions (zFlare): Certificate No. 2019610822 on state registration of computer code. Russia. January 18, 2019. Appl. date: 28.12.2018. Registr. date: 18.01.2019. Date of publ.:18.01.2019.
4. **Vlasenko V.V., Liu W., Molev S.S. Sabelnikov V.A.** Influence of heat transfer conditions and chemical kinetics on the flow structure in the ONERA LAPCAT II model combustion chamber. // Combustion and Explosion, 2020. Vol. 13, No. 2. P. 36–47. (In Russian.)
5. **Pelletier G., Ferrier M., Vicent-Randonnier A., V. Sabelnikov, A. Mura** Wall roughness effects on combustion development in confined supersonic flow // Journal of Propulsion and Power. 2020. DOI: 10.2514/1.b37842
6. **Sabelnikov V.A., Troshin A.I., Bahne S., Molev S.S., Vlasenko V.V.** Search for determining physical factors in the validation calculations of the experimental model ONERA LAPCAT II with considering roughness of the channel walls. // Combustion and Explosion. 2022. (In Russian.)
7. **Menter F.R., Kuntz M., Langtry R.** Ten years of industrial experience with the SST turbulence model // Turbulence, Heat and Mass Transfer. 2003. Vol. 4, No. 1. P. 625–632.
8. **Aupoix B.** Roughness corrections for the k–ω SST model: Status and Proposals // Journal of Fluids Engineering, 2015. Vol. 137, Art. 021202. 10 p. DOI: 10.1115/1.4028122.
9. **Davidenko D., Gökalp I., Dufour E., Magre P.** Systematic Numerical Study of the Supersonic Combustion in an Experimental Combustion Chamber // 14th AIAA/AHI Space Planes and Hypersonic Systems and Technologies Conference. 2006: AIAA 2006-7913. 25 p. DOI:10.2514/6.2006-7913.
10. **Vincent-Randonnier A., Sabelnikov V., Ristori A., Zettervall N., Fureby C.** An experimental and computational study of hydrogen–air combustion in the LAPCAT II supersonic combustor // Proceedings of the Combustion Institute. 2019. Vol. 37, No. 3. P. 3703-3711. DOI:10.1016/j.proci.2018.05.127

DOI: 10.53954/9785604788967_123

EVOLUTION OF DISTURBANCES IN SUPERSONIC BOUNDARY LAYER UNDER DISTRIBUTED INJECTION OF HELIUM FROM THE SURFACE

V.I. Lysenko, B.V. Smorodsky, A.D. Kosinov

Khristianovich Institute of Theoretical and Applied Mechanics SB RAS
630090, Novosibirsk, Russia

In a number of technological applications, the problem arises to control the boundary layer state. Experiments and computations [1, 2] showed, that it is possible to stabilize a supersonic boundary layer by distributed injection from the surface of a heavy gas, thereby favorably changing (making more stable) the flow by changing the density profile across the boundary layer. The next problem to study is the effect of injection of a gas with a high specific heat capacity C_p into the boundary layer on its stability. Such investigations have not been previously performed. Present paper presents results of the joint experimental and theoretical investigation of helium injection into a supersonic boundary layer on its stability.

Linear Stability Theory. The dynamics of a binary mixture of viscous heat-conducting compressible gases can be described by a set of partial differential equations. Equations, boundary conditions, and numerical methods are reported in detail in [3]. The linear stability theory (LST) for the boundary layer of the binary gas mixture was developed in [4].

Experimental Setup. The experiments were performed in the supersonic low-noise wind tunnel T-325 of the Institute of Theoretical and Applied Mechanics (ITAM SB RAS) at free-stream Mach number M_∞=2, flow stagnation temperature $T_0 \approx 290$ K, and the unit Reynolds number $\mathrm{Re}_1 = 5 \cdot 10^6$ m^{-1}.

The test model was a stainless-steel flat plate 440 mm long, 10 mm thick, and 200 mm wide, with a skew nose beveled at the angle 14° and with a sharp leading edge. Over the working-surface segment of 50 to 170 mm the plate was provided with a 4.3 mm deep slot where permeable insert cold be mounted flush. In this study the porous stainless-steel insert was used which had a porosity of 39 %, filtration purity (an analogue to pore size) of 10 μm, and a thickness of 2.5 mm. The insert was manufactured of porous stainless steel PNS-8 (sintered from a powder, with a grain of size about 70 μm), supplied by Vyksa Metallurgical Plant.

In the experiments, helium was used, a gas with a high specific heat capacity $C_p \approx 5200$ J/(kg·K), that is five times larger than for the air. The experiments were carried out by blowing helium into the boundary layer through a permeable porous insert on the model at various flow rates of the injected gas.

The plate under study was fixed rigidly to the sidewalls of the test section of the wind tunnel at zero angle of attack. Artificial (controlled) disturbances were introduced in the model boundary layer by means of point glow-discharge disturbance-generator [5,6]. The boundary-layer stability to disturbances was measured by a constant-resistance hot-wire anemometer operated with a single-wire sensor made of 10-μm diameter tungsten wire. The overheat ratio of the sensor was 0.8; therefore it could be assumed that the probe was sensitive predominantly to mass-flux fluctuations. Measurements of the downstream disturbance amplification have been performed in the vicinity of the disturbance maximum across the boundary layer, at $E = \mathrm{const}$ (where E is the mean diagonal voltage across the hot-wire bridge), i.e. along the line of a constant value of the mass flux. Disturbance measurements have been performed at different streamwise (x) stations in the spanwise (z) direction. Fluctuation and mean flow quantities were measured by means of the automated data acquisition system described in detail in [7].

Results. Air and helium differ in two factors: helium is much lighter than air (molecular weight is lower), while helium has five times higher specific heat capacity. As a result, two factors influence boundary layer stability in the opposite directions: the boundary layer is being destabilized due to a decrease in the density (low molecular weight of the injected gas, [1, 2]) and, simultaneously, it is being stabilized due to an increase in the specific heat capacity that leads to a reduction of near-wall flow temperature, that according to [8] facilitates to the boundary layer stabilization.

We performed measurements of the development of the artificial perturbation field, generated in the boundary layer by our source. β-spectra measured on the excitation frequency $f = 14$ kHz and local spatial amplification rates $-\alpha_i$ were determined experimentally on the model equipped with solid impermeable insert and with porous insert under various He injection rates of Q = 0; 0.25; 5.5 liter/min at $\mathrm{Re}_1 = 5\times10^6$ m^{-1}. It was established that injection of helium leads to the reduction of disturbance amplification rates on the excitation frequency $f = 14$ kHz. Thus, despite of the destabilizing influence of a low (compared to air) density, injection of a gas with a significantly higher (than air) specific heat capacity C_p can lead to a stabilization of the supersonic boundary layer in a certain range of blowing flow rates. At the same time, calculations showed that at large (Q = 20 liter/min) and small (Q = 0.15 liter/min) values of the flow-rate of injected helium, the boundary-layer under study is destabilized for all frequencies.

Basic conclusions. Results of joint experimental and theoretical study of the effect of distributed injection of helium into the supersonic (Mach 2) flat-plate boundary-layer on the amplification of disturbances are reported. It was established that injection of high heat capacity gas at a certain range of parameters can lead to the boundary layer stabilization. However linear stability computations show that at large and small values of mass flow rate the helium injection leads to boundary layer destabilization.

REFERENCES

1. **Lysenko V.I., Smorodsky B.V., Ermolaev Yu.G., Kosinov A.D.** Stability of supersonic boundary layer under the influence of heavy gas injection: experimental study // Thermophysics and Aeromechanics. 2018. Vol. 25. No. 2. P. 183–190.
2. **Lysenko V.I., Gaponov S.A., Smorodsky B.V., Yermolaev Yu.G., Kosinov A.D**. Influence of distributed heavy-gas injection on stability and transition of supersonic boundary-layer flow // Physics of Fluids. 2019. Vol. 31, Iss. 10. Art. 104103. 16 p. URL: https://aip.scitation.org/doi/10.1063/1.5112145
3. **Gaponov S.A., Smorodsky B.V**. Laminar supersonic boundary layer of binary mixture of gases // Vestnik NSU. Series: Physics. 2016. Vol. 11. No. 1. P. 5–15 (in Russian).
4. **Gaponov S.A., Smorodsky B.V**. Control of supersonic boundary layer and its stability by means of foreign gas injection through the porous wall // Int. J. Theor. & Appl. Mech. 2016. Vol. 1. P. 97–103.
5. **Kosinov A.D., Semionov N.V., Shevelkov S.G**. Investigation of supersonic boundary layer stability and transition using controlled disturbances // Int. Conf. on the Meth. of Aerophys. Research: Proc. Pt. 2. Novosibirsk: ITAM, SB RAS, 1994. P. 159–166.
6. **Lysenko V.I**. Experimental studies of stability and transition in high-speed wakes // J. Fluid Mech. 1999. Vol. 392. 26 p. DOI:10.1017/S0022112099004723.
7. **Kosinov A.D., Ermolaev Yu.G., Nikolaev N.N., Semionov N.V., Semisynov A.I**. On the measurements of the pulsation in supersonic boundary layer by constant temperature hot-wire anemometer // Int. Conf. on the Methods of Aerophys. Research: Proc. Pt. 5. Novosibirsk: Parallel, 2007. P. 81–86.
8. **Lysenko V.I., Maslov A.A**. The effect of cooling on the supersonic boundary layer stability // J. Fluid Mech. 1984. Vol. 147. P. 39–52.

DOI: 10.53954/9785604788967_125

STUDY OF CAVITATION IN THROTTLE FLOWS ON THE BASIS OF NUMERICAL SIMULATION USING EDDY-RESOLVING APPROACHES

A.V. Makhnov[1,2], D.K. Zaitsev[2], A.A. Schmidt[1]

[1]Ioffe Institute RAS
194021, Saint Petersburg, Russia

[2]Peter the Great Saint Petersburg Polytechnic University
195251, Saint Petersburg, Russia

Cavitation in throttle flows (flows in channels with sudden changes of the cross section area) has been the subject of many investigations over the past decades, since the topics of cavitation and liquid degassing are relevant for many engineering applications, such as, for example, fuel injectors and rocket propellants [1, 2]. Cavitation inception in such throttle flows is usually observed in form of cavitation clouds attached to the channel walls. These cavitation clouds mainly develop within the separated flow regions behind the inlet edges of the throttle and practically do not have any influence on the flow structure far from the channel walls [2]. However, if the flow regime corresponds to a sufficiently low value of the cavitation number, then the formation of cavitation clouds near the throttle edges is followed by their break-off, their further transport by the flow and their presence in downstream regions.

This report presents the results that have been obtained by means of numerical simulations using the open-source toolbox OpenFOAM for three-dimensional unsteady flows with cavitation. Two different channel configurations corresponding to two different experiments ([3, 4]) are considered. These geometries are shown in Figs. 1 and 2. For each of the geometries, systematic simulations have been carried out with the operating conditions (the pressure difference, the physical properties of the liquid and its vapor) defined according to the experiments [3, 4].

The simulations are based on the numerical solution of the Navier – Stokes equations and also involve eddy-resolving (LES-based) approaches for turbulence modeling. To account for cavitation, the simulation algorithm is combined with a barotropic cavitation model which assumes an equilibrium description of the liquid-vapor mixture [5]. The table below provides the information about the key operating parameters for the cavitating flow regimes considered in the experiments [3, 4] and in the present study. The working fluid in the experiment [3] is a hydrocarbonic liquid with the properties similar to the ones of real diesel fuels, in the experiment [4] the working fluid is water.

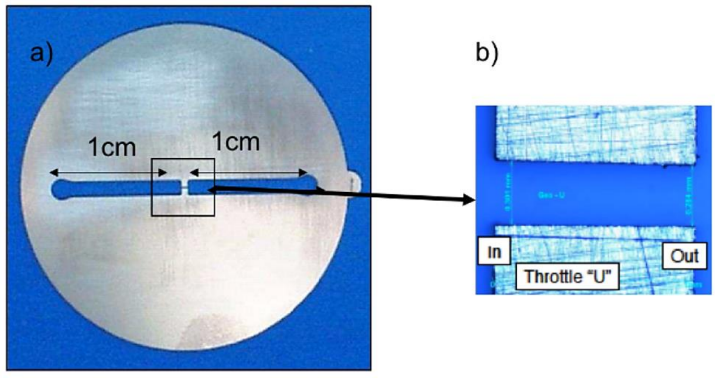

Fig. 1. Geometry of the experimental channel (*a*) and enlarged view of the sudden contraction (*b*), [3].
In – inlet of the throttle, Out – outlet of the throttle. The throttle length is 1 mm, the height and width are 0.3 mm.

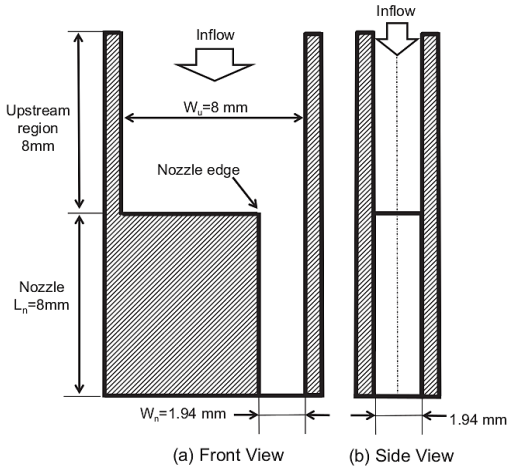

Fig. 2. Geometry of the experimental channel including the nozzle (where cavitation occurs) and the upstream region: front view (*a*) and side view (*b*). [4]

Key information about the operating conditions under study

Range of the pressure differences		Range of the Reynolds number		Range of the cavitation number	
Geometry [3] (Fig. 1)	Geometry [4] (Fig. 2)	Geometry [3]	Geometry [4]	Geometry [3]	Geometry [4]
5.5–8.5 MPa	0.05–0.21 MPa	$(1.4–1.8)\cdot10^4$	$(2.2–3.6)\cdot10^4$	0.16–0.75	0.71–1.92

The results obtained in the present study are in a sufficiently adequate agreement with the literature (experimental) data for both throttle flow configurations. Besides, the systematic variations of the operating conditions in practically relevant ranges of the cavitation number have allowed to obtain new information that in some aspects may be helpful for the development of currently existing ideas in understanding of unsteady mechanisms in cavitating flows.

REFERENCES

1. **Peters A., Sagar H., Lantermann U., el Moctar O.** Numerical modelling and prediction of cavitation erosion // Wear. 2015. Vol. 338-339. P. 189–201.
2. **Franc J.P.** Physics and control of cavitation // Design and Analysis of High Speed Pumps: Educational Notes RTO-EN-AVT-143, Paper 2. Neuilly-sur-Seine, RTO, 2006. P. 2-1–2-36. URL: http://www.rto.nato.int/abstracts.asp.
3. **Winklhofer E., Kull, E., Kelz E., Morozov A.** Comprehensive Hydraulic and Flow Field Documentation in Model Throttle Experiments Under Cavitation Conditions // Proc. of the 17 ILASS-Europe Int. Conference on Liquid Atomization and Spray Systems (Zurich, Switzerland, September 2–6, 2001). Zurich, P. 574–579. URL: https://www.ilasseurope.org/ICLASS/ilass2001/ILASS2001.pdf.
4. **Sou A., Hosokawa S., Tomiyama A.** Effects of cavitation in a nozzle on liquid jet atomization // International Journal of Heat and Mass Transfer. 2007. Vol. 50. Iss. 17-18. P. 3575–3582. https://doi.org/10.1016/j.ijheatmasstransfer.2006.12.033.
5. **Kärrholm F.P.** Numerical Modelling of Diesel Spray Injection, Turbulence Interaction and Combustion: Ph.D. Thesis / Chalmers University of Technology. Göteborg, 2008.

DOI: 10.53954/9785604788967_127

STUDY ON SPOKE-TYPE MULTICOMPONENT ROTATING SHAFT BALANCES FOR MEASURING THE LOADS ON PROPELLERS IN ROTATION

V.S. Manvelyan, V.V. Petronevich, V.V. Lytov, S.V. Zimogorov, M.M. Bogatirev, A.A. Kulikov

Central Aerohydrodynamic Institute
140180, Zhukovsky, Moscow region, Russia

Measurement of aerodynamic loads components on propellers in tests is carries out using a strain gauge measuring system, consisting of rotating shaft balances (RSB), wireless digital telemetry with a built-in inclinometer and software for data processing.

In recent years in TsAGI, the concept of a scalable design of six-component RSB with 12 spoke-type beams has been widely implemented in the design of RSB's for various load ranges [1], including a RSB for measuring loads on contra-rotating open rotor (CROR) [2].

By means of static calibration rig, six-component RSB for CROR testing formulas were obtained [3]. To transmit the signal from the RSB in rotation, a digital telemetry layout and software for working with it was developed. A cycle of dynamic tests was carried out on a TsAGI's test rig for rotor investigation, which is equipped with static two-component strain gauge dynamometer to measure thrust and torque loads. The general view of test rig with RSB and telemetry layout is shown below (see the figure).

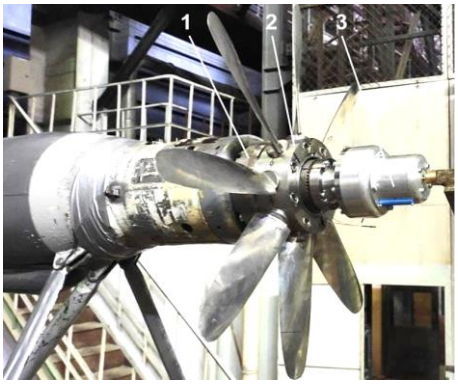

Test rig for rotor investigation equipped with RSB and telemetry layout.
1 – RSB, 2 – Propeller hub, 3 – Telemetry layout.

The result of dynamic tests revealed the operability of both the RSB and the telemetry layout with software. Minor discrepancies have been identified between the data from the two-component strain gauge dynamometer of test rig and the RSB processed data. These discrepancies are the subject of further research.

REFERENCES

1. **Petronevich V.V., V.V. Lytov, V.S. Manvelyan, A.A. Kulikov, S.V. Zimogorov** Study on six-component rotating strain-gauge balance development for helicopter tail rotor testing // Aerospace MAI Journal. 2021. Vol. 28, No. 2. P. 69–84. doi.org/10.34759/vst-2021-2-69-84.
2. **Bogdanov V.V., Lytov V.V., Manvelyan V.S.** Development of the six-component rotating shaft balances for counter rotating open rotor testing // Proc. of 18 Int. Conf. on the Methods of Aerophys. Research (ICMAR 2016): AIP Conference Proceedings. 2016. Vol. 1770. Iss. 1. Art. 030002. (6 p.). doi.org/10.1063/1.4963944.
3. **Petronevich V.V., Lytov V.V., Manvelyan V.S., Kulikov A.A., Zimogorov S.V.** Study on six-component rotating strain-gauge balance calibration for aircraft propeller testing // Aerospace MAI Journal. 2021. Vol. 28, No. 4. P. 48–61.

DOI: 10.53954/9785604788967_128

DIFFUSION DEPOSITION OF AEROSOL PARTICLES IN A FIBROUS FILTER FOR EXTENDED RANGE OF PECLET NUMBERS

R.F. Mardanov, S.K. Zaripov, V.F. Sharafutdinov

Kazan Federal University
420008, Kazan, Russia

The efficiency E of capture of aerosol particles by fibrous filters is determined though the value of the single fiber efficiency η (SFE) by the formula

$$E = 1 - \exp\left(-\frac{2\alpha H}{\pi a}\eta\right),$$

where a is the fiber radius, α is the solidity of the porous medium, H is the filter layer length. Thus, one of the main tasks in modeling the deposition of suspended particles in aerosol filters is to calculate SFE.

In the case of a small particle size, within the framework of the diffusion deposition model, the following formula was obtained in [1]

$$\eta(\mathrm{Pe}) = 2.9\,\mathrm{Ku}^{-1/3}\,\mathrm{Pe}^{-2/3} + 0.624\,\mathrm{Pe}^{-1}, \quad (1)$$

where $\mathrm{Pe} = 2aU/D$ is the Peclet number, U is the average velocity of the carrier phase flow, D is the diffusion coefficient, Ku is the hydrodynamic Kuwabara parameter, that is equal $\mathrm{Ku} = -0.5\ln\alpha - 0.75 + \alpha - 0.25\alpha^2$ for the fibrous filters and $\mathrm{Ku} = \ln(2h) - 1.33 + \frac{1}{3}\left(\frac{\pi}{2h}\right)^2$ for wire mesh screens with $h = h_0/(2a)$ (h_0 is the distance between fibers in row). In [2], a periodic cell model was proposed for the problem of convective-diffusion transport of aerosol particles and to take into account the diffusion wake from fibers located upstream the formula (1) was generalized

$$\eta(\mathrm{Pe}) = B\,\mathrm{Ku}^{\beta}\,\mathrm{Pe}^{\gamma_0+\gamma_1\mathrm{Ku}}. \quad (2)$$

The parameters values B, β, γ_0, γ_1 were calculated the fibrous filter at regular and chess order fibers packing.

Dependencies (1) and (2) are consistent with the experimental and numerical data only for relatively large numbers $\mathrm{Pe} > 10$ when the graphs $\eta(\mathrm{Pe})$ in the logarithmic axes are close to linear. At average values of the Peclet numbers $0.1 < \mathrm{Pe} < 10$, the behavior of the dependences $\eta(\mathrm{Pe})$ obtained in the experiments becomes nonlinear, and at small values $\mathrm{Pe} < 0.1$ they go to the horizontal asymptote $\eta = \eta_0$ (see [3]).

In the present work, the SFE calculations are carried out for fibrous filters with regular and chess order packing, as well as for a single-row wire mesh screen in a wide range of Peclet numbers $\mathrm{Pe} = 10^{-3}...10^{3}$ for different packing densities taking into account the diffusion wake and for various distances between fibers in row. The numerical solution of the problem of calculating the carrier phase flow in the framework of the Stokes model was performed using the boundary element method [4]. The solution of the problem of convective-diffusive transport in rectangular periodic cell was carried out by the method of boundary and domain elements [2].

An analytical approximate expressions for the dependencies $\eta(\mathrm{Pe})$ are derived that include an inclined asymptote, taken in form (1) for a wire mesh screen and in form (2) for a fibrous filter, at $\mathrm{Pe} \to \infty$ and on the horizontal asymptote $\eta = \eta_0$ at $\mathrm{Pe} \to 0$. The derived dependencies are compared with the calculated and known experimental data.

The work is performed according to the Russian Government Program of Competitive Growth of Kazan Federal University.

REFERENCES

1. **Stechkina I.B.** Diffusion precipitation of aerosols in fiber filters // Dokl. Acad. Nauk. SSSR. 1966. Vol. 167, № 6. P. 1327–1330.
2. **Mardanov R.F., Zaripov S.K., Sharafutdinov V.F.** A new periodic cell model of aerosol diffusion deposition in a fibrous filter // Separation and Purification Technology. 2021. Vol. 257, No. 117848.
3. **Kirsh V.A.** Deposition of aerosol nanoparticles in fibrous filters // Colloid Journal. 2003. Vol. 65, No. 6 H. 726–732.
4. **Mardanov R.F., Dunnett S.J., Zaripov S.K.** Modeling of fluid flow in periodic cell with porous cylinder using a boundary element method // Engineering Analysis with Boundary Elements. 2016, Vol. 68. P. 54–62.

DOI: 10.53954/9785604788967_130

NUMERICAL SIMULATION OF GAS-DYNAMICS IN A JET EMITTER WITH A SLIT CHAMBER

E.A. Marfin, A.A. Abdrashitov
Institute of Power Engineering and Advanced Technologies
FRC Kazan Scientific Center RAS
420111, Kazan, Russia

Jet emitters of pressure oscillations are widely used in various fields. One of the promising directions is the use of such devices in the oil industry to intensify oil production [1, 2]. Field tests of the jet-driven Helmholtz oscillator have confirmed its high efficiency, namely: by more than 1 ton of oil per day, the flow rate of producing wells is increased; the injectivity of the wells is restored; water cut is reduced [3]. At the same time, studies have identified directions for improving the design of the device. In particular, when water is used as a working agent, it is necessary to exclude the negative cavitation effect of a high-speed jet on a cover with an outlet. In this paper, an emitter with a modified geometry is investigated in comparison with "classical" jet-driven Helmholtz oscillator.

The studied jet emitter was an axisymmetric cylindrical chamber with a diameter of D_c = 78 mm and a length of L_c = 5 mm, closed on both sides with covers (Fig. 1). In the center of the front cover, a cylindrical hole is made – a nozzle with a diameter of d_1 = 12 mm. The cover thickness l_1 varied from 0.7 to 18 mm. Considering that the length of the chamber is much less than the diameter of the nozzle, the chamber can be called a slit chamber. In the center of the outlet cover with a thickness of l_2 = 9 mm, an outlet hole with a diameter of d_2 = 16 mm is made. When the working agent flows through the device, in this work – air, a jet is formed at the nozzle exit, which flows through the cylindrical chamber and the outlet to the outside. With an increase in the jet speed, sound vibrations are generated, the frequency of which depends on the jet speed and the geometry of the device. Within certain speed ranges, characteristic modes of pressure fluctuations are observed, in which the dependence of frequency on speed is non-linear.

Experimental studies preceded the numerical simulation of the gas-dynamics of the flow in a jet emitter of pressure oscillations. A series of experiments was carried out on the stand [2, 4, 5], in a jet velocity range from 0 to 72 m/s. The research results showed some difference in the mechanism of generation of pressure oscillations in comparison with "classical" jet-driven Helmholtz oscillator. First, a strong dependence of the maximum amplitude reduced to velocity head on the length of the cylindrical nozzle was observed. Secondly, the resonant amplification occurred at higher frequencies than the natural frequency of the device. An important result of experimental studies is the revealed dependence of the Strouhal number Sh = $l_1 f/U$ on the reduced jet velocity (U/l_1). As a consequence of this result, the dependence of the frequency of generated oscillations within the "strong" mode on the jet velocity was obtained in the form:

$$f = 0.765 \cdot l_1^{-0.31} \cdot U^{0.31}.$$

The experimental data obtained are used to determine the boundary conditions in numerical simulation. The numerical experiment was carried out using

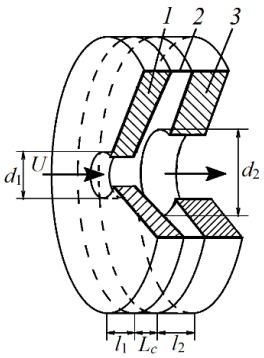

Fig. 1. Scheme of a jet emitter with a slit chamber.
1 – front cover with an inlet nozzle, *2* – resonator chamber, *3* – rear cover with an outlet.

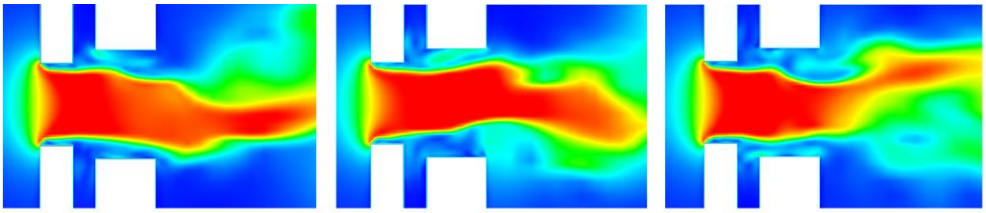

Fig. 2. Distribution of air velocity in the axial section of the emitter at different points in time with a step of 0.01 s.

the software package for three-dimensional modeling of the movement of liquid and gas FlowVision. Models were used, including: Navier – Stokes equations, continuity equation, energy conservation law, *k–e* turbulence model. To perform the calculation, a finite-volume method for solving equations at a stationary inlet pressure was used.

As a result of numerical simulation, the gas flow in the flow-through part of the device (Fig. 2) was visualized, pressure distributions were obtained, allowing a deeper understanding of the mechanism of jet generation of pressure fluctuations. The presence of a slit chamber and an outlet leads to the non-stationarity of the jet, which is the source of sound. The values of the amplitude of pressure fluctuations are comparable with the experimental data obtained earlier.

The study was financial support of the Russian Science Foundation, grant No. 22-29-01174, https://rscf.ru/project/22-29-01174/.

REFERENCES

1. **Gataullin R.N., Kadyirov A.I.** Intensifying oil extraction by wave action methods on productive layers // SOCAR Proceedings. 2020. Vol. 2020, No 2. P. 78–90. doi.org 10.5510/OGP20200200434.
2. **Abdrashitov A.A., Marfin E.A.** Short cylindrical nozzles in a jet-driven Helmholtz oscillator // Physics of Fluids. 2020. Vol. 32, No. 7. P. 121–130. doi.org /10.1063/5.0006845.
3. **Marfin E.A., Kravtsov Ya.I., Abdrashitov A.A., Gataullin R.N.** Field Tests of Wave Action on Oil Production in the Pervomaysky Field // Georesursy [Georesources]. 2014. Vol. 57, No. 2. P. 14–16. doi.org/10.18599/grs.57.2.3.
4. **Abdrashitov A.A., Marfin E.A., Chachkov D.V.** Experimental study of a borehole acoustic radiator with a ring in a long cylindrical chamber // Acoustical Physics. 2018. Vol. 64, No 2. P. 237–244. doi.org/10.1134/S106377101802001XB.
5. **Abdrashitov A.A., Marfin E.A., Plakhova E.A.** Experimental study of the jet-driven Helmholtz oscillator // Proc. of 20 Int. Conf. on the Methods of Aerophys. Research (ICMAR2020): AIP Conference Proceedings. 2020. Vol. 2351. Art. 040059. 6 p. doi.org/10.1063/5.0052206.

DOI: 10.53954/9785604788967_132

SUPERSONIC INTAKE WITH LONGITUDINAL AIR BLEED SLOTS FACILITATING ITS STARTING

I. I. Mazhul, Y. P. Gounko

Khristianovich Institute of Theoretical and Applied Mechanics SB RAS
630090, Novosibirsk, Russia

A significant problem in providing the starting and efficient operation of supersonic air intakes is the elimination of adverse effects associated with the separation of the boundary layer when shock waves fall on inlet walls. Traditional methods of preventing the boundary layer separations on the ramp wedge in the inlet duct entrance are suction of the boundary layer using perforated panels at places where the shock wave falls on the ramp wedge or the use of transverse bleed slots. In those cases when the shock wave created by the inlet cowl lip falls on the ramp wedge, the longitudinal coordinate of the place of this shock significantly depends on the free-stream Mach number, and the fixed position of the transverse bleed slots cannot be effective in a wide range of flight speeds. For the air intakes multimode by the supersonic flight speed, this can lead to a significant worthening the flow in the inlet entrance section, and, accordingly, to a degradation of the air intake performance.

A constructive solution to improve the structure of the flow in the entrance section of the multimode intakes in the said cases was proposed in [1], this solution enables controlling this flow. It is making of a compression surface in the intake duct with the longitudinal air bleed slots in a place where the shock wave created by the inlet cowl lip falls onto it. The width of these slots may be fixed or controlled. In the latter case it may be controlled with coordinated forward-return moving special longitudinal volumetric elements executed by a direction transversal to the compression surface.

To study the efficiency of a longitudinally slotted air bleeding as for the problem of the air intake starting, a simplified intake configuration was considered which is shown in Fig. 1.

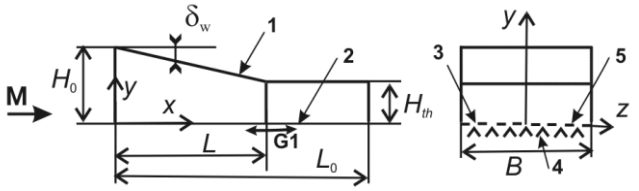

Fig. 1. Scheme of the investigated configuration.

1 – intake cowl, *2* – compression surface, *3* – longitudinal air bleed slots, *4* – longitudinal moved elements, *5* – longitudinal fixed elements corresponding to the compression surface.

Here is marked the inlet cowl lip *1* created the shock wave falling onto the compression surface *2* in the air intake duct. A part of this compression surface, in the area G1 where the shock wave falls onto it, is arranged with longitudinal slots *3* used for the boundary layer bleeding or for the air bypass. The width of these slots is regulated by the coordinated forward-return moving of the longitudinal volumetric elements *4* having a triangular cross section. Moving is carried out in a direction transverse to the compression surface. Sizes of the considered intake configuration were accepted proceeding from requirements for tests of model in the wind tunnel T-313 ITAM for operating flow Mach number M = 4.

The intake consists of an entrance converging section arranged by the cowl lip of an angle $\delta_w = 10°$ positioned at a height $H_0 = 0.04$ m, as well as a throat section of a relative height $H_{th}/H_0 = 0.58$, the intake width is $B = 0.075$ m. Note that the accepted value of the relative throat

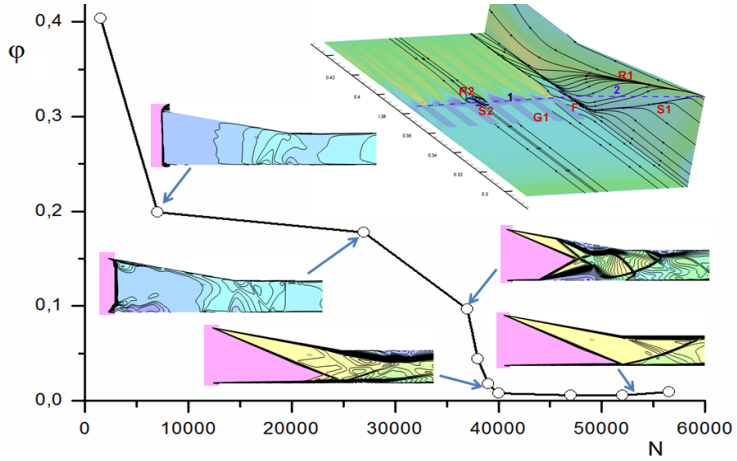

Fig. 2. Steadying the flow in the process of iterations.

area $H_{th}/H_0 = 0.58$ is less than the critical value 0.672, determined by the Kantrowitz – Donaldson criterion of the intakes starting for M = 4. This means the considered air intake was theoretically not self-starting at this velocity.

Numerical computations of the steady supersonic 3D flow over the intake were carried out using the Reynolds-averaged Navier – Stokes equations (RANS) and the k–ω SST turbulence model. Parameters of the slots positioned in an area G1 were varied. In particular there was considered the "limiting" case, when the slots were completely closed and air bleeding did not implement. A flow pattern over the non-started intake with a bow shock wave in front the intake entrance took place in this case, the flow in the intake entrance was subsonic at the entrance and it accelerated to a little supersonic velocity at the intake duct exit. Critical conditions for chocking the nonuniform flow [2] were achieved here.

Steading the flow by data of the numerical computations in the case with the air bleeding can be illustrated by changing the air flow rate φ through the slots in an area G1 depending on the number of iterations N, Fig. 2 (where the presented flow patterns refer to the plane of symmetry of the configuration). The process of flow steadying in a numerical computation with some approximation can be interpreted as the process of starting the air intake. It can be seen that bypassing a certain part of the air through the longitudinal bleed slots arranged in the compression surface is an effective way to facilitate starting of the air intake.

The research was supported by the Ministry of Science and Higher Education of the Russian Federation within the framework of the state assignment (project No.121030500158-0).

REFERENCES

1. Patent No. 2672825 RF. Supersonic inlet (with multislotted bleeding) / Yu.P. Gounko. Patent holder ITAM SB RAS. Appl. No. 2017113272. Priority 17.04.2017. Publ. 19.10.2018. Bul. No. 32.

2. Gounko Yu.P., Mazhul I.I., Nurutdinov V.I. Numerical investigation of supersonic flow breakdown at the inlet duct throttling // Thermophysics and Aeromechanics. 2014. Vol. 21, No. 2. P. 157–170.

DOI: 10.53954/9785604788967_134

INVESTIGATION OF HIGH-SPEED INTERACTION OF SOLID BODIES AND A NEW METHOD OF AEROBALLISTIC ACCELERATION

A.Yu. Melnikov

Khristianovich Institute of Theoretical and Applied Mechanics SB RAS
630090, Novosibirsk, Russia

The modern state of methods for accelerating bodies to ultrahigh velocities, as well as the possibilities of using throwing facility in aeroballistic experiments and problems of protection against meteorites, simulation of impact phenomena, etc., are discussed in reviews [1–6]. As noted in review [7], the capabilities of traditional means of accelerating bodies (gas, light gas and powder guns, explosive and railgun accelerators) are approaching the limit. In this regard, the tasks associated with increasing the throwing speed, increasing the mass of thrown objects and the efficiency of energy conversion in throwing facility are of particular interest.

In most of the existing throwing facilities, the mass of thrown objects does not exceed ten grams [8]. It should be emphasized that if the deformable bodies under study are small in size, then the wave pattern acquires exceptional complexity. This complexity is due to the fact that when stress waves propagate in objects of limited size, they experience multiple reflections from the boundary surfaces of the body and, interacting, form a very complex wave pattern inside the object. Therefore, the task of creating a ballistic plant for throwing massive bodies at high speeds, using only the energy of compressed gas (under laboratory conditions), is extremely urgent.

To be able to estimate the imparted velocities to bodies of various masses, a one-dimensional quasi-stationary theoretical calculation model was created. The one-dimensional model is based on gas-dynamic relations and the problem of gas outflow from the receiver through a hole of a given diameter is solved. It is believed that the pressure force is transferred to the accelerated body without losses and the movement along the barrel is carried out for some time, depending on the length of the barrel. The peculiarity of the scheme under consideration was the use of a large elongation barrel (up to L/D = 500), which should allow accelerating fairly heavy bodies (up to 500 g), compared with known light-gas facility.

To confirm the proposed schemes and compare with the calculations, a prototype ballistic plant (BP) was developed and manufactured (Fig. 1).

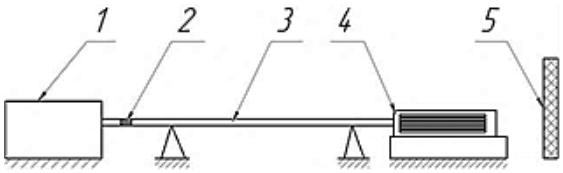

Fig. 1. Scheme of the prototype ballistic plant.
1 – pressure receiver, *2* – projectile, *3* – barrel, *4* – muzzle brake, *5* – target.

Obtained experimental data on the prototype BP on the speed of the projectile at various initial pressures. Figure 2 shows the dependence of the body's flight speed on the pressure in the receiver. The mass of the thrown body in all experiments was about 130 g. The solid line on the graph shows the dependence of the velocity obtained from the one-dimensional

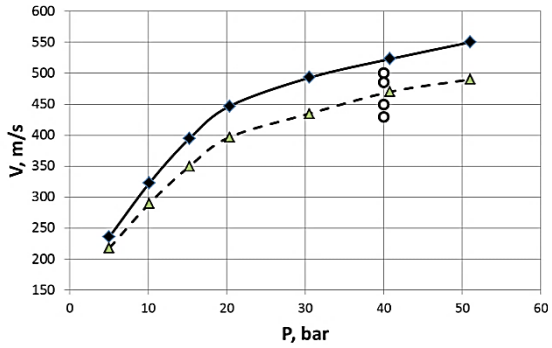

Fig. 2. Dependence of the projectile flight speed on the pressure in the receiver.

theoretical model on the pressure in the receiver for a given mass of the projectile. The dotted line shows the experimentally obtained velocity values at various initial pressures in the receiver.

It can be seen that the experimentally obtained velocity values are in good agreement with the analytical calculation. The average deviation is 10%. Also, for a pressure value in the receiver of 4 MPa, additional studies were carried out, showing the spread of the obtained velocities. The existing difference between the analytical calculation and the experimentally obtained velocities is due to the lack of consideration of the friction forces of the body, in the theoretical model, when moving along a ballistic barrel.

REFERENCES

1. **Cable A.J.** Hypervelocity Accelerators // High-Velocity Impact Phenomena / Ed. R. Kinslow. N.Y.: Academic Press, 1970. P. 1–23.
2. **Lekont K.** High-speed throwing // Kurzzeitphysik = High-speed Physics / Eds. K. Vollarth, G. Thomer. Wien; N. Y.: Springer-Verlag, 1967. **[Лёконт К.** Высокоскоростное метание // Физика быстропротекающих процессов: Пер. / Под ред. Н. А. Златина. Т. II. М.: Мир, 1971. С. 247–275.]
3. **Pilyugin B.N., Leontiev P.E.** Possibilities of increasing the speed of throwing bodies in ballistic installations. Preprint No. 52-99. Moscow: Publishing House of the Institute of Mechanics, Moscow State University, 1999. 58 p.
4. **Titov V.M., Shvetsov G.L.** Acceleration of macroparticles to high speeds // Continuum Dynamics. Vol. 78. Explosion hydrodynamics. Novosibirsk, 1986. P. 128–136.
5. **Fadeenko Yu.I.** High speed kick: Bibliographic index of domestic and foreign literature. Novosibirsk, 1967 – No. 1; 1972 – No. 2; 1976 – No. 3; 1979 – No. 4.
6. **Khvostov I.I., Shirmanov P.M.** Ballistic tubes and stands for aerodynamic research: (Based on foreign materials. seals). [Moscow], 1973. 60 p. (TsAGI. ONTI; No. 425).
7. **Ostashev V.E., Lebedev E.F., Fortov V.E.** Requirements for limiting the macrospeed of an accelerator in a magnetoplasma accelerator // TVT. 1993. Vol. 31, No. 2. P. 313–320.
8. **Golubyatnikov A.N., Leontiev N.E., Pilyugin N.N.** Methods for assessing the effectiveness of light gas ballistic installations // Advances in Mechanics. 2003. Vol. 2, No. 2. P. 97–125.

DOI: 10.53954/9785604788967_136

THE STRUCTURE OF A SUPERSONIC FREE JET FLOWING OUT AT AN ANGLE TO THE DIRECTION OF AN INCOMING FLOW

I.V. Menshchikova, V.I. Zapryagaev, I.N. Kavun

Khristianovich Institute of Theoretical and Applied Mechanics SB RAS
630090, Novosibirsk, Russia

There are a variety of approaches of drag reduction of a supersonic aircraft, such as the use of a drag-reducing aerospike [1], jet blowing towards the incoming flow [2], air heating in the area in front of the nose cone [3], etc. Each of the known methods has its advantages and disadvantages, and the search for new ones is a relevant challenge of supersonic aerodynamics.

An undescribed method was mentioned in [4, 5]. The effect of jets flowing from the propulsion system of the launch escape system on the aerodynamic characteristics of the main stage separation unit was considered. The launch escape system is a nose cone with small rocket engines installed in front of the nose cone of the spacecraft. In the case of an emergency, powering up these engines makes it possible to separate the spacecraft and send it to a safe distance. It was discovered that the powering up of this propulsion system can result in both a decrease and an increase of the drag of the spacecraft. The authors of these articles suggested that the potential causes of the drag variation could be shielding by jets of the nose cone of the spacecraft, and ejection of gas jets from the area near its surface. In these papers, a detailed analysis of the structure of the flow resulting from the interaction of the incoming flow with the engine jets has not been carried out due to the great complexity of the flow. It is reasonable to reveal the physical mechanism affecting the drag variation. The first stage is to explore the flow structure of a single free jet, with the direction of flow oriented at some angle to the incoming flow.

In this paper the results of the research of gas-dynamic parameters and shock-wave structure are presented for the flow for a supersonic single free jet flowing out into a motionless space and a single jet interacting with the incoming flow in the non-axial direction.

The figures shows the flow picture in the longitudinal symmetry plane (Fig. 1) of a single jet flowing out into a motionless submerged space (*a*) and when interacting with the incoming flow at M = 2 (*b*) and M = 6 (*c*) and the flow picture in the cross-section plane (Fig. 2) at a distance x/D_a= 16 (D_a is the nozzle section diameter) from the nozzle section of a single jet when interacting with the incoming flow at M = 2 (*a*) and M = 6 (*b*). The Mach number at

a *b* *c*

Fig. 1. The flow picture for longitudinal section.

a – the jet flowing out into a motionless space, *b* – the jet interaction with the incoming flow M = 2, *c* – the jet interaction with the incoming flow M = 6.

a *b*

Fig. 2 The flow picture for cross section.

a – the jet interaction with the incoming flow M = 2, *b* – the jet interaction with the incoming flow M = 6.

the nozzle section is $M_a = 3.5$, the ratio of the total pressure at the nozzle section to the static pressure in the incoming flow is *Npr* = 1000. The angle between incoming flow direction and jet flow direction is 30°. The line is the location of the cross section.

It is shown that the incoming flow deforms the jet in the direction of its streams: the shock waves are appeared, the length of the first shock cell is reduced, the cross section of the jet is transformed from circular to horseshoe-shaped.

The research was carried out within the state assignment of Ministry of Science and Higher Education of the Russian Federation (project No. 121030500158-0).

REFERENCES

1. **Alexander S.R., Katz E.** Flight Tests to Determine the Effect of Length of a Conical Windshield on the Drag of a Bluff Body at Supersonic Speeds: NACA RM No. L6J16a. 1947. 13 p.
2. **Lopatoff M.** Wind-flow Study of Pressure-drag Reduction at Transonic Speed by Projecting a Jet of Air from the Nose of a Prolate Spheroid of Fineness Ratio 6: NACA RM No. L51E09. 1951. 20 p.
3. **Georgievskij P.Yu., Levin V.A**. Supersonic flow around the bodies at the presence of external sources of heat release // Letters to the Journal of Applied Physics. 1988. Vol. 14. Iss. 8. P. 684–687.
4. **Andreev V.N., Borovkov A.I., Voynov I.B., Drozdov S.M., Dyadkin A.A., Kazakov M.I., Kazakov M.N., Mikhaylov M.V.** Aerogasdynamics behavior of the escape system separable nose assembly with operating propulsion system // Space Engineering and Technology. 2014. No. 4(7). P. 10–20.
5. **Dyadkin A.A., Kazakov M.I., Mikhaylov M.V., Andreev V.N., Kozlovskiy V.A.** A study of the abort rocket unit plume effects on the aerodynamics of the separation unit // Space Engineering and Technology. 2017. No. 4(19). P. 16–28.

DOI: 10.53954/9785604788967_138

DRAG COEFFICIENT OF A GAS-PERMEABLE HIGHLY POROUS PLATE IN SUPERSONIC FLOW

S.G. Mironov, T.V. Poplavskaya, I.R. Valiullin

Khristianovich Institute of Theoretical and Applied Mechanics SB RAS
630090, Novosibirsk, Russia

The study of the interaction of a supersonic flow with gas-permeable porous materials is of great scientific and applied interest in the development of a perspective aircrafts. The first experimental and numerical studies on the use of gas-permeable porous materials in supersonic aerodynamics and, in particular, in the problem of reducing aerodynamic drag are given in [1–9]. The data obtained in these works refer to the flow around axisymmetric bodies at zero angle of attack. In [8, 9], the results of studies on the flow around a cylinder with a front gas-permeable cellular-porous insert were analyzed and generalized in the form of a linear dependence of the normalized drag coefficient on a complex that includes the ratio of the cylinder diameter to the pore diameter of the insert and the free flow Mach number. The obtained empirical dependence makes it possible to predict the magnitude of the decrease in the aerodynamic drag of such bodies depending on their geometric scale and flow conditions (i.e., for different ratios of the cylinder diameter to the pore diameter and Mach numbers in the range from 5 to 21).

The design of aircraft is a combination of axisymmetric and flat elements. Therefore, it is practically important to obtain a similar dependence, which makes it possible to predict the magnitude of the reduction in the aerodynamic drag of flat bodies with a front porous insert. In the presented study, for the first time, the flow around a gas-permeable plate made of cellular-porous material was studied by an experimental-computational method and a generalized dependence of the drag coefficient on the ratio of the plate thickness to the diameter of the pores of the material was found.

The experiments were carried out in the T-327 supersonic wind tunnel of ITAM SB RAS at zero angle of attack, Mach number $M_\infty = 7$, and unit Reynolds number $1.5 \cdot 10^6$ 1/m. In the experiments, the force of aerodynamic resistance F_x of rectangular blocks of cellular-porous nickel with a size of 60×40 mm and a thickness h installed in a special fork holder was measured (Fig. 1). The material of the blocks had a porosity of 95%, the average pore diameter d = 1 mm. The width of the porous block (60 mm) was determined by the size of the homogeneous core of the wind tunnel flow. The longitudinal size of the block (40 mm) was determined from the results of numerical simulation [9], where it was shown that the oncoming flow penetrates into the porous material to a depth of less than 40 mm. In the experiments, the thickness of the porous block h was varied in the range from 4 to 20 mm with a step of 1 mm. In addition, the aerodynamic drag force Fx0 of rectangular blocks of gas-tight material of the same size was measured. The ratio of forces F_x/F_{x0} is quantitatively equal to the ratio of the drag coefficient of the porous plate to the drag coefficient of the gas-tight material plate C_x/C_{x0}, which shows the amount of drag reduction due to the porosity of the material.

Numerical simulation of supersonic flow around a gas-permeable plate made of cellular-porous material was performed using the ANSYS Fluent CFD package using a two-dimensional skeletal model of a porous material in the form of a set of round elements arranged in a checkerboard pattern. Numerical simulation makes it possible to expand the range of geometrical parameters of the model and flow conditions.

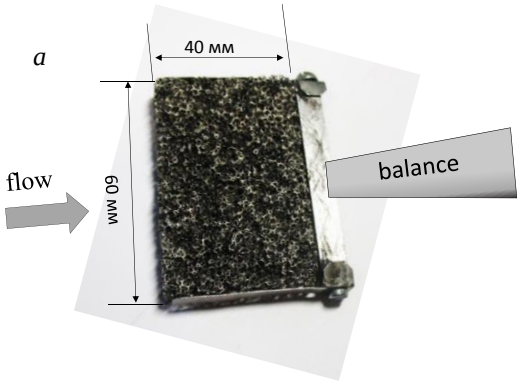

Fig. 1. Photograph of the model on the fork holder.

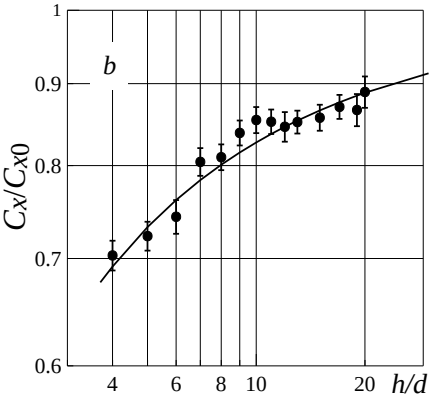

Fig. 2. Dependence of the normalized drag coefficient on the ratio h/d.

The results of measurements of the normalized resistance coefficient C_x/C_{x0} of a porous plate are given depending on the ratio of the plate thickness h to the average material pore diameter d (Fig. 2). The generalizing dependence for the flat model is described by the empirical relation $C_x/C_{x0} = 1 - 2.7\cdot[(h/d)^{-0.65}\cdot M_\infty^{-2/3}]$, and the data with measurement accuracy fall on a single curve from the ratio h/d.

The work is carried out within the framework of the Program of Fundamental Scientific Research of the State Academies of Sciences for 2021-2023 (project No. 121030500162-7). Equipment Experiments Center for Collective Use “Mechanika” (ITAM SB RAS).

REFERENCES

1. **Fomin V.M., Mironov S.G., Serdyuk K.M.** Reducing the Wave drag of bodies in supersonic flows using porous materials // Tech. Phys. Lett. 2009. Vol. 35, No. 2. P. 117–119.
2. **Fomin, V. M., Zapryagaev, V. I., Lokotko, A. V., et al.** Aerodynamic characteristics of a body of revolution with gas-permeable surface areas // J. Appl. Mech. Tech. Phys. 2010. Vol. 51, No. 1. P. 65–73.
3. **Bedarev I.A., Mironov S.G., Serdyuk K.M., et al.** Physical and mathematical modeling of a supersonic flow around a cylinder with a porous insert // J. Appl. Mech. Tech. Phys. 2011. Vol. 52, No. 1. P. 9–17.
4. **Mironov, S. G., Maslov, A. A., Tsyryulnikov, I. S.** Controlling aerodynamic forces with the aid of gas-permeable porous materials // Tech. Phys. Lett. 2014. Vol. 40, No. 10. P. 888–890.
5. **Mironov S.G. Maslov A.A., Poplavskaya T.V., Kirilovskiy S.V.** Modeling of a supersonic flow around a cylinder with a gas-permeable porous insert // J. Appl. Mech. Tech. Phys. 2015. Vol. 56, No. 4. P. 549–557.
6. **Mironov, S. G., Poplavskaya, T. V., Kirilovskiy, S. V.** Impact of frontal-porous-insert temperature on the cylinder drag in supersonic flow // Thermophys. Aeromech. 2017. Vol. 24, No. 4. P. 629–632.
7. **Kirilovskiy, S.V., Maslov, A.A., Mironov, S.G., Poplavskaya, T.V.** Application of the skeleton model of a highly porous cellular material in modeling supersonic flow past a cylinder with a forward gas-permeable insert // Fluid Dynamics. 2018. Vol. 53, No. 3. P. 9–17.
8. **Mironov S.G., Poplavskaya T.V., Kirilovskiy S.V., Maslov A.A.** A similarity criterion for supersonic flow past a cylinder with a frontal high-porosity cellular inser // Tech. Phys. Lett. 2018. Vol. 44, No. 3. P. 225–228.
9. **Maslov A.A., Mironov S.G., Poplavskaya T.V., Kirilovskiy S.V.** Supersonic flow around a cylinder with a permeable high-porosity insert: Experiment and numerical simulation // J. Fluid. Mech. 2019. Vol. 867. P. 611–632.

DOI: 10.53954/9785604788967_140

COMPARISON OF SOLUTION METHODS FOR A QUASILINEAR TRANSPORT EQUATION FOR SIMULATION OF SONIC BOOM WAVE PROPAGATION

P.A. Mishchenko, T.A. Gimon, V.A. Kolotilov

Khristianovich Institute of Theoretical and Applied Mechanics SB RAS
630090, Novosibirsk, Russia

One of the restrictions that determine the right to operate supersonic passenger aircraft and their market competitiveness is the need to ensure an acceptable level of sonic boom generated by an aircraft at supersonic speed. To develop a design that meets these requirements, high-quality and fast computational tools are needed to model this phenomenon [1].

An integrated approach is considered to be the optimal approach for modeling this phenomenon. In the near zone of the disturbed flow region behind a moving aircraft, the three-dimensional problem of a supersonic air flow around a model is usually solved. In the far zone, the quasilinear problem of propagation of a one-dimensional profile of perturbed pressure is solved using the augmented Burgers equation [2] in the following form:

$$\frac{\partial p}{\partial x} = \frac{\beta}{2\rho_0 c_0^3}\frac{\partial p^2}{\partial t`} - \frac{1}{2A}\frac{\partial A}{\partial x}p + \frac{1}{2\rho_0 c_0}\frac{\partial(\rho_0 c_0)}{\partial x}p + \frac{\delta}{2c_0^3}\frac{\partial^2 p}{\partial t`^2} + \sum_j \frac{(\Delta c)_j \tau_j}{c_0^2}\left(1+\tau_j\frac{\partial}{\partial t`}\right)^{-1}\frac{\partial^2 p}{\partial t`^2},$$

where $p(x,t')$ – pressure, x – curvilinear coordinate along the wave propagation ray, A – ray tube area, $t' = t - \int_0^x \frac{1}{c_0}\mathrm{d}x$ – retarded time, c_0 – equilibrium speed of sound, ρ_0 – ambient density, β – nonlinearity coefficient, δ – sound diffusion coefficient due to both viscosity and thermal conductivity. This equation takes into account such important properties of the medium as nonlinearity, atmospheric stratification, dissipative and dispersion effects. The splitting method allows sequentially solving the system of equations.

In the process of developing a computational tool for modeling the propagation of a disturbed pressure profile in an inhomogeneous atmosphere, oscillations in the areas of pressure shocks were observed in the calculation results. These features arose when solving the hyperbolic quasilinear transport equation, which describes the nonlinear propagation of small amplitude waves:

$$\frac{\partial p}{\partial x} = \frac{\beta}{2\rho_0 c_0^3}\frac{\partial p^2}{\partial t}. \qquad (1)$$

To solve it, the predictor-corrector scheme [3] was used, which is conditionally stable and conservative. Also, for comparison, we used the explicit and conditionally stable CABARE scheme [4] specified on a compact spatial template.

The propagation of the perturbed pressure profile in the far zone was simulated taking into account all the previously described effects. This profile was calculated in the near zone of a disturbed flow in a flow around a model with a complex structure. Two previously described methods for solving equation (1) were used. The obtained results were analyzed for the occurrence of oscillations.

The research was carried out within the state assignment of Ministry of Science and Higher Education of the Russian Federation (project No. 121030900260-6).

REFERENCES

1. **Chernyshov S.L.** Sonic Boom. Moscow: Nauka, 2011.
2. **Cleveland R.O.** Propagation of sonic booms through a real, stratified atmosphere : PhD thesis / The University of Texas at Austin, 1995.
3. **Khakimzyanov G.S., Cherny S.G.** Computational Methods: textbook : in 4 parts. Novosibirsk, 2008.
4. **Zyuzina N.A., Kovyrkina O.A., Ostapenko V.V.** On the monotonicity of the CABARET scheme approximating a scalar conservation law with alternating characteristic field // Matem. Mod. 2018. Vol. 30, No. 5. P. 76–98.

DOI: 10.53954/9785604788967_141

STEADY AND PULSATING FLOW NEAR END-TO-SIDE PROXIMAL ANASTOMOSIS OF FEMORAL ARTERY

V.M. Molochnikov[1], A.B. Mazo[2], A.N. Mikheev[1], E.I. Kalinin[2], M.A. Kluev[1], O.A. Dushina[1]

[1]*FRC Kazan Scientific Center of RAS*
420111, Kazan, Russia

[2]*Kazan Federal University*
420111, Kazan, Russia

Flows in branching channels are often encountered in power engineering facilities of various purposes. Besides, such channels are inherent in the human cardiovascular system. In this area, the research, among other directions, aims at prolongation of the lifetime of grafts that bypass the artery lesions. The post-surgery period is often complicated by intimal hyperplasia, which is the growth of the inner layer of the vascular graft in the area of its attachment to the artery (anastomosis). These processes are largely associated with hemodynamics. Femoral popliteal arteries most often need recovery of the blood flow. Hemodynamics in these arteries exhibits, among other factors, the flow rate reversal during a portion of the pulsation period. The region of intimal growth is often attributed to low skin friction and its high gradient. Local separation regions formed in the anastomosis area can result in flow turbulization at lower Reynolds numbers than in smooth channels. Its consequences in terms of the distributions of skin friction and other parameters have not been studied extensively. The present research comprises an experimental study and direct numerical simulation (DNS) of flow in the region of channel branching that models the end-to-side proximal anastomosis. Two types of flow are examined: constant flow rate and flow rate with a pulsation period typical of blood flow in the human popliteal artery [1]. Different Reynolds numbers and ratios of flow rates in the main channel and the side channel (graft) are considered.

The experimental setup is described in detail in [2]. It provided high amplitude of pulsation, reproduced the flow reversal during a fraction of pulsation period and guaranteed stability of the required flow rate pattern. The test section of the experimental setup simulated the proximal part of the end-to-side anastomosis (Fig. 1). It was made of transparent polycarbonate pipes with the inner diameter d = 17 mm; H = 150 mm. Water solution of glycerin was used as a fluid (mass fraction 51.7%). Two Reynolds numbers were considered: Re = 200 and 1500. The flow rate ratios were Q_1/Q = 0, 0.25, 0.5, and 0.75. The experiments included flow visualization and SIV measurements of instantaneous vector fields of velocity. DNS was carried out using ANSYS Fluent 19.4 software (finite volume technique with SIMPLE scheme for time and space discretization of the second order of accuracy). Three-dimensional Navier – Stokes equations were solved in non-dimensional natural variables. A structured grid with non-structured insertions in the flow branching region was employed. The total number of grid cells was 500,000 (Re = 200) or 2,000,000 (Re = 1500). The minimal linear cell size in wall-normal direction was 0.007. The time step was 0.01. Special procedure was employed for simulation of flow reversal in pulsating flows.

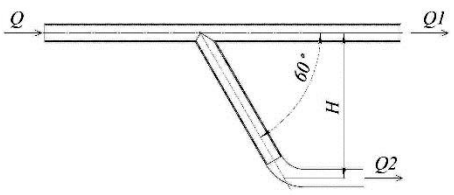

Fig. 1. Schematic of the test section.

At Q = const, essentially non-uniform flow due to flow separation was observed in the main channel (artery) and the side channel (graft). The transverse size of the separation regions

reduced with the increase in the flow rate share passing through the main channel. At Re = 200, the flow in the branching area was steady and laminar. The shear layers at the boundaries of the separation regions were stable. At Re = 1500, the onset of shear layer instability was documented at the boundaries of the separation regions. In this case, flow turbulization was observed at all the considered flow rate ratios, except for $Q_2/Q = 0.75$. Large-scale vortices regularly shed by the main flow were formed at the boundaries of the separation regions. The amplitude of flow velocity fluctuation in these regions increased up to 100% of the mean velocity (Fig. 2). The mixing layer length in the main channel was demonstrated to grow with the increase in the flow rate passing through this channel; the maximum fluctuation intensity in the mixing layer was attained at the mixing layer length of approximately 1.4 of the channel diameter. According to DNS, the lowest skin friction coefficient in steady flows was localized in the flow separation regions: (1.2 – 1.4)*d* from the vertex of acute angle in the main channel, and approximately *d* in the graft.

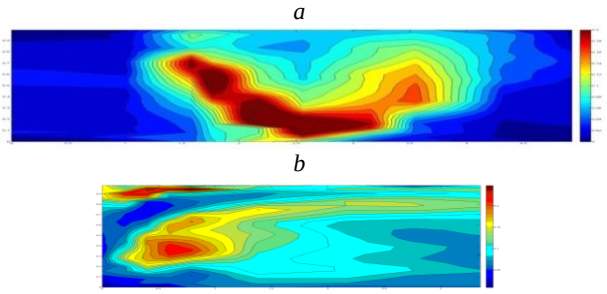

Fig. 2. Fluctuation fields of streamwise velocity component in the main channel (*a*) and side channel *(b*) in steady flows at Re = 1500.

Pulsating and steady flows exhibited different structure in the branching region even when the instantaneous Re in the pulsating flow was the same as Re in the steady flow. The size of the separation region changed significantly with the phase of forced flow rate pulsation. During flow rate reversal, the separation region in the graft disappeared. Instead, it was formed at the closest to bifurcation wall of the main channel. The average position of lowest friction zones changed accordingly. The flow in the mixing layer was intermittent for two reasons: variation of the transverse size of the separation regions with the pulsation phase and formation of large-scale vortices in the mixing layer during the acceleration phase. The level of turbulent fluctuation in both channels became approximately 1.5 – 2 times lower than in steady flows.

The study was financially supported by the Russian Science Foundation (project No. 20-61-47068) (scientific results) and government assignment for FRC Kazan Scientific Center of RAS (project No. FMEG-2021-0001) (testing of SIV technique).

REFERENCES

1. **Klein W.M. et al.** Magnetic resonance imaging measurement of blood volume flow in peripheral arteries in healthy subjects // Journal of Vascular Surgery. 2003b. Vol. 38, Iss. 5. P. 1060–1066. DOI: 10.1016/s0741-5214(03)00706-7.
2. **Molochnikov V.M., Mikheev N.I., Mikheev A.N., Paereliy A.A., Goltsman A.E.** Investigating a pulsating flow in the smooth channel and at the bifurcation section with regard to the popliteal artery hemodynamics // Journal of Physics: Conference Series. 2021. Vol. 2119. Art. 012020. (6 p.). DOI:10.1088/1742-6596/2119/1/012020.

DOI: 10.53954/9785604788967_143

NUMERICAL INVESTIGATION OF THE COMPRESSIBLE BOUNDARY LAYER STABILITY ON CONES WITH A CONCAVE SURFACE OF DIFFERENT CONFIGURATIONS

S.O. Morozov

Khristianovich Institute of Theoretical and Applied Mechanics SB RAS
Novosibirsk 630090, Russia

The investigation of compressible boundary layer stability on a concave surface is an urgent task [1]. The most appropriate configuration of the model for experimental studies of Görtler vortices at Mach numbers greater than 5 is in the form of a cone with a concave surface [1]. The aim of this work is a numerical investigation of compressible boundary layer stability on cones with a concave surface with various geometric parameters (Fig. 1).

The numerical simulation of the boundary layer is carried out for the free-stream parameters that correspond to Tranzit-M wind tunnel: Mach number M_∞ = 5.8, Reynolds number $Re_{1\infty} = 4.3 \cdot 10^6$ m^{-1}. For experimental studies of Görtler vortices, it is necessary to create a model on which Görtler vortices grow faster than the first and second Mack modes. For this purpose, the boundary layer stability is calculated on models with different control parameters (see Fig. 1): straight cone length – L_1, straight cone half-angle – a, angle between the tangent at the beginning of the concave surface and the axis – b, radius of curvature – R. Boundary layer separation may occur on the concave surface of the model. Numerical simulations have shown that, for given flow parameters, separation occurs at $R < 500$ and at the value of the transition angle from the straight to the concave part $a + b > 20$.

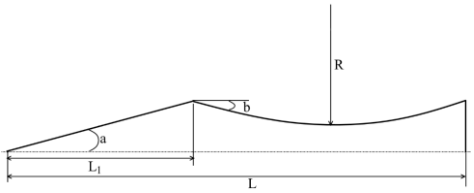

Fig. 1. Schematic of the model.

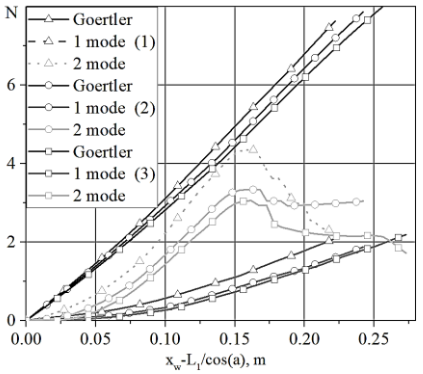

Fig. 2. Disturbances maximum N-factor on the model concave part vs. streamwise coordinate of a model.

1 – L_1 = 0,3 m; R = 0,7 m; a = 5°; b = 2°;
2 – L_1 = 0,15 m; R = 0,7 m; a = 10°; b = 4°;
3 – L_1 = 0,1 m; R = 0,7 m; a = 16°; b = 4°.

In the absence of boundary layer separation on a concave surface, Görtler vortices grow the faster, the smaller the surface curvature radius R. The influence of the straight part of the model on disturbances maximum N-factors on a concave surface with a radius of curvature R = 0.7 m is shown in Fig. 2. Maximum N-factors of Görtler vortices, first and second Mack modes decrease with an increase in the angle a. The difference between Görtler vortices N-factors and the second mode increases with increasing a. Thus, for the experimental study of Görtler vortices, the model with L_1 = 0.1 m; R = 0.7 m; a = 16°; b = 4° will be used.

The research was supported by the Russian Science Foundation (project No. 21-19-00393).

REFERENCE

1. **Gimon T.A., Lukashevich S.V., Morozov S.O., Shiplyuk A.N.** Methods for experimental study of the görtler instability in boundary layers (review) // Thermophysics and Aeromechanics. 2022. Vol. 29, No. 2. P. 159–173.

DOI: 10.53954/9785604788967_144

EXPERIMENTAL INVESTIGATION OF THE FLOW IN A GAS-VORTEX BIOREACTOR

I.V. Naumov, B.R. Sharifullin, S.G. Skripkin, M.A. Tsoy

Kutateladze Institute of Thermophysics SB RAS
630090, Novosibirsk, Russia

In technical applications, vortex mixing is a common method for intensifying mass transfer processes. In swirl combustors, swirl cells stabilize the flame and reduce harmful emissions. In chemical gas and biological two-fluid reactors, the organization of vortex motion contributes to the mixing of ingredients, which increases the yield of a useful product [1].

In many vortex devices, the interaction of a rotating working fluid with a free boundary of another fluid or air is allowed, for example, when the reactor is partially filled with a working medium. So relatively recently, the attention of researchers was attracted by two-fluid rotating flows in connection with the development of vortex aerated bioreactors [2]. The excellent characteristics of the gas-vortex bioreactor compared to traditional apparatus are explained by the use of a fundamentally new mixing method using a concentrated air vortex generated by an activator installed under the bioreactor lid above the surface of the culture medium. The mixing of the medium is carried out by creating in it a three-dimensional motion of the type of a "rotating vortex ring" – a quasi-stationary flow with an axial counterflow generated by an aerating gas vortex due to the pressure drop over the surface and the friction force of the air flow on the liquid surface. The absence of a mechanical mixing element in the liquid ensures energy-efficient (0.06-0.1W/l), soft and efficient mixing of liquids, including viscous ones, without foaming and cavitation, water hammer, highly turbulent and stagnant zones, and microzones with high temperature [2].

A convenient model of a vortex reactor is a vertical cylindrical container (see the figure), where the movement of the filling fluid is generated through an intermediate liquid or gaseous

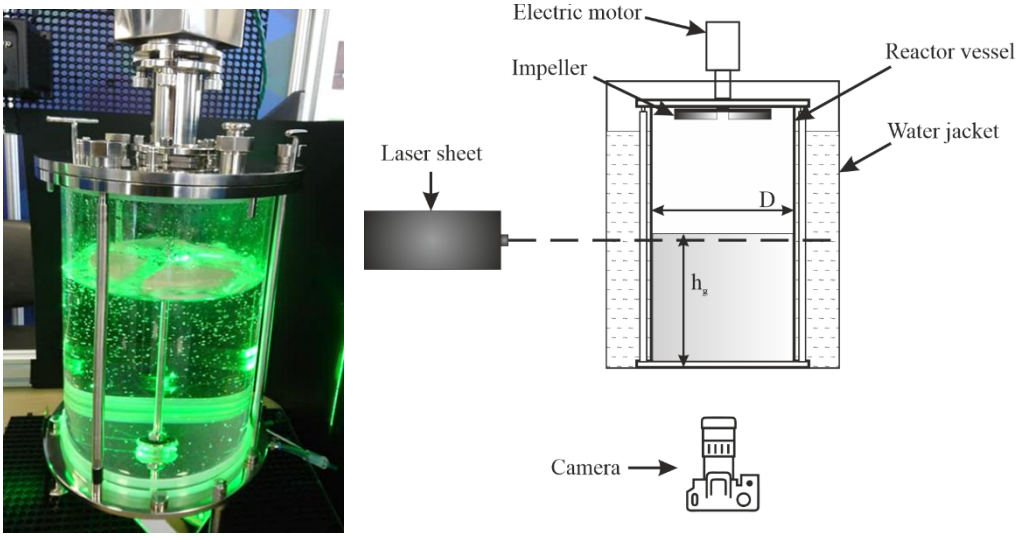

a *b*

Experimental setup.
a – gas-vortex bioreactor, *b* – scheme of the setup.

medium by rotation of one of the end disks [3, 4]. It was found that the flow topology doesn't depend on the properties of the medium (liquid or gas) at the free boundary that limits the circulation of the working fluid and the location of the disk that generates the vortex structure [5, 6].

In this work, we studied the regularities of the vortex motion of the culture medium in the glass gas-liquid bioreactor "GV FBI 10-I", with a volume of 10 liters and a diameter of the reactor vessel D = 190 mm, with its minimum filling (50%) and by continuously adding a model medium to the maximum filling (80%). A 65% water solution of glycerol was used as a model medium (density ρ = 1150 kg/m^3 and kinematic viscosity ν = 15 mm^2/s). To observe the pattern of vortex motion, the methods of digital tracer visualization and adaptive track visualization were used [5, 6].

The regularities of the vortex motion of the culture medium were determined depending on its volume and the intensity of rotation of the activator that generates the swirling motion in the air. The aerating gas interacts with the liquid only through the free surface. As a result, the intensification of interfacial mass transfer is ensured due to the high velocity of the aerating gas.

In the course of the conducted studies, it was found that, similarly to the case of two immiscible liquids, an ascending paraxial jet is formed near the axis of the gas-vortex bioreactor and the circulation movement of the working fluid is realized. It is shown that, as in the case of two-fluid systems, in a two-phase air-liquid system, the radial velocity slips to the interfaces. In this case, despite the difference in density by more than three orders of magnitude, the spiral air flow descending towards the reactor axis forms a divergent vortex motion of the model liquid medium. The results obtained are of interest for the further development of vortex devices and reactors that provide complex vortex motion of ingredients and optimization of the operation of existing plants.

The work was supported by the Russian Science Foundation (№ 19-19-00083).

REFERENCES

1. **Shtern V.** Cellular Flows. Topological Metamorphoses in Fluid Mechanics. New York: Cambridge University Press, 2018. 573 p.
2. **Mertvetsov N.P., Ramazanov Yu.A., Repkov A.P., Dudarev A.N., Kislykh V.I.** Gas-vortex bioreactors "BIOK": Use in modern biotechnology. Novosibirsk: Nauka, 2002. 117 p.
3. **Shtern V.N., Naumov I.V.** Swirl-decay mechanism generating counterflows and cells in vortex motion // J. Eng. Thermophysics. 2021. Vol. 30, No. 1. P. 19–39.
4. **Naumov I.V., Kashkarova M.V., Okulov V.L., Mikkelsen R.F.** The structure of the confined swirling flow under different phase boundary conditions at the fixed end of the cylinder // Thermophysics and Aeromechanics. 2020. Vol. 27, No 1. P. 89–94.
5. **Naumov I.V., Sharifullin B.R., Tsoy M.A., Shtern V.N.** Dual vortex breakdown in a two-fluid confined flow // Physics of Fluids. 2020. Vol. 32, No. 6. Art. 061706. 5 p. DOI:10.1063/5.0012156
6. **Naumov I.V., Skripkin S.G., Shtern V.N.** Counter flow slip in a two-fluid whirlpool // Physics of Fluids. 2021. Vol. 33, No. 6. 061705.

DOI: 10.53954/9785604788967_146

EXPERIMENTAL STUDY OF THE VISCOUS LIQUID ATOMIZATION BY SUPERSONIC UNDEREXPANDED GAS JET

A.Yu. Nesterov, V.M. Boiko, S.V. Poplavski

Khristianovich Institute of Theoretical and Applied Mechanics SB RAS
630090, Novosibirsk, Russia

Devices for liquid spraying, or atomizers, have wide applications in different technologies: they are applied for firefighting, irrigation and dispersing of chemicals into plants, in chemical and food industries, in engines, burners and furnaces, and many other industrial branches. All variety of nozzle designs can be divided into a few types according to the mechanisms of liquid spraying, one of these classes are pneumatic nozzles. In these devices liquid breaks by a high-velocity gas flow, which allows to generate a fine spray in a wide range of jet outflow parameters, also it has some technological advantages over other atomizer types. Among the large variety of pneumatic nozzle constructions coaxial injector can be distinguished, where the liquid jet is supplied into the gas flow to the nozzle cutoff through a central pipe. Although the practical application of these atomizers is limited, they are widely used for the exploring the mechanisms of gas-liquid flows forming (for example, [1]).

The widest applications of pneumatic atomizers can be found in the tasks of high-viscosity liquid spraying (for example, atomization of dyes), because the gas flow allows to form fine-sprayed jet in this case. With increasing the viscosity of liquid phase the growth of gas pressure also becomes relevant, it leads to necessity of the liquid breakup by supersonic gas jets from a certain viscosity threshold [2]. Using the supersonic jets is accompanied by forming the shock structures in the gas jet, it can radically changes the mechanisms of drop formation. Also the existence of dispersed phase in the jet changing its structure: experiments with water revealed that the Mach disk of the underexpanded jet changes into a cone-shaped shock with increasing of drops concentration [3], some minor changes of the jet geometry were also shown.

Atomization of liquids with small and high viscosities is clearly different, so the task of determining the changes caused by viscosity increases and describing this process compared with the water dispersing arises. The aim of this work is experimental investigation of gas-liquid jet of coaxial injector with supersonic gas flow forming the underexpanded jet, special attention is paid to the changes of shock structure in the two-phase region and its influence on the parameters of two-phase core.

The work was carried out on the “Gas-liquid stand” setup of ITAM SB RAS, which allows to perform the complex exploring the gas-liquid jets of pneumatic nozzles in a wide range of outflow parameters (gas and liquid pressures at the nozzle inlet is up to 8 atm). The nozzle represents confusor channel of gas supply with inlet diameter of 19 mm and outlet – 14 mm, with a central tube with inner diameter of 2 mm and outer – 3 mm, located in the middle of the gas channel. As the liquid we use water-glycerol mixture with the viscosity of 50 cSt, which corresponds to the average viscosity of oil. The data were obtained by a complex of optical methods of diagnostics for gas-liquid jets consisting of shadow method and AVT-visualization [4], laser knife, Malvern Spraytec spray analyzer and LDA prototype with direct spectral analysis [5]. Data from this complex of methods is sufficient for complete describing the outflow processes and defining all main parameters of the jet [6].

Investigation of the supersonic gas-liquid jets of glycerol mixture shows a fundamental similarity of the jet outflow pattern with the water jet: conical shock is also emerges instead of

Mach disk. However, bigger mass of droplets of the mixture leads to forming the drops cloud at a considerable distance from the shock, which demonstrates gas-dynamic nature of its forming processes. In other features, the structure of the jet outflow is similar to the water jet, and the supersonic breakup allows to generate the spray of satisfactory dispersity in the wide range of liquid flow rates.

The investigation was carried out in the framework of the Program of the Fundamental Scientific Research of the state academies of sciences in 2021-2023 (project No. 121030500158-0).

REFERENCES

1. **Lasheras J.C., Villermaux E., Hopfinger E.J.** Break-up and atomization of a round water jet by a high-speed annular air jet // Journal of Fluid Mechanics. 1998. Vol. 357. P. 351–379.
2. **Andryushkin A. Yu.** Liquid spraying by the supersonic gas-dynamic technique // Constructions from the composite materials. 2011. No. 3. P. 5–27.
3. **Poplavski S.V., Nesterov A.Yu.** On the near wake structure of a supersonic coaxial gas-liquid jet // Journal of Physics: Conference Series. 2019. Vol. 1404. Art. 012038. 6 p. doi.org/10.1088/1742-6596/1404/1/012038.
4. **Boiko V.M., Orishich A.M., Pavlov A.A., Pikalov V.V.** Methods of optical diagnostics in aerophysical experiments. Novosibirsk, 2009. 450 p.
5. **Poplavski S.V., Nesterov A.Yu., Boiko V.M.** Development and application of the laser Doppler anemometer with direct spectral analysis for studying high-velocity multiphase flows // Thermophysics and aeromechanics. 2020. Vol. 27, № 4. P. 555–563.
6. **Boiko V.M., Nesterov A.Yu., Poplavski S.V.** Liquid atomization in a high-speed coaxial gas jet // Thermophysics and aeromechanics. 2019. Vol. 26, № 3. P. 385–398.

DOI: 10.53954/9785604788967_148

PARAMETRIC IDENTIFICATION OF FLOW AND TEMPERATURE TRANSDUCER OF LIQUID AND AIR IN PIPELINES

V.N. Nikolaev

Chaplygin Siberian Aeronautical Research Institute
630051, Novosibirsk, Russia

Investigation and diagnostics of the technical condition of the hydraulic system or the air conditioning system of an aircraft requires the measurements results of the flow and temperature of liquid and air in pipelines. These parameters vary over a wide range, and the processes of their change are unsteady.

This paper considers the issues of optimal synthesis of the measuring system, including the primary and secondary transducers of liquid and air in the pipelines, which contribute to solving these problems.

The secondary transducer of flow and temperature of liquid and air in pipelines is a system for automatic regulation of the temperature of the pipeline in certain sections of it, carried out by changing the electric current in the heater. In general, the regulation law for the secondary transducer can be represented as

$$\frac{dI}{dt} = k_1 \Delta T_{set} - k_1 \Delta_{1,2} - k_1 k_3 \Delta_{3,2} - k_1 \tau_1 \frac{d\Delta_{1,2}}{dt} - k_1 k_3 \tau_1 \frac{d^2 \Delta_{3,2}}{dt^2}, \quad (1)$$

where I is the electric current in the heater; k_1, τ_1 are constant coefficients.

When developing a secondary transducer, a difficult task is to determine the optimal values k_1 and τ_1, which can be obtained using the well-known methods of the automatic control systems theory.

For this purpose, the paper proposes an experimental and theoretical method for determining the parameters of the system under consideration k_1 and τ_1 leading to the problem of estimating the vector of parameters

$$\Theta = [\vartheta_1, \vartheta_2]^T = [k_1, \tau_1]^T$$

of the transducer mathematical model.

The transducer mathematical model is described by the equation (1), where

$$\frac{d\Delta_{1,2}}{dt} = \frac{AW_{tb}}{\tau_2} e^{-mx_1} - \frac{1}{\tau_2}\Delta_{1,2};$$

$$\frac{d^2\Delta_{3,2}}{dt^2} = \frac{Ae^{-mx_3}W_{tb}}{\tau_3 \tau_4} - \frac{\tau_3 + \tau_4}{\tau_3 \tau_4}\frac{d\Delta_{3,2}}{dt} - \frac{\Delta_{3,2}}{\tau_3 \tau_4}; \quad (2)$$

$$A = \frac{(e^{mL} - e^{-mL})}{4\pi d_{tb} L \lambda_{tb} l_{tb} m^2};$$

$$W_{tb} = I^2 R_{wrm} - k_\alpha \Delta\alpha_{tb};$$

$$U_{ex} = I R_{wrm}.$$

In equations (2) k_2, k_α, τ_2, τ_3, τ_4 are constant coefficients; U_{ex} — heater output voltage; R_{wrm} — heater resistance; $\Delta\alpha_{tb}$ — change in the coefficient of parametric identification of heat transfer α_{tb}.

The equation (1) is an ordinary differential equation, which in general form can be written as follows:

$$Y_t = F(Y(t,\Theta)), t \in (0,t_t);\ Y_t = Y_\Theta, F, Y \in R^S;\ \Theta \in R^r, \tag{3}$$

where $Y = [\Delta U_{ex}]^T$ is the parameter vector of the compartments thermal state; Y_t is the vector of the first derivatives Y with respect to t; $\Theta = [\upsilon_1, \upsilon_2]^T$ is the vector of model coefficients; T is the superscript denoting the transposition operation.

To solve equations (3), it is proposed to use the following second-order approximation Rosenbrock-type numerical scheme for non-autonomous systems [1]:

The inverse problem solution, that is, the estimation of the Θ model coefficients, reduces to minimization of the discrepancy squares weighted sum between the values $\vec{Y}$ given according to the accepted criterion and the corresponding values of $\vec{Y}(t,\Theta)$, obtained during the calculations by the model equations:

$$\Phi(\Theta) = \sum_{k=1}^{N} (\vec{Y}_k - \vec{Y}_k(t_k,\Theta))^T (\vec{Y}_k - \vec{Y}_k(t_k,\Theta)), \tag{4}$$

where t_k are time points at $k = 1,...,N$.

As was noted in [2], to minimize the function (4), it is advisable to use the composition of the steepest descent method, the quasi-Newton method of Broyden – Fletcher – Goldfarb – Shanno, and the Newton method,

The model parametric identification results (1) according to the proposed method have the following values

$$\Theta = \left(0.6;\ 6.6\right)^T.$$

Determination of the parameter estimates uncertainty Θ will be carried out according to the method described in [3]. It is based on the construction and analysis of the estimation error covariance matrix.

A thermoconvective transducer of flow and temperature of liquid and air in pipelines has been developed. The optimal synthesis of the measuring system has been carried out, which makes it possible to increase the operating speed and reduce the sensitivity to changes in the thermal conductivity of the pipeline walls. The direct problem was solved by the Rosenbrock-type numerical scheme of the second order approximation for non-autonomous systems. When solving the inverse problem, an algorithm for the composition of the steepest descent, quasi-Newton and coordinate methods was used. In the quasi-Newton method, the Hessian matrix of the second partial derivatives is estimated using the Broyden – Fletcher – Goldfarb – Shanno formula.

REFERENCES

1. **Artemiev S.S., Demidov G.V., Novikov E.A.** Minimization of ravine functions by the numerical method for the stiff sets of equations solving. Novosibirsk. 1980, 13 p. (Preprint / Computational Center of the Siberian Branch of the USSR Academy of Sciences; No. 74).
2. **Nikolayev V.N., Gusev S.A., Makhotkin O.A.** Mathematical model of the convective radiant heat exchange of the blown heat-insulated unpressurized compartment of the aircraft // Aircraft strength. Strength analysis of the airframe elements: Scientific and technical collected volume. Iss. 1. Novosibirsk: SibNIA, 1996. P. 98–108.
3. **Himmelblau D.** Applied nonlinear programming. New York: McGraw-Hill 1972, 498 p. [in Russian: Иммельблау Д.М. Прикладное нелинейное программирование / Пер. с англ.; под ред. М.Л. Быховского. М.: Мир, 1975. 534 с.]

DOI: 10.53954/9785604788967_150

MATHEMATICAL MODEL OF FLOW IN A MIXED-TYPE AEROSOL FILTER FROM NANO- AND MICROFIBERS

E.R. Panina, R.F. Mardanov, S.K. Zaripov

Kazan Federal University
420008, Kazan, Russia

A mathematical model of fluid flow in a mixed filter consisting of various nano- and microfibers has been developed. The results of experimental studies of the mixed aerosol filter are presented in [1], where it is shown that the combination of the advantages of the efficient capture of aerosol particles and the low aerodynamic drag of nanofibers and the controlled uniformity of microfibers allows mixed filters to provide a higher overall filter quality factor compared to filters with monodisperse fibrous filters.

In this work, we propose a new mathematical model for the flow of an incompressible fluid in a porous medium, consisting of cylinders of various diameters in the range of nano- and micrometers, to study the characteristics of a mixed filter. A rectangular periodic cell with one microfiber and n_f nanofibers is taken as the flow domain. The mass fraction of nanofibers γ_n is defined as the ratio of the mass m_{nf} of nanofibers to the sum of the mass m_{nf} of nanofibers and the mass m_{mf} of microfibers

$$\gamma_n = \frac{m_{nf}}{m_{nf}+m_{mf}} = \frac{n_f}{n_f+a^2},$$

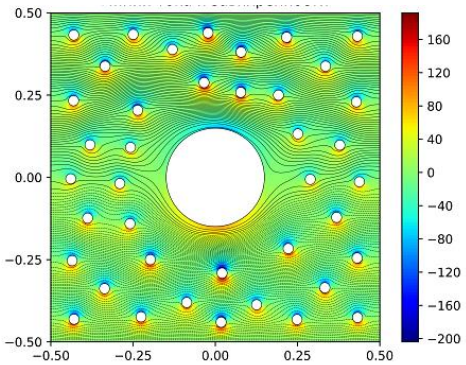

Streamlines and flow vorticity.

where $a = r_{mf}/r_{nf}, r_{nf}$, r_{mf} are the radii of nano- and microfibers.

The flow of the carrier medium is described in the approximation of the Stokes flow of a viscous fluid with no-slip boundary conditions for microfibers and slip conditions for nanofibers. The numerical method of boundary elements is applied [2]. The fluid flow and the pressure drop in the periodic cell depend on the parameter γ_n, the filter density α and the filtration rate. The streamlines and distributions of the flow vorticity at $\gamma_n = 0.1$ are shown in the figure. The developed model is used to calculate the pressure drop in the cell and the efficiency of deposition of aerosol particles.

The study was supported by the Russian Science Foundation grant No. 22-21-00176, https://rscf.ru/project/22-21-00176/

REFERENCES

1. **Choi H.J., Kumita M., Hayashi S., Yuasa H., Kamiyama M., Seto T., Tsai C.J., Otani Y.** Filtration properties of nanofiber/microfiber mixed filter and prediction of its performance // Aerosol Air Qual. Res. 2017. Vol. 17, No 4 P. 1052–1062.
2. **Mardanov R.F., Dunnett S.J., Zaripov S.K.** Modeling of fluid flow in periodic cell with porous cylinder using a boundary element method // Engineering Analysis with Boundary Elements. 2016. Vol. 68. P. 54–62.

DOI: 10.53954/9785604788967_151

INVESTIGATION OF THE INFLUENCE OF MANEUVERING CONTROL GEARS ON THE FLOW STRUCTURE AROUND A TRAPEZOIDAL UAV MODEL

A.M. Pavlenko, B.Yu. Zanin, V.S. Kaprilevskaya, N.S. Alpatskiy, E.A. Melnik

Khristianovich Institute of Theoretical and Applied Mechanics SB RAS
630090, Novosibirsk, Russia

Currently there is a high rate of development of unmanned vehicles for various purposes around the world. A special place among these types of aircraft is occupied by small-sized unmanned aerial vehicles (UAVs) used not only for military purposes but also for solving civilian problems [1–3]. Therefore, a wide variety of UAVs resulted in a rapid increase of the competition level for improved flight characteristics allowing carrying out tasks that are more complex. Thus, it became necessary to pay attention to improving the flow around when designing aircraft. The basis for this is the knowledge of the physical processes that occur during the interaction of the UAV with the surrounding air. The presented investigation is devoted to the experimental study of the influence of the maneuvering control gears (elevons) on the flow structure near the surface of the trapezoidal UAV model (Fig. 1, *a*). This work is continuation of the cycle of studies devoted to the research of separated flows and the possibilities of controlling the flow around various layouts of UAV models [4–6]. The relevance of this area of research is out of question.

Several series of experiments were carried out under different flow regimes in the test section of the T-324 wind tunnel of the Khristianovich Institute of Theoretical and Applied Mechanics SB RAS (ITAM SB RAS, Novosibirsk). The level of incoming flow turbulence for this wind tunnel does not exceed 0.04%. Dimensions of the working part 1000 × 1000 × 4000 mm. The UAV model was installed in the working part at angles of attack in the range from 0° to 20° and slip angle in the range from 0° to 30°. The free flow velocity varied from 15 to 25 m/s. The deflection angle of the elevons changed in the range from –30° to +30°. The geometrical dimensions of the model used in the experiments are comparable with the dimensions of real UAV (the span of the model is 750 mm; the maximum chord is 500 mm). Experiments were carried out for Reynolds number ranged from 4 to 6.3 × 10^5. This corresponds to the natural Reynolds numbers at which real flights of small-sized UAVs are carried out. Hot-wire anemometry and oil film technique were used to obtain experimental data.

In the aftermath of the experiments visualization pictures were obtained and the flow topology was constructed for each flow regime described above (Fig. 1, *b*). The influence of the angle of maneuvering control gears on the flow structure was studied. Also the effect for differ-

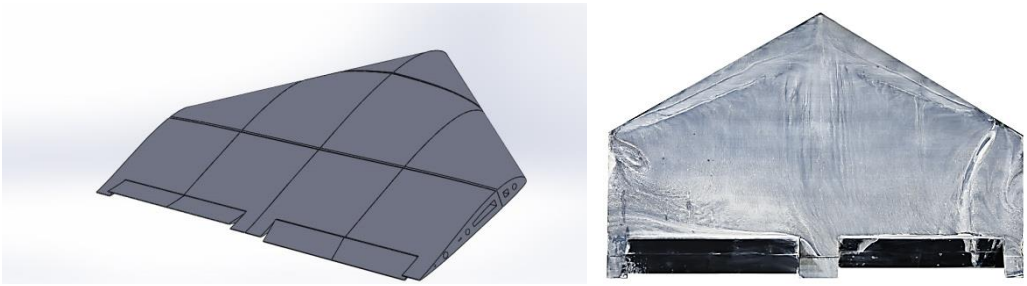

a *b*

Fig. 1. Three-dimensional image of the trapezoidal model of the UAV (*a*) and visualization of the flow under local impact at an angle of attack α = 16° and free flow velocity U_∞ = 15 m/s (*b*).

ent geometric dimensions of elevons was investigated. The distributions of the mean velocity profiles and velocity fluctuation profiles along the model chord were obtained at angles of attack of 0° and 5° and elevons deflection angles of –30°, 0° and +30°. Curves of pulsation growth and spectra for each regime were constructed. Quantitative data were obtained on the laminar-turbulent transition near the surface of the model and its relationship with the formation of local flow separation zones at angles of attack of 0 and 5°, free flow velocity of 15 m/s and various positions of elevons. It was found that on this type of UAV layout the laminar-turbulent transition mechanism is similar to the transition mechanism on a straight wing. In addition, it was shown that with the increase of the angle of attack, the transition region shifts towards leading edge. The level of fluctuations in the transition region reaches 20% of U_∞ at zero deflection angle of elevons and at the angle of attack of 0°. Deflection of the elevons results in a decrease in the level of pulsations approximately from 3 to 6% compared to a case without deflection. Increasing the angle of attack to 5° also resulted in decrease of the maximum level of pulsation by approximately 5% with zero elevon deflection. However, the deflection of the elevons by an angle of +30° at given angle of attack led to increase in the level of disturbances up to 20% of U_∞. The performed spectral analysis made it possible to determine the exact position of the region of transition to turbulence for each flow regime. From frequency distribution of pulsations, frequency ranges at which the laminar-turbulent transition occurs were determined. Results obtained are fully correlated with the data received by oil film technique.

The search for the possibilities of flow control using the influence in local points was made. The sources of disturbances were conical bump and air blowing/suction. The place of maximum flow susceptibility was found on the upper surface of the model. The possibility of changing the flow structure by this method is shown.

The study was supported by the Russian Science Foundation grant № 22-29-00309, https://rscf.ru/en/project/22-29-00309/

REFERENCES

1. **Zverkov I.D., Krukov A.V., Grek G.R.** Prospects of studies in region of low-sized aircraft (review) // Vestnik of NSU. 2014. 9(2). P. 95–115. In Russian.
2. **Singhal G., Bansod B., Mathew L.** Unmanned Aerial Vehicle Classification, Applications and Challenges: A Review // Preprints. 2018. 2018110601. DOI: 10.20944/preprints201811.0601.v1.
3. **Stewart M. P., Martin S. T.** Unmanned aerial vehicles: fundamentals, components, mechanics, and regulations. Chapter 1 // Barrera. Unmanned aerial vehicles / Ed. N. Hauppauge. NY: Nova Science Publishers. 2021. 70 p.
4. **Pavlenko A.M., Zanin B.Yu., Katasonov M.M.** Flow around a small-sized UAV model in a turbulent trace // Proc. of 19 Int. Conf. on the Methods of Aerophys. Research (ICMAR2018): AIP Conference Proceedings. 2018. Vol. 2027. Art. 040004. 7 p. doi.org/10.1063/1.5065278.
5. **Pavlenko A.M., Zanin B.Yu., Bykov A.V., Katasonov M.M.** Flow around the wing models with straight and swept leading edge in case of contact with turbulent wake // Journal of Physics: Conference Series : XXXV Siberian Thermophysical Seminar (Novosibirsk, August 27–29, 2019). S.l. IOP Publishing, 2019. Vol. 1382. Art. 012030. 6 p. DOI: 10.1088/1742-6596/1382/1/012030.
6. **Pavlenko A.M., Bykov A.V., Zanin B.Yu.** The influence of external disturbances on the flow around the model of a small-sized UAV // Proc. of the 27 Conference on High-Energy Processes in Condensed Matter: AIP Conference Proceedings. 2020. Vol. 2288. Art. 030018. 9 p. DOI: 10.1063/5.0028716.

DOI: 10.53954/9785604788967_153

MATHEMATICAL MODELING OF ETHANE-METHANE MIXTURES IN LASER REACTORS

E.E. Peskova, V.N. Snytnikov

Federal Research Center Boreskov Institute of Catalysis
630090, Novosibirsk, Russia

The development of laser technology for the conversion of methane-ethane mixtures into valuable products with the production of hydrogen, ethylene and acetylene is a promising and little-studied branch of the development of modern gas chemistry. CO_2 lasers are best suited for use, its radiation is effectively absorbed by ethylene. The gas mixture temperature rises in the zone of absorption of laser radiation. Active radicals are formed there, its superequilibrium substance promotes a significant increase target products yield. The gas-dynamic flow of hydrocarbons in laser reactors is characterized by the formation of a big number of mixture components with a large difference in molecular weight and, therefore, thermal conductivity and diffusion. Such flows with radical chain reactions and intense energy exchange require detailed investigation to achieve maximum target products yields for the initial gas mixture composition.

The development of high-performance computing and numerical methods allow to simulate reactive multicomponent gases, taking into account sharp local changes in temperature, density, velocity, diffusion, and mixture composition. The article presents a computational algorithm for investigation of ethane-methane mixtures conversion in axisymmetric laser reactors.

The mathematical model is described by the system of Navier – Stokes equations in low Mach number limit [1] for the case of axisymmetric flow and multicomponent gas [2]. Accounting for the energy introduced by means of laser radiation is included in the enthalpy form of the energy equation using the term, which is responsible for the intensity of laser radiation. The radical scheme of high-temperature methane conversion is used to describe chemical transformations.

The discrete model is built on the uniform grid of rectangles. The splitting procedure for physical processes is used for constructing a computational algorithm. The split has proven itself well in modeling the processes of ethane and propane pyrolysis [3]. This approach includes separation of one time step integration into the following blocks: solving the equations of chemical kinetics, solving the equation for the radiation intensity, solving the equations of dynamics of a viscous diffusion heat-conducting gas, solving an elliptic-type equation for the dynamic pressure component.

The time integration step in problems with radical reactions is determined by the fastest stage from the kinetic scheme. It is much less than the gas-dynamic step. The chemical kinetics system is solved separately from the Navier – Stokes equations to avoid this fact. We use the RADAU5 package at this work [4], which showed good convergence in our problems.

The initial equations are approximated in terms of spatial variables using the finite volume method for solving the Navier – Stokes equations. The Lax – Friedrichs flow functions are used to calculate the numerical flow in the convective terms of the equations, the primitive terms are approximated using schemes of the WENO type. The function of the numerical flow at the boundary between elements in the diffusion terms of the Navier – Stokes equations is calculated as a half-sum. The coefficients of viscosity, diffusion and thermal conductivity is determined taking into account each component of the mixture's one.

The radiation absorption coefficient takes into account the nonlinear dependence on the radiation intensity [5]. The RADAU5 package [4] is also used for the numerical solution of the nonlinear differential equation of transfer and absorption of laser radiation.

Fig. 1. Temperature and ethylene mass fraction distribution.

The problem is arises for an elliptic-type equation with a variable coefficient for correcting pressure and correcting the velocity vector when solving the Navier – Stokes equations in low Mach numbers limit. The resulting systems of equations are integrated using the Jacobi method, taking into account rapid convergence for small pressure changes in the computational area.

The previously described algorithm was implemented to solve problems in a flat geometric region. It has been successfully validated on the problems of ethane and propane pyrolysis [3].

This article is devoted to modeling the effect of laser radiation on ethane-methane mixtures in a cylindrical pipe, taking into account the external heating of the pipe. The distributions of the main components of the mixture were obtained under various reaction conditions (different wall temperatures and radiation power). The figure shows that the temperature reached inside the flow (Fig. 1, left) stimulates the conversion of hydrocarbons at the area of radiation absorption. The maximum concentrations of target products (ethylene, hydrogen, acetylene) are observed in the central part of the reactor (Fig. 1, right). This indicates the possibility of designing laser reactors for obtaining valuable products with decreased weight and size characteristics.

REFERENCES

1. **Day M.S., Bell J.B.** Numerical simulation of laminar reacting flows with complex chemistry // Combustion Theory and Modelling. 2000. Vol. 4. Iss. 4. P. 535–556.
2. **Peskova E.E.** Numerical modeling of subsonic axisymmetric reacting gas flows // Journal of Physics: Conference Series. 2021. Vol. 2057. Art. 012071. DOI:10.1088/1742-6596/2057/1/012071.
3. **Gubaydullin I.M., Zhalnin R.V., Masyagin V.F., Peskova E.E., Tishkin V.F.** Simulation of propane pyrolysis in a flow-through chemical reactor under constant external heating // Mathematical models and computer simulations. 2021. Vol. 13. № 3. C. 437–444.
4. **Hairer** and Wanner Solving Ordinary Differential Equations. Stiff and Difderential-Algebraic Problems. 2nd edition. Springer Series in Comput. Math. 1996. Vol. 14.
5. **Snytnikov Vl.N., Snytnikov V.N., Masyuk N.S., Markelova T.V.** The Absorption of CO2 Laser Radiation by Ethylene in Mixtures with Methane // Journal of Quantitative Spectroscopy and Radiative Transfer. 2020. Vol. 253. Art. 107119. 6 p.

DOI: 10.53954/9785604788967_155

FRACTURE OF SOLIDS AS A THERMODYNAMIC PROCESS

M.G. Petrov

Aeronautical Research Institute n. a. S. A. Chaplygin
630051, Novosibirsk, Russia

There are many approaches and methods for determining the load-bearing capacity of structures depending on the loading character and temperature, though each of these approaches and methods is applicable only in a limited range of operation conditions. The problem is difficult because the basis of the problem solution, i.e., the material itself, is ignored. The above problems cannot be solved without constructing new models of continuous media on the basis of physics and thermodynamics of internal processes that occur in loaded solids.

The processing of experimental data on the durability and creep rate at constant stresses and temperatures, called thermal activation analysis, involves the construction of dependencies

$$U(\sigma) = U_0 - \gamma\sigma \in RT\ln(\tau\nu_0) \text{ and } Q(\sigma) = Q_0 - \alpha\sigma \in RT\ln(\dot{\varepsilon}_0 / \dot{\varepsilon}_p),$$

which called the force dependences of the activation energy of fracture (AEF) and deformation (AED) and are straight lines, if the structure of the material does not undergo significant changes. Here R is the universal gas constant, $\nu_0 = 1/\tau_0 = 10^{13}\ \text{s}^{-1}$ is characteristic Debye frequency [1]. The coefficients γ and α, which depend on the structure of the material, called the activation volume, characterize the values of internal stresses in the so-called fracture centers. A typical relationship between deformation and fracture is illustrated in Fig. 1. And the temperature-force dependences of the steady-state creep rate are a mirror image of similar dependences of durability [2].

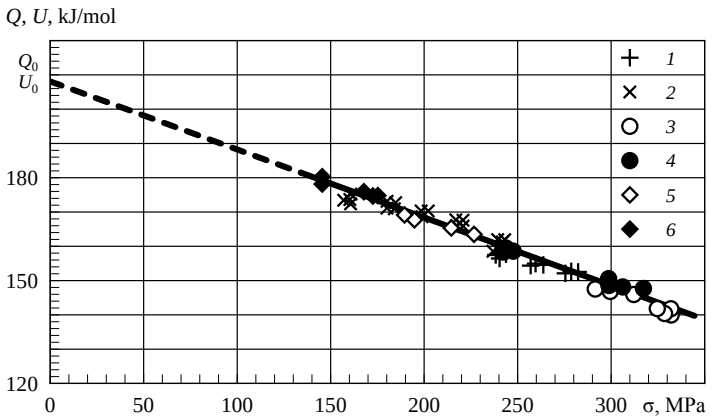

Fig. 1. Force dependence of AEF and AED of specimens of 1201 T1 alloy tested at constant temperatures and loads.
T, K: *1* – 398, *2* – 433 (creep rate); *3* – 398, *4* – 433, *5* – 448, *6* – 473 (durability).

New models describing their plastic flow have been introduced into the rheology of materials [3]. In material models, instead of viscous flow bodies N (Newton body), plastic flow bodies Zh (Zhurkov body) and Km (Kauzmann body) are used. Figure 2 shows a one-dimensional structural model of the material, describing both its general flow (creep) and local plastic strains distributed over the volume of the material, varying over time and associated with fatigue failure. Here $A = \varepsilon_* \nu_0 \exp(-Q_0 / RT)$ and $B = \alpha / RT$, M is elasticity module of Hooke's body.

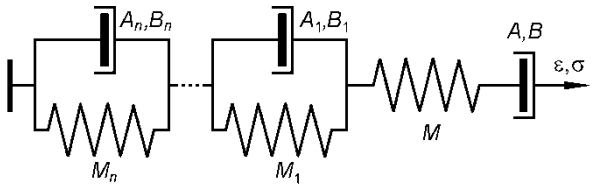

Fig. 2. Structural model of a material with sequential and parallel connection of elastic bodies (Hooke's bodies) and plastic flow bodies (Zhurkov's or Kauzmann's bodies).

Having the realization of temperature-force loading conditions, it is possible to calculate any arbitrary process by time steps [4]. Damage according to the mathematical model of the material is calculated independently from its structural elements. This is evidenced by indirect data obtained in the fatigue tests of specimens that cut from an aircraft wing panel after 25,000 hours of operation.

The approach outlined here, unlike the others currently in use, relies on a single conceptual framework: the notions of what a solid is and why it failures. Any material is an atomic-molecular system in thermal motion, and fracture occurs as a result of anharmonicity and stochasticity of the process of thermal vibrations of atoms in a solid body [1]. It follows that fracture is due to the internal energy of the solid, the measure of which is temperature [1, 4]. External effects only change the failure rate of a solid if they change its internal energy (thermal energy, electromagnetic radiation, chemical reactions).

The proposed methodology for predicting the durability of materials in structures shows that a unified approach and reproduction in mathematical models of the processes of their failure and deformation as thermodynamic, allows us to solve those problems that have not yet been solved by fracture mechanics. Only for special cases, acceptable solutions are obtained.

From the standpoint of thermodynamics, if it is possible to obtain solutions for thermocyclic loading or thermal fatigue of a material in calculations, then everything else may be treated as special cases. The difficulty lies not in the calculation algorithms, but in the properties of the material, which are subject to change. The processes of structural changes in the material have other activation parameters, and this becomes clear only from the thermo-dynamical viewpoint. Otherwise, we are doomed to invent Ersatz-theories.

REFERENCES

1. **Petrov V.A., Bashkarev A.Ya., Vettegren V.I.** Physical foundations for predicting the durability of structural materials. St Petersburg, 1993. 475 p. (in Russian).
2. **Stepanov V.A., Peschanskaya N.N., Shpeizman V.V., Nikonov G.A.** Longevity of solids at complex loading // Intern // J. Fracture. 1975. Vol. 11, No 5. P. 851–867.
3. **Petrov M.G.** Rheological properties of materials from the point of view of physical kinetics // J. of Appl. Mech. and Tech. Phys. 1998. Vol. 39, No 1. P. 104–112.
4. **Petrov M.G.** Investigation of the longevity of materials on the basis of the kinetic concept of fracture // J. of Appl. Mech. and Tech. Phys. 2021. Vol. 62, No 1. P. 145–156.

DOI: 10.53954/9785604788967_157

ON THE STUDY OF LAMINAR-TURBULENT TRANSITION IN THE LONGITUDINAL VORTICES REGION IN SUPERSONIC BOUNDARY LAYER OF A FLAT PLATE

M.V. Piterimova, A.D. Kosinov, N.V. Semionov, A.A. Yatskikh, V.L. Kocharin, Yu.G. Yermolaev

Khristianovich Institute of Theoretical and Applied Mechanics SB RAS
630090, Novosibirsk, Russia

Until recently, studies of the laminar-turbulent transition were carried out mainly at subsonic flow velocities [1, 2]. The paper [3] presents experimental and theoretical study aimed at describing the non-modal growth of stationary longitudinal (vortex) periodic in span streaks, generated by roughness elements in the boundary layer of a flat plate. The generation of stationary longitudinal vortex disturbances by *N*-wave from two-dimensional irregularities was studied theoretically in [4, 5]. The authors have shown that the perturbation generated by the leading edge of the *N*-wave leads to a shift in the position of the beginning of the laminar-turbulent transition upstream. In this case, the perturbation from the trailing edge of the *N*-wave does not affect the position of the beginning of the transition. Experiments [6, 7] made it possible to start research on the effect of longitudinal stationary vortices on the laminar-turbulent transition in the supersonic boundary layer of a flat plate. However, the experimental data [7] showed that the transient decay was not achieved in the measurements. The results of experimental studies similar to [7] and estimation of the transition Reynolds numbers obtained by measurements in the region of longitudinal vortices are presented in this paper.

Experimental set up. The experiments were conducted in the T-325 supersonic wind tunnel of ITAM SB RAS at Mach number 2. A detailed description of the T-325 setup and the experimental setup are given in [7]. The model of a flat plate with blunted leading edge was used in the experiments. A schematic representation of the experimental set up and a photo of the test chamber with the installed model are shown in Fig. 1,*a* and *b*, respectively. Weak shock waves were generated using an adhesive tape 2.5 mm wide, 130 μm thick, and about 150 mm long (2D in Fig. 1,*a*). The measurements were made with a constant temperature hot-wire anemometer.

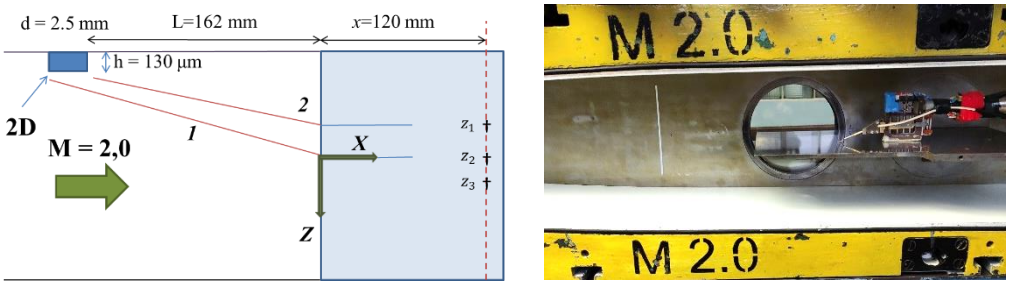

a *b*

Fig. 1. Experimental set up (*a*) and a photo of a flat plate model and a generator of weak shock waves in the test chamber of the T-325 (*b*).

The measurements were carried out in the boundary layer of the model in the cross section x = 120 mm in the region of the vortices generated by wave 2 (Z_1 = –8 mm) and wave 1 (Z_2 = 4.2 mm), away from the vortices (Z_3 =2 0 mm).

Results. Figure 2 illustrates the results of the measurements in the region of vortices generated by weak shock waves (curve *1* – measurements at Z_1, curve *2* – measurements at Z_2) and measurements away from vortices (curve *3* – measurements at Z_3). The results are presented as a dependence of the mass flow pulsations root-mean-square amplitude on Reynolds number

along the longitudinal coordinate x (Re_x). It is shown that the growth of amplitude of disturbances generated by wave 2 (see Fig. 1,*a*) starts from $\mathrm{Re}_x \approx 1.3\times10^6$, and the growth of disturbances generated by wave 1 starts from $\mathrm{Re}_x \approx 1.6\times10^6$. Reynolds numbers $\mathrm{Re}_x \approx 1.5\times10^6$ and $\mathrm{Re}_x \approx 2\times10^6$ respectively correspond to the position of laminar-turbulent transition. For measurements conducted away from the vortices area, the transient decay was not reached in these experiments.

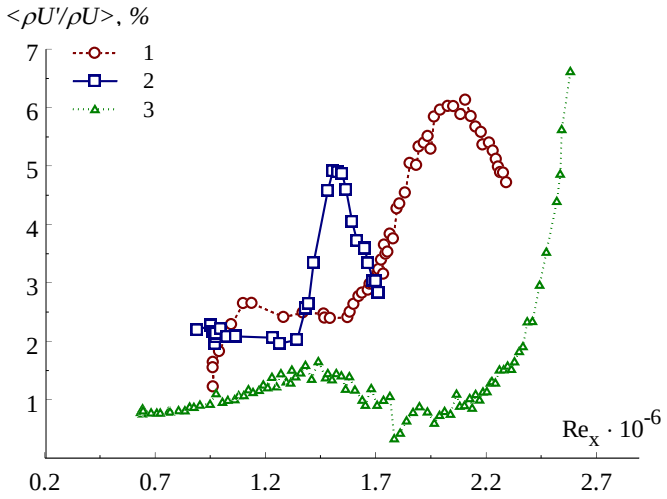

Fig. 2. The dependence of the root-mean-square amplitude of mass flow pulsations on Re_x. Measurements at Z_1 (*1*), Z_2 (*2*), Z_3 (*3*).

Conclusion. An experimental study of longitudinal vortices influence on the laminar-turbulent transition in supersonic boundary layer of a blunted flat plate was carried out. It is found that the transition in the region of the vortices generated by the leading and trailing edges of *N*-wave occurs at different Reynolds numbers: $\mathrm{Re}_x \approx 2\times10^6$ and $\mathrm{Re}_x \approx 1.5\times10^6$ respectively.

The research was carried out within the state assignment of Ministry of Science and Higher Education of the Russian Federation (project No. 121030500161-0). The study was conducted at the Equipment Sharing Center “Mechanics” of ITAM SB RAS.

REFERENCES

1. **Boiko A.V., Grek G.R., Dovgal A.V., Kozlov V.V.** The emergence of turbulence in near-wall flows. Novosibirsk: Nauka, 1999. (in Russian).
2. **Matsubara M., Alfredsson P.H.** Disturbance growth in boundary layers subjected to free stream turbulence // J. Fluid Mech. 2001. Vol. 430. P. 149–168.
3. **Fransson J.H.M., Brandt L., Talamelli A., Cossu C.** Experimental and theoretical investigation of the nonmodal growth of steady streaks in a flat plate boundary layer // Physics of Fluids. 2004. Vol. 16. P. 3627.
4. **Din Q.H., Egorov I.V., Fedorov A.V.** Interaction of Mach waves and boundary layer at a supersonic flow over a plate with a sharp leading edge // TsAGI Science Journal. 2017. Vol. 48, № 4. P. 317–329.
5. **Din Q.H., Egorov I.V., Fedorov A.V.** Mach wave effect on laminar-turbulent transition in supersonic flow over a flat plate // Fluid Dynamics. 2018. Vol. 53, No. 5. P. 690–701.
6. **Kosinov A.D., Yatskikh A.A., Yermolaev Yu.G., Semionov N.V., Kolosov G.L., Piterimova M.V.** On mechanisms of the action of weak shock waves on laminar-turbulent transition in supersonic boundary layer // Proc. of the XXV Conf. on High-Energy Processes in Condensed Matter (HEPCM 2017) (Novosibirsk, Russia 5–9 June 2017): AIP Conference Proceedings. 2017. Vol. 1893. Art. 030072. 8 p. https://doi.org/10.1063/1.5007530.
7. **Piterimova M.V., Yatskikh A.A., Kosinov A.D., Semionov N.V., Yermolaev Yu.G.** Experimental study of the impact of weak shock waves on the laminar-turbulent transition in the supersonic boundary layer of a flat plate // Problems of Mechanics: Theory, Experiment and New Technologies: Abstracts of the XIII All-Russian Conference of Young Scientists (Novosibirsk – Sheregesh, March 15–22, 2019). Novosibirsk, 2019. P. 130–131. (in Russian).

DOI: 10.53954/9785604788967_159

RESULTS OF FLIGHT EXPERIMENTS ON THE DETECTION OF A SEPARATED FLOW BY UNSTEADY SENSORS ON UAVs

P.A. Polivanov, V. Markin, V.A. Kislovsky, A.A. Sidorenko

Khristianovich Institute of Theoretical and Applied Mechanics SB RAS
630090, Novosibirsk, Russia

Small unmanned aerial vehicles (UAV) often fly in a turbulent environments, in urban areas and etc. These conditions are characterized by the presence of gusts of wind, which can lead to the UAV reaching critical angles of attack and the beginning of the flow separation. Therefore the issue of detecting of the flow separation on UAV wings based on the readings of any sensors becomes of great importance. In papers [1, 2] the issues of the applicability of microphones and high-frequency pressure sensors to determine flow separation on a small UAV in wind tunnel were studied. The purpose of this work is to test the possibility of detecting a separated flow by unsteady pressure sensors and microphones in a flight experiment.

The UAV model ZOHD Nano Talon Evo (Fig. 1) was chosen for this research. The dimensions of this UAV made it possible to carry out tests in the T-503 NSTU wind tunnel. This made it possible to compare the results of flight experiments and wind tunnel tests. The data acquisition system was based on two arduino compatible microcontrollers. The first arduino Mega2560 Pro was used to record flight telemetry data such as: position of flight control surfaces; readings of the magnetic sensor; pitch and roll angles of UAV; GPS coordinates and ground speed; pitot tube data (airspeed); power of the motor (current and voltage on the motor); barometric altitude.

The second arduino compatible Teensy 4.1 board was used to data quisition from unsteady sensors at a high frequency (up to 10 kHz). Four pressure sensors and three microphone sensors were install into the UAV wing. The pressure sensors were located at a location $X/b = 0.56$ from the leading edge of the wing, and $Z/L = \pm 0.23, \pm 0.16$ relative to the plane of symmetry. The microphones were located at a location $X/b = 0.53$ from the leading edge of the wing, and $Z/L = \pm 0.09, 0.025$ relative to the plane of symmetry.

Figure 2 shows the data found during the incipient and recovery of a stall-spin. At the top part of the figure a spectrogram of the pulsations measured by the microphone sensor can be seen. The bottom part of Fig. 2 presents the UAV airspeed and altitude data. The data gap ob-

Fig. 1. Photo of a UAV.

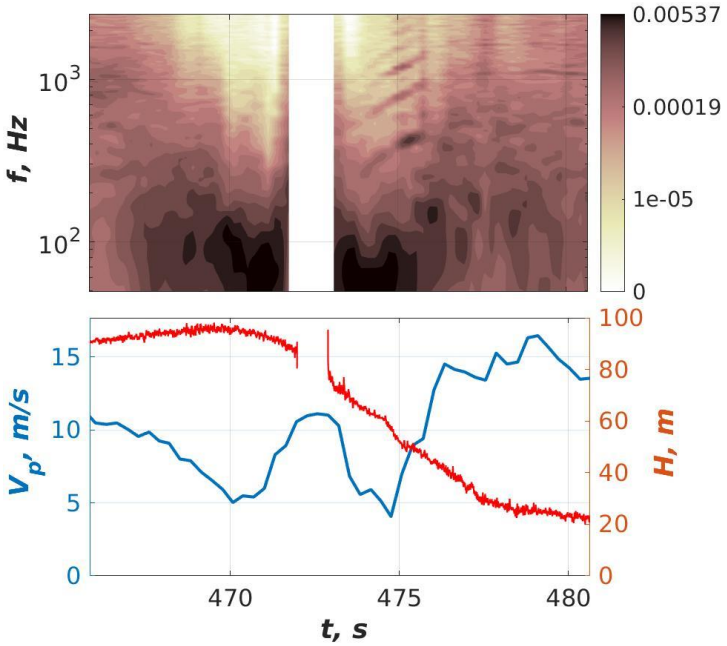

Fig. 2. An example of the spectrogram of pulsations of pressure (top) and distributions of velocity and altitude (bottom) measured during entry and exit from a stall.

served in the figure is explained by the process of saving data from RAM to SD card. During this time data from unsteady sensors are not read. The stall-spin was entered by gradually increasing the pitch angle at the motor off. This led to a drop of the velocity and an increase of the height of the UAV up to 470 seconds. After that there was an incipient into a stall accompanied by a drop of the altitude and an increase of the velocity. After several rotations the recovery was carried out with the transfer of the UAV to horizontal flight (475 second). The spectrogram shows an increase in low-frequency disturbances (less then 200 Hz) 2.5 seconds before the spin (467.5 s). It was shown in [1, 2] that the cause of low-frequency pulsations is flow separation. Accordingly in the flight experiment there is a significant delay between the appearance of flow separation and the start of stall-spin. During a spin the low-frequency pulsations dominate. When recovery of the spin the motor was turned on, which led to the appearance of high-frequency pulsations observed as several arcuate curves on the spectrogram at the time 474–476 s. After the ending of stall the low-frequency pulsations decay.

Experimental data demonstrate the possibility of detecting the occurrence of a separated flow in flight by analyzing the information from unsteady sensors. This data can improve UAV flight safety.

The work was supported by grant of RSF 20-49-08006. The study was conducted at the Joint Access Center “Mechanics” of ITAM SB RAS.

REFERENCES

1. **Polivanov P.A., Sidorenko A.A.** Determining the flow separation near a small UAV by unsteady pressure sensors // Journal of Physics: Conference Series: 6 All-Russian Conference on Thermophysics and Physical Hydrodynamics (Sevastopol, August 22–29, 2021). 2021. Vol. 2057, No. 1: Art. 012008 (6 p.) IOP Publishing. DOI:10.1088/1742-6596/2057/1/012008
2. **Polivanov P.A., Sidorenko A.A.** Problems of detection of flow separation by pressure sensors on unmanned aerial vehicles with a propeller // Letters to the Journal of Technical Physics. 2022. Vol. 48, No. 3. P. 40–43. DOI: 10.21883/PJTF.2022.03.51982.18946 (in Russian)

DOI: 10.53954/9785604788967_161

ON ANALYTICAL SOLUTION OF THE BOUNDARY-LAYER EQUATION FOR NONLINEAR DILATANT FLUID ON A PLATE WITH SUCTION-INJECTION

A.N. Popkov

Khristianovich Institute of Theoretical and Applied Mechanics SB RAS
630090, Novosibirsk, Russia

In fluid mechanics, exact analytical solutions offer a more penetrating insight into the physics of flows, and they play an important part in verification of numerical methods. In the boundary-layer theory, a finite number of such solutions are known, whose derivation and classification was given by Rosenhead.

Boundary layers in non-Newtonian fluids are governed by rather complex partial equations whose form depends on the rheological model adopted for the flow. In some cases, such equations can be rendered into the form of nonlinear ordinary differential equations with automodel solutions. Such solutions can be obtained by various numerical methods. Interestingly, in one of the particular cases such a solution can be obtained in closed form, in elementary analytical functions.

Indeed, if the non-Newtonian fluid obeys a power rheological law, then for the stationary flow over a semi-infinite plate in the particular case of $n = 2$ (dilatant fluid) the boundary-layer equation assumes the form [1]

$$|F''|F''' + FF'' = 0.$$

Here, $F' = U/U_\infty$ is the dimensionless velocity. If the velocity-profile derivative F'' is non-negative, then the starting equation separates into two linear ordinary differential equations [2],

$$F'''(y) = 0, \quad (1) \quad \text{and} \quad F'''(y) + F(y) = 0, \quad (2)$$

with boundary conditions $F(0) = A;\ F'(0) = 0$ and

$$\lim F'(y \to \infty) = 1. \quad (3).$$

The parameter A = const defines the transfer of mass on the plate surface, so that at $A < 0$ and at $A > 0$ we deal respectively with fluid injection and fluid suction through the surface.

Equation (1) governs the flow in unperturbed stream, equation (2) governs the near-wall viscous flow; this equation has the well-known solution [3]:

$$F(y) = C_1 e^{-y} + e^{-\frac{y}{2}}[C_2 \cos(\beta) + C_3 \sin(\beta)], \qquad \beta = \left(\sqrt{3}\right) * \frac{y}{2}.$$

The two solutions are to be matched together at some minimal value of y, $y = y_{\min}$. The value of $y_{\min}$ can be found from boundary condition (3), which yields $F'(y = y_{\min}) = 1$, and from an additional condition $F''(y = y_{\min}) = 0$.

All in all, for the four unknown variables, C_1, C_2, C_3, and y_{mm}, we have a nonlinear algebraic system whose solution defines the analytical solution in elementary functions to the boundary-layer equation for non-Newtonian fluid in the particular case under consideration.

1. For zero mass transfer on the plate surface, $A = 0$, we have the following simple relations between the constants:

$$C_2 = -C_1; \quad C_3 = \sqrt{3}\, C_1; \quad F''(0) = 3C_1.$$

The constant C_t is to be determined from the equation $C_1 = 2e^{-a}/(2\sqrt{3}\times \sin(\beta_{\min}) - 3e^{-3a})$; $(\beta_{\min} = \sqrt{3}\times y_{\min}/2\,;\ a = y_{\min}/2)$ using the value of $y_{\min}$; in turn, the latter value

can be found from the equation [2]: $e^{3a} + 2\times\cos(\beta_{\min}) = 0$. As a result, we obtain: $y_{\min}$ =1.83244 and $F''(0)$ = 0.7264677. The numerical values of $y_{\min}$ and $F''(0)$ obtained by direct numerical integration of the differential equations are y_{mm} = 1.8 and $F''(0)$ = 0.7265, [1].

2. Given the mass transfer on the plate surface, a system of nonlinear algebraic equations is obtained to determine the unknown constants C_1, C_2, C_3, $y_{\min}$ at different parameter values A corresponding to suction ($A > 0$) or injection ($A < 0$) into the boundary layer through the streamlined surface. By sequential exclusion it was possible to convert the system of four equations to one algebraic equation as regards to $y_{\min}$. The equation is extremely nonlinear, an analytical solution cannot be obtained, so it was solved numerically. The availability of singular points made it very difficult to find physically reasonable values of the roots of the equation $y_{\min}$ at different values of the suction-injection parameter A. The equation is written as:

$$\left\{A\left(2\mu - \frac{\gamma^3}{\sqrt{3}}\right) + \frac{2}{\sqrt{3}}\times\left[\gamma + \sqrt{\left[-(A\mu)^2 + \sqrt{3}A^2\gamma^3\mu + 2A\gamma^4 + \gamma^2 + \frac{A^2\gamma^6}{4}\right]}\ \right]\right\}\times(1-\gamma^6) -$$

$$-\{A + \gamma^4 + (1/\sqrt{3})\times\sqrt{[A^2(4\gamma^6 - 1) + 6A\gamma^4 + 4\gamma^2 - \gamma^8]}\ \}\times\left(2\mu - \gamma^3\sqrt{3}\right) = 0.$$

$$\mu = \sin(\beta_{\min})\,; \qquad \gamma = e^{-a};$$

$$C_1 = \{\ A + \gamma^4 + \sqrt{[(A+\gamma^4)^2 - (4/3)(A^2 - \gamma^2)(1-\gamma^2)]}\ \}/[2(1-\gamma^6)]\ .$$

The results of the calculations are presented in the table:

A	– 0.35	–0.3	– 0.2	– 0.1	0	0.2	0.5	1.0
C_1	–0.05994	–0.00161	0.09010	0.16934	0.24216	0.37635	0.56049	0.84164
$F''(0)$	0.17017	0.295167	0.47029	0.60801	0.72647	0.92904	1.18146	1.52492

The research was carried out within the state assignment of Ministry of Science and Higher Education of the Russian Federation (State Registration Number 121030500158-0).

REFERENCES

1. **Shul'man Z.P., Berkovsky B.M.** Boundary Layer in Non-Newtonian Fluid Flows. Minsk, 1966. 240 p.
2. **Popkov A.N.** Analytical solution of the equation of the boundary-layer of non-newton power-low fluids on the plate // Int. Conf. on the Methods of Aerophys. Research: Abstr. Pt II. Novosibirsk, 2010. P. 203–204.
3. **Kamke E.** Handbook of Ordinary Differential Equations. Moscow: Nauka, 1976. 576 p.

DOI: 10.53954/9785604788967_163

MODELING HEAT TRANSFER IN MICROCHANNELS TAKING INTO ACCOUNT THE SLEEP AND THERMAL CREEP

V.Ya. Rudyak[1,3], A.S. Lobasov[3], A.V. Minakov[2,3]

[1]*Novosibirsk State University of Architecture and Civil Engineering*
630008, Novosibirsk, Russia

[2]*Institute of Thermophysics SB RAS*
630090, Novosibirsk, Russia

[3]*Siberian Federal University,*
660041, Krasnoyarsk, Russia

The rapid implementation of microsystem technology in the last few decades is associated not only with their energy efficiency and low material consumption but also with the fact that in some cases the use of such technology is the only possible. This situation, for example, occurs when creating a new generation of computers, as well as in various biomedical applications. Most of the corresponding microdevices operate using certain fluid flows. One of the dominant research areas in modern microfluidics is developing methods for controlling flows and heat transfer in microchannels. The use of such devices makes it possible to obtain extremely high heat transfer coefficients, a sharp increase in transverse temperature and concentration gradients, reduce the dimensions of the devices, material consumption, etc.

Usually, the flows of liquids and not too rarefied gases can be described by methods of continuum mechanics [1]. From a practical standpoint, it is necessary, on the one hand, to ensure maximum heat transfer, while on the other, to minimize resistance of the microchannel. For this purpose, hydrophobic or even ultrahydrophobic coatings are used (see [2] and the references therein). When modeling, the presence of hydrophobic coatings is taken into account by the fact that slip conditions are set instead of the usual no-slip conditions.

Flow slip on the channel wall occurs, generally speaking, not only due to the presence of a flow velocity gradient near the surface, but in non-isothermal flows, slip is also due to the presence of a temperature gradient along the channel. In addition, in the general case, a temperature jump occurs on the channel wall due to the presence of a temperature gradient across the flow. Thus, the boundary conditions on the channel walls in the general case have the following form [3, 4]

$$u = u_w + k_1\left(\frac{\partial u}{\partial y}\right)_w + k_2\left(\frac{\partial T}{\partial x}\right)_w, \qquad T = T_w + k_3\left(\frac{\partial T}{\partial y}\right)_w. \tag{1}$$

Here u is the fluid velocity, u_w is the channel wall velocity, T is the temperature, the index means the value of the corresponding value on the wall; x, y are the coordinates along and across the channel wall, respectively. Coefficients k_i determine the slip lengths and value of the temperature jump.

The slip conditions (1) are typical for the rarefied gas flows [3]. In microchannels, however, slip on hydrophobic walls also takes place for liquids; moreover, the slip length can reach tens of micrometers. It is quite natural that the presence of slip on the wall significantly reduces the hydraulic resistance. At the same time, it was shown [5] that in isothermal flows, the mixing efficiency in micromixers practically does not change. However the slip effect on heat transfer in the microchannel has still not been practically studied. The purpose of this work is to study the effect of slip and temperature jump (1) on the heat transfer characteristics. The coefficients k_i are assumed to be constants and vary quite widely. The complexity of modeling such non-isothermal flows also lies in the fact that all fluid characteristics also depend on the temperature.

The problem is solved by continuous medium methods. The flows are assumed to be incompressible, and their rheology is Newtonian. The usual non-isothermal Navier – Stokes equations are used to describe the flows, and the energy conservation equation is used to determine the enthalpy. All thermophysical characteristics depend on temperature. This dependence is determined by polynomials of the fourth or fifth degree [6]. The transport equations are solved numerically using the ANSYS Fluent 19 package. It is worth noting that conditions (1) cannot be implemented within this standard package. They were implemented with the help of user–defined functions library. This also made it possible to set temperature-dependent characteristics and vary the coefficients of k_i. The used algorithm was tested on several tasks where either reliable experimental data or proven semi-empirical formulas were known.

It is shown that with an increase in the slip length k_1, the value of the heat flux density increases and may exceed the corresponding value under no-slip conditions by about 40%. As a result, the excess of the average heat transfer coefficient in comparison with the corresponding value during no-slip flow can reach up to 50%. Naturally, the pressure drop significantly reduces, that is, two beneficial effects take place simultaneously.

The presence of a thermal creep (k_2 coefficient) also leads to a decrease in the pressure drop in the channel, but this effect is much less than the effect of the slip length. The average heat transfer coefficient for thermal creep increases almost linearly with an increase in k_2 and its increase reaches 10%. This effect grows with an increase in the degree of heterogeneity of heating of the channel walls.

The existence of a temperature jump on the wall, in contrast to slip, can lead to a certain increase in the pressure drop, however, the heat transfer coefficient increases. It is worth noting that when simulating heat transfer, it is necessary to take into account the change in all thermophysical properties of fluids with temperature in the calculation process. Otherwise, significantly different results will be obtained both quantitatively and qualitatively. For example, at constant thermophysical properties of the fluid, with an increase in the coefficient k_3, a pressure drop in the microchannel does not change, whereas in fact it is growing.

The work was supported by the mega grant of the Ministry of Science and Higher Education of the Russian Federation (Agreement No. 075-15-2021- 575).

REFERENCES

1. **Rudyak V.Ya., Minakov A.V.** Modern problems of micro and nanofluidsics. Novosibirsk, 2016. 298 p.
2. **Huang Q.-Z., Fang Y.-Y., Liu P.-Y., Zhu Y.-Q., Shi J.-F., Xu G.** A novel strategy for durable superhydrophobic coating on glass substrate via using silica chains to fix silica particles // Chem. Phys. Lett. 2018. Vol. 692. P. 33–37.
3. **Gad-el-Hak M.** The fluid mechanics of microdevices: The Freeman scholar lecture // J. Fluids Engineering. 1999. Vol. 121. P. 5–33.
4. **Maxwell C.J.** On stresses in rarefied gasses arising from inadequacies of temperature // Phil. Trans. Roy. Soc. 1987. Vol. 170. P. 231–256.
5. Minakov A., Rudyak V., Dekterev A., Gavrilov A. Investigation of slip boundary conditions in the T-shaped microchannel // Int. J. Heat and Fluid Flow. 2013. Vol. 43. P. 161–169.
6. **NIST** standard reference database number 69. 2022. DOI: https://doi.org/10.18434/T4D303.

DOI: 10.53954/9785604788967_165

TRANSLATIONAL OSCILLATIONS OF A CYLINDER WITH A DISK IN THE AIR FLOW

A.N. Ryabinin, D.V. Kaufman

Saint Petersburg State University
199034, Saint Petersburg, Russia

A disk mounted coaxially at front end of the cylinder significantly reduces drag [1, 2]. In this paper, a cylinder with an elongation $L/D = 9$ is considered. L and D are the length and diameter. Recently [3] we studied the effect of a coaxially mounted disk on the damped rotational vibrations of the cylinder. In this study, translational oscillations were investigated.

The experiments were carried out in the AT-12 wind tunnel of St. Petersburg State University, which has an open test section. Figure 1 shows the scheme of the experiment.

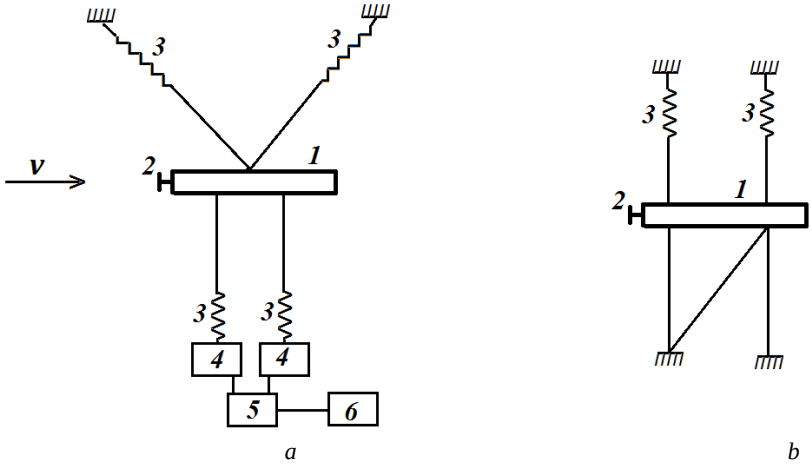

Fig. 1. The scheme of the experiment: side view (*a*) and top view (*b*).
1 – cylinder, *2* – disk, *3* – spring; *4* – strain gauge; *5* – PC oscilloscope; *6* – computer.

The suspension allowed the cylinder to move with two degrees of freedom. The elastic forces of the suspension returned the cylinder to its initial state of equilibrium. Deviated from the equilibrium position, the cylinder could perform translational oscillations, in which its center of gravity oscillated in the vertical direction, and rotational oscillations around the horizontal axis perpendicular to the axis of the cylinder.

The semiconductor strain gauges measured the tension of the lower springs. The voltage at the output of the strain gauges was transferred to the Velleman-PCS500 PC oscilloscope, which converted analog signals into digital ones. The oscilloscope was connected to a computer on which the dependence of signals on time was recorded in a file. During the experiments, the cylinder was deflected from the equilibrium position by a certain distance in the vertical direction, and then released. Oscillations began, then they damped in all experiments. The signal was recorded for 17 seconds. The spring tension values were read at a frequency of 100 Hz.

Calibration of the device was carried out by hanging the known load to the center of the cylinder. At the same time, the cylinder displacement and the change in the readings of the strain gauges were determined. In our experiments, we varied the diameter of the coaxial disk d, the distance between the disk and the end of the cylinder g and the velocity of the incoming flow.

The table shows the values of aerodynamic derivatives. 95% confidence intervals are also given, which are calculated using the t-criterion of the least significant difference [4].

Oscillatory derivatives of the cylinder with a disk

d/D	*g/D*		
	0.45	0.75	0.85
0.625	–3.97 ± 0.14	–4.03 ± 0.14	–4.06 ± 0.14
0.75	–3.52 ± 0.14	–3.69 ± 0.14	–3.63 ± 0.14
1.00	–3.77 ± 0.14	–3.66 ± 0.14	–3.69 ± 0.14

The oscillatory derivative of a cylinder without a disk is equal to -3.73 ± 0.14.

It turned out that a disk coaxially mounted in front of the cylinder end slightly changed the aerodynamic oscillatory derivative of a cylinder without a disk only if its diameter is $d = 0.625D$. The presence of a coaxially mounted disk has a much stronger effect on rotational derivatives [3].

REFERENCES

1. **Koenig K., Roshko A.** An experimental study of geometrical effects on the drag and flow field of two bodies separated by a gap // J. Fluid Mech. 1985. Vol. 156. P. 167–204.
2. **Patent** US No. 3241876 Apparatus for reducing linear and lateral wind resistance in a tractor-trailer combination vehicle / W.S. Saunders. Application number: US34162264A. Filing date: 31.01.1964. Publ. date: 03.22.1966. URL: https://www.freepatentsonline.com/3241876.pdf
3. **Ryabinin A.N., Kaufman D.V.** Determination of rotational derivatives of a cylinder with a coaxially mounted disk in an air stream // Vestnik of Saint Petersburg University. Mathematics. Mechanics. Astronomy. 2021. Vol. 8(66). Iss. 1. P. 158–166.
4. **Seber G.A.F.** Linear regression analysis. N.Y.: John Wiley & Sons, 1977. [Translation into Russian: Moscow: Mir, 1980. 456 p.]

DOI: 10.53954/9785604788967_167

LOCAL AND LARGE-SCALE INSTABILITIES OF VERTICAL THROUGHFLOW IN A TWO-LAYERED AIR-POROUS SYSTEM WITH INTERNAL HEAT SOURCE DEPENDING ON SOLID VOLUME FRACTION

R.V. Sagitov, E.A. Kolchanova

Perm State University
614990, Perm, Russia

The convective instability of a vertical throughflow in a horizontal two-layered system which consists of an air-saturated granulated heat-generating porous sublayer at the bottom and an air sublayer free of the porous matrix at the top is investigated. The volumetric heat source strength is proportional to the solid volume fraction. The system is bounded at the top and bottom by the solid air-permeable planes at which the same temperatures are maintained. Air is uniformly pumped through one plane at a velocity of $\mathbf{U}$ and sucked out through the other plane at the same velocity.

Convection equations within the Boussinesq approximation are applied to describe the air behavior. A two-domain model [1] is applied, where the Navier – Stokes equation in the air sublayer and the Darcy equation in the porous sublayer are used [2]. After introducing the scales for variables, the main control parameters are the ratio d of the air sublayer thickness to that of the porous sublayer, solid volume fraction ϕ, the Peclet number Pe which positive values correspond to the upward throughflow and negative values is for the downward one.

We have found the explicit expressions for temperature in the air sublayer and in the porous medium. The boundary of a potentially unstable region where thermal convection is excited in a heat-generating porous sublayer shifts in the direction of the throughflow. The more intense the throughflow is or the thicker the air sublayer is, the more the boundary shifts.

Depending on the value of control parameters, different types of the convective roll patterns corresponding to distinct minima of the marginal stability curves (Fig. 1) can be most dangerous for the stability of a basic convection-free solution relative to small normal disturbances. The roll patterns are either local short-wave flows which primarily form within the air sublayer or the large-scale long-wave convective flows which cover both sublayers.

It has been found that an increase in the solid volume fraction or thickness of the air sublayer has a destabilizing effect on the basic throughflow (Fig. 2). There is a minimum of the crit-

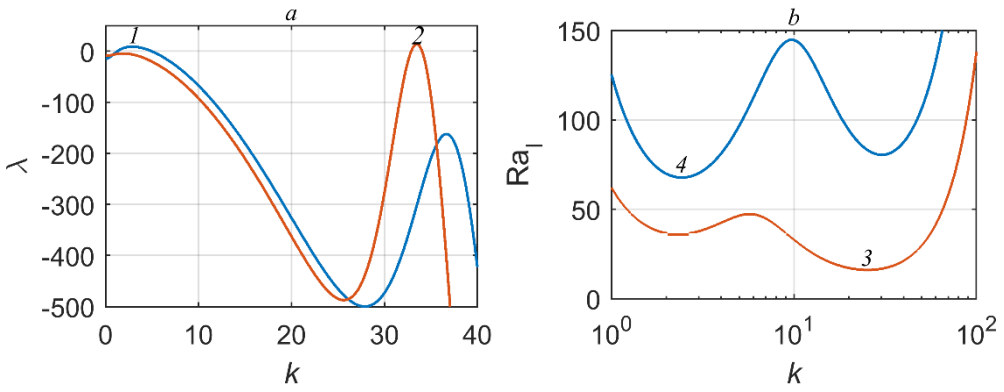

Fig. 1. The increment of disturbances (*a*) and neutral Darcy – Rayleigh number (*b*) versus the wave number at the fixed values of $d = 0.1, \phi = 0.6$.

1 – $\mathrm{Pe} = -6$, $\mathrm{Ra_I} = 101.5$, *2* – $\mathrm{Pe} = -4$, $\mathrm{Ra_I} = 27.56$, *3* – $\mathrm{Pe} = -6$, *4* – $\mathrm{Pe} = -4$.

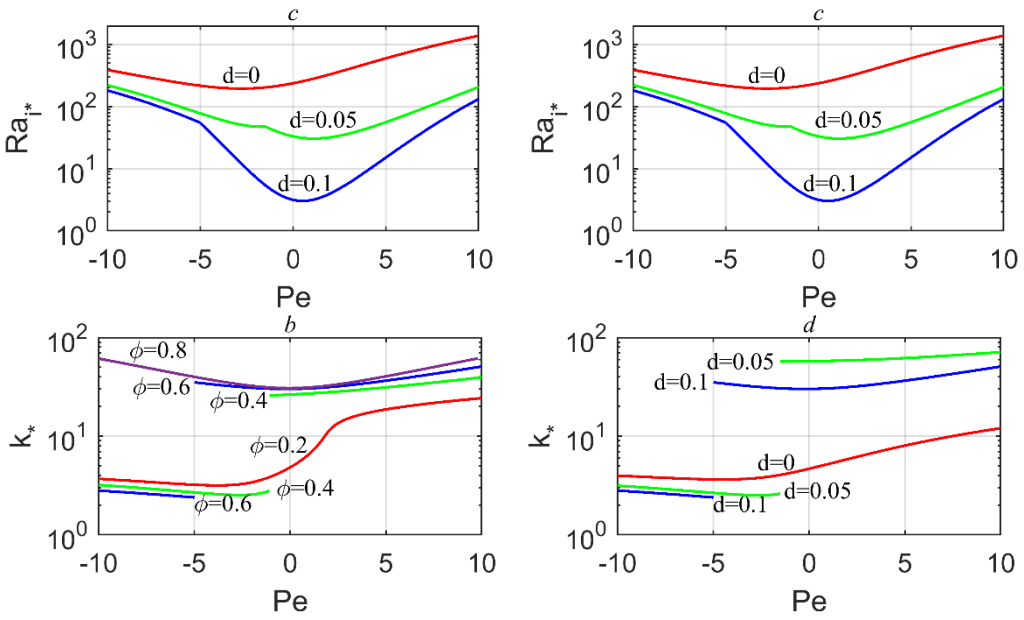

Fig. 2. The critical Darcy – Rayleigh number (*a*, *c*) and the corresponding critical wave number (*b*, *d*) versus the Peclet number.

a, *b* – $d = 0.1$, *c*, *d* – $\phi = 0.6$.

ical Darcy – Rayleigh number versus the Peclet number, which shifts towards the small Peclet numbers as the solid volume fraction or thickness of the air sublayer grows. When the instability is caused by the short-wave disturbances, this minimum is in the region of positive Peclet numbers but when the one is driven by the long-wave disturbances, it is in the region of negative Peclet numbers.

The study of the critical parameters versus the Peclet number at which there is a transition from the local to large-scale convection has shown that in the case of a relatively large solid volume fraction or thickness of the air sublayer the large-scale convection can only realize at a sufficiently strong downward throughflow. The smaller the air sublayer thickness and the solid volume fraction are, the lower the Peclet number is required. If the air sublayer thickness or solid volume fraction is small enough, the large-scale convection can also occur in the case of an upward throughflow. The smaller the air sublayer thickness and the solid volume fraction are, the stronger the flow should be.

The work was supported by the Russian Science Foundation (Grant No. 21-71-10045), https://rscf.ru/en/project/21-71-10045/.

REFERENCES

1. **Kolchanova E., Lyubimov D., Lyubimova T.** The onset and nonlinear regimes of convection in a two-layer system of fluid and porous medium saturated by the fluid // Transport in Porous Media. 2013. Vol. 97, No. 1. P. 25–42.
2. **Nield D.A., Bejan A.** Convection in Porous Media. Springer Int. Publ., 2017. 988 p.

DOI: 10.53954/9785604788967_169

REDUCTION OF CYLINDER RESISTANCE IN THE NEAR-CRITICAL RANGE OF REYNOLDS NUMBERS DUE TO THE BODY INSTALLED UP THE FLOW

S.D. Salenko, A.D. Obukhovsky, Yu.A. Gosteev, I.S. Konovalov

Novosibirsk State Technical University
630073, Novosibirsk, Russia

Reducing the resistance of cylindrical bodies is relevant in solving problems of industrial aerodynamics (wind load on building structures), designing hydraulic machines (load on elements of hydraulic fittings), stability and controllability of aircraft (transportation of various loads on an external sling). In addition, the study of the flow around a cylinder under various conditions has an enduring scientific value.

There are various ways to reduce the drag of a circular cylinder in its transverse flow in the literature. So, for this purpose, turbulators placed on the surface of the body (they work only in the subcritical range of Reynolds numbers) were used. A relatively small body (cylinder, plate, I-shape, etc.) was installed in the vicinity of the cylinder [1–4].

In this work, a corner was chosen as such a body (Fig. 1), since it was expected that it would be in some form of a fairing that favorably changes the flow structure in the vicinity of the cylinder.

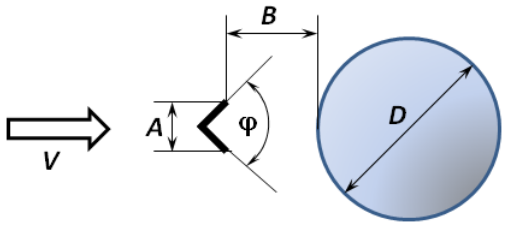

Fig. 1. Fairing installation diagram.

Fig. 2. General view of the experimental setup.

The experiments were carried out in the wind tunnel T-503 (NSTU), which has the following characteristics: flow velocity up to 60 m/s; length of the working part of the tunnel of 2 m, diameter of 1.2 m; non-uniformity of velocity head in the core of the flow with a diameter of 0.8 m, but not more than 0.75%; the degree of flow turbulence without turbulence devices is about 0.3%.

Model dimensions: cylinder diameter of 163 mm, average surface roughness of 1 mm, diameter and thickness of the end washers of 510 mm and 8 mm, respectively.

The general view of the experimental setup is shown in Fig. 2.

The experiments were carried out in the range of Reynolds numbers of $\mathrm{Re} = (1\ldots5)\cdot10^5$. The fairing parameters were varied: relative transverse dimension A/D in the range of 0.103…0.736, and console length B/D in the range of 0…2, as well as the angle φ. In the processing the results of weight tests, corrections were introduced for the resistance of the end plates and the effective elongation of the model.

Experiments have shown that the optimum is the relative transverse fairing size of 0.303 with a relative reach of 0.4 and an angle of $\varphi = 90°$. Figure 3 shows the dependence of the drag

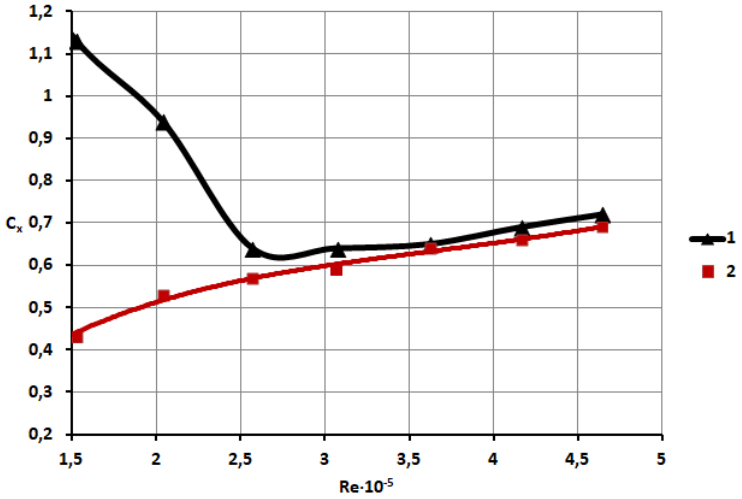

Fig. 3. The dependence of the drag coefficient of the cylinder on the Reynolds number.
1 – without fairing, *2* – with optimal fairing

coefficient of the cylinder on the Reynolds number when installing the optimal fairing in comparison with the case of its absence.

The analysis of the results show that the angle works mainly as a turbulator, significantly reducing the drag coefficient of the cylinder in the subcritical range, and to a small extent as a fairing. A decrease in cylinder resistance by 2.6 times was obtained for the Reynolds number of $Re=1.5\cdot10^5$, with the maximum number in wind tunnel experiments of $Re = 4.64\cdot10^5$.

REFERENCES

1. **Tsutsui T., Igarashi T**. Drag reduction of a circular cylinder in an air-stream // J. Wind Eng. Ind. Aerodyn. 2002. Vol. 90. P. 527–541.
2. **Mahbub A.M., Moriya M., Takai H., Sakamoto H.** Fluctuating fluid forces acting on two circular cylinder in a tandem arrangement at a subcritical Reynolds number // J. Wind Eng. Ind. Aerodyn. 2003. Vol. 91. P. 139–154.
3. **Frolov V.A., Kozlova A.S.** Experimental study of a method of reducing the drag of a circular cylinder by installing a flat plate // Vestnik of Samara University. Aerospace and Mechanical Engineering. 2017. Vol. 16, No. 3. P. 165–172. DOI: 10.18287/2541-7533-2017-16-3-165-172.
4. **Prasad A., Williamson C.H.K.** A method for the reduction of bluff body drag // J. Wind Eng. Ind. Aerodyn. 1997. Vol. 69–71. P. 155–167.

DOI: 10.53954/9785604788967_171

INFLUENCE OF SMALL ANGLES OF ATTACK AND MACH NUMBER ON THE TRANSITION ON A SWEPT WING WITH χ=72°

N.V. Semionov[1], Yu.G. Yermolaev[1], V.L. Kocharin[1], A.D. Kosinov[1, 2], A.N. Semenov[1], S.A. Shipul[1], B.V. Smorodsky[1], A.A. Yatskikh[1, 2]

[1]Khristianovich Institute of Theoretical and Applied Mechanics SB RAS
630090, Novosibirsk, Russia

[2]Novosibirsk State University
630090, Novosibirsk, Russia

Studies of the turbulence occurrence and the development of new engineering methods for transition prediction and the transition control in spatial boundary layers based on the data obtained are the focus of attention of specialists in many countries. Such studies are of practical interest, since these flows are realized around the swept wing of an aircraft. It is known that a small change in the angle of attack on swept wings, as well as on sharp cones, leads to a change in the transition Reynolds numbers [1, 2]. Data on the influence of small angles of attack on the Reynolds numbers of the transition can be of particular value in the development and verification of modern engineering methods for predicting the position of the laminar-turbulent transition, since they are obtained for the same noise conditions in the test section of wind tunnel.

The results of study of the influence of small angles of attack on the evolution of disturbances and the laminar-turbulent transition in a supersonic boundary layer on a swept wing at Mach numbers M = 2 – 4 are presented in the paper. The experiments were carried out in the supersonic low-noise T-325 wind tunnel of the ITAM. The measurements were performed on the model wing with a variable chord length along the wing span (it was 500 mm at the wing root and 200 mm at the wing end). The sweep angle of the leading edge was 72° and that of the trailing edge was 58°. This corresponds to a subsonic leading edge at M = 2, 2.5 and 3 and to a supersonic edge at M = 4. The scheme of the model and the measurement area are presented in [2]. A study of the evolution of disturbances and determination of the position of the laminar-turbulent transition was carried out using a hot-wire anemometer on the upper model surface. In more detail the setting of the experiments and the technique of measurements is described in [1, 2].

The dependences of the transition Reynolds number Re_{tr} versus the angle of attack on the wing model with the sweep angle of the leading edge (χ = 72°) at M = 2 – 4. It is shown that a change in the angle of attack has a strong effect on the transition Reynolds number for all Mach numbers. An increase in the Mach number led to a decrease in the Reynolds number of the transition. It is found that the laminar-turbulent transition in the boundary layer on a wing with a subsonic leading edge is much more sensitive to changes in the angle of attack compared to the case of flow around a model wing with a supersonic leading edge. It is shown that on a wing model with a swept angle χ = 72°, the laminar-turbulent transition occurs parallel to the leading edge of the model and the effect of the three-dimensionality of the model is not fixed. Figure 1 shows the dependences of the Reynolds number of the transition Retr on the angle of attack on a wing model with a sweep angle of the leading edge (χ = 72°) at M = 2-4 . For comparison, the same graph shows the results of measurements performed on a wing model with χ = 45° at M = 2 [1]. Note that at Mach number M = 2 the wing with χ = 45° correspond to the case with a supersonic leading edge. For experimental conditions on a wing with a sweep angle of the leading edge of 72°, calculations of the mean flow in the supersonic boundary layer and linear theory of hydrodynamic stability (LTS) were carried out. For the case M = 2, the growth curves of the

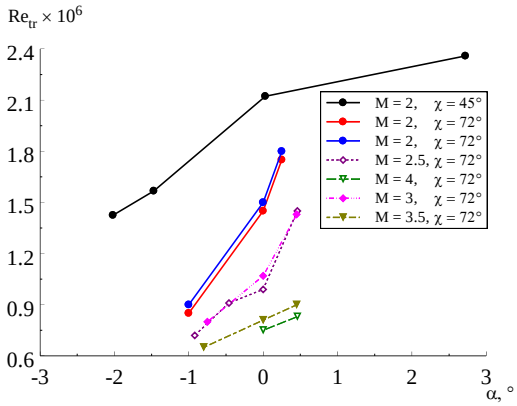

Fig. 1. Dependences of the transition Reynolds number versus the angle of attack.

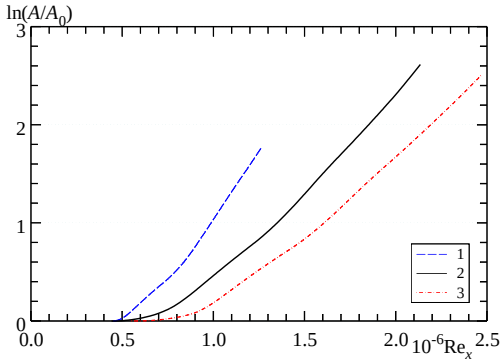

Fig. 2. Curves of increase in amplitudes of perturbations of stationary (f = 0) vortices of cross-flow instability, calculated by the e^N method for M = 2.
1 – α = –1°, *2* – α = 0°, *3* – α = 0.3°.

disturbance amplitudes of the most rapidly growing stationary (f = 0) vortices of cross-flow instability are calculated in accordance with the e^N method. It has been found that the amplitude of vortices increases most rapidly at a negative angle of attack (Fig. 2). As the angle of attack increases, the degree of growth of stationary perturbations decreases. For a zero angle, depending on the Mach number, it was obtained that the amplitude of stationary perturbations grows the slowest at M = 2, with an increase in the Mach number, the degree of growth increases. An analysis of these calculated data and the transition Reynolds numbers obtained in experiments allows us to conclude that stationary disturbances play a decisive role in the process of laminar-turbulent transition in swept wing models under low-noise flow conditions.

The research was carried out within the state assignment of Ministry of Science and Higher Education of the Russian Federation (project No 121030500161-0) at the Equipment Sharing Center “Mechanics” of ITAM SB RAS.

REFERENCES

1. **Kosinov A.D., Semionov N.V., Yermolaev Y.G., Smorodsky B.V., Kolosov G.L., Yatskikh A.A., Semenov A.N.** The influence of moderate angle-of-attack variation on disturbances evolution and transition to turbulence in supersonic boundary layer on swept wing // Journal of Aerospace Engineering: Part G. Proc. of the Inst. of Mech. Engineers. 2020. Vol. 234. No. 1. P. 96–101. DOI: 10.1177/0954410019852804.
2. **Ermolaev Y.G., Kosinov A.D., Kocharin V.L., Semenov A.N., Semionov N.V., Shipul S.A., Yatskikh A.A.** Effect of small angles of attack on laminar-turbulent transition in the supersonic boundary layer on a swept wing with χ = 72° // Fluid Dynamics. 2022. Vol. 57, No. 1. P. 30–36. DOI: https://doi.org/10.1134/S0015462822010037

DOI: 10.53954/9785604788967_173

SLENDER BODY SEPARATION IN UNSTEADY CROSSFLOW

V.I. Shalaev, D.H. Vuong

***Moscow Institute of Physics and Technology* (*National Research University*)**
140180, Zhukovsky, Moscow region, Russia

The based on the slender body theory analytical approach is developed for calculating of forces and moments acting on a body of revolution when it separates from a cavity or rigid surface at the presence of unsteady cross-flow disturbances. Solutions are found for three phases the body motion: in the cavity, at its crossing of the shear layer and in the outer freestream. Derived expressions for forces and moments and calculations results of body trajectories are presented for different conditions.

The unsteady interaction of bodies is very actual aeromechanic problem having numerous practical applications, such as a cargo separation from a from a cavity, a carrier outer hanger or aerodynamic interaction of many bodies [1]. The load unsteadiness may be defined by acoustic waves (Rossiter modes) at trans- and supersonic flights, a carrier motion or outer flow disturbances. In the present time, these problems have a large interest, what is demonstrated by many new publications [2]. Numerical modeling difficulties are determined by the aerodynamic problem complexity and time expenses needed for calculations that leads to a wide using of semi-empirical methods, which don't allow analyze possible complex phenomena, for example, trajectory bifurcations [1].

In the presented work, a modified approach is proposed including unsteady disturbances and based on the developed earlier analytical representation of the potential equation solution [1]. The body motion at the separation from a cavity is subdivided to three phases: the motion inside the cavity (Phase 1), the shear layer intersection (Phase 2) and the motion in the freestream (Phase 3). In phases 1 and 2 the only one effect, the solid or free surface (the shear layer) flow boundary on the body aerodynamic is considered. Within this framework for Phase 3 the local lift force $L_x(t,x)$ acting on a slender body of revolution is defined be the relation:

$$L_x = -\pi\left\{\frac{\partial\left[\left(2B_0 - V_e\right)a^2\right]}{\partial x} + a^2\frac{\partial\left(2B - V_e\right)}{\partial t} - 2\left(B_0 - V_e\right)aa_x + 2B_0A_{-3}a - \right.$$

$$\left. -2a\sum_{n=1}^{\infty}\left(A_{-2n-1} - A_{-2n-3}\right)B_{-2n-2}\right\}.$$

Here $V_e(t) = V(t) - x\omega(t) - \alpha(t) - V_\infty(t)$: V is vertical center of mass motion velocity, $\omega = d\alpha/dt$ is angular rotation velocity around the side axis *z*, passing the center of mass, α is angle of attack, V_∞ is vertical speed of outer unsteady disturbances. Last two terms are defined the flow boundary influence. Coefficients $A_{-2n-1}(t,x)$ and $B_{-2n-2}(t,x)$ are found from boundary conditions in the form of series by parameter $q(t,x)$. At the separation from a cavity first five coefficients have forms:

$$q(t,x) = \frac{a(x)}{2H(t,x)} \le \frac{1}{2}, \quad B = V_e\left[1 - q^2S_3(q)\right] - qa_xS_4(q),$$

$$A_{-3} = q^2\left[a_x\left(1 - 2q^2 - q^4 - 4q^6\right) + 2qV_e\left(1 - q^2 + q^4\right)\right],$$

$$B_{-4} = q^3\left[a_x\left(1-3q^2-3q^4\right)+3qV_e\left(1-q^2-3q^4\right)\right],$$

$$A_{-5} = -q^4\left[a_x\left(1-4q^2-6q^4\right)+4qV_e\left(1-q^2\right)\right],$$

$$S_3 = 1-q^2-q^4-2q^6, \quad S_4(q) = 1-q^2-3q^6.$$

Here $a(x)$ is local body radius, $H(t,x)$ is distance from the body axis to the boundary, t is time, x is coordinate along the body axis from the center of mass; all parameters are nondimensional. Similar relations are obtained for the side force, vertical and side moments.

For Phase 1 force sand moments are defined by same formulas, but the local vertical speed $V_e(t) = V_e(t) - x\omega(t) - V_\infty(t)$ and $a_x = 0$ because the longitudinal flow is absent, $u_\infty = 0$. The solution for the Phase 2 is defined using conformal mapping method under the assumption, that the shear layer is flat surface of the longitudinal velocity gap.

The problem for the body motion in cross-flow direction is formulated as:

$$\frac{d^2Y_o}{dt^2} = \frac{dV}{dt} = \dot{V} = c_l L(t) - c_g, \quad \frac{d^2\alpha}{dt^2} = \frac{d\omega}{dt} = \dot{\omega} = c_m M; \quad V(0) = V_0, \quad Y_o(0) = y_0,$$

$$\frac{d^2Z_O}{dt^2} = \frac{dW}{dt} = \dot{W} = c_l T(t), \quad \frac{d^2\beta}{dt^2} = \frac{d\omega_y}{dt} = \dot{\omega}_y = c_m M_T; \quad W(0) = W_0, \quad Z_O(0) = z_0,$$

$$c_g = \frac{gl_0}{\delta u_\infty^2}, \quad c_l = \frac{\rho_\infty l_0^3 \delta^2}{m}, \quad c_m = \frac{\rho_\infty l_0^5 \delta^2}{I}.$$

When the body moves in a uniform flow without a boundary these equations reduced to oscillation equations, the exact solution of which at the presence of unsteady crossflow disturbances was found in an analytical form [2]. This solution is general approximation for the proposed approach and it was used for them verification.

Developed approach is effective enough and it leads to the well accordance with experimental data at the absence of cross-flow disturbances [1].

REFERENCES

1. **Shalaev V.I.** Applications of Analytical Methods in Contemporary Aeromechanics. Part 2. Hydrodynamic Body Interaction. Moscow: Publ. Moscow Inst. of Phys. and Tech., 2013. 173 p.
2. **Shalaev V.I., Vuong D.H.** A slender body motion stability in the uniform freestream // Proc. of the High-Energy Processes in Condensed Matter Conference (HEPCM 2020): AIP Conference Proceedings. 2020. Vol. 2288. Art. 030061. (7 p.). DOI: 10.1063/5.0028472.

DOI: 10.53954/9785604788967_175

ACTIVE FLOW CONTROL METHODS AND SPLITTING EFFECTS IN JETS

A.K. Shevchenko, S.N. Yakovenko

Khristianovich Institute of Theoretical and Applied Mechanics SB RAS
Novosibirsk 630090, Russia

Study of flow control ways in jets is relevant in energy issues, such as various burners, in transport applications with jets used to reduce engine noise, aircraft drag, fuel consumption. In the present work, submerged and impinging jets are simulated numerically by solving the Navier–Stokes equations using OpenFOAM at varied forcing amplitudes, Reynolds ($\mathrm{Re} = UD/\nu$) and Strouhal ($\mathrm{St} = fD/U$) numbers where U is the mean inlet velocity, D is the nozzle diameter, and ν is the molecular viscosity. The active flow control ways are explored, i.e. axial and helical harmonic oscillations (with frequencies $2f$ and f, amplitude A) of the inlet velocity profile [1, 2], transverse vibrations of the nozzle (with frequency f, amplitude Z) [2, 3], and their combinations. To simulate a jet, the governing equations are solved in cylindrical or rectangular coordinates at wide range of $50 \le \mathrm{Re} \le 23\,000$. The top-hat inlet velocity profile $u(r < D/2) = U$, is chosen at the entrance section $x = 0$. The details of computation set-up are given in [2].

As in [4, 5], the branching of the jet is shown (Fig. 1) in wide ranges of amplitudes of oscillations of the inlet velocity profile ($0.01 \le A/U \le 0.2$), transversal nozzle vibration amplitudes ($0.01 \le Z/D \le 1.0$), Strouhal and Reynolds numbers ($\mathrm{Re} > 50$). Note, in the measurements [4] the jet bifurcation was caused by acoustic forcing for $\mathrm{Re} \ge 20$. The nozzle vibration here has the similar effects to those of the transverse acoustic field in [4, 5]. Only at quite low Reynolds number ($\mathrm{Re} \sim 50$), the perturbation inserted at the inlet section quickly decay downstream of the nozzle exit, so even the high-amplitude vibrational excitation is not enough to split a round jet.

The mechanism of interaction of vortex structures, leading to the jet splitting has been investigated [2, 5]. Calculations of jets demonstrate that the vibrational excitation turns out to be a more effective flow control method, than helical excitation of the inlet velocity profile [2].

The mixing enhancement (which is important for applications and produced by the jet excitation) can be parameterized by the typical jet thickness d or the expansion angles α in the bifurcation plane, as well as by centerline values of the mean velocity $\langle u \rangle$ or scalar $\langle c \rangle$ [1, 5]. It is evident that mixing efficiency increases for the stronger jet expansion with larger d and α, resulting in larger spreading area and smaller centerline values of $\langle u \rangle$ and $\langle c \rangle$.

To study the influence of St for transverse vibration, the amplitude is fixed at a high value of $Z/D = 0.5$ to guarantee the bifurcation occurrence, and runs at $0.01 \le \mathrm{St} \le 0.5$ are performed. At $\mathrm{St} = 0.01$ the jet begins to split from $x/D \approx 12$ where the forcing frequency matches the natural excitation frequency diminishing downstream. At $0.025 \le \mathrm{St} \le 0.1$ the effect grows steadily: the bifurcation point drifts closer to the inlet and the jet expansion angle increases. At $\mathrm{St} \ge 0.2$ the forcing effect degrades as its frequency becomes ever higher than the natural perturbation frequency. The thickness d shows (Fig. 2) quick growth of the expansion angle for $\mathrm{St} < 0.025$, when the forcing frequency enters an “optimal St window”. With further increase in St, the curves become steeper for $\mathrm{St} \sim 0.05$, and after that, the angle steadily declines. Similar trends are demonstrated by the centerline velocity curves. Note, that if the $\langle u \rangle / \langle u \rangle_{\max}$ value to define the typical jet thickness is changed from 0.1 to 0.5 or 1.0 than the optimal value is increased to $\mathrm{St} \approx 0.1$ (see Fig. 1) since the jet branches are much wider for $\mathrm{St} \le 0.05$ than for $\mathrm{St} \ge 0.1$.

For an impinging jet, the LES results for passive scalar dynamics show the massive jet splitting into several branches, with more efficient mixing and scalar transfer intensification when using the active control methods at forcing frequencies chosen closely to optimal values.

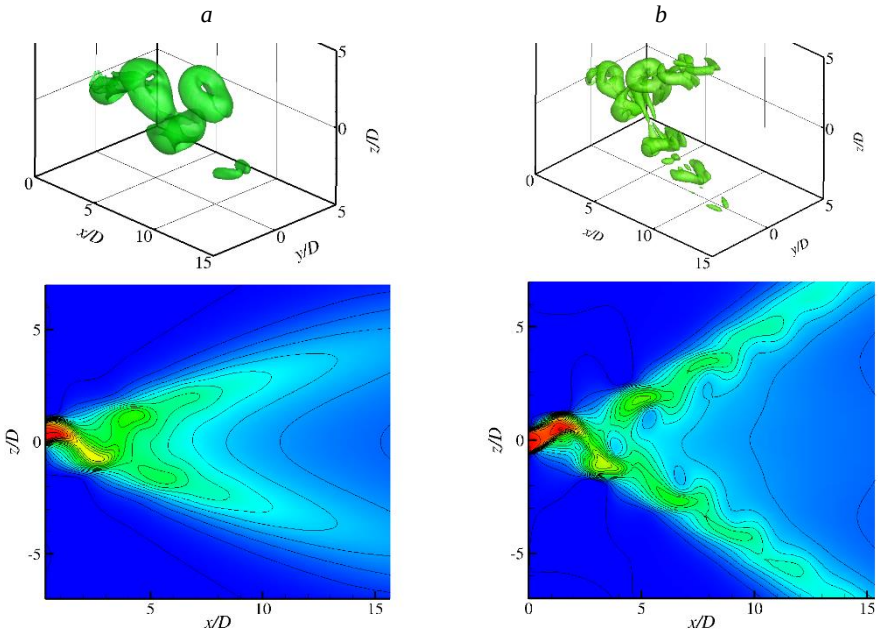

Fig. 1. 3D vortex structure, $\lambda_2 D/U$ = 500 (*a*), 0.5 (*b*), instantaneous velocity, $u(x, z)/U$, in the bifurcation plane (y = 0) with nozzle vibration at Re = 100 (*a*), 250 (*b*), $Z = 0.5D$, 'optimal' Strouhal number St = 0.1.

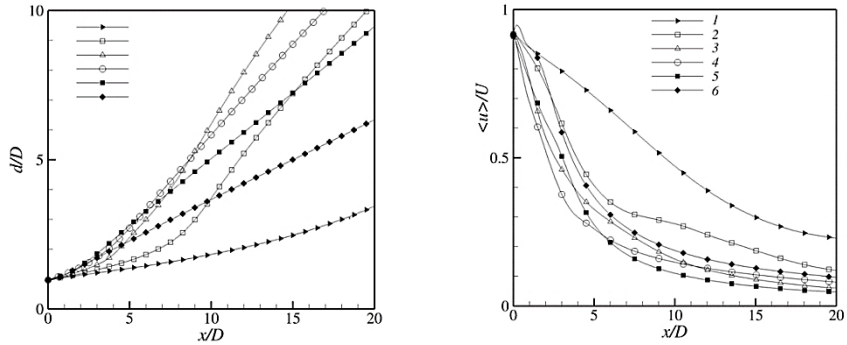

Fig. 2. Thickness $d = z(\langle u\rangle/\langle u\rangle_{max} = 0.1)$ where $\langle u\rangle_{max}$ is the maximum velocity at x = const; values of $\langle u\rangle/U$ along the jet axis.

Re = 250, Z/D = 0.5, St = 0.01 (*1*), 0.025 (*2*), 0.05 (*3*), 0.1 (*4*), 0.2 (*5*), 0.5 (*6*).

The research was carried out within the state assignment of Ministry of Science and Higher Education of the Russian Federation (project No. 121030500149-8).

REFERENCES

1. **Tyliszczak A.** Parametric study of multi-armed jets // Int. J. Heat Fluid Flow. 2018. Vol. 73. P. 82–100.
2. **Shevchenko A.K., Yakovenko S.N.** Numerical study of flow control methods and splitting effects in a round submerged jet // Thermophysics and Aeromechanics. 2021. Vol. 28, Iss. 3. P. 353–368.
3. **Yakovenko S.N.** Unsteady numerical solutions for a plane jet issuing from a narrow slit into a submerged space // Thermophysics and Aeromechanics. 2019. Vol. 26, No. 5. P. 711–721.
4. **Kozlov V.V., Grek G.R., Litvinenko Yu.A., Kozlov G.V., Litvinenko M.V.** Subsonic round and plane macro- and microjets in a transverse acoustic field // Vestnik NGU. Ser. Fiz. 2010. Vol. 5, Iss. 2. P. 28–42. (in Russian)
5. **Reynolds W.C., Parekh D.E., Juvet P.J.D., Lee M.J.D.** Bifurcating and blooming jets // Annu. Rev. Fluid Mech. 2003. Vol. 35. P. 295–315.

DOI: 10.53954/9785604788967_177

EXPERIMENTAL STUDY OF THE DISTURBANCES DEVELOPMENT IN THE SUPERSONIC BOUNDARY LAYER ON THE FLAT PLATE WITH A WAVY SURFACE

A.V. Shmakova, A.D. Kosinov, Yu.G. Yermolaev, N.V. Semionov

Khristianovich Institute of Theoretical and Applied Mechanics
630090, Novosibirsk, Russia

The paper presents experimental results continuing a series of studies on the disturbances development in inhomogeneous boundary layers [1–4]. Interest in these types of flows is due to both fundamental problems, on the one hand, and applied research, on the other. Isolated or distributed heterogeneities on the model surface can be used for passive flow control. The results of an experimental study of the natural disturbance development in a flat plate boundary layer with a wavy and smooth surface at Mach 2 are shown.

The experiments were conducted in T-325 supersonic wind tunnel of ITAM SB RAS at Mach 2. The model of a flat steel plate with a blunt radius of the leading edge r = 0.32 mm was used. In the wind tunnel the model was fixed in the central plane of the test section at approximately a zero angle of attack. Photo of the model with a wavy surface is shown in Fig. 1. To create a wavy surface on the model, longitudinal roughness elements were applied. They were additionally coated with a film to align the side sections of the roughness and give them a rounded shape. Dimensions of roughness elements: width – 2 mm, length – 150 mm, thickness – 93 microns. Distance between roughness elements 12 mm. To preserve the surface properties in experiments on a smooth surface of a flat plate, the longitudinal roughness elements were removed from the model and the flat plate was sealed with a film, the same as in the case of a wavy surface of the model. Constant temperature anemometer CTA 2017 was used for mean and pulsating flow quantities measurements [5]. The mean and pulsating characteristics of the flow were obtained after data processing using the standard technique, which is described in [1, 2, 5, 6].

To determine the mean flow distortion in the boundary layer created by longitudinal roughness elements, measurements were made with a hot-wire anemometer along a line parallel to the leading edge at x_0 = 152 mm, y_0 = const. The measurements showed that the mean flow is periodically modulated (Fig. 2), the period of flow modulation corresponding to the distance between the established roughnesses.

Measurements of the laminar-turbulent transition in the boundary layer of a flat plate with a wavy and smooth surface (Fig. 3) showed that on a smooth model the Reynolds number of the

a

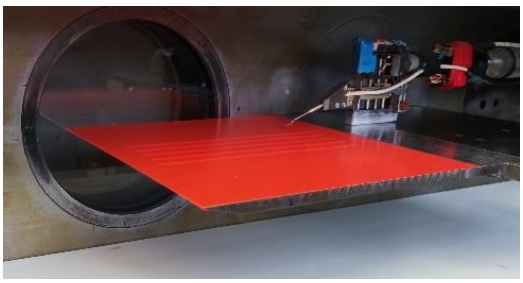

Fig. 1. Photographs of the flat plate with a wavy surface in the test section of T-325.

b

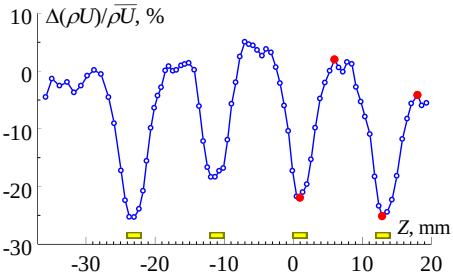

Fig. 2. Mean flow distortion in the spanwise direction for flat plate with wavy surface.

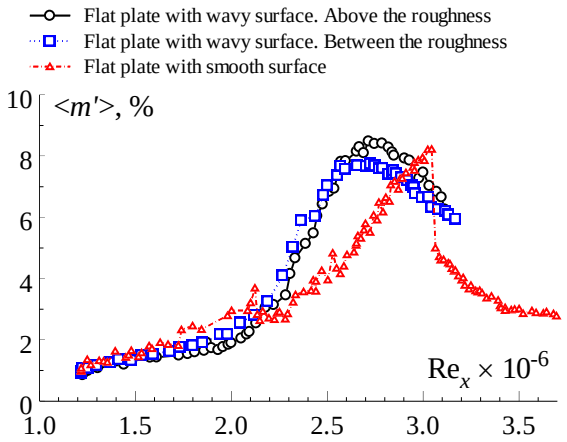

Fig. 3. The RMS mass flux pulsations for flat plate with smooth and wavy surface.

transition ($Re_{tr} = 3.06 \times 10^6$) is 12% higher than on a flat plate with a wavy surface. Perhaps this is due to the fact that measurements on a model with a smooth surface were made in a layer in which the mass flow rate fluctuations are 0.78 of the fluctuations maximum across the boundary layer, and on a model with a wavy surface – 0.9 of the maximum. More research is needed to test this assumption.

The research was carried out within the state assignment of Ministry of Science and Higher Education of the Russian Federation (project No. 121030500161-0).

The study was conducted at the Equipment Sharing Center "Mechanics" of ITAM SB RAS.

REFERENCES

1. **Panina A. V., Kosinov A. D., Yermolaev Y. G., Gorev V. N., Semionov N. V.** Experimental study of mean and pulsation flow characteristics in the 2D/3D supersonic boundary layer behind flat roughness elements // Thermophysics and Aeromechanics. 2014. Vol. 21, No. 1. P. 3–13.
2. **Kosinov A. D., Kolosov G. L., Yatskikh A. A., Semionov N. V., Ermolaev Y. G., Panina A. V.** Hot-wire measurements of the evolution of total temperature and mass flow pulsations in a modulated 3D supersonic boundary layer // Proc. of 19 Int. Conf. on the Methods of Aerophys. Research (ICMAR2018): AIP Conference Proceedings. 2018. Vol. 2027. Art. 020016. 4 p. https://doi.org/10.1063/1.5065094
3. **Panina A., Kosinov A., Semionov N., Yermolaev Yu.** Experimental study of the natural disturbance development in a supersonic flat plate boundary layer with a wavy surface // High-Energy Processes in Condensed Matter (HEPCM 2019): Proceedings of the XXVI Conference on High-Energy Processes in Condensed Matter, dedicated to the 150th anniversary of the birth of S.A. Chaplygin (Novosibirsk, Russia 3–5 April 2019): AIP Conference Proceedings. 2019. Vol. 2125. Art. 030107. 4 p. https://doi.org/10.1063/1.5117489
4. **Panina A., Yatskikh A., Kosinov A., Yermolaev Yu., Semionov N.** On the artificial wave packet development in a spanwise modulated boundary layer on the swept wing at Mach 2.5 // Nternational Conference on the Methods of Aerophysical Research (ICMAR 2020) (Novosibirsk, Russia 1–7 November 2020): AIP Conference Proceedings. 2021. Vol. 2351. Art. 040039. 4 p. https://doi.org/10.1063/5.0052064
5. **Kosinov A. D., Semionov N. V., Ermolaev Y. G., Kolosov G. L., Yatskikh A. A., Kocharin V. L.** Hot-wire measurements of the evolution of total temperature and mass flow pulsations in supersonic boundary layer on flat plate with coating permeability // Proc. of 19 Int. Conf. on the Methods of Aerophys. Research (ICMAR2018): AIP Conference Proceedings. 2018. Vol. 2027. Art. 040087. 5 p. https://doi.org/10.1063/1.5065361
6. **Yatskikh A. A., Kosinov A. D., Semionov N. V., Smorodsky B. V., Ermolaev Y. G., Kolosov G. L.** Investigation of laminar-turbulent transition of supersonic boundary layer by scanning constant temperature hot-wire anemometer // Proc. of 19 Int. Conf. on the Methods of Aerophys. Research (ICMAR2018): AIP Conference Proceedings. 2018. Vol. 2027. Art. 040041. 5 p. https://doi.org/10.1063/1.5065315

DOI: 10.53954/9785604788967_179

APPLICATION OF THE HORTON-LAPWOOD-ROGERS PROBLEM FOR DETERMINING THE PERMEABILITY OF A FIBROUS POROUS MEDIUM WITH INTERNAL HEAT GENERATION AND LOW THERMAL CONDUCTIVITY

A.S. Sidorov, N.V. Kolchanov

Perm State University
614990, Perm, Russia

The paper presents experimental results on the filtration properties of a fibrous porous medium. The medium consists of heat-generating fibers. To determine its permeability, one uses the solution of the Horton-Lapwood-Rogers problem [1]. According to this solution, convection in a horizontal porous layer is excited at the dimensionless Rayleigh – Darcy number equal to

$$Ra_{m*} = K\frac{g\beta}{\nu_f \chi_{\text{eff}}} h_m \left(\Delta T\right)_* = 4\pi^2 \tag{1}$$

where g is acceleration of gravity; β is coefficient of volumetric expansion of fluid; ν_f is kinematic viscosity; χ_{eff} is effective thermal conductivity; h_m is a thickness of the horizontal porous layer. In the Horton – Lapwood– Rogers problem, a direct measurement of the critical temperature difference allows us to find permeability of the porous medium. The application of a heat-generating porous medium with low thermal conductivity is an alternative way to determine permeability at the onset of the convective flow in a horizontal layer due to internal heat generation [2, 3].

Porous medium. In the experiment, fibers of the porous medium are made by covering each nichrome wire with a layer of plexiglass. The wire diameter is of 0.08 mm. Plexiglass occupies the most of the fiber as compared to the nichrome wire, so thermal conductivity of an individual fiber is close to that of plexiglass (0.2–0.3 W/(m·K)). The porous medium is made by weaving the fibers into a photopolymer matrix. The matrix is printed by a 3D printer. Varying a shape of the photopolymer matrix and a fiber diameter, one can change the filtration and thermophysical parameters of the medium. Figure 1 shows one of the forms of the photopolymer matrix with the fibers woven into it.

Experimental setup. The experimental setup includes a working cavity with the porous medium. It has the upper, lower, and lateral boundaries. The upper and lower boundaries are made of metal with a very high thermal conductivity as compared to the thermal conductivity of the side boundaries and fibrous porous medium. The temperature difference across the porous layer is set by means of two liquid thermostats. They pump a thermostatic liquid through the

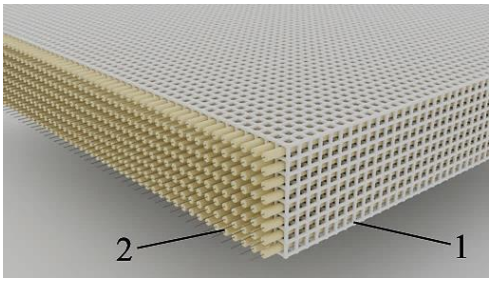

Fig. 1. Sample of a fibrous porous medium made of the photopolymer matrix 1 and interwoven fibers 2.

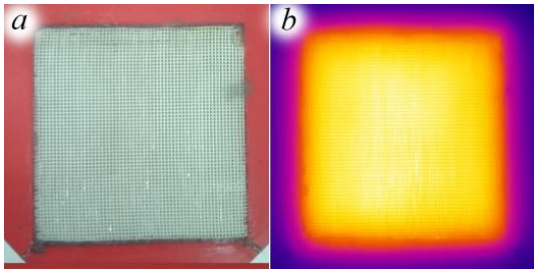

Fig. 2. External view of a sample of the fibrous heat-generating medium (*a*) and thermal image of its surface (*b*).

copper heat exchangers. The heat exchangers are connected to the metal boundaries of the cavity. The differential copper-constantan thermocouples and a device of "Thermodat" are used to measure temperatures in the porous layer. This device digitizes an analog signal from the thermocouples and transmits the data to a computer in real time.

Results. The experiments have carried out with five samples of the fibrous heat-generating porous medium. They differ by a volume fraction of the solid phase (the photopolymer matrix plus fibers), which varies from 0.2 to 0.5. Each sample has a layer with a thickness of 10–12 mm and longitudinal dimensions of just over 10 cm. Thermal imaging measurements of the temperature field on the surface of samples have shown a high degree of homogeneity of the heat generation. Fig. 2 represents the external view and thermal image for a sample with the solid volume fraction of 0.45 under voltage. The samples have been alternately placed in the working cavity of the experimental setup. The setup allows us to simultaneously find out the effective thermal conductivity of each sample by the stationary flat layer method and the critical temperature difference $(\Delta T)_*$ by the Schmidt – Milverton method [4]. To saturate the porous medium, one uses air in one series of the experiments and distilled water in the other. These experiments have showed that in a porous layer with a high solid volume fraction of 0.45, convection in the air cannot be excited even at a temperature difference of 100 °C, so for this sample and some other samples the permeability has been determined at the saturation of the porous medium with water. When the solid fraction is small (about of 0.2), the onset of convection has been observed in both air and water.

The work was supported by the Russian Science Foundation (Grant No. 21-71-10045), https://rscf.ru/en/project/21-71-10045/.

REFERENCES

1. **Nield D.A., Bejan A.** Convection in Porous Media. N.Y. et al.: Springer Int. Publ., 2017. 988 p.
2. **Carr M.** Penetrative convection in a superposed porous-medium-fluid layer via internal heating // Journal of Fluid Mechanics. 2004. Vol. 509. P. 305–329.
3. **Mukhija S., Nayak A.K.** Experimental study of transient heat transfer characteristics of single-phase natural convection in multidimensional porous bed with volumetric heat generation // Experimental Heat Transfer. 2019. Vol. 32, № 1. P. 85–101.
4. **Schmidt R. J. et al**. On the instability of a fluid when heated from below // Proc. R. Soc. Lond. A. 1935. Vol. 152, № 877. P. 586–594.

DOI: 10.53954/9785604788967_181

ANALYSIS OF THE COUPLED HEAT TRANSFER IN INTERNAL FLOW SYSTEM OF RAMJET ENGINE

N.P. Skibina, V.V. Faraponov

National Research Tomsk State University
634050, Tomsk, Russia

The processes of heat transfer and mass transfer enhancement and the formation of a separation zones accompany the deceleration of a supersonic turbulent gas flow in internal ducts of various geometry. Often such phenomena occur in nozzles, combustion chambers, air intakes, diffusers and other elements of various propulsion systems. Analysis of the flow structure, the position of the separation zones, and their effects on thermal state of the channel walls are necessary for the correct control of the deceleration process.

The aim of the research is study of coupled heat transfer influence on temperature and pressure distribution in boundary layer of internal flow system of solid-fuel ramjet (see the figure). Under study flow are formed in flow system of axisymmetric ramjet [1] in conditions of aerodynamic tests in supersonic short-duration gas-dynamic facility [2] with Mach numbers 5 and 6.

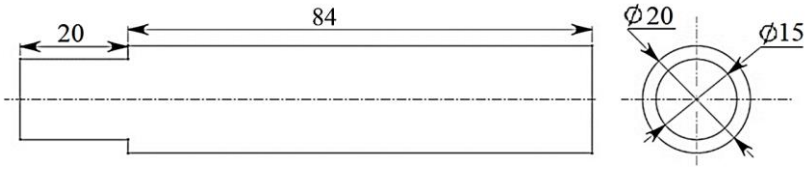

Axisymmetric internal air-duct.

The main research approach is numerical calculation. The gas motion is described by a system of non-stationary averaged Navier – Stokes equations, supplemented by the equations of the semi-empirical turbulence SST model [3]. The solution of the equations is carried out in the ANSYS Fluent. The finite volume method is used. Case with adiabatic boundary conditions on the wall and coupled heat transfer boundary are considered.

By results of a computational research range of temperature and pressure in internal flow system of ramjet are calculated. It has been established that the temperature near the adiabatic wall is, on average, 50% higher than the temperature near the coupled wall. The high temperature in boundary layer near the adiabatic wall leads to a displacement of the recirculation and separation zones upstream [4]. The interaction of shock waves with the boundary layer on the walls of the internal flow system of solid-fuel ramjet leads to the formation of an inhomogeneous temperature field in a solid material.

The work was financially supported by the Ministry of Education and Science of the Russian Federation in the framework of state assignment FSWM-2020-0036.

REFERENCES

1. **Ishchenko A.N, Maslov E.A., Skibina N.P., Faraponov V.V.** Complex investigation of nonstationary flow with shock waves in the working path of a hypersonic ramjet engine // J. Eng. Phys. Thermophy. 2021. Vol. 94. P. 450–457. https://doi.org/10.1007/s10891-021-02315-8
2. **Zvegintsev V.I.** Gas dynamic installation of short duration. Part I. Installations for scientific research. Novosibirsk: Parallel, 2014. 551 p.
3. ANSYS Fluent 12.1 Theory Guide, Solver Theory. [Canonsburg, PA, et al.:] ANSYS Inc., 2010.
4. **Chang PK**. Control of Separation. New York: McGraw-Hill, 1976.

DOI: 10.53954/9785604788967_182

NUMERICAL SIMULATION OF TURBULENT AIR MIXED CONVECTION IN RAPIDLY ROTATING ANNULAR CAVITIES

E.M. Smirnov, E.V. Kolesnik, S.I. Smirnov, A.A. Smirnovsky

Peter the Great St. Petersburg Polytechnic University
195251, St. Petersburg, Russia

The study of the motion and heat transfer effects in rotating annular cavities is of great interest and importance in turbomachinery, where such configurations are widely used to cool the rotor of axial compressors and gas turbine engines [1]. Rapid rotation creates great difficulties in obtaining accurate quantitative data on unsteady flow and local heat transfer in the experiments. Thus, the numerical simulations can reveal important details of flow inside rapidly rotating cavities.

Under conditions of high angular speed of the cavity rotation and relatively slow motion of the compressible gas inside the cavity, different approaches can be used for mathematical description of such flows. One of the main difficulties here is a high hydrostatic pressure gradient, and the most common approach to by-pass this difficulty is to use the hyposonic approximation, when the governing equations are written in the rotating coordinate system, dealing with relative velocities, and the equation of state for the gas contains only the hydrostatic pressure (variations of the absolute pressure due to the gas motion are treated as negligible). Another approach is based on the full momentum and energy equations for compressible gas relative motion and needs introducing a special technique for low-Mach flow computations.

The present work covers details and assessment of two different approaches implemented recently in the unstructured-grid finite-volume code SINF/Flag-S, which is under development at the Peter the Great St.Petersburg Polytechnic University. The hyposonic-approximation approach is implemented using the SIMPLEC algorithm. The second mentioned approach was realized using the Roe scheme for the governing equations discretization combined with a low-Mach regularization technique.

Verification of the extended version of the code SINF/Flag-S included comparisons with results obtained with ANSYS Fluent. First, the case of 2D laminar natural convection in an annular cavity segment was computed (Fig. 1). In this case, two opposite azimuthal boundaries of the segment are kept at temperatures T_1 and T_2, whereas the cylindrical walls are adiabatic. The segment rotates in the *xy* plane with angular velocity ω. The flow and heat transfer are determined by the

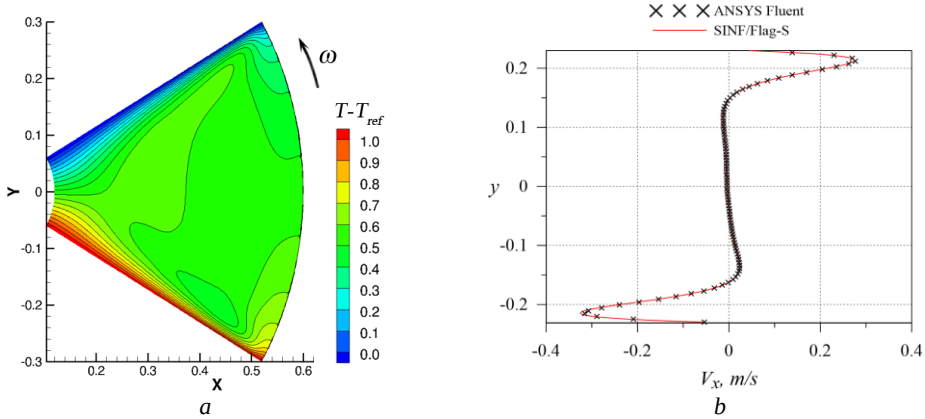

a *b*

Fig. 1. Reduced temperature distribution in the annular cavity segment (*a*) and the *x*-velocity profile at $x = 0.4$ computed at $Ra = 4.16\times10^3$, $Pr = 0.7$, $Ph = 3.45$ (*b*).

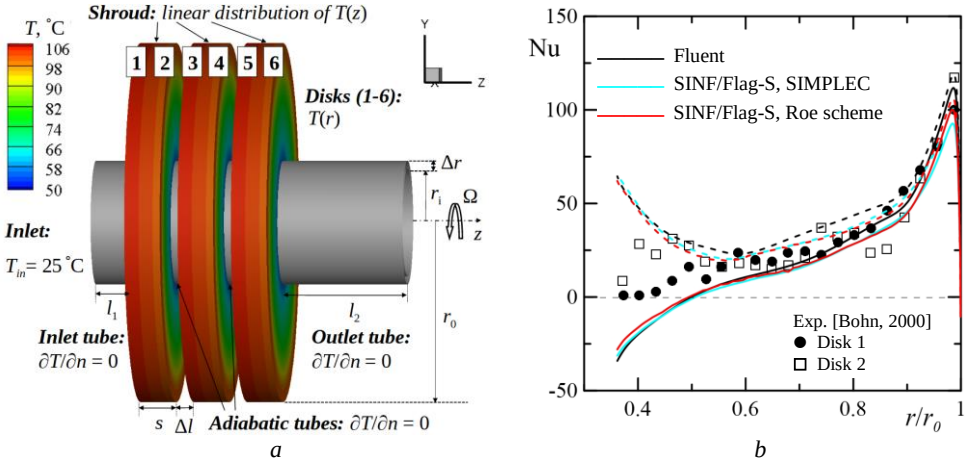

Fig. 1. Schematic illustrating the problem statement for a system of three annular cavities (*a*) and comparison of computed radial variations of local Nusselt number (Nu) on the disk surfaces (lines) with the experimental data from [2] (symbols) (*b*).

Rayleigh number, Ra, the Prandtl number, Pr, and the normalized hydrostatic pressure difference, $\mathrm{Ph} = \omega^2(R_2^2 - R_1^2)/P_1$, where P_1 is absolute pressure at the inner radius R_1. As an illustration, the temperature distribution in the computational domain is given in Fig. 1,*a* for the case of $\mathrm{Ra} = 4.16\times10^3$, Pr = 0.7, Ph = 3.45. The results obtained with SINF/Flag-S using two approaches (SIMPLEC algorithm and the Roe scheme based) are practically identical and in very good agreement with the Fluent results (Fig. 1,*b*).

The second presented case covers the problem of turbulent air mixed convection in a system with three rapidly rotating annular cavities of the same shape, heated from both disk surfaces and from the periphery, sequentially subjected to axial throughflow of cooling gas (Fig. 2,*a*). The system rotates around the *z*-axis with a constant angular velocity Ω. The geometry of the cavities and the annular axial channel, as well as the flow rate and the thermal conditions are taken from [2], where the case of a single cavity was studied experimentally.

The flow under these conditions is turbulent, and the Implicit LES approach was used in our simulation. The results obtained with SINF/Flag-S using the two implemented approaches were compared with data from our recent paper [3], where computations for the same case were performed using ANSYS Fluent [3]. As an example, Fig. 2,*b* shows the radial distributions of the local Nusselt number, averaged over time and circumferential coordinate. As seen, the distributions obtained with SINF/Flag-S for the first-cavity disks are close to the ANSYS Fluent data, and are in satisfactory agreement with the measurements. Notably that generally ANSYS Fluent predicts a higher peak values of Nusselt number, and the approach based on the Roe scheme implemented in SINF/Flag-S predicts slightly higher Nusselt numbers, as compared with the hyposonic model approach.

The study was supported by the Russian Foundation for Basic Research (grant 20-08-01090).

REFERENCES

1. **Owen J. M., Tang H., Lock G.D.** Buoyancy-Induced Heat Transfer inside Compressor Rotors: Overview of Theoretical Models // Aerospace. 2018. Vol. 5, No 1. 22 p. DOI:10.3390/AEROSPACE5010032
2. **Bohn D., Deutsch G., Simon B., Burkhardt C.** Flow visualisation in a rotating cavity with axial throughflow // Proceedings of the ASME Turbo Expo 2000: Power for Land, Sea, and Air (Munich, Germany, 8–11 May 2000); GT2000-280. 8 p. DOI:10.1115/2000-GT-0280
3. **Smirnov E.M., Smirnov S.I., Abramov A.G., Galaev S.A.** Turbulent mixed convection within rapidly rotating heated annular cavities with an axial throughflow // St. Petersburg Polytechnical State University Journal. Physics and Mathematics. 2021. Vol. 14, No.3. P. 21–34.

DOI: 10.53954/9785604788967_184

NUMERICAL AND EXPERIMENTAL STUDIES OF AERODYNAMICS OF CIVIL AIRCRAFT AT HIGH ANGLES OF ATTACK

V.G. Soudakov, A.A. Efremov, A.V. Voyevodin

Central Aerohydrodynamic Institute
140180, Zhukovsky, Moscow region, Russia

At high angles of attack a flow separation arises on the upper surface of the wing of an aircraft, which leads to a qualitative change (degradation) of aerodynamic characteristics of the aircraft. Separation evolution can lead to the aerodynamic stall. One of the complex problems of the aircraft design is to ensure that the aircraft doesn't fall into this off-design range of regimes as well as to predict behavior of the aircraft on stall regimes.

In the present work, numerical investigations of the flow around the model of typical civil aircraft are performed at high angles of attack in the range from 0 to 90 degrees. Configuration consists of wing, body, nacelle under the wing with pylon, horizontal and vertical tail (Fig. 1). Calculations are carried out on the basis of methods of computational fluid dynamics using Reynolds averaged Navier-Stokes equations. The computational grid was designed as structured multi-block and has approximately 90 million nodes. The size of the first cell from the surface corresponds to the condition $y_{+1}<1$.

Three-dimensional Reynolds Averaged Navier – Stokes equations are solved numerically. The fluid is a perfect gas having the specific heat ratio 1.4 and laminar Prandtl number 0.72. Laminar viscosity-temperature dependence is approximated by Sutherland law with Sutherland constant 110.4 K. *k*–ω SST turbulence model is used for simulations. Fully turbulent boundary layer is considered. The model surface is considered to be an adiabatic no-slip wall. Far-field boundaries are placed at distance of approximately 50 wing spans from the surface. Computational geometry of the model corresponds to experiments without wind tunnel walls and support.

Experimental investigations are carried out in T-105 subsonic wind tunnel of Central Aerohydrodynamic Institute (TsAGI), Zhukovsky, Russia. T-105 is a vertical, continuous-operation, closed-layout atmospheric wind tunnel with a round open test section (nozzle diameter is 4.5 m, length of test section – 7.5 m). A fan driven by an electric motor of 450 kW generates the flow. The wind tunnel is designed to investigate spin modes by testing dynamically similar models of aircraft and other flight vehicles in free flight. It is also widely used for investigations of aerodynamic characteristics of flight vehicles and their elements using special equipment with balance measurements (Fig. 1).

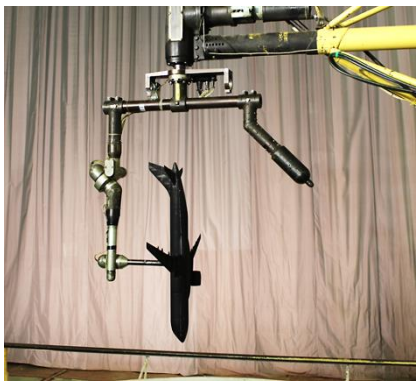

Fig. 1. Experimental setup in T-105 wind tunnel TsAGI.

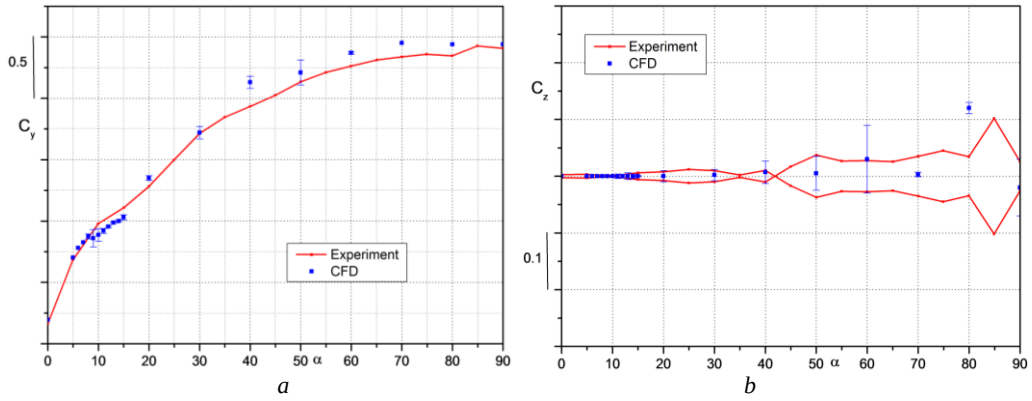

Fig. 2. Comparison of numerical and experimental data.

Solid curves – experiment, points – averaged force coefficients predicted by CFD, bars – oscillation amplitudes predicted by CFD.

Experimental and 3D numerical simulations of the flow past this configuration are carried out for the regime with velocity V = 25 m/s and Reynolds number based on free-stream parameters and mean aerodynamic chord length $\mathrm{Re} = 0.16\times10^6$. Analysis of numerical and experimental data is performed. Physical peculiarities of the flow around the model of aircraft in the extended range of flight envelope are considered.

Comparison of numerical results with experimental data is performed. It is shown that the results are in a good agreement (Fig. 2) for normal and side force coefficients. Averaged values are presented in the figure, while bars correspond to the oscillation amplitude. For angles of attack in the range 10–40°, the near-surface streamlines can show asymmetry at given moment in time. Although the averaged value of side force is about zero for this range. Asymmetry of the averaged side force begins from the angle of attack higher than 40°. It should be noted that side force can be realized of both signs due to different small disturbances. For this reason, Fig. 2,*b* shows original experimental results and the curve of opposite sign.

At the present work, different flow features at high angles of attack in the range 0–90° are presented and visualized by near-surface streamlines and flow fields at wing span sections. Interaction of the wake from the body with the wing and tail as well as interaction of the wake from the wing with horizontal and vertical tail are discussed. All peculiarities of axial, normal and side forces as well as all moments are shown in conjunction with flow features.

Effect of Reynolds number influence is discussed also in the paper. For this reason, numerical studies of the flow past this model is presented for natural Reynolds number about 6 million.

Moreover, the results of numerical simulations of aerodynamic characteristics of the model in the regime of rotation with constant angular velocity are presented. In this case, side force predicted by numerical simulation is in good agreement with side force obtained in experiment. Particularly, all changes of sign of side force are in good agreement between CFD and experiment.

This work was supported by grant of Russian Scientific Foundation No. 21-19-00659, https://rscf.ru/en/project/21-19-00659/.

DOI: 10.53954/9785604788967_186

THEORETICAL CALCULATION OF POWER CAPACITY FOR ISLAND WIND FARM ACCORDING TO METEOROLOGICAL DATA

S.V. Strijhak

Ivannikov Institute for System Programming RAS
109004, Moscow, Russia

Issues related to the development of wind energy and the study of the design for wind farms are relevant at the present time. As a rule, the onshore wind farms are now being built in the Russian Federation. Currently, it is planned to build new wind farms on Sakhalin Island and the Kuril Islands, where there is a large wind potential [1].

The tasks associated with the development of accurate calculation methods for estimating the dynamics of vortex wakes and the generated total annual capacity of a wind farm are interdisciplinary.

To solve such problems, various calculation methods and geodata can be used. These methods include analytical methods using differential equations and integral calculus, empirical coefficients, numerical methods for solving partial differential equations on detailed grids.

At the same time, it is important to compare the calculation results with the available data in open sources. The availability of meteorological data in the form of time series for 10-20 years, obtained from weather stations from an open source (https://www.rp5.ru), makes it possible to correctly assess the annual generation of electricity from a wind farm.

In this case, it is necessary to take into account such parameters as wind direction, wind speed, humidity, temperature, pressure. The choice of a site on the island and the mutual arrangement of wind turbines depends on the relief, weather conditions, altitude, transport and energy communications, and the impact on the ecology of the region.

This paper presents the results of calculating model wind farms with 2 and 8 wind turbines using FLORIS open source library. FLORIS library, developed in the Python programming language, is based on various analytical models for calculating the velocity profile behind the wind turbine, models of mutual influence and superposition of vortex wakes, and a model for optimizing the position of the nacelle by the yaw angle [2].

To describe the operation of the wind turbine, the "Actuator Disk Model", the selected dependencies for the power and thrust coefficient of the wind turbine were used. To test the performance of the models, examples were considered with the 8th wind turbine KOMAIHALTEC Inc. with a power of 0.3 MW, with a diameter of D = 32 meters (Fig. 1), with 2 wind turbines NREL with a power of 5 MW, with a diameter of D = 126 meters (Fig. 2).

Wind turbine data (wind wheel diameter, tower height, power and thrust coefficients versus speed) were taken from open sources. For the case of a wind farm with 8 wind turbines, the distance between wind turbine rows was chosen equal to 5D, between wind turbines vertically 3D – 4D. For the case of a wind farm with 2 wind turbines, the distance between wind turbines in the horizontal direction was set to 500 meters.

The data for wind speed and direction were set to 8 m/s and 270, 210, 330 degrees, respectively. The data was taken for April 2021 for a specific geographical location on the selected island. According to the results of calculations using the Jupyter Lab software, the velocity fields were obtained (see Fig. 1). Additionally, calculations were carried out for data with different wind roses.

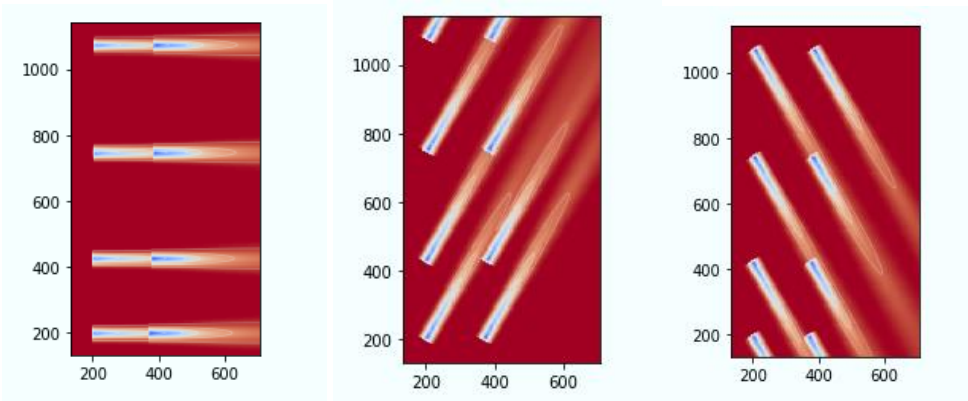

Fig. 1. Computational area with 8 wind turbines and velocity field for different wind directions.

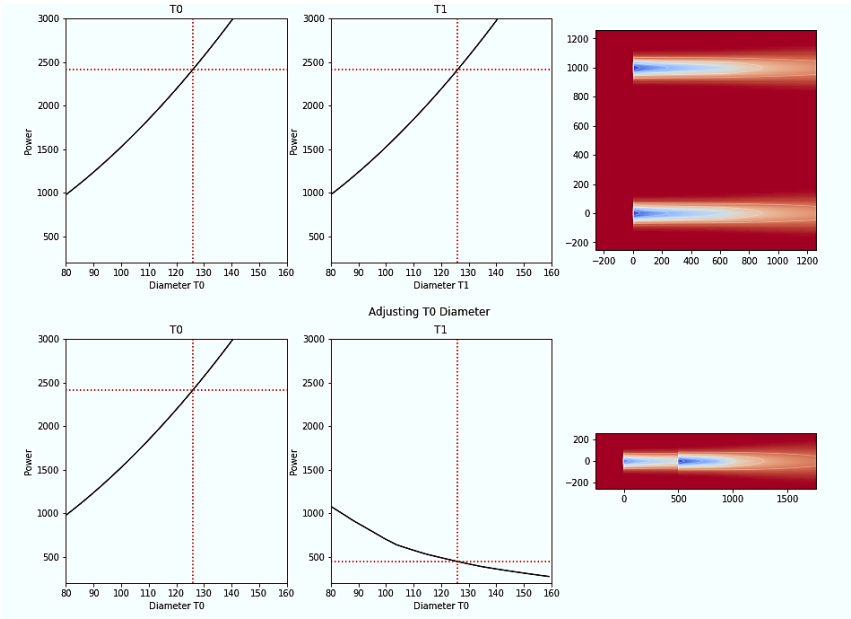

Fig. 2. Dependence of wind turbine power on the diameter of wind wheel and the velocity field.

For the case with 2 wind turbines, the mutual influence of the location of the wind turbine on the generated power for each wind turbine, the influence of the wind turbine diameter on the generated power for a given wind direction of 270 degrees were evaluated.

REFERENCES

1. Kovalev P.D., Kovalev D.P., Shevchenko G.V. Renewable energy resources of the Sakhalin region. Vladivostok: Dalnauka, 2015. 216 p. [in Russian: **Ковалев П.Д., Ковалев Д.П., Шевченко Г.В.** Возобновляемые энергетические ресурсы Сахалинской области. Владивосток: Дальнаука, 2015. 216 с.].
2. **Gebraad P.M.O. et al.** Wind plant power optimization through yaw control using a parametric model for wake effects — a CFD simulation study // Wind Energy. 2016. Vol. 19. P. 95–114.
3. **Doekemeijer B.M., van der Hoek D., van Wingerden J.W.** Closed-loop model-based wind farm control using FLORIS under time-varying inflow conditions // Renewable Energy. 2020. Vol. 156. P. 719–730.

DOI: 10.53954/9785604788967_188

NUMERICAL STUDY OF THE ATTENUATION OF GAS DETONATION IN A CHANNEL SEPARATED BY WALLS

V.M. Temerbekov, D.A. Tropin

Khristianovich Institute of Theoretical and Applied Mechanics SB RAS
630090, Novosibirsk, Russia

Currently, gaseous fuels are actively used in production and technology. The high heat release of combustible gases contributes not only to high efficiency in their operation as a fuel, but also creates a great danger of emergency situations. In this regard, studies aimed at identifying the possibility of attenuation and failure gaseous detonation are of great interest.

This work is devoted to the numerical study of the passage of a detonation wave (DW) through a flat rectangular channel with a rigid permeable barrier installed in it. The barrier was modeled as a set of longitudinal walls of finite thickness, dividing the original channel into several small channels of different thickness, and also as sets of finite-size plates regularly installed in the simulated area. The width of the initial channel was 100 mm, the width of the small channels, the dimensions and the installation step of the finite-size plates were varied. The thickness of the longitudinal walls and plates was 2 mm, for these objects the conjugate problem of heat conduction was solved. Dinas ceramics and the corresponding material parameters of thermal conductivity, heat capacity, and density were chosen for these walls.

The computational domain was filled with a premixed stoichiometric hydrogen-air mixture at the initial pressure P = 100 kPa and the initial temperature T = 300 K. Under such initial conditions, the width of the detonation wave is equal to λ = 12.5 mm. Immediately in front of the obstacles, the preliminarily calculated cellular detonation wave was set as the initial conditions. The DW front velocity was D_{CJ} = 1937 m/s.

The calculations were performed using the ANSYS Fluent software package. Within the framework of the mathematical model used, the Favre-averaged Navier – Stokes equations for a multicomponent gas mixture were solved. This system of equations is complemented by the equation of state and SST modification of the k–ω turbulence model. To simulate the chemical kinetics, the reduced kinetic scheme was used, which includes one combustion reaction of the hydrogen with oxidizer. Previously, this kinetic scheme was verified by experimental data on the ignition delay time, the propagation velocity of the detonation wave [1] and the size of the detonation cell under various conditions [2]. In this work, the “Density based” solution method was chosen, an implicit second-order scheme was used for approximation in time, a second-order upstream scheme with the AUSM flux vector splitting was used for spatial approximation. In the work, a structured computational grid, consisting of quadrangular shape elements, was used. Also, the dynamic adaptation of the computational grid along the density gradient was used.

As a result of the calculations, it was found that changing of the width of small channels in the considered range from 0.5λ to 2λ practically does not affect the propagation velocity of the detonation wave, despite the destruction of its cellular structure when the width of small channels is less than the size of the detonation cell of the mixture. As a result, the velocity of propagation of the detonation wave decreases by 5–6% compared to the velocity of propagation of the DW through the channel without obstacles.

The usage of finite-size plates made it possible to reduce the velocity of wave propagation in comparison with small channels (see the figure). This effect is caused by the presence of regularly repeating reflections throughout the entire length of the barrier. When the detonation wave is reflected from the end walls of the plates, it loses some of its energy, attenuates, and slows down. At the same time, the barrier porosity increased in comparison with the porosity for small channels (88%).

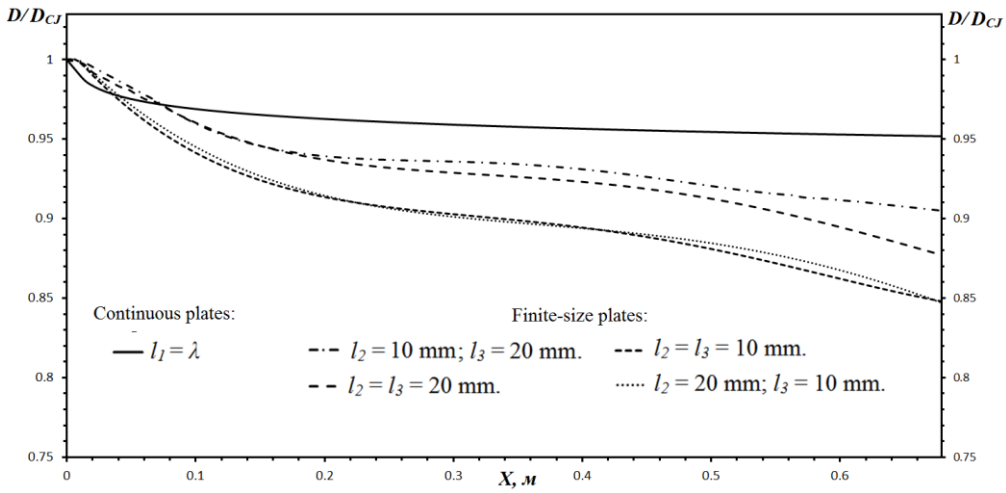

Comparison of DW propagation velocities for various configurations.

When the plate sizes are 20 mm and the distance between them is 20 mm, the normalized detonation velocity (D/D_{CJ}, where D is the detonation wave propagation velocity over the area with a barrier, D_{CJ} is the detonation wave propagation velocity in the free channel) decreases to $D/D_{CJ} = 0.89$. Reducing the size of the plates to 10 mm and the distance between them to 10 mm leads to decreasing of the normalized velocity to $V/D_{CJ} = 0.85$, while the porosity remains unchanged (94%). This effect is achieved by increasing the number of plates, which leads to increasing of the number of reflections and, thereby, increasing of energy losses by the wave. For a plate size of 20 mm and a distance between them of 10 mm, the barrier porosity decreased to 92%, which should lead to decreasing of the DW velocity. However, the number of plates also decreased, as a result of which the DW propagation velocity remained comparable to the previous case. With a plate size of 10 mm and a distance between them of 20 mm, the number of plates remained the same as in the previous case, while the barrier porosity increased to 96%, and it led to increasing of the detonation wave propagation velocity.

The work was supported by Russian Science Foundation, project No. 21-79-10083, https://rscf.ru/project/21-79-10083/

REFERENCES

1. **Bedarev I.A., Rylova K.V., Fedorov A.V.** Application of detailed and reduced kinetic schemes for the description of detonation of diluted hydrogen–air mixtures // Combustion, Explosion, and Shock Waves. 2015. Vol. 51, No. 5. P. 528−539.
2. **Bedarev I.A., Temerbekov V.M.** Estimation of the energy of detonation initiation in a hydrogen-oxygen mixture by a high velocity projectile // Thermal Science. 2021. Vol. 25, No. 5. P. 3889−3897.

DOI: 10.53954/9785604788967_190

SPECTRUM AND LINEAR INSTABILITY BY LYAPUNOV OF THE RESTING STATE FOR FLOWS OF INCOMPRESSIBLE POLYMERIC FLUID IN A PLANE CHANNEL

D.L. Tkachev

Sobolev Institute of Mathematics SB RAS
630090, Novosibirsk, Russia

We study the linear stability of a resting state for the flows of incompressible viscoelastic medium in an infinite plane channel; as a model we use Pokrovski – Vinogradov model [1], which has shown its high efficiency for numerical research of polymeric flows in areas with complex boundary geometry [2].

In paper [3] it was proven that the spectrum points of the linearized problem (there are no-slip conditions on the channel boundaries) can't lay in the right open complex half-plane. In current work this result is strengthened.

1. We prove that the linear problem solution amplitude in the one-dimensional case (perturbations do not depend on the variable, changing along the channel side) growth faster than any exponent $e^{\mu t}$ with the growth of time, where $\mu > 0$ is constant.

2. Spectrum of the linear problem is situated in the left open complex half-plane.

3. For the perturbation class of harmonic functions with respect to the variable, changing along the infinite channel side, the base solution, i.e. the resting state, is linearly unstable by Lyapunov. This happens because the solution amplitude growth faster than exponent $e^{\mu t}$, $\mu > 0$.

Note that the study of linear instability of a Poiseuille-type flow for both base and modified Pokrovski – Vinogradov model was conducted in works [4–9].

This study was carried out within the framework of the state contract of the Sobolev Institute of Mathematics SB RAS (project No. FWNF-2022-0008).

REFERENCES

1. **Pokrovski V.N.** The mesoscopic theory of polymer dynamics. Dordrecht: Springer, 2010. 256 p.
2. **Altukhov Yu.A., Pishnograi G.V.** Entering flows in 4:1 channel of fluid linear polymers // Mechanics of Composite Materials and Constructions. 2001. Vol. 7, No. 1. P. 16–23.
3. **Blokhin A.M., Goldin A.Yu.** On linear stability of an incompressible polymer liquid at rest // J. Math. Sci. 2015. Vol. 230, No. 1. P. 14–24.
4. **Blokhin A.M., Yegitov A.V., Tkachev D.L.** Linear instability of solutions in a mathematical model describing polymer flows in an infinite channel // Comput. Math. Math. Phys. 2015. Vol. 55, No. 5. P. 848–873.
5. **Blokhin A.M., Yegitov A.V., Tkachev D.L.** Asymptotics of the spectrum of a linearized problem of the stability of a stationary flow of an incompressible polymeric fluid with a space charge // Comput. Math. Math. Phys. 2018. Vol. 56, No. 1. P. 102–117.
6. **Blokhin A.M., Tkachev D.L., Yegitov A.V.** Spectral asymptotics of a linearized problem for an incompressible weakly conducting polymeric fluid // Z. Angew. Math. Mech. 2018. Vol. 98, No. 4. P. 589–601.
7. **Blokhin A.M., Tkachev D.L.** Stability of Poiseuille-type flows for an MHD model of an incompressible polymeric fluid // Journal of Hyperbolic Differential Equations. 2019. Vol. 16, No. 4, P. 793–817. DOI: 10.1142/S0219891619500243.
8. **Blokhin A.M., Tkachev D.L.** MHD model of an incompressible polymeric fluid. Linear instability of the resting state // Complex Variables and Elliptic Equations. 2021. Vol. 66, No. 6-7. P. 929–944.
9. **Blokhin A.M., Tkachev D.L.** On linearly unstable steady states of an MHD model of an incompressible polymeric fluid in the case of absolute conductivity // Sib. Adv. in Math. 2022. Vol. 32, No. 1. P. 1–12.

DOI: 10.53954/9785604788967_191

MULTI-DISCHARGE ACTUATOR SYSTEM FOR SEPARATION CONTROL ON THE STRAIGHT WING MODEL

S.N. Tolkachev

Central Aerohydrodynamic Institute
140180, Zhukovsky, Moscow region, Russia

There is an interest among researchers in the use of plasma actuators to control flows in the boundary layer [1–7]. From the point of view of safety of use and the possibility of integration into the design of an aircraft, actuators using a dielectric barrier discharge (DBD) stand out.

There is a problem associated with low induced velocity by volumetric forces. TsAGI developed a design that allows increasing this parameter – a multi-discharge actuator system (MAS), which implements a unidirectional air jet. This advantage renews interest in the study of separation control. In this work, the turbulent state of the boundary layer and a positive pressure gradient were implemented in order to create conditions that are realized on the flap.

Experimental conditions. A flat plate 15 mm thick was chosen as an experimental model. The leading and trailing edges of the model are cylindrical with a radius of 7.5 mm. The chord of the model was 557 mm.

The model was installed in the test section of the T-03 TsAGI wind tunnel (WT) equipped with an Eiffel chamber. At the outlet of the nozzle, a jet core 580×370 mm (W×H) is formed. Walls were installed flush with the nozzle exit to minimize edge effects. The typical turbulence level *Tu* for this setup is 0.35%. The experiments were carried out at freestream velocities V_0 18 and 36 m/s.

A positive pressure gradient was created by a structure consisting of a displacement body (Eppler E662 profile) set at an angle of attack of –15° and a slat providing attached flow around the displacement body.

Velocity distribution over the model surface and in the boundary layer was measured using particle image velocimetry (PIV). Using a pitot comb located at a distance of 30 mm from the trailing edge of the model, the distribution of the total pressure in the wake behind the model was measured and the integral pressure losses were estimated.

The parameters of the MAS actuator are as follows: the electrode pitch is 6 mm, the size of the area with the discharge is 160×180 mm, the leading edge of the discharge is located 274 mm from the leading edge, and the rear edge is 454 mm. The position of the displacement body was selected in such a way that the separation point in the natural case was located at $394 < X < 454$ mm.

Results. The measurements showed that the use of MAS at freestream velocity of 18 m/s leads to a noticeable displacement of the separation point downstream: when a voltage of 5 kV is applied, it is 18.3δ*, which is 30 mm. An increase in speed reduces the distance by which the separation point is displaced.

The Pitot comb allows you to compare the wake behind the model in the natural case and when voltage is applied to the actuator. Turning on the MAS led to a decrease in the total pressure loss simultaneously with a decrease in the cross dimension of the wake behind the model. As the flow velocity increases, the relative contribution made by the actuator decreases.

The integral effect of MAS was estimated using the specific force f (dimension N/m), determined by the following formula:

$$f = \int_{-12.5}^{Y_s} (P - P_{\text{tot}})\ dY$$

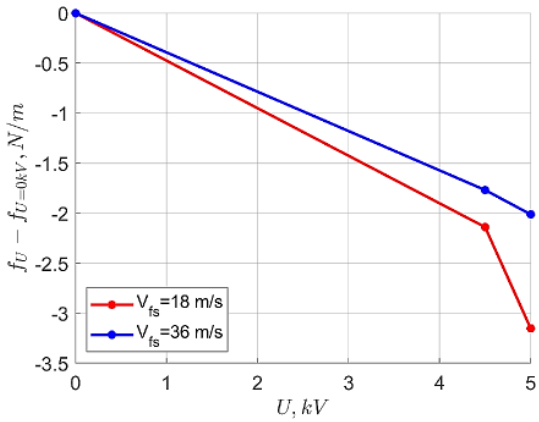

Change in specific force under the influence of MAS from the applied voltage.

where P is the pressure measured by the total pressure comb, P_{tot} is the total pressure in the control section of the WT outlet nozzle, Y_s is the position on the comb corresponding to the velocity defect created by the slat.

The results of measuring the average force depending on the applied voltage are shown in the figure. With an increase in the voltage across the actuator, the pressure loss decreases, and this is typical for the entire investigated range of speeds.

Acknowledgments. The work is prepared in the implementation of the program for the creation and development of the World-Class Research Center "Supersonic" for 2020-2025 funded by the Ministry of Science and Higher Education of the Russian Federation (Grant agreement of December, 8, 2020 № 075-11-2020-023).

REFERENCES

1. **Moreau E.** Airflow control by non-thermal plasma actuators // Journal of Physics D: Applied Physics. 2007. Vol. 40, № 3.
2. **Cattafesta L.N., Sheplak M.** Actuators for active flow control // Annual Review of Fluid Mechanics. 2011. Vol. 43.
3. **Corke T.C., Post M.L., Orlov D.M.** SDBD plasma enhanced aerodynamics: concepts, optimization and applications // Progress in Aerospace Sciences. 2007. Vol. 43, № 7–8.
4. **Wang J.J. et al.** Recent developments in DBD plasma flow control // Progress in Aerospace Sciences. 2013. Vol. 62.
5. **Benard N., Moreau E.** Electrical and mechanical characteristics of surface AC dielectric barrier discharge plasma actuators applied to airflow control // Experiments in Fluids. 2014. Vol. 55, Art. 1846. 43 p. https://doi.org/10.1007/s00348-014-1846-x
6. **Kriegseis J., Simon B., Grundmann S.** Towards In-Flight Applications? A Review on Dielectric Barrier Discharge-Based Boundary-Layer Control // Applied Mechanics Reviews. 2016. Vol. 68, № 2.
7. **Corke T.C., Enloe C.L., Wilkinson S.P.** Dielectric barrier discharge plasma actuators for flow control // Annual Review of Fluid Mechanics. 2010. Vol. 42.

DOI: 10.53954/9785604788967_193

THE INVESTIGATION OF HIGH FLOW RATE SUCTION ON THE SWEPT WING BOUNDARY LAYER STABILITY

S.N. Tolkachev, A.Ph. Kiselev, D.S. Sboev

Central Aerohydrodynamic Institute
140180, Zhukovsky, Moscow region, Russia

One of the most effective and versatile methods of laminarization is the suction of the boundary layer. Despite the fact that the implementation of this technique on real aircraft is associated with a number of technical difficulties, it is considered the most promising.

The concept of critical suction is encountered in the literature. Due to the local effect of suction above the perforated surface, three-dimensional perturbations are introduced into the structure of the boundary layer, which leads to a decrease in its stability and, finally, such a strong suction can lead to turbulence of the boundary layer instead of its stabilization. In this work, the main attention is paid to measuring the level of critical suction on an experimental model simulating the flow around a swept wing. Ellis and Poll [1], Pfenninger [2], Goldsmith [3] criteria were used as starting points. Exceeding the oversuction criteria of MacManus and Eaton [4], Campe [5] in the experimental configuration was not possible, since this would require a suction velocity in the holes of the order of 1000 m/s.

Experimental conditions The experiments were carried out in subsonic low-turbulence wind tunnel (WT) T–124 TsAGI. The experimental model is a flat plate with a swept leading edge having a sweep angle of 35°, a span of 998 mm, a chord of 2100 mm, and a thickness of 20 mm, made of plexiglas. The front edge of the model has the shape of an ellipse with a large semi-axis of 80 mm. A three-dimensional boundary layer, similar to that of a swept wing, was created using profiled side walls and a top insert. This method of creating a three-dimensional boundary layer is widely used [6, 7].

The freestream velocity was V_{fs} = 37.2 m/s; the free flow turbulence level was about 0.12%; the air temperature during the experiments was in the range T_{air} = 303–311°K; the unit Reynolds number was $Re_1 = 2.6\times10^6$ 1/m.

The experimental model is equipped with five ultraperforated panels 484×32×0.49 mm in size and a perforated area 460×9.5 mm formed by 20 rows of holes with a diameter of 80 μm located at the nodes of a square grid with a 0.5 mm edge. This provides a porosity of 2%. The average positions of the panels were located at distances from the leading edge: X = 304 mm; 404 mm; 504 mm; 654 mm and 804 mm.

The coordinate system used in the work: the X-axis is orthogonal to the leading edge and originates from it, the Z-axis is parallel to the leading edge, the Y-axis is orthogonal to the X and Z axes and originates from the model surface. To minimize the influence of the coordinate device on the flow, it was installed taking into account the streamlines; therefore, measurements were carried out along the Z' axis, which has an angle of 10° to the Z axis.

Constant temperature hot-wire anemometry was used for measurements. To study the structure and flow regime, a series of measurements was carried out on a two-dimensional grid (in the YZ' plane). The size of the two-dimensional grid along the Z' direction was chosen so as to capture at least three periods of stationary vortices.

Results. Hot-wire studies of the boundary layer in the area of the negative pressure gradient showed an increase in stability when using suction in the entire range of flow rates studied. An increase in the suction rates leads to the suppression of stationary and travelling disturbances.

Quantitatively, the part with a turbulent flow regime on the entire velocity oscillogram is called intermittency γ. The dependence of the suction rate on the intermittency in the position

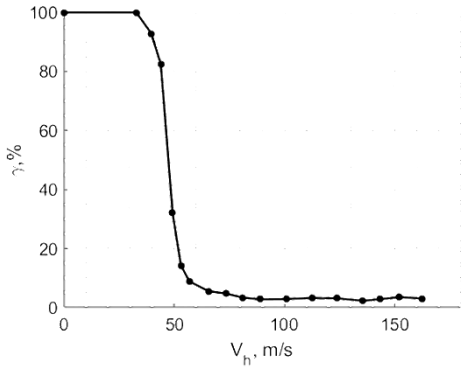

Dependence of intermittency on suction speed in holes (V_h) at distance X = 979 mm.

X = 979 mm is shown in the figure. There is a sharp decrease in intermittency with an increase in the suction rate. The use of even the maximum realized suction velocity V_h = 162 m/s did not lead to an increase in intermittency and, moreover, no signs of abrupt turbulization of the flow by suction were observed, despite the excess of the suction criteria of Ellis and Poll [1], Pfenninger [2] and Goldsmith [3].

The results obtained make it possible to expand the effective limit of applicability of suction as a method of laminarization of the boundary layer above the swept wing.

Acknowledgments. The work was supported by the Ministry of Industry and Trade of the Russian Federation (government contract 20411.1770290019.18.010).

REFERENCES

1. **Ellis J.E., Poll D.I.A.** Laminar and laminarizing boundary layers by suction through perforated plates // 2nd European Forum on Laminar Flow Technology. Bordeaux, 1996. P. 8.17–8.26.
2. **Pfenninger W.** Laminar Flow control, laminarization, Special Course on concepts of drag reduction: AGARD Report No 654. 1977.
3. **Goldsmith J.** Critical laminar suction parameters for suction into an isolated hole or a singlerow of holes: Rep. BLC-95. Northrop Aircraft. 1957.
4. **MacManus D.G. et al.** Mapping the flow field induced by a HLFC perforation using a high resolution LDV // 34th Aerospace Sciences Meeting and Exhibit (Reno, NV, 15–18 Jan., 1996): AIAA-96-0097.
5. **Campe R.** A two-dimensional model for the conceptual design for a LFC equipped sailplane: Msc thesis report / Delft Univeristy of Technology. Delft, 2004.
6. **Deyhle H., Bippes H.** Disturbance growth in an unstable three-dimensional boundary layer and its dependence on environmental conditions // Journal of Fluid Mechanics. 1996. Vol. 316. P. 73–113.
7. **Gaponenko V.R. et al.** Swept-wing boundary-layer receptivity to surface non-uniformities // Journal of Fluid Mechanics. 2002. Vol. 461, P. 93–126. DOI:10.1017/S0022112002008297

DOI: 10.53954/9785604788967_195

PHYSICAL AND MATHEMATICAL MODELING OF DETONATION FAILURE IN A HYDROGEN-AIR MIXTURE BY A SYSTEM OF POROUS FILTERS

D.A. Tropin, K.A. Vyshegorodcev

Khristianovich Institute of Theoretical and Applied Mechanics SB RAS
630090, Novosibirsk, Russia

During the transition of hydrogen-air mixtures in the pipes, accidents may occur, leading to explosions. It is known that detonation waves (DW) can be attenuated by adding inert particles or filters to the reacting mixture of gases [1–5]. This paper devoted to the numerical study of the effect of a system of two porous filters located at the walls of the channel on the propagation of detonation. Such a filter system can suppress the detonation wave, and when the gas pipeline is works under normal conditions, it allows gas to flow in the gap between the filters without additional resistance.

Let us consider a flat channel filled with a hydrogen-air mixture at atmospheric parameters, as well as a system of two filters located at the upper and lower walls of the channel (Fig. 1). A cellular detonation wave falls on the filter system, which, depending on the filter parameters, is either attenuated by them or suppressed. The physical and mathematical model describing these processes presents the laws of mass, momentum and energy conservation for gas, supplemented by the energy equation for porous filters [4] and the equations of the reduced chemical kinetics of hydrogen combustion [5].

Figure 1,*a* shows the fields of pressure maximum when the DW interacts with the filter system with particle diameters of 50 microns, volume concentration of $2\cdot10^{-3}$ and a gap of 2λ, where λ = 14.29 mm is the size of the detonation cell in pure gas. In this case, it can be seen that the propagation regime of a stationary attenuated cellular DW is realized and the size of the detonation cell increased to the width of the channel.

At constant diameter of the particles, increasing their volume concentration to a certain critical value ($m_2^* = 4\cdot10^{-3}$ for $d = 50$ μm), the detonation failure regime is realized. In this regime, at some distance from the beginning of the filter, the detonation wave is divided into a frozen shock wave and a combustion front lagging behind it. In addition, the cellular structure of the detonation wave is destroyed (Fig. 1,*b*). It can be seen from the numerical Schlieren image

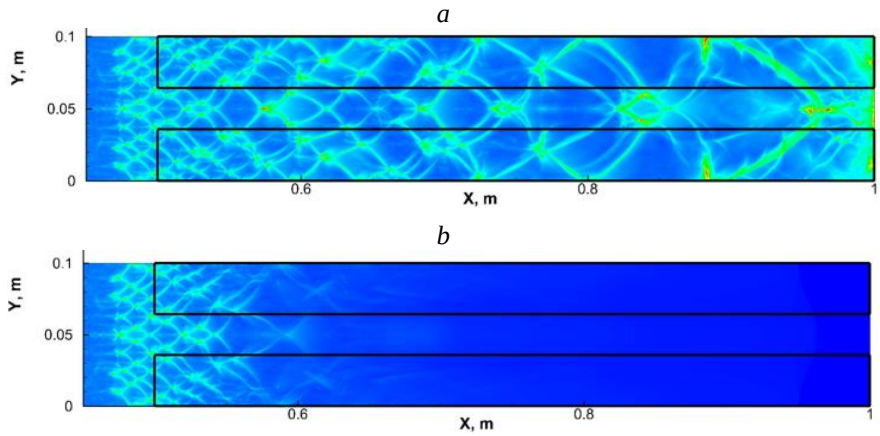

Fig. 1. Fields of pressure maximum in the channel.

Filter with parameters: *a* – $m_2 = 2\cdot10^{-3}$; $d = 50$ μm; gap width 2λ; propagation of attenuated detonation wave. *b* – $m_2 = 4\cdot10^{-3}$; $d = 50$ μm; gap width 2λ; failure of detonation wave with the destruction of cellular structure.

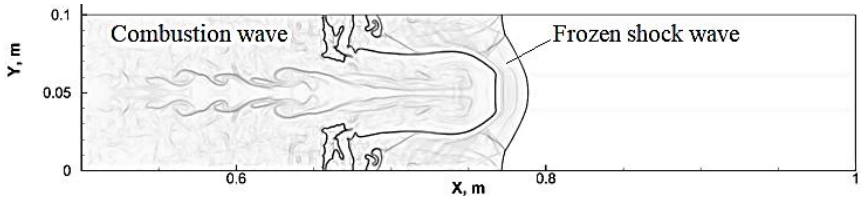

Fig. 2. Numerical Schlieren.

Filter with parameters: $m_2 = 4 \cdot 10^{-3}$; d = 50 μm; gap width 2λ, moment of time t = 27 ms; failure of detonation wave.

(Fig. 2) that there is almost a complete termination of combustion in the filters, while the combustion in the gap between the filters continues, and the shock wave front takes the form of an arc (see Fig. 2). At the same time, as it propagates, the combustion front in the gap lags behind the frozen shock wave.

Regimes of detonation failure by the porous filter system were obtained in the following cases: for particles with a diameter d = 50 μm, with volume concentration $m_2 = 4 \cdot 10^{-3}$ with gaps λ, 2λ and 3λ; for particles with a diameter d = 100 μm, with volume concentration $m_2 = 8 \cdot 10^{-3}$ with gaps λ and 2λ; for particles with a diameter d = 200 μm, with volume concentration $m_2 = 9 \cdot 10^{-3}$ and $18 \cdot 10^{-3}$ with a gap λ. In other cases, the attenuated detonation wave regime was observed.

The work was supported by Russian Science Foundation, project No. 21-79-10083, https://rscf.ru/project/21-79-10083/

REFERENCES

1. **Fedorov A.V., Tropin D.A.** Modeling of detonation wave propagation through a cloud of particles in a two-velocity two-temperature formulation // Combustion, Explosion, and Shock Waves. 2013. Vol. 49, No. 2. P. 178–187.
2. **Tropin D.A., Fedorov A.V.** Mathematical modeling of detonation wave suppression by cloud of chemically inert solid particles // Combustion Science and Technology. 2014. Vol. 186, No. 10-11. P. 1690–1698.
3. **Papalexandris M. V.** Numerical simulation of detonations in mixtures of gases and solid particles // Journal of Fluid Mechanics. 2004. Vol. 507. P. 95–142.
4. **Tropin D.A., Fedorov A.V.** Physical and mathematical modeling of interaction of detonation waves in mixtures of hydrogen, methane, silane, and oxidizer with clouds of inert micro- and nanoparticles // Combustion Science and Technology. 2019. Vol. 191, No. 2. P. 275–283.
5. **Tropin D.A., Bedarev I.A.** Problems of Detonation Wave Suppression in Hydrogen-Air Mixtures by Clouds of Inert Particles in One- and Two-dimensional Formulation // Combustion Science and Technology. 2021. Vol. 193, No. 2. P. 197–210.
6. **Fedorov A.V., Tropin D.A., Bedarev I.A.** Mathematical modeling of detonation suppression in a hydrogen-oxygen mixture by inert particles // Combustion, Explosion, and Shock Waves. 2010. Vol. 46, No. 3. P. 332–343.
7. **Bedarev I.A., Rylova K.V., Fedorov A.V.** Application of Detailed and Reduced Kinetiic Schemes for the Description of Detonation of Diluted Hydrogen-Air // Combustion, Explosion and Shock Waves. 2015. Vol. 51, No. 5. P. 528–539.

DOI: 10.53954/9785604788967_197

DEVELOPMENT OF AN IMPROVED DIFFERENTIAL REYNOLDS STRESS MODEL FOR THE NEAR-WALL PART OF NON-EQUILIBRIUM BOUNDARY LAYERS

A.I. Troshin, L.A. Usov, I.A. Kursakov, K.S. Anisimov

Central Aerohydrodynamic Institute
140180, Zhukovsky, Moscow region, Russia

There is currently growing interest in hybrid RANS/LES modelling. Hybrid models can simulate large scale turbulent structures in the outer part of a boundary layer while staying in RANS mode in the inner part. Such models are promising for predicting non-equilibrium and separated flows at reasonable computational costs, much lower than pure LES at high Reynolds numbers. As the flow near a separation point is typically controlled by underlying RANS model, it is preferably to involve advanced models such as differential Reynolds stress models (DRSM) for the simulations of flows involving strong pressure gradients. The fact that the RANS model within hybrid approach is highly specialized, being active only in thin near-wall regions (typically, $0 \le y^+ \le 200$), gives hope for the possibility of its sufficiently accurate calibration without using the trade-offs of "general purpose" RANS models.

Reynolds stress tensor equation reads as follows:

$$\frac{\partial \overline{u_i' u_j'}}{\partial t} + \frac{\partial}{\partial x_k}\left[\overline{u_i' u_j'} \cdot \overline{u}_k + \underbrace{\overline{u_i' u_j' u_k'}}_{T_{ijk}} - \frac{\nu}{2}\frac{\partial \overline{u_i' u_j'}}{\partial x_k} \right] = \underbrace{-\overline{u_i' u_k'}\frac{\partial \overline{u}_j}{\partial x_k} - \overline{u_j' u_k'}\frac{\partial \overline{u}_i}{\partial x_k}}_{P_{ij}} \underbrace{- \frac{1}{\rho}\left(\overline{u_i' \frac{\partial p'}{\partial x_j}} + \overline{u_j' \frac{\partial p'}{\partial x_i}} \right)}_{\Pi_{ij}} - \varepsilon_{ij}^h .$$

Pressure diffusion and pressure-strain tensors are combined to form velocity-pressure gradient tensor Π_{ij}. It is more convenient to model near a wall than its constituent parts due to the property $\Pi_{ij} \to 0$ as $y \to 0$. Inhomogeneous dissipation rate tensor,

$$\varepsilon_{ij}^h = 2\nu \overline{\frac{\partial u_i'}{\partial x_k}\frac{\partial u_j'}{\partial x_k}} - \frac{\nu}{2}\frac{\partial^2 \overline{u_i' u_j'}}{\partial x_k \partial x_k},$$

is introduced because its anisotropy follows that of Reynolds stress tensor near a wall [1].

Several near-wall DRSMs aimed at term-by-term Reynolds stress budget modelling are published in the literature, e.g. [1, 2]. They were developed in the 1990s and calibrated based on available experimental data and early DNS of near-wall flows, inevitably at low Reynolds numbers. In the current paper, an attempt is made to use more recent DNS data to advance the closures for Π_{ij} and T_{ijk} originally proposed in [1]. Turbulent channel flow at Re_τ up to 5200, converging-diverging channel flow at $\mathrm{Re}_\tau \approx 600$, and turbulent separation bubbles at $1500 \le \mathrm{Re}_\tau \le 3000$ data collected at website [3] are involved. The following form of the closures are considered:

$$\Pi_{ij} = \varepsilon^h \left(C_1 \delta_{ij} + C_2 a_{ij} - C_3 s_{ij} - C_4 p_{ij} \right),$$

$$T_{ijk} = \sum_{perm\{i,j,k\}} \left[-C_{T1} kT \frac{\partial k}{\partial x_k}\delta_{ij} - C_{T2} kT \frac{\partial \overline{u_i' u_j'}}{\partial x_k} - C_{T3} kT^2 \frac{\partial \overline{u}_k}{\partial x_l}\frac{\partial \overline{u_i' u_j'}}{\partial x_l} - C_{T4} kT^2 \overline{u_i' u_j'}\frac{\partial (\varepsilon^h / k)}{\partial x_k} \right],$$

where $a_{ij} = \overline{u_i' u_j'}/k - 2\delta_{ij}/3$ is Reynolds stress anisotropy tensor, s_{ij} is mean strain tensor divided by its norm, $p_{ij} = 2P_{ij}/P_{kk} - 2\delta_{ij}/3$ is production anisotropy tensor, $k = \overline{u_i' u_i'}/2$ is turbulent

kinetic energy, $\varepsilon^h = \varepsilon^h_{ii}/2$ is homogeneous dissipation rate, and $T = \sqrt{\left(k/\varepsilon^h\right)^2 + C_T^2 \nu/\varepsilon^h}$ is a hybrid time scale similar to that proposed in [4]. Summation in the right-hand side of T_{ijk} is over all cyclic permutations of three indices *i, j, k*, which makes the closure fully symmetric. All coefficients, $C_1 - C_4$ and $C_{T1} - C_{T4}$, are considered to be the functions of wall-normal turbulent Reynolds number

$$\mathrm{Re}_{tn} = \frac{\left(\overline{u_i' u_j'} n_i n_j\right)^2}{\nu\varepsilon_h}, \qquad \mathbf{n} = \frac{\nabla \mathrm{Re}_t}{\mathrm{Re}_t}, \qquad \mathrm{Re}_t = \frac{k^2}{\nu\varepsilon_h}.$$

After a priori calibration, the model was implemented in computational code *zFlare* (TsAGI). First results of its a posteriori testing in channel and boundary layer flows in the near-wall domains covering $0 \le y^+ \le 100 \div 200$ are presented. Promising results compared to the JHh model [2] are demonstrated. Next steps involving formulation of a DRSM-based hybrid RANS/LES model are discussed.

The research was supported by a grant from the Russian Science Foundation No. 21-71-10105, https://rscf.ru/en/project/21-71-10105/.

REFERENCES

1. **Jakirlić S., Hanjalić K.** A new approach to modelling near-wall turbulence energy and stress dissipation // Journal of Fluid Mechanics. 2002. Vol. 459. P. 139–166.
2. **Craft T.J.** Developments in a low-Reynolds-number second-moment closure and its application to separating and reattaching flows // International Journal of Heat and Fluid Flow. 1998. Vol. 19, No. 5, P. 541–548.
3. Langley Research Center. Turbulence Modeling Resourc (Website). URL: https://turbmodels.larc.nasa.gov/other_dns.html
4. **Durbin P.A.** Near-wall turbulence closure modeling without “damping functions” // Theoretical and Computational Fluid Dynamics. 1991. Vol. 3, P. 1–13.

DOI: 10.53954/9785604788967_199

HIGH-PRESSURE LAYER IN SUPERSONIC SEPARATION FLOW PAST SPIKED CONE

L.P. Trubitsyna, V.I. Zapryagaev, I.N. Kavun

Khristianovich Institute of Theoretical and Applied Mechanics SB RAS
630090, Novosibirsk, Russia

The high-velocity supersonic separation flow past a compression corner has an interesting feature. In the flow reattachment zone above the boundary layer, another layer emerges – the high-pressure layer [1, 2], in which the stagnation pressure can reach 80–95% of the freestream stagnation pressure.

The high-pressure layer was detected at freestream Mach number $M_\infty = 6 – 8$ and Reynolds number based on the length L of the horizontal plate $Re_L = 0.3 – 2.9$ million. Figure *a* shows a schlieren photograph of laminar separation compression corner flow at the Mach number $M_\infty = 6$. Number 1 marks the experimental model. The high-pressure layer *HPL* is visible on schlieren-photographs of the flow as a narrow dark band behind the reattachment line, parallel to the inclined surface of the model. Other visible flow features are the shock waves (C_1 is the leading-edge shock, C_2 is the separation shock, and C_3 is the reattachment shock), the shear layer *SL*, the reverse flow zone *RF*, the compression wave fan *CF* and the reattachment zone *RZ*. The high-pressure layer *HPL* emerges in the reattachment zone when the gas flow from the shear layer *SL* passes through the compression wave fan *CF* with small total pressure losses compared to the flow passing through the shock C_3.

Number 2 marks the Pitot probe used to obtain the distribution of the total pressure (Pitot pressure) along the dashed line *r*. The high-pressure layer is visible on the measured pressure distribution (Fig. *b*) as a local near-wall peak of total pressure *HPL*. Here p_{Pt} is the total pressure measured by the Pitot probe, $p_{0\infty}$ is the freestream total pressure and *r* is the measurement direction line, perpendicular to the ramp surface.

The high-pressure layer was recorded by independent experimental (schlieren visualization and measurement of the total pressure distribution with a Pitot probe) and numerical methods [1, 2]. Its existence was also detected in the numerical works of other authors [3, 4].

The physical mechanism of the high-pressure layer *HPL* formation, its structure and gas-dynamic parameters were previously studied for various three-dimensional and quasi-two-dimensional geometry of the compression corner model and various freestream parameters. The present report shows the structure and characteristics of the high-pressure layer near a cone equipped with sharp or blunt spike of various length (Fig. *c*).

The experiments were performed in the T-326 blowdown wind tunnel based at the Khristianovich Institute of Theoretical and Applied Mechanics of the Siberian Branch of the Russian Academy of Sciences at freestream Mach number $M_\infty = 6.03$. The experimental model is a cone with a set of interchangeable spikes of various length. The cone diameter is 60 mm, its semi-vertex angle is 30°, and the diameter of spikes is 8 mm. Two sets of spikes were used: the sharp spike (semi-vertex angle $\varphi_s = 10°$, spike length $L_s = 35$, 60 and 100 mm) and the flat-faced spike (semi-vertex angle $\varphi_s = 90°$, spike length $L_s = 25$, 60 and 95 mm). The geometry of the model is chosen so that the flow reattachment line is located on the surface of the cone [5]. The distance from the junction between the spike and the cone to the probing cross-section is $L_{Pt} = 38$ mm.

Figure *d* shows the Pitot pressure distribution for the cone with a sharp spike $L_s = 60$ mm, the cone with a flat-faced spike $L_s = 95$ mm and the compression corner with the ramp angle $\varphi = 30°$, obtained in previous studies for the same flow parameters in the cross-section $L_{Pt} = 17.3$ mm.

The *HPL* peak of the high-pressure layer is consistent in terms of amplitude and location above the model wall for the cases of compression corner and the cone with a sharp spike. In the case of the cone with a flat-faced spike, the high-pressure layer *HPL* was not detected. Thus, the presence of a high-pressure layer near the point of reattachment of the separated flow has been experimentally confirmed for the axisymmetric case.

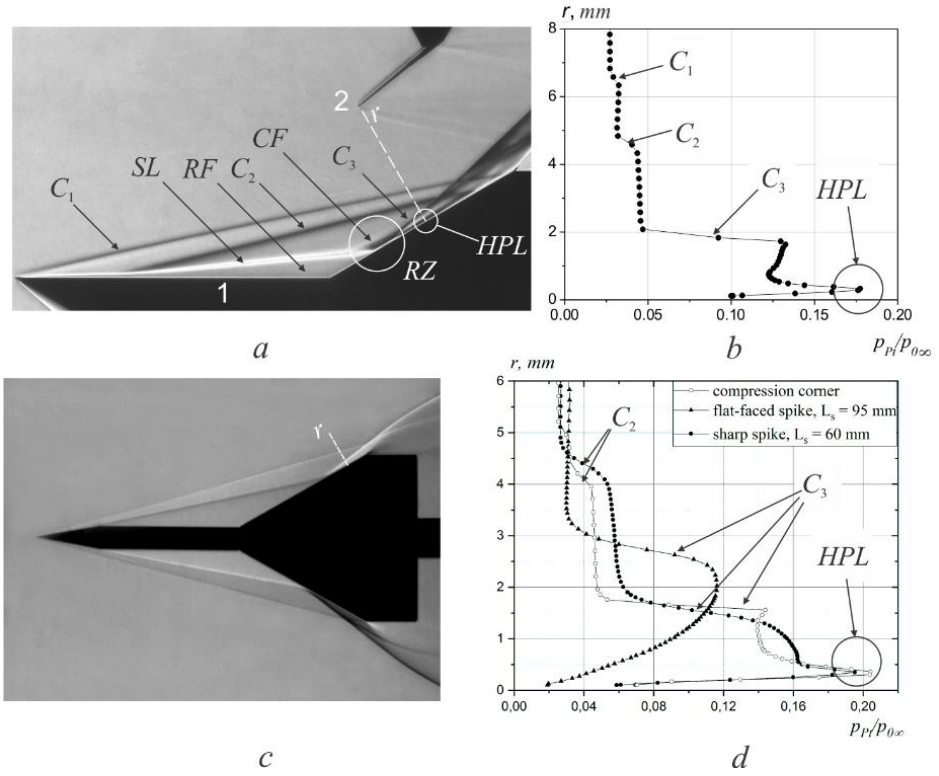

Supersonic laminar separated flow: compression corner flow (*a*), Pitot pressure distribution along the line *r* (*b*), flow past a cone with a sharp spike (*c*), Pitot pressure distribution for the compression corner and the cone with sharp and flat-faced spikes (*d*).

The research was carried out within the state assignment of Ministry of Science and Higher Education of the Russian Federation (project No. 121030500158-0).

REFERENCES

1. **Kavun I.N., Lipatov I.I., Zapryagaev V.I.** Flow effects in the reattachment region of supersonic laminar separated flow // International Journal of Heat and Mass Transfer. 2019. Vol. 129, No. 27. P. 997-1009.
2. **Zapryagaev V.I., Kavun I.N., Trubitsyna L.P.** Reattachment of a Laminar Separated Flow At a Hypersonic Velocity of the Flow // Journal of Applied Mechanics and Technical Physics. 2020. Vol. 61, № 5. P. 710–716.
3. **Chetverushkin B.N., Khankhasaeva Y.V., Lutskii A.E.,** Compact quasi-gas-dynamic system and high performance computing // J. Comput. Appl. Math. 2020. Vol. 375. P. 1–9.
4. **Han G., Jiang Z**. Hypersonic Flow Field Reconfiguration and Drag Reduction of Blunt Body with Spikes and Sideward Jets // International Journal of Aerospace Engineering. 2018. Vol. 2018. Art. 7432961 (16 p.). DOI:10.1155/2018/7432961.
5. **Wood C.** Hypersonic flow over spiked cones // Journal of Fluid Mechanics. 1962. Vol. 12, № 4. P. 614–624.

DOI: 10.53954/9785604788967_201

RESONANT THREE-WAVE INTERACTION OF WAVES IN SUPERSONIC SPATIAL FLOW AROUND A PLATE

R.Ya. Tugazakov

Central Aerohydrodynamic Institute
140180, Zhukovsky, Moscow region, Russia

A theoretical analysis of the laminar-to-turbulent transition in a supersonic gas flow has been carried out. The law of similarity of the burst formation frequency has been confirmed. The spectral flow analysis has indicated that a resonant three-wave interaction was realized in the turbulent boundary layer among the waves. The influence of the plate temperature on the turbulence of the gas flow and the spectral composition of pressure fluctuations have been studied.

Most authors whose works are dedicated to the study of the laminar-turbulent transition in subsonic and supersonic gas flows around a flat plate (Fig. 1), where the results are either obtained experimentally [1] or by numerical simulation [2], seek to confirm the theoretical results discovered in the weakly nonlinear approach. To confirm, in other words, that the greatest nonlinear contribution to the development of unstable perturbations in shear flows should come from the resonant three-wave interaction [3]. The weakly nonlinear approach in the frequency space, though, only describes the occurrence of a gradient catastrophe, which can lead to a transition. The real picture of the transition can be described only in a nonlinear formulation [4]. This is what this work aspires to do, where based on the results of direct numerical simulation of the Navier – Stokes equations, the theoretical results obtained in the framework of a weakly nonlinear model of a developed boundary layer [5] have been confirmed. In addition, one of the main provisions of the developed turbulent boundary layer found in the experiment has also been obtained in the work: the burst formation frequency. Thus, according to Fig. 2 and Fig. 3, it turns out that this frequency is equal to 5.98. The law of similarity is therefore fulfilled.

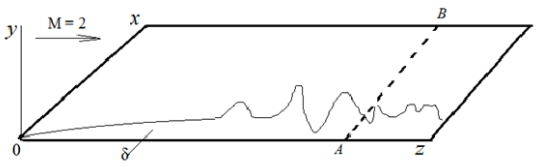

Fig. 1. The pattern of a supersonic flow of a viscous gas around a plate.
Line AB – the boundary of the heat-insulated and cooled parts of the plate.

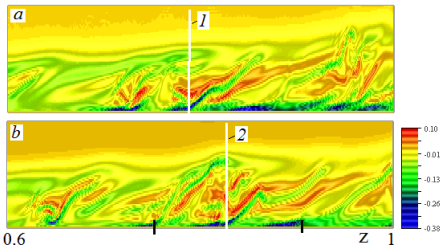

Fig. 2. Burst positions for two moments of time.

The development of the stochastization process can be traced along the spectrum. Figure 4,*a* demostrates a spectrum of pressure fluctuations of a uniformly heated plate with an indication of the relative frequency of the corresponding components. This spectrum confirms to some extent the subharmonic-harmonic transition scenario [3]. Indeed, if we take the frequency $f = 2.934$ as a basis, then the subharmonic frequency close to it is equal to $f = 1.331$. Multiple frequencies are also not difficult to guess. The difference from the exact values can be explained by the excitation of subharmonics in the form of oblique waves, the dispersion dependences of which cause a three-wave resonance at frequencies slightly different from the canonical ones.

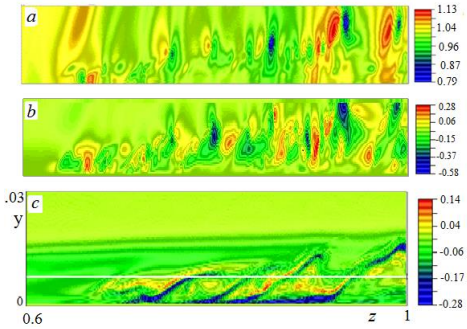

Fig. 3. Flow patterns inside the boundary layer. *a* – pressure field, *b* – normal velocity component, *c* – quasi-periodic ejections of a viscous fluid (bursts) from the near-wall region; the horizontal light line is the average boundary between subsonic and supersonic gas flows.

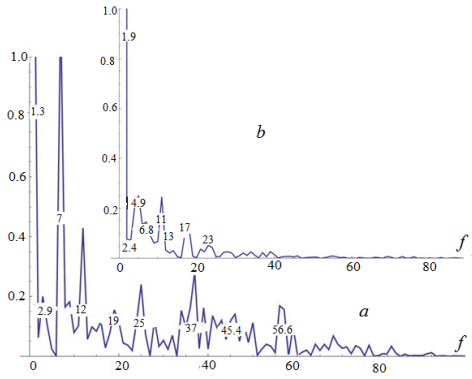

Fig. 4. Spectrum of pressure fluctuations (relative values) in turbulent flow.

The spectrum of pressure fluctuations on the plate has been examined depending on the cooling temperature. It is found that with a change in the plate temperature, the scenario for the development of pulsations is preserved (as subharmonic-harmonic), although the frequency spectrum becomes narrower (Fig. 4,*b*).

Analysis in this work has shown that increased external perturbations at $\mathrm{Re} \approx 10^6$ lead to an unstable state of the viscous sublayer, the rearrangement of which leads to the appearance and rapid growth of the transverse and normal velocity components. As a result, a transition to turbulent flow occurs. The paper formulates the condition under which flow turbulization occurs.

The work was supported by the RFBR grant (No. 20-01-00184).

REFERENCES

1. **Gaponov S.A., Maslov A.A**. Development of disturbances in compressible flows. Novosibirsk: Nauka, 1980. 134 p.
2. **Kudryavtsev A.N., Khotyanovsky D.V.** Direct numerical modeling of the transition to turbulence in a supersonic boundary layer // Thermophysics and Aeromechanics. 2015. Vol. 22. No. 5. P. 559–568.
3. **Kachanov, Y.S**. On the resonant nature of the breakdown of a laminar boundary-layer // J. Fluid Mech. 1987. Vol. 184. P. 43–74
4. **Tugazakov R.Ya.** Three-dimensional turbulent supersonic flow over a plate // Fluid Dynamics. 2019. Vol. 54. № 5. P. 705–713
5. **Zharov V.A.** On the wave theory of a developed turbulent boundary layer // Uch. zap. TsAGI. 1986. Vol. XVII, No. 5. P. 28–38.

DOI: 10.53954/9785604788967_203

STUDYNG OF SUBSTRATE HEATING BY SUPERSONIC JET AT COLD GAS DYNAMIC SPRAYING

S.Yu. Usynin, S.V. Klinkov, V.F. Kosarev

Khristianovich Institute of Theoretical and Applied Mechanics SB RAS
630090, Novosibirsk, Russia

The heat transfer of the jet with the substrate during cold gas-dynamic spraying (CGDS) plays an important role, since heating and cooling of both the substrate and the resulting coating can affect the deposition coefficient residual stresses, and adhesion, ultimately. A small number of published works (see review [1]) devoted to the study of this topic do not fully cover the required amount of knowledge to understand actual situation, which makes this topic relevant. Particularly important are numerical studies, which can significantly reduce the time and means spent on experiments. In addition, the dimensions of the jet streams characteristic for CGDS are small, which additionally complicates the measurement of their heat transfer with obstacles. In this study, the Ansys Fluent package is used to simulate the heat exchange of a jet with a barrier under CGDS conditions, with special attention paid to the temperature distribution in the substrate, the distribution of the stagnation temperature and air velocity in the near-wall jet, and the distribution of surface heat flux.

The main parameters of the problem corresponded to the conditions of practical spraying of a coating from aluminum powder. The supersonic jet was formed using an axisymmetric de Laval nozzle 145 mm long, with diameters of critical and exit section of 2.8 mm and 6.5 mm, respectively. A cylindrical aluminum plate was used as a substrate, which radius and thickness were 20 mm and 5 mm. The substrate axis coincided with the nozzle axis. The nozzle did not move relative to the substrate; thus, a stationary distribution of temperature and velocity was found when the supersonic jet impinged on the substrate. The distance from the nozzle exit to the substrate was 30 mm. Air was used as the working gas. The stated problem is solved in an axisymmetric formulation. The turbulence model k–ω SST was chosen to close the Navier–Stokes equations. Input conditions: air stagnation pressure 3.75 MPa and stagnation temperature 573 K. The jet outflows into the surrounding space with an air pressure of 0.1 MPa and a temperature of 300 K.

The calculation results show that the maximum velocity in the near-wall jet first increases to ~700 m/s at a radius of ~7 mm, and then decreases monotonically to the sonic velocity (~460 m/s) near the edge of the substrate (at the radius of 20 mm). The maximum stagnation temperature in the near-wall jet drops monotonically, reaching ~500 K at the edge of the substrate. The surface heat flux first increases, reaching a maximum value of $\sim 10^6$ W/m^2 at the radius of ~1.5 mm, then drops monotonically to zero at the radius of ~15 mm, and then becomes negative, which indicates that heat escapes from the substrate near its edges.

The temperature of the front surface of the substrate near the axis turns out to be lower than the stagnation temperature (573 K) and lies at the level of ~540 K, and then it decreases monotonically, reaching a value of ~520 K at the edge of the substrate. The temperature of the rear surface of the substrate also decreases monotonically from ~530 K on the axis to the value almost equal to the temperature of the front surface.

REFERENCE

1. **Klinkov S.V., Kosarev V.F., Shikalov V.S.** Evolution of substrate temperature during nozzle movement under cold spraying conditions // Thermophysics and Aeromechanics. 2021. Vol. 28, No. 4. P. 533–548.

DOI: 10.53954/9785604788967_204

EXPERIMENTAL STUDY OF THE REACTION OF A SUPERSONIC BOUNDARY LAYER TO LOCALIZED PULSED HEATING OF THE SURFACE OF A FLAT PLATE

Yu.I. Usynina, Yu.G. Yermolaev, A.A. Yatskikh

Khristianovich Institute of Theoretical and Applied Mechanics SB RAS
630090, Novosibirsk, Russia

In studies of the stability of an incompressible boundary layer, various methods of excitation of controlled disturbances in a shear flow are used: a vibrating tape, blowing-suction, electric discharge, etc. [1]. In a supersonic experiment, the most used method for introducing controlled perturbations is an electric discharge ignited at a high frequency (for example, [2–4]). With its help, the linear theory of hydrodynamic stability for the case of supersonic velocities was experimentally confirmed. Significant progress has also been made in studying the mechanisms of nonlinear interaction and the development of instability waves.

It was noted in [4] that a significant part of the surface discharge energy is transformed into thermal energy in a submillimeter near-surface gas layer in less than 1 μs, which leads to rapid heating of the gas. However, when a low-temperature plasma occurs, a hemispherical shock wave is formed, which contributes to the generation of disturbances from the discharge. There are also other difficulties. Therefore, the aim of the work was: to develop a method for excitation of perturbations of the supersonic boundary layer using pulsed heating of a thin wire located on the surface of a flat plate. Experimentally study the reaction of a supersonic boundary layer to localized pulsed heating.

The studies were carried out in the T-325 low-turbulent supersonic wind tunnel of ITAM SB RAS at Mach number M = 2 and unit Reynolds number $\mathrm{Re}_1 = 8 \cdot 10^6$ m^{-1}. In the experiments, a flat plate with a sharp leading edge was used, which was installed in the working part of the tube at a zero angle of attack. Thermal perturbations were introduced by heating a thin wire located on the surface of a flat plate. Nichrome wire welded on steel electrodes was used. The length of the working part of the wire and its diameter, respectively, were $l_w = 2.1 \pm 0.01$ mm and $d_w = 0.1 \pm 0.01$ mm. The diameter of the electrodes and the distance between them are respectively equal to $d_e = 1.0 \pm 0.01$ mm and $l_{1,2} = 2 \pm 0.01$ mm. The electrodes were located parallel to the incoming flow and were mounted flush with the working surface of the wing. The origin of *x*, *y*, *z* coordinates was set at the electrode farthest from the leading edge. Schematically, the location of the source of pulsed heating is shown in Fig. 1. A photo of the finished source built into the model is shown in Fig. 2.

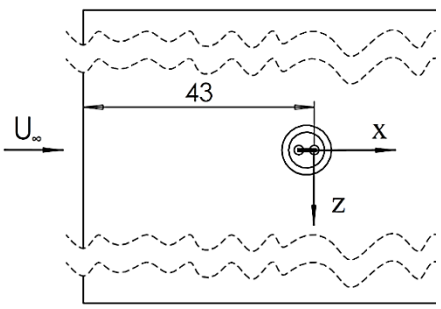

Fig. 1. Location of the source of controlled disturbances. View from above.

Fig. 2. Source built into the model.

Measurements of the average and pulsation characteristics of the flow were carried out using a constant resistance thermoanemometer.

Experimental studies were carried out in the near field from the disturbance source both along the normal to the plate surface and in the transverse direction at x = 10 mm. Thermoanemometric measurements in the cross section along z were carried out both without pulsed heating of the wire and with heating. The measurements showed a weak reaction of the supersonic boundary layer to pulsed heating. Small deviations in the dependences are most likely associated with changes in the flow stagnation temperature during pipe start-up, rather than with pulsed heating. An analysis of oscillograms of fluctuations obtained by the method of synchronous data averaging did not reveal areas where pulsed heating affects the supersonic boundary layer.

Measurements along the normal to the plate surface were carried out only for the case of pulsed heating of the wire at z = 0 mm. The boundary layer at x = 53 mm from the leading edge from the leading edge of the plate has a thickness of about 0.9 mm. The maximum of integral pulsations is located at y = 0.4 mm. For a detailed analysis, oscillograms of the filtered signal were considered.

The research was carried out within the state assignment of Ministry of Science and Higher Education of the Russian Federation (project No. 121030500161-0).

The work was carried out using the equipment of the Equipment Sharing Center "Mechanics" of ITAM SB RAS).

REFERENCES

1. **Boyko A.V., Grek G.R., Dovgal A.V., Kozlov V.V.** Physical mechanisms of transition to turbulence in open flows. M.; Izhevsk, 2006. 304 p.
2. **Kosinov A.D., Maslov A.A., Shevelkov S.G.** Experiments on stability of supersonic boundary layers // J. Fluid Mech. 1990. Vol. 219. P. 621–633.
3. **Casper K.M., Beresh S.J., Schneider S.P.** Pressure fluctuations beneath instability wavepackets and turbulent spots in a hypersonic boundary layer // J. Fluid Mech. 2014. Vol. 756. P. 1058–1091.
4. **Znamenskaya I.A., Latfullin D.F., Lutsky A.E., Mursenkova I.V.** Energy contribution to the near-wall gas layer during the initiation of a nanosecond sliding surface discharge // JETP Letters. 2010. Vol. 36, Iss. 17. P. 35–41.

DOI: 10.53954/9785604788967_206

NUMERICAL SIMULATION OF HELIUM ENRICHMENT FROM AIR-HELIUM GAS MIXTURE USING A BIFUNCTIONAL SORBENT WITH GLASS MICROSPHERES

A.S. Vereshchagin, I.V. Kazanin, V.N. Zinovyev, V.M. Fomin

Khristianovich Institute of Theoretical and Applied Mechanics SB RAS
630090, Novosibirsk, Russia

The membrane-sorption method for separating helium from mixtures is a new approach proposed by the author (in co-authorship) of this work [1; 2]. The essence of the method is the use of microspheres, which are closed microspherical membranes, selectively permeable to helium and practically impermeable to other gases. Under the influence of the difference in helium partial pressures inside and outside the microspheres, helium is selectively absorbed by them into the internal cavity and can be extracted from them by creating a reverse partial pressure gradient [3]. As a sorbent, a bifunctional sorbent with a matrix of pseudoboehmite with the inclusion of microspheres can be used [4].

To describe the flow of an air-helium mixture over a porous layer of granular sorbent, a mathematical model [5, 6] is used, which consists of convective and diffusion parts. The convective part is a classical model of a multiphase medium, described by the equations of the laws of conservation of mass, momentum and energy for a mixture of gases (air and helium) and a granular stationary medium. The diffusion part of the model describes the diffusion of gases in a cylindrical adsorbent particle, taking into account the absorption of helium by the microspheres it contains. To simulate the mass flows of helium and air between the granules and the free volume of the adsorber, the flow of gases absorbed / released by the particles of the adsorbent in the vicinity of each point of the adsorber is determined. As a result, at each point of the adsorber, it is necessary to solve the problem of diffusion of air and helium into some "isolated" cylindrical adsorbent particle. The total flow is calculated by multiplying the obtained flow for the "isolated" particle by the average volumetric content of adsorbent particles in the vicinity of the considered point.

As part of the current study, the problem of pumping out an adsorber filled with an air-helium mixture at a pressure of 3.15 atm with a volume content of helium of 5 % (approximately 0.7 % by weight) is considered. It is assumed that the process of initial preparation of the mixture in the adsorber led to the fact that the same ratio of air to helium is contained in the porous skeleton of the granular adsorbent, and the microspheres are filled with helium to their limiting equilibrium value (for the conditions under consideration). The results of numerical simulation are shown in Figs. 1, 2. For various initial temperatures of the adsorber (20, 30, 60, 75, 90, 120 °C), the instantaneous helium concentration in the outlet section (Fig. 1,*b*) was obtained and

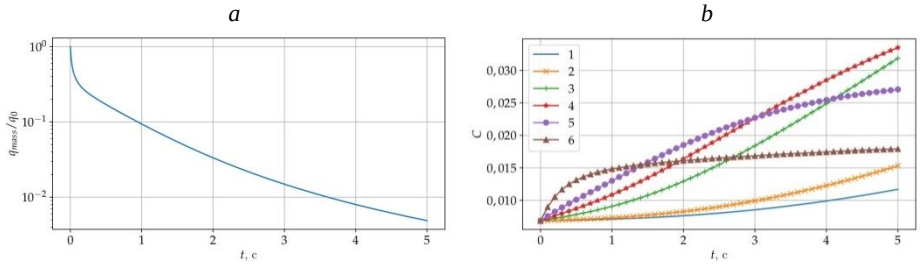

Fig. 1. Mass flux (*a*) and helium mass concentration (*b*) at the outlet of an adsorber for various initial temperatures.
1 – 20 °C; *2* – 30 °C; *3* – 60 °C; *4* – 75 °C; *5* – 90 °C; *6* – 120 °C.

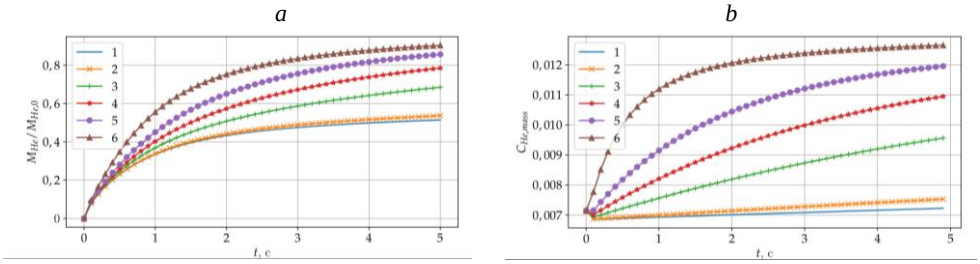

Fig. 2. Helium recovery ratio (*a*) and helium mass concentration (*b*) in the mixture taken from the adsorber for various initial temperatures.

1 – 20 °C; *2* – 30 °C; *3* – 60 °C; *4* – 75 °C; *5* – 90 °C; *6* – 120 °C.

the instantaneous mass flow rate normalized to its initial value (Fig. 1,*a*). Fig. 2,*a* shows a dependence of the degree of helium extraction versus time for various temperatures. Figure 2,*b* shows a dependence of the mass concentration of helium in the mixture taken from the adsorber. The simulation of the enrichment phase in the short cycle adsorption (PSA) method using a bifunctional sorbent based on microspheres showed the possibility of increasing the helium concentration in the air-helium mixture by almost two times (from 0.7 to 1.3 % by weight) at a helium recovery ratio of 90.4 %.

This work was supported by Russian Foundation for Basic Research and Government of Novosibirsk State [grant No. 20-41-540002] and Program of Fundamental Scientific Research of the state academies of sciences [registration No. 121030900260-6].

REFERENCES

1. **Patent** No. 2508156 RF. Method of multicomponent gas-vapor mix separation / Fomin V.M., Zinovyev V.N., Kazanin I.V., Lebiga V.A., Pak A.Yu., Vereshchagin A. S., Fomina A. F., Anshits A.G., Buluchevskii E.A., Lavrenov A.V. Appl. 2012118350/05, Date of filing: 03.05.2012. Date of publ.: 27.02.2014. Bull. No. 6.
2. **Patent** No 2291740 RF. System and the method for separation of the gas mixture / Fomichev V.P., Fomin V.M., Puzyrev L.N., Dolgushev S.V., Vereshchagin A.S., Anshits A.G. Appl. No 2005105093/15. Date of filing: 24.02.2005. Date of publ.: 20.01.2007. Bull. 2.
3. **Vereshchagin A.S.** Glass Spheres for Solar Gas // Science First Hand. 2010. Vol. 27. No 3. P. 44–49.
4. **Zinovyev V.N., Kazanin I.V., Lebiga V.A., Pak A.Yu., Vereshchagin A.S., Fomin V.M.** Co-extraction of water vapor and helium from natural gas // Thermophysics and Aeromechanics. 2016. Vol. 23, No. 5. P. 741–746. DOI: 10.1134/S0869864316050127.
5. **Vereshchagin A.S., Zinovyev V.N., Kazanin I.V., Pak A.Y., Lebiga V.A., Fomin V.M..** Model of helium and water vapor adsorption by a microsphere-based porous composite sorbent // Doklady Physics. 2020. Vol. 65, No. 2. P. 46–50. DOI: 10.1134/S1028335820020093.
6. **Vereshchagin A.S.** Accounting for resistance and temperature in a flow of a vapor-helium mixture through a layer of a porous composite sorbent based on microspheres // Journal of Applied Mechanics and Technical Physics. 2021. Vol. 62, No. 2. P. 245–254. DOI: 10.1134/S0021894421020085.

DOI: 10.53954/9785604788967_208

APPLICATION OF CONTINUOUS HIGH-SPEED SHOOTING UNDER CONDITIONS OF VARIABLE FREQUENCY OF PULSATING OPTICAL DISCHARGE PLASMA

M.A. Yadrenkin, T.A. Gimon, V.B. Shulyatiev, V.I. Yakovlev

Khristianovich Institute of Theoretical and Applied Mechanics SB RAS
630090, Novosibirsk, Russia

In contrast to the thermal action of laser radiation, the mechanisms of action of high-enthalpy and high-velocity plasma microjets during optical breakdown are currently less studied. The aim of this work is to obtain experimental data on the plasma structure in an optical discharge with absorption of repetitively pulsed (40 kHz) CO_2 laser radiation, an average power of 1.6 kW [1]. In the experiment, the dynamics of the glow of the plasma of an optical repetitively pulsed discharge in a subsonic (200 m/s) argon flow was recorded by the method of continuous high-speed shooting with a FASTCAM SA-Z (Type 480K) camera. The main difficulty was that the time interval between radiation pulses (respectively, between breakdowns) varied within (0–1 μs) randomly due to the use of a mechanical modulator in the laser design. Therefore, different stages of the breakdown process can be recorded at a fixed sampling rate.

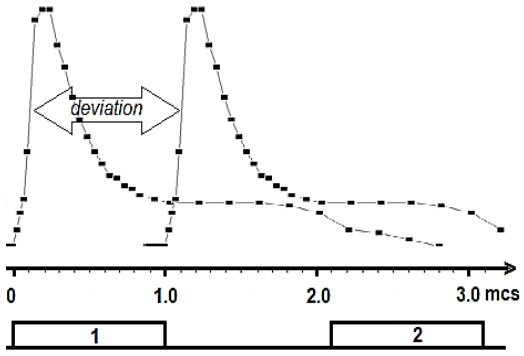

Fig. 1. Registration conditions: variation in the appearance of absorbed energy profiles relative to frames.

The experimental conditions are illustrated in Fig. 1, where two maximum possible positions of the pulse profile of the absorbed radiation energy are presented on the time scale relative to the frames where the plasma glow first appears after the previous breakdown. Intermediate positions of the pulse are also possible in the indicated interval of their deviation. The frame repetition period is 2.083 μs at a shooting frequency of 480,000 fpc, the exposure time is 1 μs. In the experiment, one breakdown corresponded to 5–6 frames with luminescence; in subsequent frames, the luminescence strongly weakened and was not observed by the time of the next breakdown. It can be seen that different stages of breakdown can be recorded in the first frame, from the initial one (profile on the right) to breakdown after the maximum of absorbed energy (profile on the left). Correspondingly, various patterns of plasma glow will be recorded. Typical experimental results selected from the data array (2500 shots, 400 breakdowns) are shown in Fig. 2. Three characteristic samples I, II and III were used, of which data I and III correspond to the above positions of the profiles in Figs. 1, and sample II corresponds to an intermediate position between them. Each of them presents a sequence (from top to bottom) of 5 frames, with the appearance of a glow in the first frame. After the end of the first frame, the time interval for recording the 2nd frame is Δt_2 = 1.083–2.083 μs, and then, respectively: Δt_3 = 3.166–4.166 μs, Δt_4 = 5.25–6.25 μs, and Δt_5 = 7.33–8.33 μs. In all cases, on subsequent second frames (2nd row in Fig. 2), the plasma glow is recorded closer to the end of the absorption pulse, and on the third, etc. – already in the absence of a laser radiation flux.

The approach used in data analysis made it possible to reveal the characteristic structure of the plasma at an early stage of breakdown. In its initial stage, in the first frame (Fig. 2, pos. I and

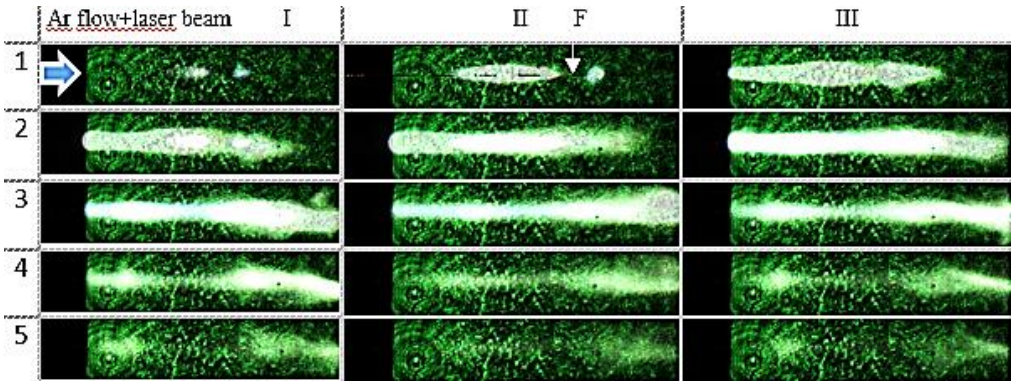

Fig. 2. Plasma glow dynamics.

The length from the edge of the channel to the end of the frame is 11.5 mm.

II), for the most part, two glow zones (two-point or extended-point) are observed on both sides of the beam focusing point *F*. At the same time, the second (downstream) zone, with very rare exceptions, is a "point", while the first (upstream) is extended. The distance between the glow zones varies within 0–1.0 mm. Thus, for the first time, a two-lobe structure of the initial stage of breakdown was revealed for the radiation of a CO_2 laser, which indicates the passage of radiation through the primary breakdown plasma, as in the region of short wavelengths [2–5]. Previously, it was assumed that long-wave radiation is absorbed more strongly and does not pass through the plasma beyond the focus point. Therefore, such an effect was not observed in studies with TEA CO_2 laser radiation, since the breakdown was carried out on the target surface due to the laser radiation intensity below the breakdown threshold in the gas. It is also determined that the average displacement velocity of the plasma glow core (of the order of 1–2 km/s) is 4–5 times higher than the flow velocity. Later (frames 4 and 5), the glow weakens and these two luminous regions separate with the destruction of the extended plasma structure. Based on the displacement of individual luminous fragments and the time interval between frames, it is determined that their speed approaches the flow velocity.

REFERENCES

1. **Malov A., Orishich A., Shulyatyev V.** High-power repetitively pulsed CO2 laser with mechanical Q-switching and its application to studies in aerodynamic installations // Quantum Electronics. 2011. Vol. 41. P. 1027–1032.
2. **Mori K., Komurasaki K., Arakawa Y.** Influence of the focusing f number on the heating regime transition in laser absorption waves // J. Appl. Phys. 2002. Vol. 92, No. 10. P. 5663–5667.
3. **Mori K., Komurasaki K., Arakawa Y.** Threshold laser power density for regime transition of a laser absorption wave in a reduced-density air atmosphere // Appl. Phys. Lett. 2006. Vol. 88. Art. 121502. (3 p.) doi.org/10.1063/1.2183812.
4. **Ushio M., Komurasaki K., Kawamura K. et al.** Effect of laser supported detonation wave confinement on termination conditions // Shock Waves. 2008. Vol. 18. P. 35–39.
5. **Shimamura K., Ofosu J.A., Komurasaki K, Koizumi H.** Predicting propagation limits of laser-supported detonation by Hugoniot analysis // Jpn. J. Appl. Phys. 2014. Vol. 54, No. 1. P. 016201.

DOI: 10.53954/9785604788967_210

FEATURES OF HIGH-SPEED MICROPARTICLES FLOW ACCELERATED BY RAILGUN

M.A. Yadrenkin, R.E. Tyustin

Khristianovich Institute of Theoretical and Applied Mechanics SB RAS
630090, Novosibirsk, Russia

Modification of the surface layer of solid bodies using a high-speed flow of microparticles is an urgent and significant task, the solution of which will allow obtaining new properties of materials used, for example, to create working surfaces of metalworking tools or the mining industry. One of the promising ways to accelerate microparticles is the use of a electrodunamic accelerator (railgun), which makes it possible to achieve high velocities of bodies up to 5 km/s and higher. Usually in the case of acceleration of microparticles in an electrodynamic or electrothermal accelerator [1–3], as in the case of using the detonation and cumulative deposition method [4], particles interact with combustion products or plasma, which can lead to a significant change in their temperature, chemical composition and even aggregate state. Therefore, there is a need to improve the methods of acceleration of particles in order to save their initial state. This paper presents a method for accelerating a powder sample of microparticles of heavy metals and alloys placed in a dielectric container, which excludes their interaction with a heated gas up to a collision with a target.

Figure 1 shows the principal scheme of the experiment. The acceleration of the container *1* with microparticles *2* occurs in the channel of the railgun, which has a square cross section and consists of two conductive (rails) *3* and two dielectric walls. When a large current pulse *4* is applied to the rails, a plasma armature appears *5*, which exerts pressure on the accelerated object under the action of the Ampère force in the induced magnetic field (Fig. 1,*b*). At the moment of acceleration, the particles are enclosed in a dielectric polycarbonate container, so their contact with the plasma armature is excluded. We used microparticles of tungsten and tungsten carbide with a diameter of 9 to 30 μm. When the container approaches the target *6*, it collides with the cutter *7*, which is a steel blunted cone with a cylindrical hole. After stopping and destroying the container, most of the powder continues its movement in the direction of the target by inertia (Fig. 1,*c*). The target, a cylinder made of instrument steel, was located at a distance of 20 mm from the cutter, so the drop in velocity due to the aerodynamic drag of the particles is negligible. The process under study was recorded using a Photron SA-Z camera with a frequency of 240 kHz. This made it possible to determine the speed of the front of a dense two-phase flow of microparticles (700–1600 m/s), as well as to observe the process of their interaction with the surface.

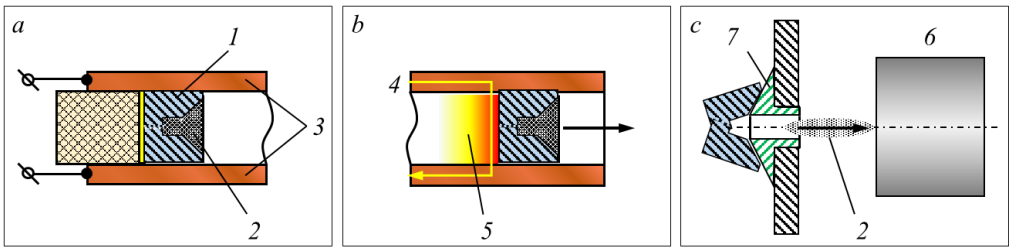

Fig. 1. Scheme of the experiment.

1 – container, *2* – microparticles, *3* – rails, *4* – current pulse, *5* – plasma armature, *6* – target, *7* – cutter.

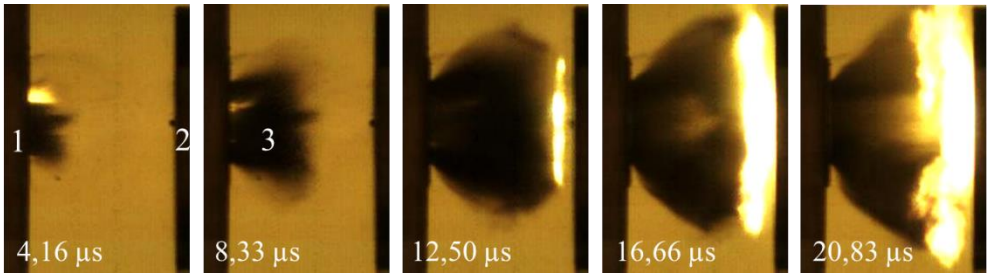

a *b* *c* *d* *e*

Fig. 2. Process visualization of micropowder impact with target surface.
1 – cutter outlet section, *2* – target, *3* – microparticles flow.

An experimental study of the interaction of a microparticles swarm with a target was carried out at atmospheric air pressure; therefore, a significant effect of gas-dynamic processes on the structure of an essentially two-phase flow was found on video frames. In particular, it was shown, that the particle flow expands significantly after exiting the cutter channel (Fig. 2,*a–d*). In some cases, it was found, that when microparticles are closed to the target, there is a sharp drop in velocity and an increase in the particle concentration along a certain boundary located parallel to the target surface (Fig. 2,*c*). It is noted, that in the case when the stagnation temperature of the gas flow exceeds the oxidation temperature of the particle material, a bright flash is observed in the region of this conditional boundary (Fig. 2,*c–e*). In this case, the frames clearly show that at this moment no interaction of microparticles with the target surface is observed. Probably, this effect is associated with the interaction of particles and the reflected shock wave formed as a result of air acceleration in the cutter channel in front of the moving volume of micropowder. Then the flow of microparticles reached the surface of the model and the expansion of the powder from the place of interaction was observed. Craters with a non-standard asymmetric shape were found in the target surface, which clearly differs from the case of plastic deformation at the classical collision of a macroimpactor with a solid body. Thus, the process of interaction between the flow of microparticles and the target material can be represented in the hydrodynamic approximation.

The developed method for accelerating microparticles made it possible to realize high speeds of particle-target collisions. However, the description of the process requires taking into account the gas and hydrodynamic effects both before the collision and during the interaction.

REFERENCES

1. **Lazarenko B.R.** Acceleration of gas-discharge plasma powder particles and their interaction with a solid body // Electronic Processing of Materials. 1973. No. 5(53). P. 31–33.
2. **Gasin D.A., Grishin S.D., Leskov L.V., Kozlov N.P.** Plasma accelerators. Moskow: Mashinostroenie, 1983. 226 p.
3. **Shcolnikov E.Ya., Chebotarev A.V. et al.** Acceleration of powder materials in an electrothermal launcher // IEEE Transactions on Magnetics. 1995. Vol. 31. P. 758–763.
4. **Andilevko S.K., Shilkin V.A., Usherenko S.M., Romanov G.S.** Specific features of mass transfer of discrete microparticles in the process of metallic target treatment with a powder flux // International Journal of Heat and Mass Transfer. 1993. № 4(36). P. 1113–1124.

DOI: 10.53954/9785604788967_212

TURBULENCE DEVELOPMENT IN STABLY STRATIFIED FLOWS WITH PYCNOCLINE AND OROGRAPHY

S.N. Yakovenko

Khristianovich Institute of Theoretical and Applied Mechanics SB RAS
Novosibirsk 630090, Russia

The study is intended to explore the turbulence development scenarios in a stably stratified fluid with the breaking lee wave generated by orography. Zones of strong orographic turbulence arise with certain free-stream and relief parameters. Exploration of these zones is of interest for solving the problems of meteorology and aviation security: hundreds of cases of intense clear-air turbulence, often associated with breaking internal waves, are recorded annually.

The breaking lee waves above the obstacle of height h in a stably stratified flow with constant inflow velocity U is studied by DNS and LES. Ranges of Froude numbers $F_h = U/(Nh)$, where N is Brunt–Väisälä frequency based on the inflow density gradient, Reynolds numbers, $50 \le \mathrm{Re}\ (= Uh/\nu) \le 4\times10^4$, relate to tank measurements. Prandtl or Schmidt numbers correspond to natural and laboratory conditions ($1 \le \mathrm{Pr} \le 2000$). The case of Re = 4000, Pr = 1 was tested in [1, 2]. The density field instability arising after wave overturning reveals a range of spanwise spectra modes. The $\lambda_y \sim 0.5h$ mode represents Rayleigh–Taylor instability with periodic convective structures. At late transition times, larger vortices appear with the dominant mode $\lambda_y \sim 2.5h$ when the large-scale toroidal structures become evident in computations and experiments [2–4].

The present study also considers the lee wave overturning region for various obstacle shapes and initial density distributions, e.g. constant-gradient or step-like one with pycnocline (Figs. 1 and 2) which can occur for internal waves and bores over the shelf [5], and examines the effects of F_h, Re, Pr and the density distribution on the routes of transition to turbulence.

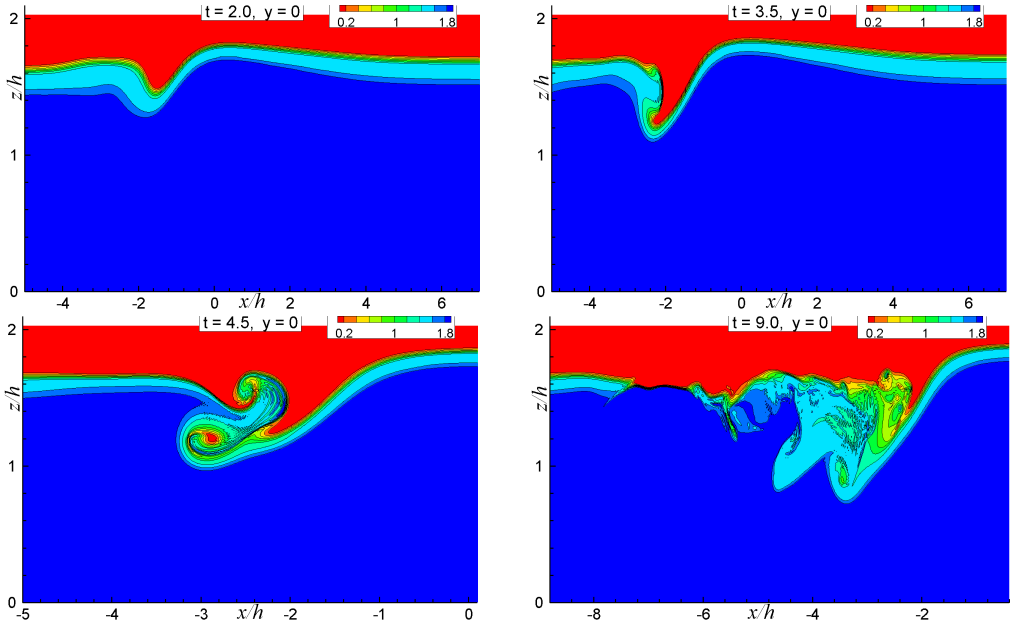

Fig. 1. Density field evolution for $y = 0$ in a flow above a triangular hill at $F_h = 0.19$, Pr = 2000, Re = 783.

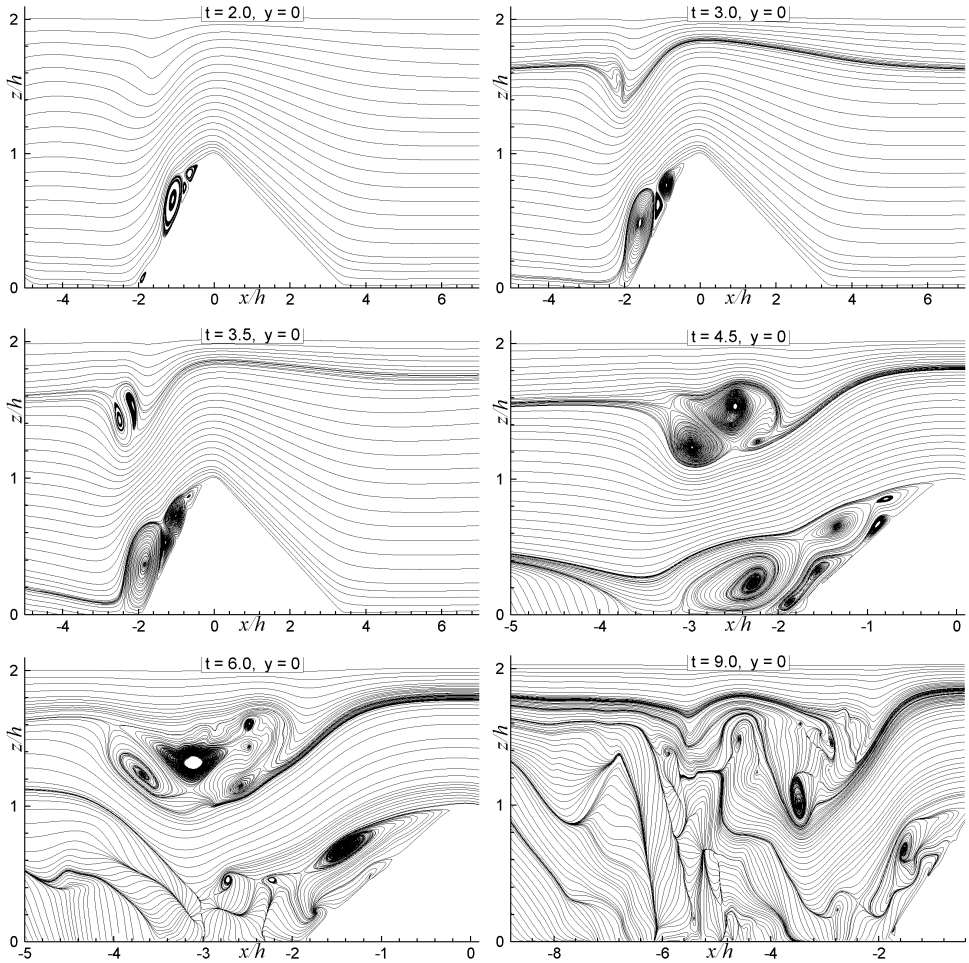

Fig. 2. Streamlines for $y = 0$ in a flow above a triangular hill at $F_h = 0.19$, Pr = 2000, Re = 783.

A studied flow (see Figs. 1 and 2) is above the triangle-like obstacle, which shape has straight sides of different angles to the horizontal plane and the semicircle fragment between them. The flow blockage is quite large: the open channel height is $D = 2h$. The initial density distribution has multiple layers of constant density values and gradients like the pycnocline in oceans, Pr = 2000 relates to sugar solution in water, and $F_h = 0.19$ is based on the density drop in the pycnocline.

The research was carried out within the state assignment of Ministry of Science and Higher Education of the Russian Federation (project No. 121030500149-8).

REFERENCES

1. **Yakovenko S.N., Thomas T.G., Castro I.P.** A turbulent patch arising from a breaking internal wave // J. Fluid Mech. 2011. Vol. 677. P. 103–133.
2. **Yakovenko S.N., Thomas T.G., Castro I.P.** Transition through Rayleigh–Taylor instabilities in a breaking internal lee wave // J. Fluid Mech. 2014. Vol. 760. P. 466–493.
3. **Yakovenko S.N.** Lee wave breaking region: the map of instability development scenarios // Journal of Physics: Conference Series. 2017. Vol. 894. Art. No. 012112.
4. **Eiff O.F., Bonneton P.** Lee-wave breaking over obstacles in stratified flow // Phys. Fluids. 2000. Vol. 12. P. 1073.
5. **Liapidevskii V.Yu., Novotryasov V.V., Khrapchenkov F.F., Yaroshchuk I.O.** Internal wave bore in the shelf zone of the sea // J. Appl. Mech. Tech. Phys. 2017. Vol. 58. P. 809–818.

DOI: 10.53954/9785604788967_214

EXPERIMENTAL STUDY OF ADAPTIVE WING MECHANIZATION WITH TANGENTIAL JET BLOWING

V.S. Zamaraev, A.A. Krutov, A.V. Petrov, E.A. Pigusov

Central Aerohydrodynamic Institute
140180, Zhukovsky, Moscow region, Russia

The main way to increase the load-bearing characteristics of aircraft is the use of take-off and landing wing mechanization. The experience of using a single-slotted flap of the Fowler type on mainline passenger airliners along the trailing edge of the wing revealed the need to simplify the design of the wing mechanization while maintaining its effectiveness, which led to the implementation of adaptive wing mechanization, in which a rotary flap and a downward deflecting spoiler are used [1, 2]. However, when the flap is deflected at large angles, a significant downward deflection of the spoiler is also required to ensure the required high values of the lift coefficient. As a result, a separation of the flow occurs on the upper surface of the tail part of the wing due to a sharp increase in curvature, which reduces the effectiveness of the wing high lift devices. In [3, 4], to increase the efficiency of adaptive wing mechanization, active flow control using jet vortex generators was proposed. As a result of using this method, it is possible to suppress the flow separation on the deflected down spoiler and increase the bearing characteristics of the wing.

The authors of this paper consider an alternative solution for suppressing the flow separation on the spoiler surface and increasing the load-bearing characteristics of wing high lift devices using of boundary layer control (BLC) by tangential jet blowing from a slot nozzle on a spoiler deflected down. This paper presents the results of experimental studies of a regional aircraft model with adaptive wing mechanization with BLC in the T-104 TsAGI wind tunnel.

In the design of the model, the possibility of conducting studies of the effect of tangential jet blowing on the aerodynamic characteristics of adaptive wing mechanization is realized. The tangential jet blowing on a spoiler deflected by an angle $\delta_S = 16°$ is investigated for two variants of deflection of the inner flap $\delta_F = 36°$ and $\delta_F = 45°$. The external flaps and spoiler in all studied configurations were set to the position $\delta_F = 36°$ and $\delta_S = 10°$. The velocity of the incoming flow in the wind tunnel was 65 m /s, which corresponds to the value of the Reynolds number of $Re \approx 2 \cdot 10^6$, calculated from the average aerodynamic chord of the wing. The momentum coefficient of the blown jet varied in the range $C\mu = 0 \div 0.1$.

It is shown that the tangential jet blowing on the upper surface of the spoiler with an intensity of $C\mu = 0.1$ makes it possible to increase the lift coefficient of the wing with the flap deflected by an angle of $\delta_F = 36°$ by the value of $\Delta C_L \approx 0.2$ in the entire studied range of angles of attack $\alpha = 3 \div 15°$. At the same time, the maximum lift coefficient of the wing increases from 2.4 to 2.6 and, accordingly, the critical angle of attack increases from 12 ° to 15°. Blowing on the spoiler with intensity $C\mu = 0.1$ on a wing with an inner flap deflected by an angle $\delta_F = 45$ °, increases the lift coefficient by the value of $\Delta C_L \approx 0.4 \div 0.35$ at angles of attack $\alpha = 3 \div 5$ ° and the maximum lift coefficient from 2.3 to 2.6

The results obtained indicate the effectiveness of the use of adaptive wing mechanization with tangential jet blowing to increase the bearing properties of the wing during takeoff and landing flight modes.

REFERENCES

1. **Reckzeh D.** Multifunctional wing moveables: design of the A350XBW and the way to future concepts // Proc. of 29th Congress of the International Council of the Aeronautical Sciences (ICAS 2014): ICAS 2014-0133. 2014. https://icas.org/ICAS_ARCHIVE/ICAS2014/data/papers/2014_0133_paper.pdf.
2. **Henning S.** The aerodynamic design of the A350 XWB-900 high lift system // Proc. of 29th Congress of the International Council of the Aeronautical Sciences (ICAS 2014): ICAS 2014-0298. 2014. https://icas.org/ICAS_ARCHIVE/ICAS2014/data/papers/2014_0298_paper.pdf.
3. **Radespiel R., Burnazzi M., Casper M., Scholz P.** Active Flow control for high lift with steady blowing // The Aeronautical Journal. 2016. Vol. 120, Special Issue 1223. P. 171–200. https://doi.org/10.1017/aer.2015.7.
4. **Scholz P., Mahmood S.S., Casper M., Wallin S., Skoogh D., Addenk S.** Design of Active Flow Control at a Drooped Spoiler // Proc. of 31st AIAA Applied Aerodynamics Conference: AIAA 2013-2518.2013. https://doi.org/10.2514/6.2013-2518.

DOI: 10.53954/9785604788967_216

METHOD OF PRESSURE AVERAGING OVER TIME FOR COMPARISON OF NUMERICAL RESULTS WITH EXPERIMENTAL DATA FOR NONSTATIONARY COMBUSTION IN A SUPERSONIC FLOW

V.P. Zamuraev, A.P. Kalinina

Khristianovich Institute of Theoretical and Applied Mechanics SB RAS
630090, Novosibirsk, Russia

Numerical simulation of unsteady combustion in a supersonic flow is an economical and safe alternative to experiment. However, a comparison between the numerical simulation results and the experiment one is not an easy task. Among the reasons, one can mention a rather long duration of the process, as well as the several spatial and temporal scales that differ by an order of magnitude. All this caused the various simplifications in numerical simulation such as modifications of the system geometry, or consideration a very small interval of the duration of real modeled process, or modeling of a small part of the system only. Therefore, it is difficult to compare the results of experiment and calculation. However, data comparison can be performed in some cases at the condition which are taking into account in the numerical simulation the most important properties of the real process.

The initiation of combustion in a supersonic flow when it is throttled by a jet of compressed air was considered in this paper. A feature of the process under consideration is the predetonation nature of combustion, as noted by the authors of the experiments [1, 2]. Numerical results confirm that the combustion front moves along with the shock wave front. However, the pressure distributions presented in the experiment have the form of smooth curves. It is possible to resolve such a contradiction using knowledge or hypotheses about the instantaneous properties of the process. The experimental pressure distributions at the stage of combustion initiation at Mach numbers M = 1.7 and M = 2 was analyzed in the paper. Combustion was initiated in a channel of variable cross section. The simulated system is shown in Fig. 1.

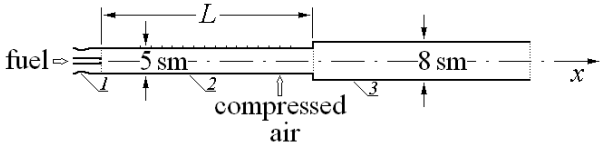

Fig. 1. The channel scheme.

1 – the nozzle block with an axial injector, *2* – the first section with a constant cross section, *3* – a section with a sudden expansion.

A Laval nozzle was disposed at the entrance to the channel for creation a flow with the required Mach number. A channel part of constant cross section was adjoined to the nozzle. Gaseous hydrocarbon fuel flows out through the injector at the beginning of the section of constant section. An annular slot was disposed downstream to the injector. Compressed air enters to the channel through the slot. The shock wave caused by the jet of compressed air was initiated combustion. The amount of fuel supplied was limited by the requirement that the flow must remain transonic.

Numerical simulation of this process was carried out. The problem was solved in the framework of a non-stationary axisymmetric formulation based on the Reynolds-averaged Navier – Stokes equations closed by the k–ε turbulence model [3]. Chemical kinetics was modeled by one gross reaction. As a result of numerical simulation, it was found that the combustion front propagates upstream with a constant speed. The combustion front propagated directly

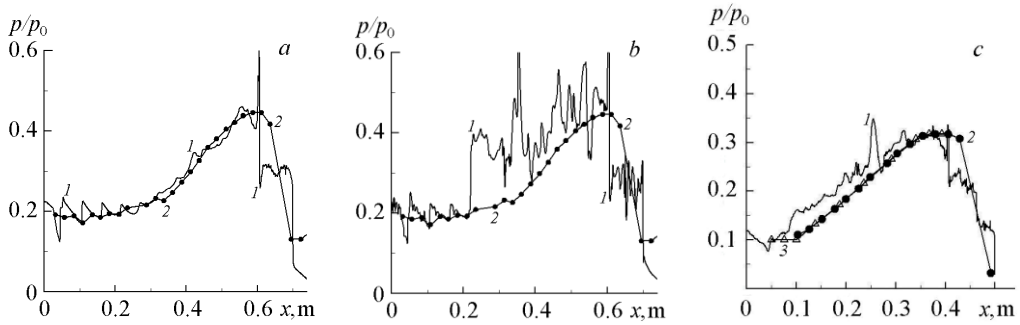

Fig. 2. Pressure distribution along the channel length.

a – M = 1.7: *1* – numerical simulation (averaged one), *2* – experiment one [2];
b – M = 1.7: *1* – numerical simulation (instantaneous one), *2* – experiment [2];
c – M = 2: *1* – numerical simulation (averaged one), *2* – the experiment simulation [2] (•),
3 – analytical simulation (△).

behind the shock wave, so that the instantaneous pressure distribution near the combustion front is actually a "step" in this case.

The analytical model of the process is a "pressure step" moving upstream with a constant velocity. It is shown that if the pressure in the "step" coincides with the maximum pressure in the experiment, and the boundaries of the averaging interval evaluating from the spatial features of the flow (the position of the "step" in the analytical and numerical instantaneous distributions) coincide with the appearance of pressure gradients on the experimental graph, then the experimental, numerical and analytical pressure distributions coincide with good accuracy (Fig. 2).

The coincidence of the experimental distributions pressure with numerical one leads to the two conclusions: the combustion front propagates upstream with a constant velocity, and the velocity of the combustion front propagation upstream in the laboratory reference system is 0.75 m/s (the velocity can be calculated from the analytical model of combustion), which corresponds to the pre-detonation combustion regime.

The study was performed within the framework of the program of fundamental scientific research of the state academies of sciences in 2021–2023 (project No. 121030500157-3) and with the financial support of the Russian Foundation for Basic Research (grant No. 20-08-00245).

REFERENCES

1. **Tretyakov P.K.** Organization of effective combustion of kerosene in a channel at high flow velocities // Combustion, Explosion and Shock Waves. 2020. Vol. 56, No 1, P. 36–40.
2. **Tretyakov P.K., Tupikin A.V., Zudov V.N.** Kerosene combustion in a pseudoshock with varied conditions at the supersonic ramjet combustor model // Combustion, Explosion and Shock Waves. 2021. Vol. 57, No. 6, P. 635–639.
3. **Zamuraev V.P., Kalinina A.P.** Modeling of kerosene combustion in a supersonic flow under the action of a throttling jet // Journal of Applied Mechanics and Technical Physics. 2020. Vol. 61, No. 5. P. 763–768.

DOI: 10.53954/9785604788967_218

MATHEMATICAL MODEL OF THE FLOW AROUND A NANOFIBER IN A PERIODIC CELL

S.K. Zaripov, R.F. Mardanov, V.F. Sharafutdinov

Kazan Federal University
420008, Kazan, Russia

Aerosol filters, consisting of a packing of cylindrical microfibers, are used in industrial and living rooms for air cleaning. Along with this, so-called fine filters are used, consisting of nanofibers, the cross-sectional size of which is an order of magnitude smaller than the size of microfibers. Nanofiber filters have lower aerodynamic drag and can provide better particulate capture. The air flow model around the fibers of aerosol filters is determined by the Knudsen number $\mathrm{Kn} = l / r_c$, that is the ratio of the mean free path of molecules l to the radius r_c of the fiber circular section. For nanofibers, in the case of small Knudsen numbers $\mathrm{Kn} < 0.1$, the study of the flow of a viscous fluid around the nanofiber can be carried out, remaining within the framework of continuum mechanics, with a slip condition on the fiber surface instead a non-slip condition [1]

$$v_\tau = \lambda \tau_{12}, \tag{1}$$

where v_τ is the tangential velocity component of the gaseous medium, τ_{12} is the tangential stress component on the solid surface, λ is then proportionality coefficient.

The main quantity determined when calculating the hydrodynamics of flow in a porous medium of a fibrous filter is the aerodynamic drag force F. Experiments for filters with nanofibers [2] showed that the value of F^{-1}, the inverse quantity to the drag force, linearly depends on the Kn number. At the same time, the generally accepted model of fluid flow with the slip boundary condition (1) does not provide the linearity of the dependence $F^{-1}(\mathrm{Kn})$. It was shown in [3] that the experimental results are in good agreement with the tangent to the calculated dependence $F^{-1}(\mathrm{Kn})$ drawn at the point $\mathrm{Kn} = 0$. Thus, the developed models of flow around nanofibers with condition (1), strictly speaking, do not correspond to experimental data.

We propose a new boundary condition on the surface of nanofibers that establishes a relationship between the tangential velocity component v_τ and the flow vorticity ω

$$v_\tau = \lambda \omega. \tag{2}$$

It is shown that condition (2) provides invariance with respect to the transformation of the coordinate system, in contrast to condition (1). Within the framework of the Kuwabara cell model with a circular fiber [4], an analytical solution to the problem of flow past a nanofiber with condition (2) was obtained. The function $F^{-1}(\mathrm{Kn})$ calculated with the new slip boundary condition (2) is linear. Based on the boundary element method [5], the drag force of nanofibers was calculated for a rectangular periodic hydrodynamic cell, which more accurately models the flow of a viscous fluid in a fibrous porous medium. A series of calculations has been carried out for fibers with different cross-sectional shapes in the case of regular and chess order packing. In all cases, it was confirmed that the new boundary condition provides the linearity of the dependence $F^{-1}(\mathrm{Kn})$. For all calculated cases, approximate dependences for $F^{-1}(\mathrm{Kn})$ are derived.

The study was supported by the Russian Science Foundation grant No. 22-21-00176, https://rscf.ru/project/22-21-00176/

REFERENCES

1. **Pich J.** Pressure drop of fibrous filters at small Knudsen numbers // The Annals of occupational hygiene. 1966. Vol. 9. P. 23–27.
2. **Kirsch A.A., Stechkina I.B., Fuchs N.** Effect of gas slip on the pressure drop in fibrous filters // Journal of Aerosol Science. 1973. Vol. 4. P. 287–293.
3. **Kirsh V.A., Budyka A.K., Kirsh A.A.** Simulation of nanofibrous filters produced by the electrospinning method: 2. The effect of gas slip on the pressure drop // Colloid Journal. 2008. Vol. 70, No. 5. P. 584–588.
4. **Kuwabara S.** The forces experienced by randomly distributed parallel circular cylinders or spheres in a viscous flow at small Reynolds numbers // Journal of Physical Society of Japan. 1959. Vol. 14. P. 527–532.
5. **Mardanov R.F., Dunnett S.J., Zaripov S.K.** Modeling of fluid flow in periodic cell with porous cylinder using a boundary element method // Engineering Analysis with Boundary Elements. 2016. Vol. 68. P. 54–62.

DOI: 10.53954/9785604788967_220

VALIDATION OF SHOCK-WAVE/TURBULENT BOUNDARY-LAYER INTERACTION FLOWS BY HIGH-FIDELITY NUMERICAL SIMULATIONS

A.A. Zheltovodov[1], J. Fang[2], Yu. Yao[3]

[1]Khristianovich Institute of Theoretical and Applied Mechanics SB RAS
630090, Novosibirsk, Russia

[2]Scientific Computing Department, STFC Daresbury Laboratory
Warrington WA4 4AD, UK

[3]Department of Engineering Design and Mathematics, Faculty of Environment and Technology, University of the West of England
Bristol BS16 1QY, UK

Shock-wave/turbulent-boundary-layer interactions (SWTBLI) are prevalent phenomena around high-speed vehicles. The resultant strong adverse pressure gradient will induce large flow separation, high wall heat flux, and strong pressure fluctuation, along with other complex physical phenomena. The research on SWTBLI has been conducted persistently for more than 70 years, although some fundamental flow mechanisms are still not completely understood and the prediction of its aerodynamic performance is still unsatisfactory [1]. Four key configurations involving a high-speed vehicle are studied using DNS and LES, which are respectively the oblique shock-wave/flat plate boundary layer interaction (OSWFPBLI) flow, the compression-expansion corner (ComExpCor) flow, the expansion-compression corner (ExpComCor) flow and the flow past a single fin (SFIN). The sketch of these configurations are presented in Fig. 1. The in-house code ASTR was adopted to solve the compressible Navier – Stokes (NS) equations. The 7th-order MP-LD scheme [2] is used to solve the convection terms, and the diffusion terms are solved with the 6th-order compact central scheme. The 3rd-order Runge – Kutta method is used to advance the solution in time.

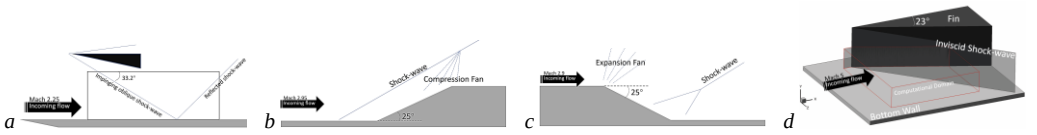

Fig. 1. Sketch of the SWTBLI configurations studied.
a – OSWFPBLI (M = 2.25, ε_{sw} = 33.2°), *b* – ComExpCor (M = 2.9, α = 25°), *c* – ExpComCor (M =2.9, α = –25°), *d* – SFIN (M = 5, β_{fin} = 23°).

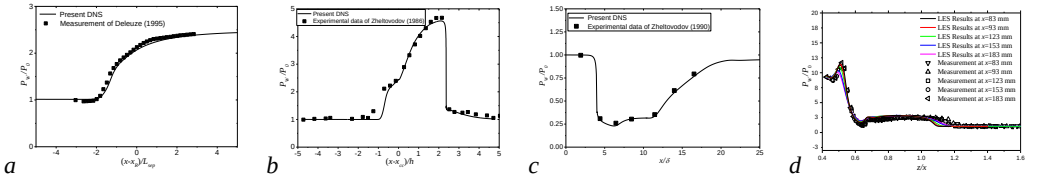

Fig. 2. Distribution of mean wall pressure in the interaction zone.
a – OSWFPBLI (Re_θ = 3.26), *b* – ComExpCor (Re_θ =3.008), *c* – ExpComCor (Re_θ = 1.532), *d* – SFIN (Re_θ = 6.29).

Results and Discussions. The validation of the simulations in the interaction zone is mainly done by comparing the mean wall pressure with the measured data, as presented in Fig. 2. For all the studied case, good agreements between simulations and experiments can be confirmed,

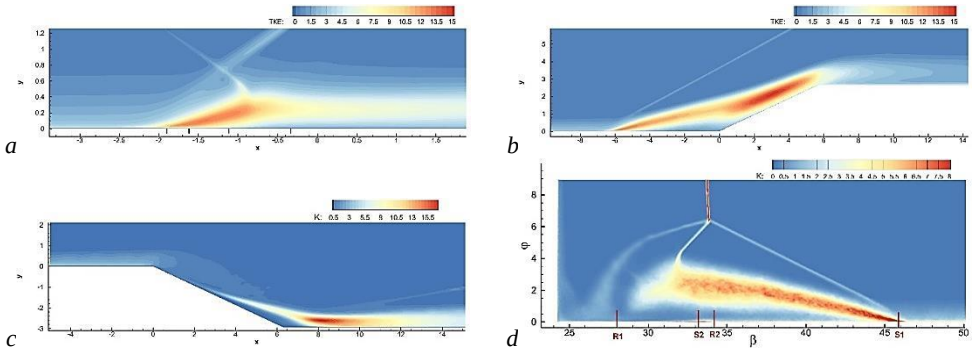

Fig. 3. Turbulent kinetic energy of cases: OSWFPBLI (*a*), ComExpCor (*b*), ExpComCor (*c*), and SFIN (*d*).

validating the numerical method for DNS/LES of SWTBLI flows. The amplification of turbulence is a key feature in SWTBLI, which is closely connected to flow separation, wall heat flux peak, skin-friction, and acoustic radiation in high-speed flows. The distribution of the turbulent kinetic energy (TKE) is presented in Fig. 3. A common phenomenon observed in Fig. 3 is a large area of high TKE zone in the interaction region for all the cases studied, indicating the amplification of turbulence is a universal characteristic in SWTBLIs. For the flat plate case, we can see that the turbulent kinetic energy is amplified with its peak moving away from the wall, indicating a free shear-layer is formed and the main contributor to the amplification of turbulence. For the compression-expansion corner case, we can also see the contribution of the free shear layer. But a two-zone structure of the amplified TKE can be identified. For the expansion-compression corner configuration, the reduction of turbulent kinetic energy downstream the expansion corner can be first seen, indicating the suppression of turbulence in a re-laminarization process. After the interaction with the shock-wave, a similar free shear-layer structure with a high level of turbulence kinetic energy. In the 3-D single fin case, high turbulent kinetic energy in the free shear-layer is obvious. Different from 2-D cases, the free shear-layer is terminated at the rear shock-wave, rather than moving downstream. In a very thin layer close to the wall, high values of turbulence kinetic energy can be seen meaning the flow inside the reverse flow is also highly turbulent, while the flow in a 2-D separation zone is less fluctuating and normally considered as the "dead zone".

Conclusions. A series of key SWTBLI flows abstracted from hypersonic flights are studied using the DNS and LES approaches using the ASTR code. Some interesting flow structures are discovered, including the chaotic turbulent structures in the free shear-layer generated during the interaction, the large-scale Görtler vortices created in the re-laminarization process in the expansion-compression corner flow, and the strong near-wall turbulence in the thin layer of the 3-D SWTBLI flow. The present study has demonstrated that DNS and LES relying on high performance computing are effective in studying turbulence of high-speed flow.

Acknowledgment. The research by the first author was carried out within the state assignment of Ministry of Science and Higher Education of the Russian Federation (project No. 121030500161-0).

REFERENCES

1. **Knight D.D., Zheltovodov, A.A.** Ideal-Gas Shock Wave – Turbulent Boundary-Layer Interactions (STBLIS) in Supersonic Flows and Their Modeling: Two-Dimensional Interactions // Shock Wave – Boundary-Layer Interactions / Eds. H. Babinsky, J. Harvey. Cambridge: Cambridge University Press, 2011. P. 137–201.
2. **Fang J., Li Z., Lu L.** An Optimized Low-Dissipation Monotonicity-Preserving Scheme for Numerical Simulations of High-Speed Turbulent Flows // J. Sci. Comput. 2013. Vol. 56. P. 67–95.

DOI: 10.53954/9785604788967_222

INVESTIGATING POSSIBILITIES TO USE A GLASS-CERAMIC COATING FOR METAL MODELS IN A HEAT EXPERIMENT

B.E. Zhestkov, A.S. Rtishcheva

Central Aerohydrodynamic Institute
140180, Zhukovsky, Moscow region, Russia

Expanding the capabilities of a wind tunnel heat experiments to study the aerothermodynamics of hypersonic aircraft follows the path of widespread use of panoramic methods for determining the surface temperature of the body under study, increasing the testing time, and using metal bodies as test samples and models. All this requires the use of high emissivity coatings. Such coatings prevent destruction of the model at long-term testing, make its surface smooth, which in practice makes it possible to reduce flow turbulence and improve the accuracy and quality of the experiment.

This study dealt with the possibility of using a new erosion-resistant glass-ceramic coating for metal models in a heat experiment conducted in TsAGI wind tunnels.

Description of Erosion Resistant Glass-Ceramic Coating. Erosion-resistant glass-ceramic coating has emissivity factor $\varepsilon = 0.85$. The main thermophysical properties of this coating were obtained within the temperature range T = 300-573 K. The thermal conductivity coefficient in the temperature range under consideration changes slightly: $\lambda = 1.21 \pm 0.01$ W/(m·K). To determine the possibilities of conducting a heat experiment with this coating, it became necessary to study its thermophysical properties at higher temperatures.

Experimental study of an erosion-resistant glass-ceramic coating. The tests were carried out in the TsAGI VAT-104 facility with the parameters: p_0 = 4668 Pa, T_0 = 6000–6500 K. The model was a steel cylinder, on the frontal surface of which an erosion-resistant glass-ceramic coating was applied. Three thermocouples were installed on the side surface of the cylinder. As a result of the experiment, the duration of which was $\Delta\tau \approx 200$ s, the temperature distributions of the cylinder surface (using a pyrometer) and thermocouple readings were obtained. The surface temperature of the cylinder was $T_w \approx$ 1000–1200 K, and the temperature change at the points of installation of thermocouples was $-\Delta T/\Delta\tau \approx$ 1.2–1.4 K/s.

Computational study of the external flow and non-stationary heating of a cylinder coated with an erosion-resistant glass-ceramic material. To determine the coefficient of thermal conductivity of the coating, the external flow and non-stationary heating of the cylinder were numerically simulated in the VAT-104. Using the ANSYS FLUENT software package, the laminar flow of chemically reacting components of the gas mixture was simulated: O_2; N_2; O; N; NO [1, 2]. The condition of radiative heat transfer was set on the surface of the cylinder. To solve the problem of non-stationary heating of a solid structure, the conditions for convective and radiative heat transfer were set. In this case, the distribution of the value of the heat transfer coefficient over the surface of the cylinder was obtained as a result of solving the problem of external flow.

Both problems were solved in a two-dimensional axisymmetric formulation. In this case, structured computational grids were used (~ 1 million cells).

A series of calculations for non-stationary heating of a solid-state cylinder structure was performed with different values of the thermal conductivity coefficient of the glass-ceramic coating. This was done in order to find the value of λ, that satisfies the data of the heat experiment (the temperature distribution on the surface of the model and the rate of temperature change at the points of thermocouple installation). In the course of calculations, the value of the

thermal conductivity coefficient of the coating was obtained: $\lambda = 3.6 \cdot 10^{-2}$ W/(m·K). The revealed decrease in the value of the thermal conductivity coefficient while the temperature increases imposes restrictions on its use in a heat experiment (the surface temperature of the model should not exceed $T_w = 600$ K).

Application of erosion-resistant glass-ceramic coating in thermal testing. Testing of the erosion-resistant glass-ceramic coating was carried out in a heat experiment conducted in the TsAGI T-117 wind tunnel, at M = 10.5 and 13.8. In this case, a model made of steel grade 12X18H10T and having a fairly simple configuration (in the form of a segmental-conical body) was used. The coating thickness was δ = 55–60 μm. The model surface temperature was measured using a FLIR SC7750L infrared camera. Temperatures at control points were also measured using thermocouples. The experiment time was $\Delta\tau \leq 20$ s in each of the indicated modes, while the surface temperature of the model did not exceed T_w = 450-473 K. Also, numerical modeling of the external flow and non-stationary heating of the model was performed. From the conditions of coincidence of numerical and experimental data, the distributions of the values of the heat flux density and the heat transfer coefficient on the surface of the model were obtained at different times during the experiment.

At M = 10.5 (p_0 = 95 at, T_0 = 1200 K), the maximum calculated value of the heat flux density(at the front critical point) varied within: q_{max} = 19.5…16.5 W/cm^2, at M = 13.8 (p_0 = 100 at, T_0 = 1900 K) – they varied within: q_{max} = 23.2…20.9 W/cm^2.

It should also be noted that at present TsAGI is developing a method for reconstructing the heat flux density from the surface temperature data obtained in the experiment (without modeling the external flow around the model).

Thus, the developed coating has shown its effectiveness in heat tests under conditions where the surface temperature of the model is $T_w < 600$ K.

REFERENCES

1. **Roop N. Gupta R., Yos J., Thompson R.** A review of reaction rates and thermodynamic and transport properties for the 11-species air model for chemical and thermal nonequilibrium calculations to 30000 K: NASA Technical Memorandum 101528, 1989.
2. **McBride B, Gordon S., Reno M.** Coefficients for calculating thermodynamic and transport properties of individual species: NASA Technical Memorandum 4513, 1993.

DOI: 10.53954/9785604788967_224

DETERMINATION OF AIR-JET ENGINE THRUST

V.I. Zvegintsev

Khristianovich Institute of Theoretical and Applied Mechanics SB RAS
630090, Novosibirsk, Russia

The traditional approach to measuring of air-jet engines thrust was proposed by B.S. Stechkin in 1929 and consists in defining thrust as the difference between the momentum of the gas flow at the inlet and outlet of the engine [1]. This approach contains both methodological and terminological problems. Based on a critical analysis of existing ideas, this paper proposes to consider the thrust of the air-jet engines as a decrease in the drag of the entire composition "aircraft + engine" during the power plant operation with fuel supply and energy release. To highlight the introduced concept further in the text, the term "real thrust" R_t is used.

The concept of "real thrust", as a drag decrease, removes all existing problems in the classification of acting forces. With this definition, there is no need to divide forces into external and internal ones. "Real thrust" can be created both along the internal path of engine and on the external flying vehicle surface (for example, during a bottom gas generator operation). The formation of "real thrust" may be accompanied by an increase in external drag or by a change in the flow characteristics at the input of the air intake. "Real thrust" is, by definition, always positive and acts against drag force. The same "real thrust" can reduce the aerodynamic drag, can compensate for the drag, can exceed the drag (then the amount of excess is called "excessive" thrust).

As an example, the application of the concept of "real thrust" is considered in determining the thrust of the air-jet engine of the simplified scheme shown in Fig. 1.

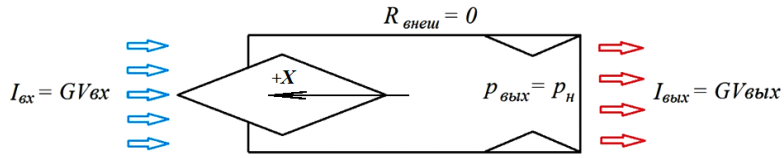

Fig. 1. Simplified scheme of the air-jet engine.

The simplifications of the scheme under consideration are as follows: a) external aerodynamic drag is assumed to be equal to zero; b) the gas flow rate at the inlet and outlet is considered as a constant; c) the static pressure at the outlet is equal to atmospheric pressure; d) the flow momentum at the inlet remains constant during engine operation.

Figure 2 shows the conditional values of the input and output momentum as the fuel consumption G_F increases. In the initial situation without fuel combustion (see Fig. 2a), the negative

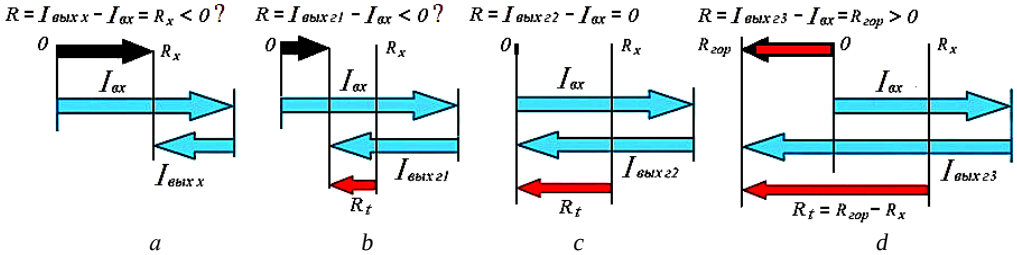

Fig. 2. Change in momentum distribution for a simplified air-jet engine.

momentum at the input – I_{in} exceeds the positive momentum of the flow at the output I_{out}, as a result the drag force of the considered engine is formed. This force R_x will be shown by the force-measuring device in the experiment as the total force acting on the engine.

When a small amount of fuel is supplied and burned in the combustion chamber (see Fig. 2,*b*), the speed and momentum of the outgoing flow $I_{\text{out } h1}$ increase and, accordingly, the drag of the engine (of the internal engine path) decreases. It is this decrease in the initial engine drag that is called "real thrust", the creation of which begins to consume the energy of the supplied fuel.

With a further increase in the flow rate of the supplied fuel, the momentum of the outgoing flow continues to increase and, in the end, can be equal to the value of the momentum at the inlet (see Fig. 2,*c*). At this moment, the total force acting on the entire engine is zero. However, the "real thrust", for the creation of which the energy of the supplied fuel continues to be expended, is not equal to zero and now it is equal to the aerodynamic drag force of the engine without combustion.

At a sufficiently high fuel consumption, the momentum of the outgoing jet exceeds the momentum of the flow at the inlet, and an excess (or effective) thrust R_{th} appears (see Fig. 2,*d*). It is this excess thrust, defined as the difference between the output and input momentum, that is considered the correct value of the thrust of the considered air-jet engine, which corresponds to the well-established classical concepts [1, 2]. In fact, the excess traction force R_{th} is underestimated compared to the "real thrust" R_t proposed in the paper by the value of the initial resistance of the internal engine path R_x: $R_h = R_t - R_{\text{x}}$

From Fig. 2 it can be seen that the value of "real thrust", the creation of which consumes the energy of the supplied fuel, is easily determined by measuring the total force acting on the engine during and without fuel combustion: $R_t = R_h - R_{\text{x}}$

The presentation includes a large number of examples of the definition of "real thrust" in various situations of application and simulation of the WFD. In particular, "real thrust" is easily determined in flight experiments to measure the acceleration of an aircraft and in bench tests to change the total force acting on the test model with and without fuel combustion. The value of "real thrust" can be effectively used in calculating the trajectories of an aircraft with an air-jet engine in the Earth's atmosphere.

REFERENCES

1. **Stechkin B.S.** Selected articles: Theory of heat engines. Section 1. Theory of jet engines and blade machines. Moscow: Fizmatlit, 2001. 432 p.
2. **Cherny G.G.** Gas Dynamics: Textbook for Universities and Higher Educational Institutions. Moscow: Nauka. Ch. ed. Fiz.-mat. lit., 1988. 424 p.

DOI: 10.53954/9785604788967_226

MODELING AND STUDY OF RICHTMAYER-MESHKOV INSTABILITY IN A BINARY SYSTEM OF LIGHT AND HEAVY GAS

K.I. Zyryanov[1], V.Y. Rudyak[1,2,3]

[1]Novosibirsk State University of Architecture and Civil Engineering (*Sibstrin*)
630008, Novosibirsk, Russia

[2]Novosibirsk State University
630090, Novosibirsk, Russia

[3]Institute of Thermophysics SB RAS
630090, Novosibirsk, Russia

The Richtmayer – Meshkov instability (R–M), which occurs during pulsed acceleration of the interface between two fluids with different densities, is characterized by the appearance of baroclinic vorticity on it [1, 2]. Such instability occurs in many practically important tasks. At the same time, there are tasks where the development of this instability should be maximally delayed or suppressed altogether (for example, during inertial compression of matter to trigger thermonuclear fusion). On the other hand, in supersonic modes of operation of a jet engine, it is necessary to ensure good mixing of the fuel components. And here the instability of R–M turns out to be a positive factor. Thus, managing the development of the instability of the R–M is practically an extremely important task. Since the mechanisms of the development of the R–M instability are quite subtle and are accompanied by the appearance of other complicating factors, in particular, Kelvin – Helmholtz and Rayleigh – Taylor instabilities, its study also has an important fundamental component.

This type of instability has been intensively studied experimentally for many years (see, for example, [3-5] and the literature cited there). A typical laboratory experimental staging of the study of this instability is the study of the evolution under the action of a plane shock wave of an expanding cylinder (or several cylinders) heavy gas flowing through the light gas under the influence of gravity. This is how instability was modeled in [6], which develops when a plane shock wave falls on a drop of heavy gas in the atmosphere of a light one (the problem was solved in a flat staging). It was shown that a pair of vortices forms at the boundary of the droplet after the shock wave passes through it, the interaction of which determines the further evolution of the system. Comparison of simulation data with experimental data [7] showed the adequacy of the model used and their fairly good consistency. Later, the same algorithm was used to simulate the Richtmeier – Meshkov instability that develops when a shock wave falls on a system of two drops of heavy gas [8]. In this work, the intensity of the shock wave, the distance between the droplets and some other parameters varied. It is shown that several critical distances can be distinguished at which the nature of the development of the Richtmayer – Meshkov instability changes qualitatively. In general, a complex four-vortex structure is formed here. However, its character significantly depends on the distance s between the centers of the droplets. A decrease in s leads to a decrease in the density gradient in the region between the droplets and, as a consequence, to a decrease in the corresponding vorticity field. As a result, a full–fledged four-vortex structure develops only at s/D (D is the diameter of the drop) greater than some. It was found that there are some critical distances at which other qualitative and quantitative changes occur in the dynamics of the evolution of the system. They depend on the intensity of the shock wave and the density gradient at the boundary of the two gases.

In real and laboratory conditions, however, systems of regularly located drops (gas pillars) can often take place, on which an intense shock wave falls. Such a situation is realized, for example, during the initialization of thermonuclear fusion. The simplest system of this kind con-

sists of three drops of heavy gas, on which a flat shock wave falls. The geometry of the system can vary from rectilinear to triangular with different localization of the sides. In addition, the density of droplets and other parameters may change. It is in such systems that the instability of R–M is studied in this paper. The intensity of the shock wave, the distance between the centers of the droplets, their density and configuration vary. The shock wave passes through the air and falls on SF_6 droplets. The physical mechanism for generating swirling is that the velocity of the shock wave decreases monotonically with increasing density of the mixture, as a result of which shear streams having swirling of the opposite sign occur in the upper and lower segments of each drop.

The problem is solved numerically within the framework of two-fluid hydrodynamics [6, 8]. Three configurations of droplets are considered: linear across and along the shock wave, as well as two symmetrical triangular ones with a base and a vertex closer to the front of the incoming shock wave. Different mutual distances between droplets are considered. In the case of triangular configurations, the influence of the initial distance of one cylinder from a pair of others is also considered. The critical value of this distance is determined, at which both quantitative and qualitative changes occur in the evolution of the entire system. Various asymmetric configurations of droplets are also considered. It is shown how the ratio of cylinder densities affects the qualitative changes in the evolution of the system. Flow patterns, qualitative and quantitative characteristics of the evolution of various configurations of three drops are compared with the corresponding characteristics of the evolution of a solitary drop and a pair of drops. The nature of the developing instability and the structure of the emerging vorticity regions, their dependence on the Mach number (shock wave intensity), droplet density, their configuration, etc. are systematically studied. It is established that there is a certain kind of self-similarity, which makes it possible to predict the nature of the developing instability in arbitrary similar systems.

The work was supported by megagrants of the Ministry of Science and Higher Education of the Russian Federation (Agreements No. 075-15-2021- 575).

REFERENCES

1. **Richtmayer R.D.** Taylor instability in shock acceleration of compressible fluids // Comm. Pure Appl. Math. 1960. Vol. 13. P. 297–319.
2. **Meshkov E.E.** Instability of the interface between two gases accelerated by a shock wave // The Proceedings of the USSR Academy of Sciences. Fluid and Gas Mechanics. 1969. No. 5. P. 151–157.
3. **Tomkins C., Prestrige K., Rightly P., Marr-Lyon M., Vorobieff P., Benjamin R.** A quantitative study of the interaction of two Richtmyer – Meshkov-unstable gas cylinders // Phys. Fluids. 2003. Vol. 15. P. 986–1004.
4. **Kumar S., Orlicz G., Tomkins C., Goodenough C., Prestridge K., Vorobieff P., Benjamin R.** Stretching of material lines in shock-accelerated gaseous flows // Phys. Fluids. 2005. Vol. 17. Art. 082107. 11 p. DOI:10.1063/1.2031347.
5. **Zhou Y**. Rayleigh – Taylor and Richtmyer – Meshkov instability induced flow, turbulence, and mixing // Physics Reports. 2017. Vol. 720–722. P. 1–136.
6. **Zyryanov K.I., Ruev G.A., Fedorov A.V.** Development of the Richtmayer – Meshkov instability as a result of the passage of a shock wave through the cylindrical structure of a heavy gas // Engineering and Physics Journal. 2017. Vol. 90, No. 2. P. 458–464.
7. **Tomkins C., Kumar S., Orlicz G., Prestridge K**. An experimental investigation of mixing mechanisms in shock accelerated flow // J. Fluid Mech. 2008. Vol. 611. P. 131–150.
8. **Zyryanov K.I., Rudyak V.Ya., Ruev G.A.** On critical interaction distances of heavy gas droplets in the presence of Richtmayer – Meshkov instability // The works of NSUACE. 2019. Vol. 22, No. 4. P. 19–37.

Content

Научное издание

Международная конференция по методам
аэрофизических исследований
8–14 августа 2022 г.,
Новосибирск, Россия
Тезисы докладов
Часть I

На английском языке

INTERNATIONAL CONFERENCE ON THE METHODS
OF AEROPHYSICAL RESEARCH
August 8 – 14, 2022,
Novosibirsk, Russia
Abstracts
Part I

Ответственный за выпуск А.Д. Косинов
Технический редактор Т.В. Ветровская

Подписано в печать 1.07.2022. Формат бумаги 70×100 1/16
Усл. печ. л. 19,0. Уч.-изд. л. 18,4. Тираж 230 экз. Заказ № 232

Сибирское отделение РАН
630090, просп. Акад. Лаврентьева, 17
Отпечатано в Сибирском отделении РАН
630090, г. Новосибирск, Морской просп., 2
Тел. (383) 330-84-66, e-mail: e.lyannaya@sb-ras.ru